

August 2015

Migration of Myeloid-derived Suppressor Cells to Tumor and Tumor-Draining Lymph Node in a Murine Model of Breast Cancer

Vyara Matson

University of Wisconsin-Milwaukee

Follow this and additional works at: <https://dc.uwm.edu/etd>



Part of the [Allergy and Immunology Commons](#)

Recommended Citation

Matson, Vyara, "Migration of Myeloid-derived Suppressor Cells to Tumor and Tumor-Draining Lymph Node in a Murine Model of Breast Cancer" (2015). *Theses and Dissertations*. 1012.

<https://dc.uwm.edu/etd/1012>

This Dissertation is brought to you for free and open access by UWM Digital Commons. It has been accepted for inclusion in Theses and Dissertations by an authorized administrator of UWM Digital Commons. For more information, please contact open-access@uwm.edu.

**MIGRATION OF MYELOID-DERIVED SUPPRESSOR CELLS TO TUMOR
AND TUMOR-DRAINING LYMPH NODE IN A MURINE MODEL OF BREAST
CANCER**

by

Vyara Matson

**A Dissertation Submitted in
Partial Fulfillment of the
Requirements for the Degree of**

**Doctor of Philosophy
in Biological Sciences**

at

The University of Wisconsin-Milwaukee

August 2015

ABSTRACT

MIGRATION OF MYELOID-DERIVED SUPPRESSOR CELLS TO TUMOR AND TUMOR-DRAINING LYMPH NODE IN A MURINE MODEL OF BREAST CANCER

by

Vyara Matson

**The University of Wisconsin-Milwaukee, 2015
Under the Supervision of Professor Douglas A. Steeber**

Myeloid-derived suppressor cells (MDSC) consist of two major subsets, monocytic MDSC (M-MDSC) and polymorphonuclear MDSC (PMN-MDSC), both of which expand in cancer and suppress the activation of naïve T cells in the tumor-draining lymph node (TDLN) and the function of effector T cells in the tumor microenvironment. Thus, the ability of MDSC to enter the TDLN and the tumor is likely to be critical for suppression of the anti-tumor immune response. L-selectin mediates the homing of circulating naïve lymphocytes to lymph nodes and the migration of conventional myeloid cells, such as neutrophils and monocytes, to sites of inflammation, but its contribution to MDSC migration is unknown. Using the 4T1 murine breast cancer model, we demonstrated that MDSC express L-selectin and integrins necessary for migration to TDLN and inflammatory sites, such as the tumor. We then demonstrated involvement of L-selectin in the migration of PMN-MDSC, but not M-MDSC, to tumors and TDLN. This suggests that M-MDSC may utilize L-selectin-independent mechanisms for migration. After entry into the tumor, MDSC migrated through the tumor parenchyma

and associated with MDSC aggregates localized in the immediate vicinity of hypoxic areas. BrdU incorporation experiments showed that approximately 20% of tumor-infiltrating MDSC were undergoing *in situ* proliferation in the tumor microenvironment. Thus, in addition to MDSC recruitment to tumors, intratumoral proliferation of MDSC may also contribute to MDSC accumulation. Hypoxia-inducible factor (HIF) is an intracellular sensor of hypoxia, which functions to activate the expression of genes necessary for adaptation to hypoxic conditions. There are several HIF isoforms with both overlapping and opposing roles in various processes, including proliferation. Although our preliminary experiments did not confirm a role for HIF in inducing proliferation of tumor-infiltrating MDSC, the specific roles of the different HIF isoforms in MDSC recruitment, proliferation, and function in the tumor microenvironment requires further study. These studies provide insights into the mechanisms of MDSC migration and accumulation in the tumor and TDLN. Further studies may create a basis for novel immunotherapeutic approaches for the treatment of cancer.

**© Copyright by Vyara Z. Matson, 2015
All Rights Reserved**

TABLE OF CONTENTS

LIST OF FIGURES	vii
LIST OF TABLES	ix
LIST OF ABBREVIATIONS	x
ACKNOWLEDGEMENTS	xiv
<u>CHAPTER 1</u> – GENERAL INTRODUCTION	1
Figure Legends and Figures.....	31
<u>CHAPTER 2</u> – ROLE OF L-SELECTIN IN TUMOR PROGRESSION AND ACCUMULATION OF MYELOID-DERIVED SUPPRESSOR CELLS	35
Abstract.....	36
Introduction.....	38
Materials and Methods.....	45
Results.....	55
Discussion.....	67
Figure Legends and Figures.....	74
Tables and Table Legends.....	92
<u>CHAPTER 3</u> – INVOLVEMENT OF L-SELECTIN IN MDSC MIGRATION TO TUMOR AND TUMOR-DRAINING LYMPH NODE	98
Abstract.....	99
Introduction.....	101
Materials and Methods.....	108
Results.....	113

Discussion.....	119
Figure Legends and Figures.....	126
Tables and Table Legends.....	135
<u>CHAPTER 4 – TUMOR-INFILTRATING MYELOID-DERIVED SUPPRESSOR CELLS AGGREGATE NEAR REGIONS OF HYPOXIA WITHIN THE PRIMARY TUMOR</u>	139
Abstract.....	140
Introduction.....	142
Materials and Methods.....	145
Results.....	152
Discussion.....	159
Figure Legends and Figures.....	164
<u>CHAPTER 5 – CONCLUSIONS</u>	177
Figure Legends and Figures.....	182
REFERENCES	185
CURRICULUM VITAE	204

LIST OF FIGURES

Figure 1.	Adhesion cascade.....	33
Figure 2.	Oxygen-dependent regulation of hypoxia inducible factor-1 alpha expression.....	34
Figure 3.	The kinetics of systemic MDSC accumulation correlate with tumor growth rate.....	81
Figure 4.	PMN-MDSC and M-MDSC from spleen and blood of 4T1 tumor-bearing mice express L-selectin.....	82
Figure 5.	MDSC accumulation in tissues of wild type and L-selectin ^{-/-} mice with advanced stage 4T1 tumors.....	83
Figure 6.	High M-MDSC/PMN-MDSC ratio in PLN of mice with advanced stage 4T1 tumors is dependent on L-selectin.....	84
Figure 7.	MDSC from spleen of 4T1 tumor-bearing mice suppress T cell proliferation in a dose-dependent manner.....	85
Figure 8.	Localization of MDSC in the spleen of advanced stage 4T1 tumor-bearing mice.....	86
Figure 9.	Localization of PMN-MDSC in the TDLN of advanced stage 4T1 tumor-bearing mice.....	87
Figure 10.	Localization of M-MDSC in the TDLN of advanced stage 4T1 tumor-bearing mice.....	88
Figure 11.	Localization of MDSC in advanced stage 4T1 tumors.....	89
Figure 12.	PMN-MDSC are present in the thymus of advanced stage 4T1 tumor-bearing mice.....	90
Figure 13.	MDSC from 4T1 tumor-bearing mice express folate receptor β	91
Figure 14.	Flow cytometric identification of PMN-MDSC and M-MDSC subpopulations.....	130
Figure 15.	Expression of α_L and β_2 integrins on PMN-MDSC and M-MDSC.....	131
Figure 16.	Expression of α_4 , β_1 , and β_7 integrins on PMN-MDSC and M-MDSC...	132

Figure 17.	<i>In vivo</i> migration of adoptively transferred 4T1 tumor-induced MDSC.....	133
Figure 18.	Localization of migrated MDSC relative to blood vessels and endogenous MDSC clusters in the tumor microenvironment.....	134
Figure 19.	Co-localization of MDSC clusters next to hypoxic regions in 4T1 tumors.....	170
Figure 20.	Quantitation of co-localized MDSC clusters next to hypoxic regions in 4T1 tumors.....	171
Figure 21.	Quantitation of contact between MDSC clusters and hypoxic regions in 4T1 tumors.....	172
Figure 22.	Quantitation of blood vessels in areas of hypoxia, areas near hypoxia, and areas far from hypoxia in 4T1 tumors.....	173
Figure 23.	MDSC enter tumors in areas located outside of MDSC clusters and accumulate within MDSC clusters over time.....	174
Figure 24.	Quantitation of MDSC proliferation within bone marrow, spleen and tumor from mice with 4T1 breast cancer.....	175
Figure 25.	Effect of <i>in vivo</i> DMOG treatment on the proliferation of tumor-infiltrating MDSC.....	176
Figure 26.	Roles of L-selectin and hypoxia in MDSC migration to TDLN and tumor in the 4T1 breast cancer model.....	184

LIST OF TABLES

Table I.	Tumor growth rate and kinetics of MDSC accumulation in 4T1 tumor-bearing wild type and L-selectin ^{-/-} mice.....	92
Table II.	Frequencies of MDSC subsets in tissues of wild type and L-selectin ^{-/-} mice with advanced stage 4T1 tumors.....	94
Table III.	Numbers of MDSC subsets in tissues of wild type and L-selectin ^{-/-} mice with advanced stage 4T1 tumors.....	96
Table IV.	Tissue cellularity of wild type and L-selectin ^{-/-} mice with advanced stage 4T1 tumors.....	97
Table V.	Efficiency of MDSC migration quantified as numbers and percent of injected PMN-MDSC and M-MDSC recovered 16 h after adoptive transfer.....	135
Table VI.	Tissue cellularity of recipient mice bearing mid stage 4T1 tumors.....	137
Table VII.	Numbers of endogenous PMN-MDSC and M-MDSC in wild type recipient mice bearing mid stage 4T1 tumors.....	138

LIST OF ABBREVIATIONS

1. ADAM17 - ADAM metallopeptidase domain 17; also known as TNF- α converting enzyme (TACE)
2. APC - allophycocyanin
3. ARNT - aryl hydrocarbon nuclear translocator
4. BCL-2 - B-cell lymphoma 2
5. BCL-XL - B-cell lymphoma XL
6. bHLH-PAS protein - basic helix-loop-helix-Per-ARNT-Sim protein
7. BM - bone marrow
8. CCR - CC chemokine receptor(s)
9. CFSE - carboxy-fluorescein succinimidyl ester
10. C-TAD - C-terminal transactivation domain
11. CTL - cytotoxic T lymphocyte(s)
12. CXCR - CXC chemokine receptor(s)
13. DAMP - damage-associated molecular pattern(s)
14. DC - dendritic cell(s)
15. DMOG - dimethyl-oxalyl-glycine
16. EGF - epidermal growth factor
17. FITC - fluorescein isothiocyanate
18. FR - folate receptor(s)
19. G-CSF - granulocyte colony stimulating factor
20. GlyCAM-1 - glycosylation-dependent cell adhesion molecule-1
21. GM-CSF - granulocyte/monocyte colony stimulating factor
22. h – hour(s)

23. HDAC - histone deacetylase
24. HEV - high endothelial venule(s)
25. HIF - hypoxia-inducible factor(s)
26. HRE - hypoxia response element(s)
27. ICAM-1 - intercellular adhesion molecule-1
28. IFN – interferon
29. IL – interleukin
30. i.p. – intraperitoneal
31. iNOS - inducible nitric oxide synthase
32. i.v. - intravenous
33. LFA-1 - lymphocyte function-associated antigen-1
34. Mac-1 - macrophage-1 antigen
35. MAdCAM-1 - mucosal vascular addressin cell adhesion molecule-1
36. MDSC - myeloid-derived suppressor cell(s)
37. MHC - major histocompatibility complex
38. min – minute(s)
39. M-MDSC - monocytic myeloid-derived suppressor cell(s)
40. MMTV - mouse mammary tumor virus
41. NDLN - non-draining lymph node(s)
42. NF- κ B - nuclear factor-kappa B
43. NK cells - natural killer cells
44. NO - nitric oxide
45. NS cells - natural suppressor cells

46. N-TAD - N-terminal transactivation domain
47. ODDD - oxygen-dependent degradation domain
48. PALS - periarteriolar lymphatic sheath
49. PAMP - pathogen-associated molecular pattern(s)
50. PHD proteins - prolyl hydroxylase domain proteins
51. PLN - peripheral lymph node(s)
52. PMN-MDSC - polymorphonuclear myeloid-derived suppressor cell(s)
53. PNAd - peripheral node addressin(s)
54. PRR - pattern recognition receptor(s)
55. PSGL-1 - P-selectin glycoprotein ligand-1
56. pVHL - von Hippel-Lindau protein
57. RNS - reactive nitrogen species
58. ROS - reactive oxygen species
59. s.c. - subcutaneous
60. SCR - short consensus repeat(s)
61. sE-selectin - soluble E-selectin
62. sLe^x - sialyl Lewis^x
63. sL-selectin - soluble L-selectin
64. sP-selectin - soluble P-selectin
65. STAT - signal transducer and activator of transcription
66. TAA - tumor-associated antigen(s)
67. TCR - T cell receptor(s)
68. TDLN - tumor-draining lymph node(s)

- 69. TGF- β - transforming growth factor- β
- 70. T_{reg} - regulatory T cell(s)
- 71. TRITC - tetramethylrhodamine
- 72. VCAM-1 - vascular cell adhesion molecule-1
- 73. VEGF - vascular endothelial growth factor
- 74. VLA-4 - very late activation-4
- 75. WT – wild type

ACKNOWLEDGEMENTS

I thank Dr. Douglas Steeber for being an amazing mentor. Providing guidance when needed is valuable, but what makes you such a great teacher is understanding and addressing the unique needs of each of your students, creating a positive and collaborative environment, giving the space and freedom for active learning, and most importantly, caring for our success and well-being. After spending almost 6 years in your lab, I have seen in you many positive qualities as a researcher, a teacher, and a person and hope to adopt at least some of them.

I also thank the rest of my committee members: Dr. Julie Oliver, Dr. Heather Owen, Dr. Jeri-Annette Lyons, and Dr. Reinhold Hutz for the guidance as my project developed. I thank Dr. Julie Oliver and her lab for sharing the tissue culture equipment, as well as Dr. Michael Laiosa and his lab for their help with cell sorting.

Several undergraduate and high school students have contributed to this work: Kate Rose, Daniel Schloegel, Samantha Willms, Ahmed Al-Muhairi, Rishi Sharma, Louis Palen, Amber Huffine, Margaret Linden, Jeffrey Denninger, Stephanie Bora, Jenna Lieungh, Alyssa Myszewski, and Nancy Gao; it was a pleasure working with all of you.

I am also grateful for the wonderful graduate students I shared the lab with during my time at UWM: Dr. Jamison Grailer taught me most of the techniques I used in this work; Dr. Jessica Loppnow always gave great counsel; there was never a dull moment with Abner Fernandes; and Sreya Biswas always cheered me up with an optimistic comment.

Finally, I thank my Bulgarian and American family and friends for their encouragement, as well as my husband Adam Matson who supported and inspired me and believed in me more than I did.

CHAPTER 1

GENERAL INTRODUCTION

I. Introduction

Tumor cells contain mutations or epigenetic abnormalities that result in an altered gene expression compared to healthy cells. This altered phenotype can be recognized by the adaptive immune system, as tumor-associated antigens (TAA) are presented in the tumor-draining lymph node (TDLN). This is of particular relevance to the development of immunotherapeutic strategies for the treatment of cancer. The major player in the anti-tumor immune response are cytotoxic T lymphocytes (CTL), which after their activation in the TDLN, can infiltrate the tumor and kill tumor cells upon contact. Various promising immunotherapeutic approaches are under investigation with that concept in mind. However, in many cancer patients the tumor microenvironment is characterized by overpowering immunosuppressive events due to a large extent to the expansion and accumulation of myeloid-derived suppressor cells (MDSC). In addition to suppressing the function of activated CTL within the tumor, MDSC can also suppress T cell activation within the TDLN (1, 2). Importantly, CTL responses are not systemically suppressed (3), suggesting that TAA-specific T cell suppression occurs primarily in the tumor and the TDLN (4, 5). The mechanisms of MDSC migration to these sites remain largely unknown.

II. Overview of the immune system

A. Function

The function of the immune system is, while sparing healthy host tissues and cells, to recognize and eliminate pathogenic foreign organisms (including bacteria, fungi, and various parasites); virus-infected, neoplastic, and dying host cells; as well as to aid in the repair of damaged tissues throughout the body. These functions constitute a complex

process called an immune response that is dependent on the ability of leukocytes, generated in the bone marrow and released into the bloodstream, to migrate to virtually all tissues in the body.

B. Cells and organs of the immune system

There are two major lineages of leukocytes, myeloid and lymphoid, which are generally responsible for the innate and adaptive branches of the immune response, respectively. The myeloid lineage consists of polymorphonuclear cells (including neutrophils, eosinophils, and basophils), monocytes, and myeloid dendritic cells (DC). Tissue-resident monocytes and basophils become macrophages and mast cells, respectively. The lymphoid lineage consists of lymphocytes, including T cells and B cells, natural killer (NK) cells, and lymphoid DC. All leukocytes are generated in the bone marrow via a process called hematopoiesis and released into the bloodstream. Progenitor T cells then migrate to the thymus for an additional process of selection and maturation, after which they are once again released into the bloodstream. Because the bone marrow and thymus function in the generation and maturation of leukocytes, these tissues are also referred to as primary lymphoid organs. In addition, secondary lymphoid organs such as spleen, peripheral lymph nodes (PLN) and mucosa-associated lymphoid tissues, among others, are the sites where the adaptive immune response is activated. These tissues are uniquely positioned for exposure to and surveillance against pathogens in the blood, in the peripheral tissues and ingested pathogens, respectively. For instance, blood-borne pathogens are filtered through the spleen, while pathogens in the periphery are transported with the lymph to the nearest PLN.

The spleen is located in the abdominal cavity and is the largest secondary lymphoid organ in the body. The spleen is especially equipped for filtering blood and surveillance against blood-borne pathogens and is responsible for mounting an immune response against systemic infections. It is fed by the splenic artery, which delivers substantial amounts of blood to the organ. In addition, the spleen contains networks of specialized capillaries, called sinusoids, which are characterized by fenestrated walls allowing for easier passage of large molecules and even cells between the blood and the spleen parenchyma. The sinusoids are enriched within the red pulp, one of the two major compartments of the spleen, which contains myeloid cells, especially macrophages, as well as red blood cells. In fact the red pulp is the site of deposition of aged or damaged red blood cells, followed by their phagocytic clearance by resident macrophages. The other compartment of the spleen, the white pulp, is located around arterioles, which branch from the splenic artery to feed all parts of the spleen. The white pulp is the site where the immune response to blood-borne pathogens is generated and contains the T cell-rich periarteriolar lymphatic sheath (PALS) immediately surrounding the arterioles and the B cell-rich follicles and marginal zone located around the PALS.

PLN are positioned throughout the body and filter lymph, which drains nearby tissues and enters the PLN via the afferent lymphatic vessels. The lymph is the major vehicle for delivery of antigens to the PLN, thus potentiating immune responses to infections in nearby tissues. In addition, the lymph also carries leukocytes from nearby tissues to lymph nodes. After its passage through the PLN, the lymph fluid is returned to the bloodstream, thus providing a route for leukocyte recirculation between blood and PLN. In addition to the lymphatic route, leukocytes primarily enter PLN from the

bloodstream, through specialized postcapillary venules called high endothelial venules (HEV). Similar to the spleen, the PLN are rich in B cells and T cells. B cells are organized in follicles in the cortex, a superficial zone, while T cells are localized deeper, in the paracortex. The innermost region in the PLN is the medulla, which contains macrophages and specialized antibody-secreting B cells called plasma cells.

C. Innate immune response

Neutrophils, macrophages and DC are phagocytic and express pattern recognition receptors (PRR) with broad specificity, which recognize classes of molecules commonly found in pathogens (pathogen-associated molecular patterns, PAMP) or associated with damaged or dying host cells (damage-associated molecular patterns, DAMP) (6). Engagement of these receptors at a site of infection or tissue injury, where there is abundant presence of PAMP and/or DAMP, initiates signaling resulting in increased phagocytic activity and release of inflammatory mediators (cytokines and chemokines) that recruit more leukocytes in a process called inflammation. Inflammation involves the function of both the innate and the adaptive immune responses. During the initial stages of inflammation, activated neutrophils release reactive oxygen and nitrogen species (ROS and RNS, respectively), which function locally to destroy the pathogens (along with some host cells), thus serving as the first line of defense against the infection. However, prolonged activation of the inflammatory process (chronic inflammation) is undesirable, because it leads to excessive tissue damage. Therefore, an important trait of the immune system are built-in mechanisms for contraction of the immune response and resolution of inflammation, followed by tissue remodeling/wound healing, mediated by myeloid cells.

D. Adaptive immune response

While activation of the innate immune response relies on PRR with very broad specificities, the receptors necessary for activation of the adaptive immune response recognize unique molecules, called antigens. The majority of antigens are peptide sequences derived from the processing of larger proteins of endogenous or exogenous origin. To be “visible” to the adaptive immune system, antigens must be presented in complex with cell surface molecules called major histocompatibility complex (MHC) molecules. MHC class II (MHC II) molecules are expressed only by professional antigen-presenting cells (including DC, macrophages, and B cells) and are used to present exogenous antigen processed from phagocytosed material. On the other hand, MHC class I (MHC I) molecules are expressed by all host cells and present endogenous antigens derived from self components within the cells or from an intracellular pathogen in the case of infected host cells. In addition, some DC can use MHC I to present exogenous antigens, a process called cross-presentation. Activated DC from the site of infection migrate via the lymph to the nearby lymph nodes, where they present antigens derived from the phagocytosed pathogens in complex with MHC II and, in some cases, MHC I. Antigen-MHC II complexes are recognized by the T cell receptor (TCR) complex of a subset of T cells, $CD4^+$ T cells, also called T helper cells. These cells do not possess cytolytic activity and cannot directly kill target cells, but via secretion of cytokines, can activate other leukocytes, as well as endothelial cells. For instance, T helper cells can aid in the activation of $CD8^+$ T cells. Activated $CD8^+$ T cells proliferate and differentiate into effector T cells (cytotoxic T cells, CTL) capable of lysing infected host cells that present a cognate pathogen-derived antigen in complex with MHC I on their surface. In addition,

T helper cells can also activate B cells, which secrete antibodies able to bind to their cognate antigen on the surface of pathogenic bacteria, fungi, and parasites, thus opsonizing the pathogen. These surface bound antibodies can then be recognized by receptors on phagocytic leukocytes which eliminate the pathogen. In addition, especially in the case of blood-borne infections, opsonized pathogens can be recognized and lysed by the coordinated function of serum proteins, collectively called the complement system.

III. The immune response to cancer

The immune system can distinguish between self and non-self molecules and generate a response that specifically eliminates infections as described above. Tumors, except those induced by a viral infection, arise from self rather than non-self cells, and thus were long thought to be “invisible” to the immune system. However, it is now known that tumors contain multiple genetic and epigenetic alterations, which result in TAA that are often immunogenic (7, 8). In fact, the current understanding is that the immune system eliminates most tumors before they become clinically detectable. If tumors are not completely eliminated, they enter an equilibrium state, in which tumor growth is balanced against tumor destruction. This state may last decades, but is eventually followed by tumor escape from immune surveillance and manifestation of clinically detectable cancer. Both innate and adaptive immune mechanisms are implicated in the immune response against cancer; however, the CTL response is the major contributor.

A. Generation of CTL-mediated anti-tumor response

In the TDLN, precursors of CTL, via the TCR, recognize TAA presented on MHC, which provides the first signal necessary for T cell activation and expansion. The second signal is provided by binding of co-stimulatory molecules to cognate receptors on the T cell. In response, the T cell starts to express the interleukin-2 (IL-2) receptor, which upon binding to its cognate ligand, IL-2, induces the T cell to proliferate and become capable of killing target cells, expressing the cognate TAA.

B. Generation of the NK cell-mediated anti-tumor response

Another component of the anti-tumor immune response are the NK cells, which also recognize and kill tumor cells, albeit via a different mechanism. Specifically, NK cell function is modulated by a balance of inhibiting and activating signals resulting from the ligation of inhibitory and activating receptors, respectively. For instance, class I MHC molecules, expressed by all healthy nucleated cells in the body, are recognized by receptors on NK cells that send a dominant inhibitory signal that prevents NK cell activation and cytotoxicity against healthy cells. By contrast, NK cell activating receptors bind ligands induced by tumor transformation or cell damage and initiate NK cell-mediated attack of the target cell. Thus, if a cell lacks or underexpresses MHC I, which is often the case with tumor cells, and/or overexpresses activating ligands, NK cells eliminate it by releasing cytotoxic substances or inducing apoptotic signals in the target cell.

IV. Myeloid-derived suppressor cells

In order to evade the CTL and NK cell response, tumors utilize a plethora of immunosuppressive strategies. One of these involves the induction and accumulation of MDSC.

A. Generation and activation of MDSC

MDSC, as do all white blood cells, arise in the bone marrow. In a healthy individual, immature myeloid cells in the bone marrow differentiate to dendritic cells, monocytes, and granulocytes, including neutrophils, basophils, and eosinophils. During pathologic conditions such as cancer, infections, traumatic stress, *etc.*, various soluble factors drive the expansion of immature myeloid cells and facilitate their activation to immunosuppressive MDSC. In the context of cancer progression, MDSC expansion is driven by pro-inflammatory cytokines and tumor-derived factors such as vascular endothelial growth factor (VEGF) (9), granulocyte/monocyte colony stimulating factor (GM-CSF) (10, 11), IL-1 β (12), IL-6 (13), stem cell factor (SCF) (14), S100A8/9 proteins (15), transforming growth factor- β (TGF- β), prostaglandin E₂ (PGE₂) (16, 17), and macrophage colony-stimulating factor (M-CSF) (16), among others. Most of these factors affect myelopoiesis and tumor progression via the signal transducer and activator of transcription 3 (STAT3) signaling pathway (18-20), and thus MDSC expansion is decreased by STAT3 knock-out or inhibition (21-23). Activated STAT3 increases the survival and proliferation of immature myeloid cells possibly via upregulation of B-cell lymphoma XL (BCL-XL), cyclin D1, c-Myc, and survivin (18, 24). Further activation of MDSC is driven by factors secreted by activated T cells and tumor stromal cells, possibly in response to tumor cell death (24). Among these factors are interferon γ (IFN γ), toll-like

receptor (TLR) ligands, IL-4, IL-13 and TGF- β . These factors trigger signaling via STAT1, STAT6, and nuclear factor-kappa B (NF- κ B), which induces expression of arginase-1, inducible nitric oxide synthase (iNOS), and TGF- β involved in MDSC-mediated immunosuppression (24).

B. Mechanisms of MDSC-mediated immunosuppression

Immunosuppressive functions of myeloid cells were first acknowledged in the late 1970s and early 1980s and the term “natural suppressor (NS) cells” was initially used for them (25-29). These NS cells were implicated in previously observed fetal and neonatal immunosuppression in the context of allogeneic graft transplantation experiments in mice (30). Importantly, a role for NS cells in the suppression of tumor-specific CTL was also recognized at that time (28). Indeed, the heterogeneous cell population that we know today as MDSC is no different than the NS cells described several decades ago (29). However, it was not until fairly recently that the mechanisms of MDSC-mediated immunosuppression became better understood.

Many of the suppressive functions of MDSC are due to upregulated arginase-1 and/or iNOS, which control L-arginine metabolism. Arginase-1 metabolizes L-arginine to L-ornithine and urea and is induced in myeloid cells by anti-inflammatory cytokines such as IL-10, IL-4 and IL-13 (31, 32), as well as TGF- β (33) and GM-CSF (34), and is primarily regulated by STAT6 activity (35). iNOS converts L-arginine to L-citrulline and nitric oxide (NO) and can be induced by pro-inflammatory cytokines such as IFN- γ , IL-1, IFN- α , IFN- β , and tumor necrosis factor (TNF) via NF- κ B and STAT1 signaling (36). Thus, the expression of these enzymes is differentially regulated. Furthermore, inhibition of arginase-1 results in an increase of iNOS function (37), while upregulation of arginase-

1 depletes L-arginine leading to a decrease in iNOS translation and NO production (38, 39). However, iNOS function may activate arginase-1 via NO-induced nitrosylation of cysteine residues in arginase-1 (40). L-arginine depletion from the tumor microenvironment by arginase-1 and/or iNOS causes T cell unresponsiveness by decreasing the mRNA stability and/or translation of important factors involved in T cell signaling and proliferation. Specifically, lack of L-arginine interferes with TCR signaling by downregulating the main signaling component, the CD3 ζ -chain, of the TCR complex, as well as inhibiting nuclear translocation of the downstream transcription factor NF- κ B (41-43). Lack of L-arginine also interferes with IL-2 receptor signaling in T cells by inhibiting the upregulation of the tyrosine kinase Jak-3 necessary for activation of STAT5-dependent transcription in response to IL-2 (43). In addition, IL-2 receptor signaling is also inhibited by exposure to NO, the product of iNOS (44, 45), and NO also inhibits the production and release of IL-2 by activated lymphocytes (46, 47) and induces T cell apoptosis (48). Importantly, L-arginine depletion also causes proliferative arrest of activated T cells by decreasing the mRNA stability and translation of cell cycle regulators such as cyclin D3 and cyclin-dependent kinase 4 (49, 50). These effects of L-arginine depletion are likely due to decreases in global translation rather than inhibition of the translation of specific proteins.

It has been suggested that arginase-1 and iNOS may cooperatively convert NO to ROS and RNS, such as hydrogen peroxide and peroxynitrites, respectively (51), which can exert multiple inhibitory effects on T cells. For instance, hydrogen peroxide, an electrically neutral and stable molecule that diffuses across membranes, has been implicated in the downregulation and functional impairment of the CD3 ζ -chain both in

tumor-bearing mice and in cancer patients (52, 53). In addition, peroxynitrite, a highly reactive cell-permeable molecule, inhibits T cell function by nitration and nitrosylation of cysteine, methionine, tryptophan and tyrosine in multiple protein targets, both extra- and intracellular. For instance, antigen-specific T cell unresponsiveness has been linked to nitration of the T cell receptor and the CD8 co-receptor molecule, as well as a general increase in intracellular nitro-tyrosine levels, while inhibition of arginase-1 and iNOS abrogated these effects (1, 54). Furthermore, both hydrogen peroxide and peroxynitrite cause apoptosis in antigen-activated T cells, possibly by downregulating the anti-apoptotic protein B-cell lymphoma 2 (BCL-2) and by upregulating the pro-apoptotic FAS ligand (55, 56).

MDSC also inhibit the function of other components of the anti-tumor immune response, such as NK cells and macrophages. For instance, MDSC block the expression of the activating receptor NKG2D on NK cells (57) and MDSC depletion in tumor-bearing mice results in restoration of NK activity (58). MDSC also downregulate IL-12 production by macrophages, thus skewing the immune response to favor tumor progression (59). In addition, MDSC indirectly suppress anti-tumor responses by promoting the function of other immunosuppressive populations such as regulatory T cells (T_{reg}). Specifically, MDSC activate both the clonal expansion of existing T_{reg} and the conversion of naïve $CD4^+$ T cell into T_{reg} via various mechanisms, including secretion of IL-10 and TGF- β as well as arginase-1 function (60-62).

In addition to their immunosuppressive functions, MDSC can directly promote tumor progression by driving the formation of new blood vessels within the tumor, a process called angiogenesis. This process is dependent on MDSC-mediated production of

matrix metalloproteinase 9 (MMP9), an enzyme that degrades the extracellular matrix and also increases the bioavailability of the pro-angiogenic signal VEGF (63). In addition, MDSC can directly incorporate into the tumor endothelium and differentiate into endothelial cells (63).

V. Leukocyte migration

Leukocyte migration to lymph nodes or sites of inflammation occurs via a multi-step process, called the adhesion cascade, which involves adhesive and signaling interactions between the leukocyte and the endothelium. These interactions are sequentially organized into 3 basic stages: 1) leukocyte capture and rolling over the endothelium, 2) firm adhesion (arrest), and 3) transendothelial migration (diapedesis) (Fig. 1) (64). Each of these stages is characterized by interactions between distinct groups of molecules. The adhesion cascade starts with leukocyte margination followed by a transient interaction with the endothelium, known as tethering or capture, and further transition to leukocyte rolling along the vascular wall. The capture and rolling events are dependent on interactions between selectins and their ligands (65, 66). The importance of these events is that they allow the leukocyte to slow down and sense chemokines displayed on the endothelial surface. The chemokines signal via G protein-coupled receptors to induce conformational changes increasing the adhesiveness of leukocyte-expressed integrins, which, via interactions with endothelial immunoglobulin-like superfamily molecules, are involved in decreasing the rolling speed and transitioning to the next stage of the adhesion cascade, firm adhesion (64, 67-72). Integrins are also involved in the subsequent events in the adhesion cascade including locomotion from the site of firm adhesion to a nearby junction between endothelial cells (a process also known

as intraluminal crawling) followed by transendothelial migration. In addition, integrins participate in leukocyte migration in the extracellular matrix and through epithelial layers to reach sites of tissue injury or inflammation (73).

Leukocyte migration to PLN occurs in specialized post-capillary venules, the HEV, morphologically characterized by a plump cuboidal shape of their endothelial cells. In addition, HEV differ from other blood vessels by the constitutive expression of HEV-restricted adhesion molecules, which are especially important for the homing of lymphocytes to PLN. On the other hand, the post-capillary venules of peripheral tissues do not express sufficient adhesion or signaling molecules to support migration of most leukocytes. Thus, in physiologic conditions, peripheral tissues are not readily infiltrated by leukocytes, except for some tissue-resident leukocytes. However, activation of these tissue resident leukocytes by PAMP and/or DAMP results in the secretion of inflammatory mediators, such as TNF- α or IL-1 β , which induce the expression of adhesion and signaling molecules on the vascular endothelium necessary for additional leukocyte recruitment. Thus, lymphocyte homing to PLN is constitutive, while leukocyte migration to peripheral non-lymphoid tissues is strongly enhanced only in inflammatory conditions.

A. Selectins mediate leukocyte capture and rolling

In the initial stages of the adhesion cascade the leukocyte is captured and starts rolling over the endothelium. These initial events are carried out via rapid interactions of association and release between selectins and their ligands. There are three selectins named after their location: P-selectin was initially identified on activated platelets (74, 75), but is also expressed, as is E-selectin, on activated endothelial cells (76, 77), while

L-selectin is expressed on leukocytes. P-selectin is not found on the membrane in resting platelets and resting endothelial cells, but is stored in α granule membranes and Weibel-Palade bodies, respectively, and upon activation, is rapidly distributed to the surface membrane. By contrast, expression of E-selectin on the endothelium requires *de novo* synthesis and takes hours (65), while L-selectin expression on leukocytes is constitutive (66). L-selectin is localized on the tips of the leukocyte microvilli to improve interactions with the endothelium. In addition, there is co-localization of some integrins on the leukocyte microvilli promoting synergism between L-selectin and integrins in mediating leukocyte adherence to the endothelium (66). The initial capture and fast rolling of the leukocyte is mediated by P- and L-selectin, while E-selectin is involved in the subsequent slower rolling and the transition to firm adhesion (66). Leukocyte rolling along the endothelium consists of rapid association between selectins and their ligands at the leading edge and their rapid dissociation at the trailing edge of the leukocyte. The nature of the bonds formed between L-selectin and its ligands confers a shear-dependent character to L-selectin-mediated rolling, meaning that a minimal hydrodynamic shear threshold against the blood vessel wall must be reached for capture and rolling to occur (78).

1. Selectin structure

The three selectins show some structural similarities and differences. Specifically, the N-terminal lectin domain, the epidermal growth factor (EGF)-like domain, and the short consensus repeat (SCR) domains (nine SCR in P-selectin, six SCR in E-selectin, and two SCR in L-selectin) are well conserved among selectins, while the transmembrane and intracellular domains show little sequence identity (66). Ligand binding occurs via

the lectin domain and is calcium dependent; however, the EGF-like domain also contributes (79-81). The SCR repeats are also thought to promote ligand binding, but their major role seems to be increasing the reach of the lectin and EGF-like domains for better ligand interactions. With only two SCR domains, L-selectin is the shortest of the selectins, but that is compensated by its strategic localization on leukocyte microvilli, allowing sufficient reach for ligand interactions. In addition to the above domains, L-selectin contains an endoproteolytic cleavage site, which upon leukocyte activation is targeted by endogenous membrane-bound proteases such as the ADAM metallopeptidase domain 17 (ADAM17; also known as TNF- α converting enzyme or TACE) (66). This cleavage generates a soluble form of L-selectin (sL-selectin) which is relatively stable ($t_{1/2} \sim 20$ h) and able to bind ligand. sL-selectin competes with membrane L-selectin for endothelial binding partners, thus interfering with L-selectin-dependent leukocyte adhesion and migration (79, 82, 83). In addition, studies have also identified soluble forms of P- and E-selectin. The levels of sP- and sE-selectin are especially increased in inflammatory settings or upon thrombin-mediated platelet activation, likely due to cleavage of the membrane-bound forms as a result of these stimuli (65). The function of soluble selectins is unclear; however, it has been suggested that they serve as a regulatory mechanism to tune down over-activated immune responses by interfering with leukocyte migration, or, in the case of sP- and sE-selectin, initiating signaling in leukocytes (65, 66).

2. Selectin ligands

The selectin ligands comprise a group of glycoproteins expressed on HEV or inflamed endothelium, leukocytes, and platelets. A variety of glycoproteins bind selectins

in vitro, but confirming their physiologic relevance as selectin ligands is challenging due to the nature of the recognition epitope, as well as the redundancy among ligands. In general, the ligands consist of various protein scaffolds displaying serine/threonine-rich domains that are post-translationally modified by attachment of oligosaccharide chains. Specifically, the lectin domain of the selectins recognizes the carbohydrate components of the ligand. For instance, binding of all three selectins depends on the presence of sialic acid within the carbohydrate moiety of the ligand. In addition, the presence of fucose and sulfate are necessary for biologically relevant ligand recognition for P- and L-selectin but not for E-selectin (84). Thus, the generation of physiologic selectin ligands requires the function of glycosyl- and sulfo-transferases. The spatial and temporal regulation of the expression and activity of these groups of enzymes in endothelial cells, leukocytes, or platelets is an important determinant of the patterns of leukocyte migration. Consistent with the requirement for sialylation, fucosylation and sulfation for selectin binding, the tetrasaccharide sialyl Lewis^x (sLe^x) composed of N-acetylglucosamine, galactose, sialic acid, and fucose (structure: Sia α 2 \rightarrow 3Gal β 1 \rightarrow 4[Fuc α 1 \rightarrow 3]GlcNAc) binds to all selectins, but with low affinity (85). For L-selectin, the sulfated form 6-sulfo-sLex confers high affinity binding. Studies using anti-sLex blocking antibodies suggest that the tetrasaccharide participates in the structure of physiologic L-selectin ligands (86, 87). Interestingly, selectin binding occurs even if the required sialic acid, fucose and sulfate moieties are not located on the same oligosaccharide. In fact, in some cases the sulfate is directly added to tyrosine residues of the protein scaffold, rather than the carbohydrate component (84). This discontinuous character of the carbohydrate epitope is reminiscent of antibody-binding epitopes composed of amino acids from different parts of the

polypeptide chain that are spatially brought together as a result of protein folding. In a similar manner, the protein scaffolds may play a vital role in the construction and the display of the carbohydrate epitopes. Specifically, the presence and correct localization of amino acid residues targeted by appropriate glycosyl- and sulfo-transferases may dictate not only the exact types of post-translational modifications, but also the order in which these reactions are carried out so as to generate the appropriate carbohydrate epitope. In addition, the overall three-dimensional structure of the protein may dictate the correct orientation and display of the carbohydrate epitopes. Furthermore, the protein scaffold may sequester the carbohydrate epitope on favorable areas of the cell surface for enhanced contact with the selectins. The protein scaffolds are likely involved in transmitting outside-in signals upon selectin binding.

Functionally expressed on leukocytes and inflamed endothelium, P-selectin glycoprotein ligand-1 (PSGL-1) is the most widely studied selectin ligand and is considered to be a major physiologic ligand of P-selectin, although it also binds E- and L-selectin (88, 89). There are not sufficient *in-vivo* studies for the identification of a major physiologic E-selectin ligand, but some potential partners include E-selectin ligand-1 (ESL-1) and CD44, the latter of which also binds L-selectin (65).

The major physiologic L-selectin ligand is also not unequivocally identified due to a high degree of redundancy between ligands. Among the protein scaffolds capable of displaying appropriate carbohydrate epitopes for L-selectin binding *in vitro* are CD34, glycosylation-dependent cell adhesion molecule-1 (GlyCAM-1), podocalyxin, nepmucin, endomucin, Spg200, endoglycan, mucosal vascular addressin cell adhesion molecule-1

(MAdCAM-1), PSGL-1, and hematopoietic cell E- and L-selectin ligand (HCELL, a glycosylated form of CD44) (65, 66).

3. Role of selectins in leukocyte migration to PLN

Expression of L-selectin ligands in PLN drives lymphocyte homing to PLN in the steady state as part of the immune surveillance process. L-selectin ligands expressed on HEV in PLN are collectively called peripheral node addressins (PNAd), and include CD34, GlyCAM-1, podocalyxin, nepmucin, and endomucin (65, 66). L-selectin-deficiency, or antibody-mediated blockade of L-selectin binding renders lymphocytes largely unable to migrate to PLN *in vivo* (90, 91). Thus, it is not surprising that L-selectin^{-/-} mice show a 70% decrease in PLN cellularity (92).

4. Role of selectins in leukocyte migration to sites of inflammation

L-selectin also plays a role in leukocyte migration to sites of inflammation. As described above, inflammation is part of the immune response and involves the recruitment of leukocytes to sites of tissue injury or infection where their purpose is to eliminate the pathogen and repair the damaged tissue. Various chronic inflammatory diseases exhibit blood vessels with enhanced ability to support lymphocyte migration due to the upregulation of L-selectin ligands. Inflammatory cytokines, such as TNF- α or IL-1 β , or bacterial components such as lipopolysaccharide (LPS) cause an upregulation of adhesion molecules, including L-selectin ligands, on the endothelium in inflamed tissues, thus leading to increased leukocyte migration to the inflammatory site (66). Contribution of L-selectin in leukocyte migration to sites of inflammation has been documented in various conditions (66). For instance, L-selectin is involved in the recruitment of neutrophils (93, 94) and T cells (95) to the inflammatory site in ischemia-reperfusion

injury, and concanavalin A-induced liver injury, respectively. Furthermore, L-selectin plays a role in the recruitment of T cells (96) as well as neutrophils, macrophages, lymphocytes and eosinophils (97, 98) to the site of pulmonary inflammation in murine and sheep models of asthma, respectively. As another example of pulmonary inflammation, mice with pulmonary fibrosis showed an L-selectin-dependent infiltration of neutrophils and lymphocytes in the lung (99).

The major role of P-selectin in platelets appears to be in coagulation (100), but it can also mediate interactions between platelets and neutrophils, monocytes, or inflamed endothelium, as well as interactions between neutrophils and inflamed endothelium (101-103). One implication of such interactions is providing for an L-selectin-independent mechanism of leukocyte migration to PLN or sites of inflammation. For instance, platelet-expressed P-selectin may mediate lymphocyte rolling on HEV through interactions with PNA_d (104, 105). In addition platelet-expressed P-selectin may be involved in the recruitment of leukocytes to sites of inflammation by signaling through PSGL-1 binding (106-111).

B. Integrins are involved in multiple events of the adhesion cascade

Integrins are a family of heterodimeric cell adhesion molecules, composed of an α and a β chain, which bind immunoglobulin superfamily molecules or molecules of the extracellular matrix. Integrins are the major cell adhesion transmembrane receptors and can mediate outside-in and inside-out signaling. There are 18 α and 8 β subunits, which form 24 known $\alpha\beta$ heterodimers, involved in various biologic processes, such as development, immune responses, leukocyte migration, and hemostasis. Some leukocyte-expressed integrins with major roles in migration include $\alpha_L\beta_2$, $\alpha_M\beta_2$, $\alpha_4\beta_1$, and $\alpha_4\beta_7$.

The $\alpha_L\beta_2$ integrin (CD11a/CD18) and $\alpha_M\beta_2$ integrin (CD11b/CD18) are also known as lymphocyte function-associated antigen-1 (LFA-1) and macrophage-1 antigen (Mac-1), respectively (112, 113). LFA-1 is expressed on various leukocytes, while Mac-1 is restricted to myeloid cells and the nonconventional B-1 B cells. These integrins have various binding partners with some overlap between the two groups. For instance, both bind intercellular adhesion molecule-1 (ICAM-1), a member of the immunoglobulin-like gene superfamily (114-117). ICAM-1 is expressed on various cells, including endothelial cells, fibroblasts, epithelial cells, monocytes, macrophages, and activated lymphocytes among others, and is transcriptionally upregulated in response to inflammatory mediators, such as TNF- α , IL-1 β , IFN- γ , as well as ROS, and virus or bacterial infections (118). LFA-1 or Mac-1 interactions with ICAM-1 play a role in various stages of leukocyte migration, including slow rolling, transition to firm adhesion, and diapedesis, as well as migration through the extracellular matrix at sites of inflammation (73). LFA-1 and Mac-1 functions are not restricted to leukocyte migration. For instance, interactions between LFA-1, co-localized with TCR on T cells, and ICAM-1, co-localized with MHC on antigen-presenting cells, aids in stabilization of cell-cell adhesion and T cell activation (119). In addition, Mac-1 is also known as complement receptor type-3, and its recognition of the complement protein iC3b on opsonized bacteria aids in phagocytosis by neutrophils and macrophages. Furthermore, Mac-1 expressed on activated neutrophils also interacts with dendritic cell-specific intracellular adhesion molecule-3-grabbing non-integrin (DC-SIGN, CD209) on dendritic cells, and this adhesion aids in neutrophil-induced dendritic cell maturation (120).

The $\alpha_4\beta_1$ and $\alpha_4\beta_7$ integrins are involved in leukocyte migration to sites of inflammation and to the gut, respectively. The $\alpha_4\beta_1$ integrin (CD49d/CD29) is also known as very late activation-4 (VLA-4) antigen. VLA-4 and $\alpha_4\beta_7$ integrin are expressed on hematopoietic stem cells, as well as mature lymphoid and myeloid cells. Specifically, both integrins are expressed on naïve lymphocytes, but high levels of $\alpha_4\beta_7$ integrin are associated with gut-homing of T and B cells (121, 122). Both VLA-4 and $\alpha_4\beta_7$ integrin are also expressed on eosinophils, basophils, NK cells, neutrophils and monocytes, although $\alpha_4\beta_7$ integrin expression on monocytes is not constitutive. Neutrophils express lower levels of VLA-4, but sufficient to support migration to inflammatory sites (123). Both VLA-4 and $\alpha_4\beta_7$ integrin can bind to fibronectin, as well as to vascular cell adhesion molecule-1 (VCAM-1), a member of the immunoglobulin-like gene superfamily, which is upregulated on inflamed endothelium, although $\alpha_4\beta_7$ integrin binds with lower affinity (124-126). Conversely, MAdCAM-1, constitutively expressed on HEV of mucosa-associated lymphoid tissues in the gut, is a primary binding partner for $\alpha_4\beta_7$ integrin, while VLA-4 binds with very low affinity (127). Interestingly, VLA-4 expressed by some tumors suppresses metastasis, possibly by supporting tumor cell adhesion within the primary tumor (128).

VI. Tumor-associated hypoxia

The rapid proliferation of cancer cells causes tumors to outgrow their existing blood vessels, reducing blood flow and consequently oxygen supply, a condition called hypoxia. Hypoxia activates the expression of genes that stimulate formation of new blood vessels (angiogenesis), growth of existing blood vessels (vasculogenesis), metabolic

switch to glycolysis, cell survival, and proliferation, thus helping the tissue to adapt to, and counteract, oxygen deficiency.

A. Hypoxia-inducible factor

The major transcription factor responsible for sensing and adaptation to hypoxia is hypoxia-inducible factor-1 (HIF-1), a heterodimer of HIF-1 α and HIF-1 β basic helix-loop-helix-Per-ARNT-Sim (bHLH-PAS) protein subunits, which is regulated by cellular oxygen tension (129). HIF-1 β is constitutively expressed and was originally identified as the aryl hydrocarbon nuclear translocator (ARNT), a binding partner of the aryl hydrocarbon receptor (AHR) (130). HIF-1 α is ubiquitously and constitutively expressed (131), but rapidly degraded ($t_{1/2} \sim 5$ min) in well-oxygenated (normoxic; $\sim 21\%$ O₂) environments via post-translational modifications of an oxygen-dependent degradation domain (ODDD) (Fig. 2) (132, 133). Specifically, hydroxylation of proline residues Pro402 and Pro564 and acetylation of lysine residue Lys532 favor HIF-1 α binding to the von Hippel-Lindau (pVHL) protein component of the ubiquitin E3 ligase complex, which ubiquitinates HIF-1 α , thus marking it for degradation by the 26S proteasome (134-137). By contrast, hypoxic conditions ($\sim 1\%$ O₂) result in stabilization of HIF-1 α (129, 131, 138) and its translocation to the nucleus, where it dimerizes with HIF-1 β via interactions between the HLH motifs and binds to hypoxia response elements (HRE; 5'-RCGTG-3', where R = A or G) of target genes via the basic region of the bHLH domain (139, 140). In addition to HIF-1 stabilization, full activation of HIF-1 is achieved by recruitment of coactivators such as CBP/p300, SRC-1, and TIF2 to the N-terminal and C-terminal transactivation domains (N-TAD and C-TAD, respectively) within the C-terminal region of HIF-1 α (141, 142). The need for coactivators allows for additional layers of HIF-1

regulation. For instance, hydroxylation of the C-TAD asparagine residue Asn803 under normoxia inhibits the binding of CBP/p300 (143, 144), while hypoxia reverses this effect (145), thus further activating the transcription of target genes.

Several HIF-1 α -related proteins have been identified, including HIF-2 α and HIF-3 α , which in humans has at least six splice variants, designated hHIF-3 α 1, hHIF-3 α 2 (also called inhibitory PAS; IPAS), hHIF-3 α 3, hHIF-3 α 4, hHIF-3 α 5, and hHIF-3 α 6 (146). HIF-2 α and some HIF-3 α variants also bind HIF-1 β and HRE, but can induce the expression of genes distinct from the HIF-1 target genes (147-151), while IPAS binds the N-terminal region of HIF-1 α and prevents DNA binding, thus acting as a dominant negative regulator of HIF-1 function (152). In addition, some HIF-3 α variants inhibit HIF-1 and HIF-2 function by competing for HIF-1 β binding (153, 154). HIF-2 α was initially found to be expressed in lung and endothelium (147, 148), but later it was demonstrated that the isoform is detectable in hypoxic conditions in a wide range of tissues and cell types, including myeloid cells (155). HIF-3 α is expressed in a variety of tissues, and IPAS is expressed in Purkinje cells in the cerebellum and corneal epithelium (152), but can also be induced by hypoxia in the heart and lung (156). Similar to HIF-1 α , in normoxic conditions, both HIF-2 α and HIF-3 α protein levels are regulated by proline hydroxylation within the ODDD, and CBP/p300 coactivator binding to HIF-2 α is inhibited by asparagine hydroxylation in the C-TAD (134).

B. Oxygen-dependent regulation of HIF function

A family of three 2-oxoglutarate- and Fe²⁺-dependent dioxygenases serve as oxygen sensors and catalyze the hydroxylation of two proline residues in HIF- α , which marks the transcription factor for ubiquitination (157). These proline residues are

conserved among all HIF- α isoforms and belong to a consensus sequence LXXLAP, with only the second proline of HIF-3 α belonging to the sequence LXXLHP (134). The human dioxygenases of HIF- α are called prolyl hydroxylase domain (PHD) proteins and there are three isoforms: PHD1, PHD2, and PHD3. Of these isoforms, PHD2 has the highest activity *in vitro* and is the limiting enzyme that regulates HIF-1 α *in vivo* (158). All isoforms require 2-oxoglutarate and molecular oxygen as substrates and use Fe²⁺ and ascorbate (vitamin C) as cofactors. During the reaction, one oxygen atom from O₂ is used to hydroxylate the proline residue, while the other reacts with 2-oxoglutarate resulting in production of succinate and CO₂. Dimethyl-oxalyl-glycine (DMOG), a 2-oxoglutarate analog, binds all PHD proteins and inhibits their function in a reversible manner, thus stabilizing HIF-1 α and, in effect, mimicking hypoxia, even when normoxic conditions are present (159). In addition, PHD protein function requires binding of Fe²⁺ to two histidine and one aspartate residues within the active site. Iron chelators or metal ions, including Co²⁺, Ni²⁺, and Mn²⁺, sequester or replace Fe²⁺ at the active site, thus inhibiting PHD protein function and stabilizing HIF-1 α (160, 161); while ascorbate maintains Fe²⁺ levels in its reduced state and is needed for complete activation of PHD proteins (161, 162).

Once hydroxylated, HIF-1 α binds with high specificity to a conserved hydroxyproline-binding pocket in pVHL (163), which together with the transcription elongation factors B and C (also called elongin B and elongin C), cullin 2, and the RING finger protein RBX1, forms the pVHL-elongin C-elongin B-cullin 2-RBX1 (VCB-CR) E3 ubiquitin ligase complex that ubiquitinates and targets HIF-1 α for degradation (164, 165).

Interestingly, a hereditary disease causing pVHL deficiency is associated with cancer development in various tissues, defining *VHL* as a tumor suppressor gene (165). The majority of evidence suggests that the carcinogenic effect of pVHL dysfunction is due to HIF-2 α stabilization, while there are conflicting reports regarding the role of HIF-1 α in tumor development and progression (166) and insufficient research on the contribution of the HIF- α -independent effects of pVHL dysfunction (165). Some of the HIF- α -independent functions of pVHL include assembly and regulation of the extracellular matrix, microtubule stabilization, maintenance of the primary cilium, regulation of apoptosis and cell senescence, and transcriptional regulation via effects on RNA polymerase II or modulation of transcription factors other than HIF (165).

C. Oxygen-independent regulation of HIF function

There is substantial evidence that ROS, such as superoxide radical and hydrogen peroxide, can cause HIF-1 α stabilization in normoxia. For example, exogenous hydrogen peroxide stabilized HIF-1 α and HIF-2 α in Hep3B and HEK293 cells in normoxic conditions (167). Similar results were observed with the addition of glucose oxidase, which generates hydrogen peroxide (167) and this effect was abolished by the addition of catalase, which converts hydrogen peroxide to water and O₂ (168). Furthermore, inhibition of superoxide dismutase (which converts superoxide to O₂ and hydrogen peroxide) or use of the DMNQ redox cyler (which generates superoxide) also increased the HIF-1 α levels in normoxic conditions (169, 170). These effects may be due to superoxide radical-mediated oxidation of the Fe²⁺ co-factor causing inhibition of PHD protein function, and thus, inability of pVHL to bind to HIF-1 α and mark it for degradation (171).

In addition to superoxide, NO produced by iNOS activation also stabilizes HIF-1 α in normoxia (172). This NO-mediated HIF-1 α stabilization may be due to direct nitrosation of thiol groups within HIF-1 α , an effect that is reversible in the presence of antioxidants such as ascorbate (173, 174). In addition, normoxic NO-mediated HIF-1 α stabilization may be due to PHD protein inhibition (175).

NO and superoxide are both generated as a result of altered oxygenation states and can interact with each other to produce ROS and RNS that nitrate, nitrosate and oxidize proteins. In regard to HIF-1 α regulation in the presence of NO and superoxide, there are conflicting observations: generally, co-incubation with low concentrations of NO and superoxide inhibit HIF-1 α , while high concentration of these reagents synergistically stabilize HIF-1 α . To consolidate these observations, it has been suggested that superoxide serves as a co-signal for NO-mediated HIF-1 α stabilization, but this effect is countered by the decrease in NO availability as a result of interaction with superoxide. Thus, more NO is needed in the presence of superoxide to achieve HIF-1 α stabilization (171, 176). In addition to post-translational modification of HIF-1 α and PHD proteins, NO and superoxide can upregulate HIF-1 α transcription and translation via activation of ERK and PI3K in normoxia (177, 178). Furthermore, ROS upregulate inflammatory mediators such as TNF- α and IL-1 β , which in turn induce transcription and translation of HIF-1 α under normoxia (179, 180).

VII. Study rationale

The major effector cells in the anti-tumor immune response are the CTL. T cell priming by antigens from solid tumors occurs in TDLN, as TAA and antigen-presenting cells are transported from the tumor and enter these secondary lymphoid structures via

the lymph. Thus, for an effective anti-tumor T cell activation to occur, T cells must be able to enter the TDLN. The importance of leukocyte migration to lymph nodes in mounting an effective immune response extends to most pathologies and constant homeostatic lymphocyte recirculation between bloodstream and lymph nodes is a vital part of immune surveillance.

However, in many cancer patients there is stronger tumor-induced immunosuppression rather than T cell activation, which is due to a large extent to the expansion and accumulation of MDSC. In fact, the accumulation of MDSC limits the success of immunotherapy, and correlates with poor prognosis. MDSC accumulate primarily in the spleen, liver and blood and to a lesser extent in the tumor and TDLN. Despite the less abundant presence of MDSC in tumors and TDLN, it has been shown that MDSC-mediated TAA-specific T cell suppression occurs primarily at these two sites (4, 5). For instance, tumor-infiltrating MDSC express elevated mRNA and protein levels of iNOS and arginase-1 compared to low or undetectable expression of these enzymes in splenic MDSC (4, 24, 181, 182). This suggests that MDSC upregulate arginase-1 and iNOS production after entering the tumor microenvironment. In addition, MDSC induce T cell tolerance in the TDLN (1, 2), suppressing not only the priming of naïve TAA-specific T cells in the TDLN, but also the secondary response of primed anti-tumor T cells (5). Importantly, CTL responses are not systemically suppressed in tumor-bearing mice (3), which further supports the notion that T cell suppression may primarily occur *in situ* at the site of tumor growth (3, 183) and within the TDLN (5). Thus MDSC migration to the TDLN and tumor may be a limiting factor in MDSC-mediated suppression of the anti-tumor T cell response. Because these are considered the sites of MDSC-mediated

immunosuppression *in vivo*, interfering with the ability of MDSC to enter these tissues may provide an approach to augment cancer therapy.

A significant number of studies have been published focused on elucidating the mechanisms of MDSC-mediated immunosuppression, as well as on developing strategies for MDSC depletion and inhibition of their function. By contrast, there are far fewer studies of MDSC migration, most of which focus on the involvement of chemokines in MDSC recruitment. However, the involvement of adhesion molecules in MDSC migration remains largely unknown. In general, the initial stages of the leukocyte migration cascade are largely dependent on L-selectin, but the contribution of this molecule to MDSC migration is unknown. We hypothesized that MDSC migration to tumor and TDLN depends on L-selectin.

L-selectin^{-/-} mice have been generated (92) to study various aspects of L-selectin biology. Whether L-selectin is involved in MDSC migration can be tested with adoptive transfers of cell tracker-labeled wild type or L-selectin^{-/-} MDSC into the circulation of tumor-bearing mice, followed by enumeration of the labeled MDSC in the tumor and TDLN shortly thereafter. The 4T1 transplantable murine breast cancer model was selected for the *in vivo* study of MDSC migration. The 4T1 cell line was derived from a spontaneous mammary tumor in a female BALB/cfC3H mouse (184, 185). BALB/cfC3H is a BALB/c subline infected with mouse mammary tumor virus (MMTV), with virion transmittance to offspring via the mother's milk. In mice, this retrovirus has been recognized as an etiological agent for breast cancer and BALB/cfC3H mice exhibit 87% tumor incidence at 16 months of age, compared to less than 1% in BALB/c mice (186). Although the involvement of MMTV or related viruses in the development of human

breast cancer remains an issue of much controversy, the murine 4T1 cell line is widely used to model human breast cancer, because its metastatic pattern is very similar to that of stage IV human breast cancer (187).

In the preliminary part of the study, we aimed to compare the growth rates of 4T1 tumors and the kinetics of 4T1 tumor-induced MDSC accumulation after tumor induction in wild type *vs.* L-selectin^{-/-} BALB/c mice. The results from these preliminary experiments allowed for the design of further functional studies in which the wild type and L-selectin^{-/-} genotypes would be equivalent sources of 4T1 tumor-induced MDSC for adoptive transfer experiments. It was of specific interest to determine the involvement of L-selectin in MDSC migration to the tumor and TDLN. MDSC are a heterogeneous population, but morphologically, functionally, and phenotypically, they can be divided into two major subsets, monocytic MDSC (M-MDSC) and polymorphonuclear MDSC (PMN-MDSC). These subsets have distinct contributions to immunosuppression and tumor growth and it was important to address them as separate populations in the migration studies.

MDSC in the tumor microenvironment upregulate their expression of arginase-1 and iNOS, possibly due to HIF-1 α signaling (181). Therefore, it was of interest to learn more about the localization of MDSC relative to hypoxic regions within the tumor microenvironment. After observing that MDSC are not uniformly distributed throughout the tumor, but aggregate next to hypoxic regions, we followed up by quantifying the extent of this co-localization, as well as by addressing aspects of the dynamics of MDSC aggregation.

FIGURE LEGENDS

Figure 1. Adhesion cascade

The adhesion cascade is a process that can occur in post-capillary venules, via which circulating leukocytes exit the bloodstream and enter peripheral tissues. Specialized post-capillary venules, called high endothelial venules (HEV) in lymph nodes and post-capillary venules near sites of inflammation express adhesion molecules and display chemokines, which are recognized by adhesion molecules and chemokine receptors on the leukocyte, respectively. The interactions between these molecules support leukocyte migration. The first stage of the adhesion cascade (1), involves capture and rolling events supported by interactions between leukocyte-expressed L-selectin and its ligands expressed on the endothelium. In addition, interactions with endothelial P- and E-selectins with leukocyte-expressed ligands (not shown) also contribute. The rolling process allows the leukocyte to slow down and, via chemokine receptors during the activation stage (2), to sense chemokines displayed on the endothelial surface. The chemokine signals induce conformational changes in leukocyte-expressed integrins, thereby activating them and increasing their binding activity. The activated integrins, via interactions with endothelial immunoglobulin-like superfamily molecules, mediate leukocyte arrest (3) and diapedesis (4).

Figure 2. Oxygen-dependent regulation of hypoxia inducible factor-1 alpha expression

Hypoxia inducible factor-1 alpha (HIF-1 α) is ubiquitously and constitutively expressed. In normoxic cells, HIF-1 α is hydroxylated (OH) by dioxygenases, called prolyl hydroxylase domain (PHD) enzymes, which consist of three isoforms: PHD1,

PHD2, and PHD3. All isoforms require 2-oxoglutarate and molecular O₂ as substrates and use Fe²⁺ and ascorbate as cofactors. Hydroxylation of HIF-1 α is required for binding to von Hippel-Lindau (pVHL) protein component of the ubiquitin E3 ligase complex, which ubiquitinates (Ub) HIF-1 α , thus marking it for proteasomal degradation. Acetylation (Ac) of HIF-1 α also contributes to the binding affinity. PHD proteins do not function in hypoxic conditions due to insufficiency of O₂ as their substrate and HIF-1 α degradation does not occur. HIF-1 α is translocated to the nucleus where it dimerizes with HIF-1 β and the dimer binds to hypoxia response elements to induce the expression of target genes. Maximal activity of the HIF-1 α / HIF-1 β dimer is achieved by recruitment of coactivators such as CBP/p300. DMOG, a 2-oxoglutarate analog, binds all PHD protein isoforms and inhibits their function in a reversible manner, thus stabilizing HIF-1 α and, in effect, mimicking hypoxia, even when there is sufficient O₂.

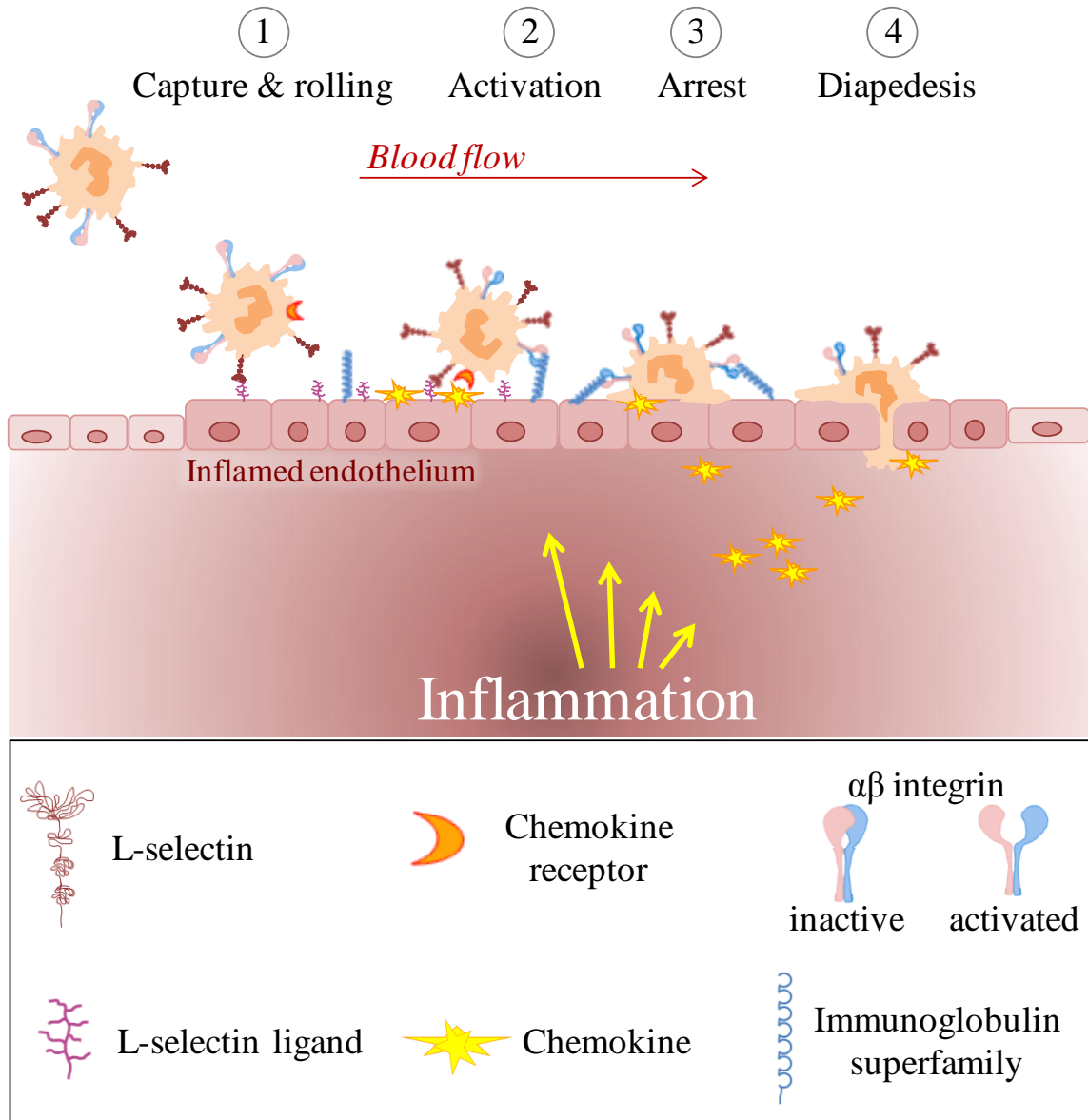


Figure 1

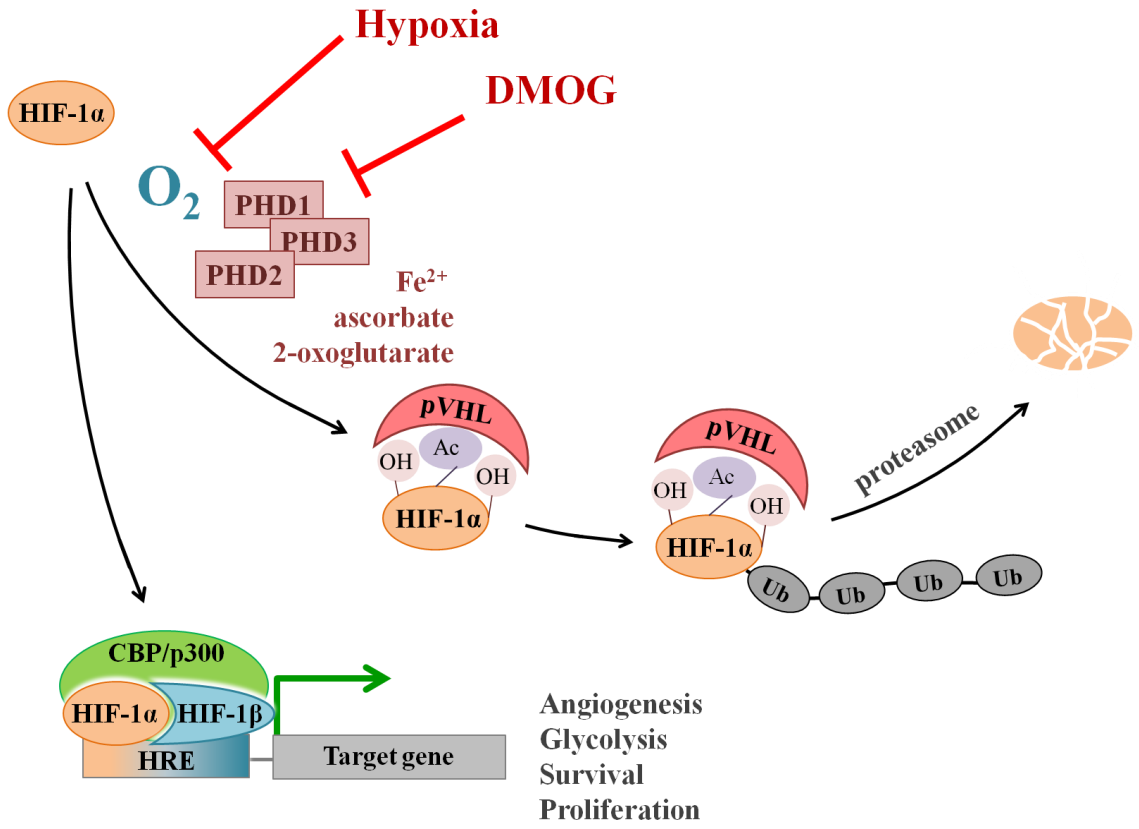


Figure 2

CHAPTER 2

ROLE OF L-SELECTIN IN TUMOR PROGRESSION AND ACCUMULATION OF MYELOID-DERIVED SUPPRESSOR CELLS

ABSTRACT

Myeloid-derived suppressor cells (MDSC) consist of two major subsets, monocytic MDSC (M-MDSC) and polymorphonuclear MDSC (PMN-MDSC), both of which expand in cancer and suppress the activation of naïve T cells in the tumor-draining lymph node (TDLN) and the function of effector cells in the tumor microenvironment. Thus, the ability of MDSC to enter TDLN and the tumor is likely to be critical for suppression of the anti-tumor immune response and elucidating the mechanisms of MDSC migration to these sites may create a basis for novel immunotherapeutic approaches for the treatment of cancer. L-selectin mediates the homing of circulating naïve lymphocytes to lymph nodes and the migration of conventional myeloid cells, such as neutrophils and monocytes, to sites of inflammation, but its contribution to MDSC migration is unknown. In this part of the study we sought to characterize and validate a model system for further investigation of L-selectin function in MDSC migration to the TDLN and tumor. Using the 4T1 transplantable murine breast cancer model, we observed similar tumor growth rates and kinetics of tumor-induced MDSC accumulation in the blood of wild type *vs.* L-selectin^{-/-} mice. In the blood, PMN-MDSC accumulated in greater numbers than did M-MDSC, with a M-MDSC/PMN-MDSC ratio of 0.06 in the late stages of tumor progression. Quantification of MDSC accumulation in peripheral tissues revealed a 26-fold higher M-MDSC/PMN-MDSC ratio in the TDLN of wild type mice relative to blood, suggesting preferential accumulation of M-MDSC. In L-selectin^{-/-} mice, the increase of the M-MDSC/PMN-MDSC ratio was less dramatic, suggesting a role of L-selectin in the preferential accumulation of M-MDSC in the TDLN. Importantly, MDSC accumulated in large numbers in the spleen of both wild type and L-

selectin^{-/-} mice and splenic wild type MDSC expressed L-selectin at levels similar to those on MDSC in the blood. Therefore, the spleen is a convenient source of MDSC for further studies of L-selectin function in MDSC migration. Thus, we herein described relevant parameters of 4T1 tumor progression in L-selectin^{-/-} mice and validated their use for the study of L-selectin function in MDSC. Additional findings include: 1) presence of small numbers of PMN-MDSC in the thymus, which correlated with a decrease in thymic cellularity and a tendency for decreased numbers of CD4⁺CD8⁺ double-positive thymocytes; 2) preferential aggregation of tumor-infiltrating MDSC in the immediate vicinity of hypoxic regions; and 3) expression of the high-affinity folate receptor beta (FR β) on both MDSC subsets, which may provide a potential strategy for the targeted elimination of MDSC. Respectively, these additional findings suggest: 1) an inhibitory role of MDSC in thymic T cell maturation during cancer; 2) a role of hypoxia in MDSC localization in the tumor microenvironment; and 3) a potential use of FR β for the targeted elimination of MDSC in immunotherapy.

INTRODUCTION

The major effector cells in the anti-tumor immune response are the CD8⁺ cytotoxic T lymphocytes (CTL) (7, 8, 188, 189). The CTL response depends on the ability of naïve CD8⁺ T lymphocytes, via their unique T cell receptor (TCR) complexes, to recognize tumor-associated antigens (TAA). In the context of additional stimulatory signals provided by antigen-presenting cells and other cells of the immune system, TAA recognition leads to intracellular signaling causing activation (also referred to as T cell priming) and clonal expansion of the primed CD8⁺ T cells. The majority of the resulting CD8⁺ T cells further differentiate into highly cytotoxic effector cells capable of lysing target tumor cells upon contact, while a minority of CD8⁺ memory T cells acquire longevity and the ability to quickly mount a response upon a second encounter of the cognate tumor antigen. Because the CTL cytolytic function is contact-dependent, activated CTL must infiltrate the tumor and studies with cancer patients show a correlation between tumor infiltration by CD8⁺ T cells and a positive prognosis (190-194). However, the prior stage of the immune response, T cell priming by antigens from solid tumors, occurs in peripheral lymph nodes (PLN), that are located in the vicinity of the tumor (tumor-draining lymph nodes, TDLN), as antigens are transported from the tumor and enter these secondary lymphoid structures via the lymph. Thus, efficient homing of naïve T cells to TDLN is required for an effective anti-tumor T cell response. Lymphocyte migration to lymph nodes is crucial for the generation of effective immune responses in a variety of pathologies and a constant homeostatic lymphocyte recirculation between bloodstream and lymph nodes is a vital part of immune surveillance.

The ability of circulating lymphocytes to enter lymph nodes is highly dependent on their expression of L-selectin (also known as CD62L), an adhesion molecule that mediates the initial interactions between the lymphocyte and the endothelium during migration to peripheral tissues (195, 196). These initial interactions are followed by a cascade of downstream interactions, which potentiate firm adhesion between the lymphocyte and the endothelium, ultimately resulting in lymphocyte extravasation into the lymph node. Thus, L-selectin-deficient (L-selectin^{-/-}) mice show a dramatic reduction in lymphocyte migration to PLN (90, 92), decreased PLN cellularity (92) and a blunted inflammatory response (64, 197, 198). L-selectin is expressed by most leukocytes (195, 199) and interestingly, in addition to its role in leukocyte migration, has a pro-metastatic role in cancer progression (200, 201).

Despite the ability of the immune system to recognize and kill cancer cells, tumors constantly adapt and outgrow the immune control. This adaptability is due to the high heterogeneity and mutability of tumor cells. In addition, tumors interact with the immune system and modulate some of its components. For instance, tumor progression is associated with suppression of the immune response in the TDLN (202-204). In addition, tumor-derived factors cause hematopoietic abnormalities, resulting in generation and release from the bone marrow of underdifferentiated myeloid cells with immunosuppressive function. Though historically known as natural suppressor cells, the more detailed characterization of these cells in recent years has led to the acceptance and wide use of the term myeloid-derived suppressor cells (MDSC) (205).

MDSC are generated in the bone marrow and accumulate in the spleen in response to various pathologic conditions, including cancer, infection, inflammation and

traumatic stress, among others (24). MDSC accumulation correlates with chronic inflammation in the context of the pathologic conditions, and it is likely that their generation constitutes an internal regulatory mechanism used to keep immune responses in check and minimize immune-mediated harm to the host. The MDSC population is heterogeneous, but the current view divides it into two major subsets: polymorphonuclear and monocytic MDSC, abbreviated PMN-MDSC and M-MDSC, respectively. Both subsets express the common myeloid marker CD11b. In addition, murine PMN-MDSC show a high expression of Ly-6G and low levels of Ly-6C. On the contrary, murine M-MDSC express high levels of Ly-6C and stain negative for Ly-6G. Thus PMN-MDSC are phenotypically identified as $CD11b^+Ly6G^+Ly-6C^{low/-}$, while M-MDSC are identified as $CD11b^+Ly-6G^-Ly-6C^{high}$ (24, 206). Of these subsets, PMN-MDSC are the more predominant population, but M-MDSC have higher immunosuppressive activity on a per-cell basis (207). The suppressive effects of MDSC result from upregulation of the enzymes inducible nitric oxide synthase (iNOS) and arginase-1. Both subsets suppress antigen-stimulated T cell proliferation *in vitro*, albeit via different mechanisms. When pre-incubated with T cells, M-MDSC are also able to suppress T cell proliferation induced by antibody stimulation of the signaling component of the TCR complex (207). Authors refer to these effects on T cell proliferation as antigen-specific and antigen-nonspecific suppression, respectively. This terminology only refers to the design of the *in vitro* assays used to measure MDSC-mediated suppression and is irrelevant in physiologic conditions, where T cell activation can only be induced by appropriately displayed antigen. Thus, the term “antigen-nonspecific” T cell suppression does not mean that all T cells *in vivo* are suppressed regardless of their specificity or location. Indeed, T

cell function in various tumor models is not systemically suppressed and there is no increase in the incidence of opportunistic infections in cancer patients, which would be indicative of diminished T cell function (3). This may indicate that although MDSC accumulate systemically, their function in suppressing the anti-tumor T cell response may be limited to the sites of exposure to TAA.

It is noteworthy that most studies of MDSC function thus far have used primarily MDSC isolated from the spleen and added to *ex vivo* formats of T cell function assays. Most often in these assays T cells are activated to proliferate by co-incubation with a cognate antigen, by antibody-induced TCR signaling, or by a general inducer of proliferation, such as concanavalin A. Of further note, the suppressive functions of MDSC are largely induced by interferon- γ (IFN- γ) signaling and a major source of this pro-inflammatory cytokine are activated T cells. Thus, in the context of *in vitro* T cell/MDSC co-culture assays, T cell activation may induce suppressive activities of MDSC that have not been in place *in vivo* at the time of MDSC isolation. This has led Haverkamp and colleagues to address the possibility that the *in vivo* suppressive effects of MDSC are only occurring at the sites of ongoing inflammation and T cell activation, rather than systemically (4). This study demonstrated that MDSC isolated from the inflammatory site in a model of acute prostate inflammation were more suppressive than MDSC from the spleen of the same mice in 48-h and 72-h assays of antigen-induced T cell proliferation. When IFN- γ signaling was blocked with an anti-IFN- γ antibody in the context of this *in vitro* assay, MDSC from the inflammatory site retained their suppressive potential, while MDSC from the spleen exhibited lower suppressive activity. In a short-term assay with minimized exposure to IFN- γ , MDSC from the inflamed

prostate, but not MDSC from the spleen, exhibited the ability to suppress the proliferation of CD8⁺ T cells, pre-activated with cognate antigen. When prostate tumor-bearing mice were used, an example of chronic inflammation, the MDSC isolated from the tumor, but not those from the spleen, exhibited suppressive function in this short-term assay format. Importantly, MDSC depletion *in vivo* resulted in increased abundance and activation potential of T cells in the inflammatory site, but had no effect on the abundance and function of T cells in the spleen. The results from the functional characterization of MDSC from the inflammatory site and the spleen are in agreement with the observation that MDSC from inflamed prostates and prostate tumors express elevated mRNA and protein levels of iNOS and arginase-1 (4), a finding that extends to other types of cancer (181). The authors concluded that MDSC exhibit immunosuppressive activity only at the inflammatory site and further suggest that MDSC function at that site to regulate T cells that are already activated, rather than to suppress T cell priming (4). It appears likely that in the context of cancer, these considerations would be valid during the earlier stages of solid tumor growth, before the establishment of distant metastases and the systemic spread of tumor cells and TAA.

Although the above study did not address a possible role of MDSC in the suppression of anti-tumor T cell activation in the TDLN, other *in vivo* studies demonstrate MDSC-mediated T cell tolerization at that site (1, 2). It was further demonstrated that MDSC suppress not only the priming of naïve TAA-specific CD4⁺ and CD8⁺ T cells in the TDLN, but also the secondary response of primed anti-tumor T cells (5). Thus, it appears that MDSC in the tumor microenvironment and in the TDLN suppress the T cell response against the tumor. The mechanisms of MDSC-mediated T

cell suppression have been well studied but not much is known about the mechanisms of MDSC migration to tumors and TDLN. Because these are considered the sites of MDSC-mediated immunosuppression *in vivo*, interfering with the ability of MDSC to enter these tissues may provide an approach to augment cancer therapy. In general, the initial stages of the leukocyte migration cascade are largely dependent on L-selectin, but the contribution of this molecule to MDSC migration in particular, is unknown.

L-selectin^{-/-} mice have been generated (92) to study various aspects of L-selectin biology. Whether L-selectin is involved in MDSC migration can be tested with adoptive transfers of cell tracker-labeled wild type or L-selectin^{-/-} MDSC into the circulation of tumor-bearing mice, followed by enumeration of the labeled MDSC in the tumor and TDLN shortly thereafter. In this part of the study, we sought to compare tumor progression and MDSC accumulation in wild type and L-selectin^{-/-} mice and to validate a model system, in which tumor-bearing wild type and L-selectin^{-/-} mice would be equivalent MDSC sources for adoptive transfer experiments, except for the lack of L-selectin on MDSC from L-selectin^{-/-} mice.

The 4T1 transplantable murine breast cancer model was selected for the *in vivo* study of MDSC migration. The 4T1 cell line was derived from a spontaneous mammary tumor in a female BALB/cfC3H mouse (184, 185). BALB/cfC3H is a BALB/c subline infected with mouse mammary tumor virus (MMTV), with virion transmittance to offspring via the mother's milk. In mice, this retrovirus has been recognized as an etiological agent for breast cancer. The exogenously introduced viral particles in concert with endogenously carried viral DNA integrated in the host genome, cause breast cancer in these mice via a complex, but well-characterized process resulting in activation of

proto-oncogenes in the mammary tissue (208). As a result, BALB/cfC3H mice exhibit 87% tumor incidence at 16 months of age, compared to less than 1% in BALB/c mice (186). Although the involvement of MMTV or related viruses in the development of human breast cancer remains an issue of much controversy, the murine 4T1 breast cancer is widely used to model human breast cancer (187). The major advantage to this model in modeling human disease is the spontaneous spread of 4T1 metastases to the draining lymph nodes, lung, liver, bone, and brain, a metastatic pattern very similar to that of stage IV human breast cancer.

In this part of the study, we demonstrated that 4T1 tumors exhibit similar growth rates and similar kinetics of tumor-induced MDSC accumulation when transplanted into wild type *vs.* L-selectin^{-/-} mice. Thus, these genotypes are equivalent sources of 4T1 tumor-induced MDSC for further functional studies. We also observed a decrease in MDSC numbers in the TDLN of L-selectin^{-/-} mice relative to wild type, which could be indicative of a role of L-selectin in MDSC migration to the TDLN. In addition, we visualized the localization of MDSC relative to B cell and T cell regions within the spleen and the TDLN, as well as relative to areas of low oxygenation (hypoxia) in the tumor. While we did not observe a particularly strong preference for MDSC co-localization with either T cell or B cell regions in the spleen and TDLN, we found that in the tumor, MDSC were primarily localized in aggregates next to hypoxic regions. Unique to the tumor microenvironment, this relationship between hypoxia and MDSC may have functional consequences, which require further investigation.

MATERIALS AND METHODS

Cell lines and reagents

The 4T1 murine mammary carcinoma cell line (ATCC CRL 2539) was purchased from ATCC (Manassas, VA). The line was originally derived from a spontaneous mammary tumor from a BALB/cfC3H mouse (185, 209). When transplanted ectopically into syngeneic BALB/c mice, the 4T1 cell line generates a solid, highly metastatic tumor, which spreads to nearby lymph nodes, lungs, bones, brain, and liver, thus resembling stage IV metastatic breast cancer in humans.

Antibodies used in the flow cytometry and fluorescence microscopy experiments included: fluorescein isothiocyanate (FITC)-conjugated, allophycocyanin (APC)-conjugated, or biotinylated anti-CD11b (Clone M1/70, BD Biosciences, San Jose, CA); phycoerythrin (PE)-conjugated or FITC-conjugated anti-Ly-6G (Clone 1A8, BD Biosciences); peridinin-chlorophyll protein-cyanine 5.5 (PerCP-Cy5.5)-conjugated or PE/Cy7-conjugated anti-Ly-6C (Clone HK1.4, BioLegend, San Diego, CA; Clone AL-21, BD Biosciences); PE-conjugated anti-CD4 (Clone RM4-5, BD Biosciences); APC-conjugated anti-CD8 (Clone 53-6.7, BD Biosciences); biotinylated anti-Thy1.2 (Clone 53-2.1, BD Biosciences) and anti-L-selectin (Clone LAM1-116, (210)); rat anti-mouse IgD antibody (Clone 11-26, SouthernBiotech, Birmingham, AL); polyclonal rabbit anti-FR β antibody (Cat. #PA5-24963, ThermoFisher Scientific, Waltham, MA). Biotinylated antibodies were detected with Alexa Fluor[®] 488- or AlexaFluor[®] 350-conjugated avidin (Life Technologies, Grand Island, NY), or APC- or tetramethylrhodamine (TRITC)-conjugated neutralite avidin (SouthernBiotech). The primary rat anti-mouse IgD antibody was detected with a secondary TRITC-conjugated goat anti-rat IgG antibody

(SouthernBiotech). The primary rabbit anti-FR β antibody was detected with a secondary AlexaFluor[®] 647-conjugated goat anti-rabbit IgG antibody (Jackson ImmunoResearch, West Grove, PA). Hypoxiprobe[™] RedAPC Kit, containing pimonidazole·HCl and APC-conjugated anti-pimonidazole antibody (Clone 4.3.11.3) was purchased from Hypoxiprobe (Burlington, MA) and used to detect hypoxic regions in the tumor microenvironment with fluorescence microscopy.

Mitomycin C (Cayman Chemical, Ann Arbor, MI) was used to inhibit proliferation of stimulator cells and Vibrant[®] carboxy-fluorescein diacetate succinimidyl ester (CFDA-SE) cell tracer kit (Life Technologies) was used to detect proliferation of responder T cells in a mixed lymphocyte reaction assay. Normal goat serum (Sigma, St. Louis, MO) and HyClone[®] normal horse serum (ThermoFisher Scientific) were used in buffers to reduce non-specific binding of antibodies. 5-Bromo-2-deoxyuridine (BrdU), a thymidine analog used to measure cell proliferation, was purchased from Sigma. Deoxyribonuclease I (DNase I) from bovine pancreas and collagenase type VIII from *Clostridium histolyticum* used for tissue digestion, were both purchased from Sigma. Bovine serum albumin fraction V (also used in the tissue digestion buffer), was purchased from ThermoFisher Scientific.

Animals

BALB/c (wild type) and C57BL/6 mice were originally purchased from the Jackson Laboratories (Bar Harbor, ME) and further housed and bred in a specific pathogen-free barrier facility at the University of Wisconsin-Milwaukee and screened regularly for pathogens. L-selectin^{-/-} mice were generated as described (92) and back-crossed against the BALB/c genetic background for twelve generations. All procedures

were approved by the Animal Care and Use Committee of the University of Wisconsin-Milwaukee.

Tumor induction

The 4T1 cells were cultured at 37°C and 5% CO₂ in RPMI-1640 medium (Life Technologies), supplemented with 10% fetal bovine serum (Atlanta Biological, Forest Hills, NY), 100 U/ml penicillin, 100 µg/ml streptomycin, 2 mM L-glutamine and 55 µM 2-mercaptoethanol (all from Life Technologies). At approximately 70% confluency, the cells were lifted with Cellstripper purchased from Mediatech (Manassas, VA), and 1x10⁴ 4T1 cells in 50 µl supplement-free RPMI-1640 medium were injected subcutaneously into the mammary fat pad of 8-12 week old wild type or L-selectin^{-/-} BALB/c female mice. In some of the mice, 50 µl supplement-free RPMI-1640 medium was injected into the contralateral mammary fat pad as an internal negative control. Tumor growth was monitored by caliper measurements of the major (L, length; mm) and minor (W, width; mm) axes and tumor volume (V, volume; mm³) was calculated by the formula: $V = (L \times W^2) / 2$.

Kinetics of MDSC accumulation in blood of 4T1-tumor bearing mice

At different time points (0, 1, 2, 3, 4 and 5 weeks) after tumor induction, 50-100 µl of blood per mouse were collected from the retro-orbital sinus using a heparinized Pasteur pipette. Leukocyte counts were determined using a hemacytometer after a 10- to 1000-fold sample dilution in 0.2% glacial acetic acid. Fifty microliters of a 2X optimal dilution of anti-CD11b, anti- Ly-6G, and anti-Ly-6C antibodies in PBS containing 2% normal horse serum, were added to 50 µl of blood and incubated for 30 min on ice with occasional light vortexing. The samples were then washed in PBS, and the red blood cells

were lysed in BD FACS Lysis buffer (BD Biosciences) for 10 min at room temperature. After two subsequent washes in PBS, the labeled leukocytes were fixed in 1.5% formaldehyde in PBS. The frequencies of M-MDSC and PMN-MDSC were determined using a FACSCalibur flow cytometer (BD Biosciences) and BD CellQuest™ Pro software. Counts of each MDSC subset per 1 ml of blood were calculated from the obtained frequencies.

L-selectin labeling

To confirm L-selectin expression on MDSC, single-cell suspensions from spleens of advanced stage (4-5 weeks) 4T1 tumor-bearing wild type BALB/c mice were immunolabeled as above against the MDSC markers CD11b, Ly-6G, and Ly-6C. A biotinylated anti-L-selectin antibody was also added to the labeling antibody mix, but omitted from negative control samples. The samples were then washed with PBS and incubated for an additional 30 min on ice with APC-conjugated neutralite avidin. The samples were then washed again in PBS and fixed in 1.5% formaldehyde in PBS. L-selectin expression was also tested on MDSC in the blood. Whole blood was labeled as above and red blood cells were lysed with BD FACS lysis buffer and fixed. Alternatively, the whole blood was washed with a 20-fold excess of PBS to remove the plasma components, including soluble L-selectin, before labeling.

Tissue preparation for flow cytometry

To assess the tissue distribution of MDSC during 4T1 tumor progression, control mice without tumors and 4T1 tumor-bearing mice at the 4-week stage were euthanized. The following tissues were harvested: bone marrow, thymus, spleen, liver, lung, tumor, tumor-draining lymph node (TDLN, the inguinal lymph node next to the primary tumor),

and non-draining lymph node (NDLN, the contralateral inguinal lymph node next to the site of the vehicle control RPMI-1640 medium injection). Single-cell suspensions were prepared as follows: 1) bone marrow was flushed from both femurs with a 27G needle and collected in PBS; after centrifugation, red blood cells were lysed in ACK buffer (0.15 M NH₄Cl, 10 mM KHCO₃, 0.1 mM Na₂EDTA, pH 7.4), filtered through a 70 µm mesh-filter and washed three times in PBS; 2) spleen, thymus, and lymph nodes were teased apart in a dish filled with PBS as previously described (90), the suspensions were filtered through 70 µm mesh and centrifuged; red blood cells from the spleen were lysed in ACK buffer, filtered again and washed three times in PBS; 3) liver, lung, and tumor were minced with scissors into ~1 mm pieces and incubated for 30-60 min at 37°C and 5% CO₂ in digestion buffer, containing 562 U/ml collagenase, 20.6 U/ml deoxyribonuclease I, and 5 mg/ml bovine serum albumin in PBS. The red blood cells were then lysed in ACK buffer, the suspensions were filtered through 70 µm mesh and washed three times in PBS.

Cell counts and viability were determined using a hemacytometer following appropriate dilution in trypan blue exclusion dye. The concentrations were adjusted to 20x10⁶ cells/ml and 1x10⁶ cells of each tissue were immunolabeled for MDSC markers and analyzed by flow cytometry as described above. Thymus suspensions were additionally labeled with anti-CD4 and anti-CD8 antibodies to determine the frequencies of double-negative (CD4⁻CD8⁻), double-positive (CD4⁺CD8⁺), and single-positive CD4⁺ and CD8⁺ thymocytes.

Analysis of MDSC suppressive activity with a mixed lymphocyte reaction assay

The suppressive activity of MDSC was quantified in the context of a one-way mixed lymphocyte reaction. In this assay, stimulator spleen cells from a C57BL/6 mouse (haplotype b) were used to activate responder T cells from the spleen of a BALB/c mouse (haplotype d). In this combination the responder T cells recognize and react to foreign histocompatibility antigens expressed on the allogeneic stimulator cells, and proliferate, while the proliferation of any T cells within the stimulator cell population is inhibited by pre-treatment with mitomycin C (211). The number of divided responder T cells served as a quantitative measure of maximum responder T cell activation. Division of T cells was quantified via the carboxy-fluorescein succinimidyl ester (CFSE) dilution method. In this approach, the responder cells are incubated with the cell permeable CFDA-SE fluorogenic substrate. Intracellular esterases remove the acetate groups converting the substrate to a cell impermeable fluorescent CFSE product, which accumulates inside of the cell. CFSE via its succinimidyl group attaches covalently to lysine groups within intracellular proteins and is retained in the cytoplasm of live cells. Upon cell division, the fluorescent product is divided evenly between the two daughter cells, thus halving the original fluorescence intensity. This decrease can be detected with flow cytometry and the number of CFSE^{low} T cells is a direct measure of T cell proliferation. Addition of MDSC sorted from the spleen of a 4T1 tumor-bearing mouse to the stimulator/responder cell co-culture should cause a decrease in the number of CFSE^{low} T cells (divided responder T cells) and this decrease is a measure of the suppressive activity of MDSC.

Spleens were harvested from non-tumor-bearing C57BL/6 (for stimulator cells) and BALB/c (for responder cells) mice. Single-cell suspensions were prepared as

described above and the responder spleen suspension was labeled with antibodies against CD4 and CD8 and analyzed by flow cytometry to determine the frequency of responder T cells. Fifty million C57BL/6 stimulator spleen cells were treated for 30 min at 37°C with 50 µg/ml mitomycin C in 1 ml PBS. The cells were then washed three times in PBS and added to a 96-well plate at 0.1×10^6 cells/100 µl/well in RPMI-1640 medium, supplemented as above. Forty-two million BALB/c responder spleen cells were incubated in 0.25 M CFDA-SE in 14 ml PBS at 37°C for 30 min. The cells were then centrifuged and resuspended in 10 ml RPMI-1640 medium, supplemented as above, and incubated for a further 30 min at 37°C. The cells were then washed and 0.1×10^6 cells/50 µl/well were added to the stimulator cells or added to 100 µl of culture medium as a negative control for proliferation without stimulation. Spleens were also harvested from BALB/c mice bearing 4-week stage 4T1 tumors. The spleen suspension was labeled with MDSC markers as described above and the MDSC population, including both M-MDSC and PMN-MDSC subsets, was sorted using a FACSAria III cell sorter (BD Biosciences), with purity > 95%. The sorted MDSC were seeded into the wells containing stimulator and responder cells at various ratios (1:1, 1:2, 1:4, 1:8, 1:16, 1:32 and 1:64) relative to the responder T cell number pre-determined with flow cytometry. Each combination was seeded in triplicate wells and the cells were co-cultured for 4 days. On the fourth day, the triplicate wells were pooled, labeled with antibodies against CD4 and CD8, and the number of CFSE^{low}CD4⁺ and CFSE^{low}CD8⁺ cells (divided CD4⁺ and CD8⁺ T cells, respectively) was determined by flow cytometry. Two independent experiments gave similar results.

Immunofluorescence labeling of frozen tissue sections

Spleen, tumor and TDLN were harvested from advanced stage 4T1 tumor-bearing wild type BALB/c mice. The tissues were then snap-frozen in tissue freezing medium (Triangle Biomedical Sciences, Inc, Durham, NC) in liquid nitrogen or on dry ice and 5 μ m thick tissue sections were cut on a cryostat and adhered onto poly-L-lysine-coated microscope slides. The sections were fixed in -20°C acetone for 5 min and stored at -20°C until labeling. The sections were thawed for 5 min and rehydrated in PBS for 10 min. The sections were then incubated in 5% normal goat serum in PBS to block non-specific antibody binding. Antibody dilutions were prepared in 2% normal horse serum in PBS. The spleen and TDLN sections were immunolabeled against the MDSC markers CD11b, Ly-6G, and Ly-6C in a combination with the T cell marker Thy1.2 and the B cell marker IgD by incubation with the corresponding antibodies for 30 min at room temperature. The slides were then washed twice for 5 min each in 2% normal horse serum in PBS and further incubated for 30 min at room temperature with AlexaFluor[®] 350-conjugated avidin to detect the biotinylated anti-Thy1.2 antibody and with TRITC-conjugated goat anti-rat IgG antibody to detect the rat anti-mouse IgD antibody. The sections were washed twice in PBS for 5 min and mounted in ProLong[®] Gold antifade mounting medium (Life Technologies). The mounting medium was allowed to cure overnight before imaging on a Nikon Eclipse TE2000-U epifluorescence microscope (Nikon Instruments Inc., Melville, NY) equipped with a Cool Snap ES digital camera (Photometrics, Tuscon, AZ). MetaVUE[™] software (Universal Imaging Corporation, Downington, PA) was used for imaging and analysis.

To visualize hypoxic regions within the tumor microenvironment, the tumor-bearing mice were first injected, 1 h prior to euthanasia, with a single intraperitoneal dose of 60 mg/kg body weight pimonidazole-HCl in PBS. This cell permeable reagent binds to the thiol groups that result from reduction of protein disulfide bonds in hypoxic conditions, and forms stable adducts with intra- and extracellular proteins. Any unbound pimonidazole is cleared within 1 h of injection. The tumors were harvested, frozen, sectioned, fixed, and stored as above. After thawing, rehydrating and blocking as above, the sections were incubated with anti-pimonidazole antibody for 1 h at 37°C in a humidified chamber. This step was followed by a 30-min incubation at room temperature with antibodies against the MDSC markers CD11b, Ly-6G, and Ly-6C to visualize the localization of MDSC relative to hypoxic regions within the primary tumor. All samples were imaged as above.

Folate receptor beta (FR β) labeling

Blood and spleen suspensions from mice with advanced stage 4T1 tumors were tested for FR β expression. One hundred microliters of 2X anti-FR β rabbit polyclonal antibody in 2% normal horse serum in PBS were added to 100 μ l of blood or 100 μ l of spleen suspension adjusted to 5×10^6 cells/100 μ l. Negative controls received 100 μ l of 2% normal horse serum in PBS without antibody and all samples were incubated for 30 min on ice with occasional light vortexing. The samples were then washed with 2% normal horse serum in PBS and incubated for 30 min on ice with AlexaFluor[®] 647-conjugated goat anti-rabbit IgG antibody. The samples were washed again in 2% normal horse serum in PBS and blocked for 15 min on ice with 5% normal rabbit serum and 2% normal horse serum in PBS, followed by another wash in 2% normal horse serum in PBS.

The samples were then incubated for 30 min on ice with antibodies against the MDSC markers CD11b, Ly-6G, and Ly-6C, followed by washing in PBS. The spleen samples were then fixed in 1.5% formaldehyde in PBS and analyzed by flow cytometry. The red blood cells from the blood samples were lysed with BD FACS lysis buffer. The blood samples were then washed twice in PBS, fixed in 1.5% formaldehyde in PBS and analyzed.

Statistical analysis

Except for the MDSC suppression assays, data are presented as mean \pm SEM. Significant differences between sample means were determined using a Student's *t* test with $p < 0.05$ considered significant.

RESULTS

Accelerated 4T1 tumor growth in L-selectin^{-/-} mice

Cytotoxic T cell activation in the tumor-draining lymph nodes is necessary for anti-tumor immunity and control of tumor growth. Being critical for the homing of naïve lymphocytes to PLN, lack of L-selectin may hinder access of naïve CD8⁺ T cells to appropriately presented tumor antigens in the presence of relevant co-stimulatory signals. Thus, L-selectin deficiency may play an inhibitory role in the generation of anti-tumor cytotoxic T cell responses, resulting in accelerated tumor progression. To determine the contribution of L-selectin in the control of 4T1 tumor progression, wild type and L-selectin^{-/-} BALB/c mice were injected subcutaneously into the mammary fat pad with 1×10^4 4T1 cells and tumor growth was monitored over a period of 5 weeks. The tumor growth curve for both wild type and L-selectin^{-/-} mice was characterized by an initial lag phase of 2-3 weeks, followed by an exponential increase in tumor volume during the period from 3- to 5-weeks (Fig. 3A). Interestingly, L-selectin deficiency resulted in a modest but significant increase in tumor volume (by 14 to 47%) relative to wild type control mice during the 2-5 week time period (Table I). Therefore, in this tumor model loss of L-selectin expression results in a modest acceleration of tumor growth.

The kinetics of systemic MDSC accumulation during 4T1 cancer progression in wild type and L-selectin^{-/-} mice are equivalent and correlate with tumor growth rate

Cancer progression drives the generation of MDSC and MDSC accumulation corresponds to tumor burden. We asked whether the small increase in tumor growth rate in L-selectin^{-/-} mice relative to wild type controls correlated with accelerated systemic MDSC accumulation. Blood was collected from tumor-bearing wild type and L-selectin^{-/-}

mice at the 1-, 2-, 3-, 4-, and 5-week time points or from mice without tumors. The blood samples were immunolabeled against the MDSC markers CD11b, Ly-6G, and Ly-6C, and each MDSC subset was quantified by flow cytometry. Figure 3B shows representative flow cytometry data plots and gating analysis for quantification of CD11b⁺Ly-6G⁺Ly-6C^{low} PMN-MDSC and CD11b⁺Ly-6G⁺Ly-6C^{high} M-MDSC. The accumulation kinetic curves (Fig. 3C) of both MDSC subsets resemble the tumor growth curve with an initial lag phase of 2-3 weeks, followed by an exponential increase in MDSC numbers during the period from 3- to 5-weeks. There was a tendency for accelerated accumulation of both PMN-MDSC and M-MDSC in the L-selectin^{-/-} tumor-bearing mice relative to the corresponding wild type control mice (Table I, Fig. 3C); however, these did not reach statistical significance. Therefore, the kinetics of systemic MDSC accumulation during 4T1 cancer progression in wild type and L-selectin^{-/-} mice were equivalent and correlated with tumor growth rate.

PMN-MDSC and M-MDSC from spleen and blood of late-stage 4T1 tumor-bearing mice express L-selectin

L-selectin is expressed on all classes of leukocytes, including neutrophils and monocytes, the respective conventional counterparts of PMN-MDSC and M-MDSC in physiologic conditions. We asked whether L-selectin is also expressed by pathologically generated PMN-MDSC and M-MDSC during 4T1 tumor progression. In studies with small experimental animals, such as mice, the spleen is the most commonly used source in the cases when large numbers of MDSC are needed. Spleen suspensions from wild type mice with advanced stage 4T1 tumors were immunolabeled against L-selectin and the MDSC markers CD11b, Ly-6G, and Ly-6C, and the expression level of L-selectin by

PMN-MDSC and M-MDSC was analyzed by flow cytometry. Both subsets expressed L-selectin (Fig. 4A). Interestingly, the M-MDSC subset expressed L-selectin at 66% higher levels than the PMN-MDSC subset.

L-selectin is responsible for leukocyte migration from the bloodstream to PLN or sites of inflammation and the expression of L-selectin by blood-borne MDSC has important biologic relevance. Therefore, in addition to spleen, we also analyzed the L-selectin expression levels on MDSC in the blood of wild type mice with advanced tumors. Various inflammatory conditions are characterized by elevated soluble L-selectin (sL-selectin) in the bloodstream as a result of proteolytic cleavage from the surface of activated leukocytes (66). Importantly, the presence of sL-selectin in the test samples may cause false negative results in immunolabeling experiments, due to competitive binding to the anti-L-selectin antibody. Therefore, the test samples included non-washed blood, as well as blood that was washed with an excess volume of PBS to remove soluble plasma proteins. L-selectin labeling on PMN-MDSC and M-MDSC in non-washed samples showed only a small increase in fluorescence intensity compared to the negative control (Fig. 4B). By contrast, the removal of soluble plasma proteins dramatically improved L-selectin labeling of both subsets, with the fluorescence intensity reaching similar levels to those detected in the spleen. Although the splenic PMN-MDSC expressed lower levels of L-selectin compared to PMN-MDSC from the blood, the difference was not statistically significant. Thus, MDSC from spleen and blood of late-stage 4T1 tumor-bearing mice expressed similar levels of L-selectin, validating the spleen of tumor-bearing mice as an appropriate source of MDSC for functional studies of L-selectin.

Decreased numbers of MDSC in TDLN of L-selectin^{-/-} 4T1 tumor-bearing mice

To determine whether L-selectin deficiency affects the tissue distribution of MDSC, advanced stage 4T1 tumor-bearing wild type and L-selectin^{-/-} mice were euthanized and bone marrow, thymus, blood, lung, liver, spleen, tumor, TDLN and contralateral non-draining lymph node (NDLN) were harvested. Single-cell suspensions of these tissues were immunolabeled for the MDSC markers CD11b, Ly-6G, and Ly-6C. The frequencies of PMN-MDSC (CD11b⁺Ly-6G⁺Ly-6C^{low/-}) and M-MDSC (CD11b⁺Ly-6G⁺Ly-6C^{high}) were quantified by flow cytometry. Non-tumor bearing control wild type BALB/c mice were used to quantify the physiologic levels of conventional myeloid cells, which have similar expression of CD11b, Ly-6G, and Ly-6C, including CD11b⁺Ly-6G⁺Ly-6C^{low/-} neutrophils and CD11b⁺Ly-6G⁻Ly-6C^{high} monocytes/macrophages. Overall, the presence of advanced stage 4T1 tumors correlated with increased MDSC frequencies and counts in all tested tissues from either wild type or L-selectin^{-/-} mice, compared to conventional myeloid cells in control healthy mice (Tables II and III, Fig. 5). Specifically, in the bone marrow of either wild type or L-selectin^{-/-} tumor-bearing mice, the frequency of PMN-MDSC showed a modest but significant increase, compared to the frequency of polymorphonuclear myeloid cells in the healthy bone marrow, while the frequency of the monocytic myeloid subset remained the same (Table II, Fig. 5A). However, the total number of both MDSC subsets in bone marrow from tumor-bearing mice were increased by an average of 2.2-fold compared to the levels of polymorphonuclear and monocytic cells in healthy mice (Table III, Fig. 5B), correlating with an overall increase in bone marrow cellularity with tumor progression (Table VI, Fig. 5C). Similar to the results from the kinetics study of MDSC accumulation in blood,

there was an approximately 7.5-fold increase in PMN-MDSC frequency and a rather modest 1.5-fold increase in M-MDSC frequency in the blood of tumor-bearing wild type or L-selectin^{-/-} mice compared to the physiologic levels of polymorphonuclear and monocytic cells, respectively (Fig. 5A). The lung, a known site of 4T1 tumor metastasis, showed an approximately 12-fold increase in PMN-MDSC frequency while relatively little change in frequency of M-MDSC was found in either wild type or L-selectin^{-/-} tumor bearing mice, compared to the corresponding conventional myeloid subsets in the healthy lungs (Fig. 5A). However, the number of both PMN-MDSC and M-MDSC were increased by approximately 37-fold and 6-fold, respectively (Fig. 5B) with a concomitant increase in total lung cellularity (Fig. 5C), likely due to the presence of metastatic burden (visual observations). The liver, another typical 4T1 metastatic site, as well as a major site of hematopoiesis during fetal development, also exhibited increased myeloid cell frequency: ~5.3-fold for PMN-MDSC and 3-fold for M-MDSC of either wild type or L-selectin^{-/-} tumor-bearing mice. In the spleen, an average 7.7-fold increase in PMN-MDSC frequency and an average 3.3-fold increase in M-MDSC frequency was found in wild type and L-selectin^{-/-} mice with advanced stage 4T1 cancer (Fig. 5A). This result corresponded to dramatic 82-fold and 36-fold increases in cell numbers of PMN-MDSC and M-MDSC, respectively (Fig. 5B), that correlated with an ~11-fold increase in splenic cellularity during cancer progression (Fig. 5C). Advanced stage 4T1 tumors from either wild type or L-selectin^{-/-} mice contained similar frequencies of both PMN-MDSC and M-MDSC (Fig. 5A) while the total number of each subset was increased by 2-fold and 3.7-fold, respectively, in the L-selectin^{-/-} mice relative to wild type mice (Fig. 5B). This finding may, at least in part, be due to the increased tumor volume and cellularity in L-

selectin^{-/-} mice at advanced time points after tumor injection (Figs. 3A and 5C). Interestingly, during cancer progression, the cellularity of the TDLN in wild type mice increased by 2.9-fold, while the contralateral NDLN retained a size typical of the inguinal PLN of a healthy control mouse (Fig. 5C). This increase may in part be due to immune activation in the TDLN, resulting in increased recruitment of lymphocytes from the bloodstream and subsequent proliferation, and/or in part due to the establishment and growth of tumor metastases within the TDLN. Importantly, the L-selectin^{-/-} TDLN did not significantly increase in cellularity, even in the late stage of 4T1 cancer, and relative to the corresponding tissue from wild type tumor-bearing mice, remained 9.9-fold smaller (Fig. 5C). In general, differences in numbers of MDSC subsets in the TDLN between wild type and L-selectin^{-/-} tumor-bearing mice correlated with tissue cellularity. Specifically, numbers of PMN-MDSC and M-MDSC were reduced by 3.3-fold and 6.5-fold, respectively, in the TDLN of L-selectin^{-/-} tumor-bearing mice relative to wild type controls (Fig. 5B). Thus, the 4T1 tumor-driven accumulation of MDSC in the blood, spleen, lung, and liver was similar between wild type and L-selectin^{-/-} mice. However, advanced stage 4T1 tumors of L-selectin^{-/-} mice were bigger and accumulated more MDSC compared to similar stage 4T1 tumors of wild type mice. By contrast, TDLN of L-selectin^{-/-} mice were smaller and accumulated fewer MDSC compared to TDLN of wild type mice.

Surprisingly, while the PMN-MDSC were much more abundant than M-MDSC in most tested tissues from tumor-bearing wild type or L-selectin^{-/-} mice, both the frequencies and numbers of PMN-MDSC and M-MDSC were equivalent in the TDLN from these mice (Fig. 5A and 5B). To emphasize this difference, the ratio between the

frequencies of M-MDSC and PMN-MDSC (M-MDSC/PMN-MDSC ratio) for each tested tissue was plotted and compared to the M-MDSC/PMN-MDSC ratio in the circulation (Fig. 6). Relative to blood, there was a small but statistically significant increase in the M-MDSC/PMN-MDSC ratio in bone marrow and spleen of both wild type and L-selectin^{-/-} tumor-bearing mice. The increase was more prominent in lung and liver, though due to greater sample variability, it remained statistically non-significant in the lung of L-selectin^{-/-} mice. Importantly, the increase in M-MDSC/PMN-MDSC ratio was greatest in the TDLN and NDLN of wild type mice. It is of further importance that relative to wild type, this ratio was dramatically decreased, by 6.4-fold, in the NDLN of L-selectin^{-/-} mice. However, in the TDLN, the decrease in M-MDSC/PMN-MDSC ratio as a result of L-selectin deficiency was more modest, 2.4-fold, and only approached significance with a p value of 0.1.

MDSC from the spleen of 4T1 tumor-bearing mice suppress T cell proliferation in a dose-dependent manner

MDSC were thus far identified based on their phenotypic expression of the markers CD11b, Ly-6G, and Ly-6C. To further confirm the suppressive identity of these cells, we tested their ability to suppress antigen-induced T cell proliferation *in vitro*. In a mixed lymphocyte reaction, sorted MDSC from spleens of advanced stage tumor-bearing mice were added at different ratios relative to the number of responder T cells. The proliferation of the responder T cells was quantified with the CFSE dilution method using flow cytometry. With this technique, each cell division causes the fluorescence intensity of the CFSE-labeled cells to drop by 50% and the CD4⁺ and CD8⁺ subsets of responder T cells with decreased CFSE fluorescence can be enumerated. In the absence of antigen

stimulation delivered by allogeneic stimulator cells (negative control), there was negligible CFSE dilution among the responder T cell populations (Fig. 7). In contrast, the addition of stimulator cells (positive control) caused a 66-fold and 14-fold increase in divided CD4⁺ and CD8⁺ T cells, respectively. As expected, the addition of MDSC caused a dose-dependent decrease in responder T cell proliferation. Specifically, the inhibition of proliferation was strongest (by 70 to 93%) when MDSC were half as abundant as the responder T cells (MDSC/T cell responders ratio = 1:2) while at a MDSC/T cell ratio of 1:16, there was virtually no decrease in T cell proliferation. Thus, the combined addition of CD11b⁺Ly-6G⁺Ly-6C^{low} PMN-MDSC and CD11b⁺Ly-6G⁻Ly-6C^{high} M-MDSC suppressed T cell proliferation in response to alloantigens in a dose-dependent manner, functionally confirming the identity of these cells as an immunosuppressive population.

Splenic MDSC localize in the red pulp, while MDSC in the TDLN localize near boundaries between T cell regions and B cell follicles.

Studies of MDSC biology rarely address the location of these cells within tissues of interest. Considering the nature of the immunosuppressive mechanisms of these cells and their dependence on target cell proximity, it was of interest to visualize the localization of MDSC within the lymphoid tissue architecture of the spleen and TDLN, as well as in the tumor microenvironment. Spleen and TDLN sections were labeled with antibodies against CD11b, Ly-6G, and Ly-6C to identify the CD11b⁺Ly-6G⁺Ly-6C^{low} PMN-MDSC and the CD11b⁺Ly-6G⁻Ly-6C^{hi} M-MDSC, and with antibodies against Thy1.2 to identify T cell zones and IgD to identify B cell follicles. Consistent with a previous observation of MDSC localization in the splenic red pulp (205), we observed a profound exclusion of both MDSC subsets from the T cell zones and B cell follicles in

the spleen (Fig. 8). Visually, the M-MDSC/PMN-MDSC ratio in the labeled spleen sections appeared similar to that determined with flow cytometry.

MDSC in the TDLN sections were rare events and the abundance of M-MDSC was similar to that of PMN-MDSC, thus confirming the flow cytometry results. Relative to T cell zones or B cell follicles, there was no clear preference for localization of either PMN-MDSC (Fig. 9) or M-MDSC (Fig. 10). Individual PMN-MDSC were occasionally found within either T cell or B cell zones, but more often a group of several PMN-MDSC together with M-MDSC were found near boundaries between T cell and B cell zones. Of note, in addition to $CD11b^+Ly-6G^-Ly-6C^{hi}$ M-MDSC, there were other $Ly-6C^+$ cells detected in the tumor-draining lymph node, and to a lesser extent in the spleen, which were localized primarily in the T cell regions. These cells did not express the myeloid marker CD11b and were thus not identified as M-MDSC. In addition to myeloid cells, the Ly-6C marker is expressed by subsets of memory lymphocytes, as well as some plasma, NK, and endothelial cells (212-215). Indeed, the majority of the $CD11b^-Ly-6C^+$ cells also expressed Thy1.2, suggesting a memory T lymphocyte identity, and some Ly-6C labeling, showed blood vessel morphology. Taken together these results show no strong preference for co-localization of MDSC with T cell regions or B cell follicles in the spleen and TDLN.

Tumor-infiltrating MDSC aggregate next to areas of hypoxia.

Tumors do not have the distinct lymphoid architecture as found in the spleen and lymph nodes, but a hallmark of solid tumors are areas of low oxygen tension (hypoxia) due to insufficient blood supply. Tissue oxygenation, or lack thereof, is emerging as a major regulator of tumor progression, as it generates intracellular signals that modulate

tumor cell metabolism, increase the metastatic potential of tumor cells, trigger the formation of new blood vessels feeding the tumor, thus leading to a more aggressive tumor phenotype (216). We used hypoxia as a marker of tumor tissue architecture in the MDSC localization experiments. Low oxygen tension within tumors was indirectly detected by binding of the intraperitoneally injected cell permeable chemical pimonidazole·HCl to exposed thiol groups in the structure of proteins and peptides. Due to the reduction of protein disulfide bonds in hypoxic conditions, regions of low oxygen tension contain more thiol groups and retain the bound pimonidazole, which is then detected by antibody labeling. The relative abundance of M-MDSC and PMN-MDSC confirmed the expectations based on the flow cytometry results. In addition, PMN-MDSC and M-MDSC were not uniformly distributed within the tumor but rather were localized together forming aggregates with only a few individual cells being observed around the aggregates. Interestingly these MDSC clusters were often localized immediately next to areas of hypoxia.

PMN-MDSC are detected in the thymus of mice with advanced stage 4T1 tumors

MDSC suppress the function of mature T cells after their release from the thymus. To the best of our knowledge, there are no reports of MDSC-mediated effects on T cell maturation in the thymus. Considering the large accumulation of MDSC in mice with advanced stage tumors, we asked whether MDSC are also detectable in the thymus. Of the two major MDSC subsets, PMN-MDSC were detected with both flow cytometry and fluorescence microscopy, albeit in low numbers, in the thymus of tumor-bearing mice (Fig. 12). M-MDSC were also detected with flow cytometry in a quantity statistically greater than that of conventional monocytic cells in healthy mice. However, the numbers

of M-MDSC were so low that these cells were virtually undetectable in tissue sections, and thus are unlikely to have much functional significance in the thymus. In addition to the observed PMN-MDSC presence in the thymus, advanced 4T1 tumors also correlated with a decrease in overall thymus cellularity and a trending decrease in the number of double positive ($CD4^+CD8^+$) thymocytes (p value = 0.16) relative to the healthy controls. It remains unclear whether PMN-MDSC in the thymus contribute to these effects or interfere in any way with T cell maturation.

MDSC generated in mice with 4T1 tumors express folate receptor β (FR β): potential use of FR-targeted therapies for MDSC elimination?

The high-affinity folate receptor alpha (FR α) has limited expression on healthy epithelia, but is overexpressed in a large number of cancers (217, 218). Therefore, FR-targeting strategies using folate or anti-FR antibody as the targeting ligand have been pursued as methods for tumor-specific drug or imaging agent delivery, hyper-thermal or mechanical destruction of tumor cells, as well as for visualization of primary and metastatic tumors for improved surgical removal (217, 219-224). On the other hand, the beta isoform of FR (FR β) is expressed on some myeloid cells, including myeloid leukemias (225-227), but reportedly is only functional on activated macrophages (227, 228). We asked whether MDSC, as immature myeloid lineage cells, express FR β , providing potential for the therapeutic elimination of these immunosuppressor cells in cancer. Blood and spleen cells from late-stage 4T1-bearing mice were immunolabeled against FR β and the MDSC markers CD11b, Ly-6G, and Ly-6C, and analyzed with flow cytometry. Both PMN-MDSC and M-MDSC from spleen and blood expressed comparable levels of FR β (Fig. 13). Whether FR β expressed on MDSC is capable of

binding and internalizing folate remains to be determined. It is of further interest to determine whether FR β is also expressed on MDSC in patients with various cancers, thus serving as a potential target for the selective elimination of MDSC to alleviate immunosuppression and increase the patient's anti-tumor immune response.

DISCUSSION

CTL can kill tumor cells upon contact and are the most potent effectors in the anti-tumor immune response. To acquire tumor cytolytic ability, CTL must be first activated by appropriate exposure to tumor antigens in the context of co-stimulation, a process that occurs in the TDLN. Thus, the ability of T cells to enter TDLN is vital for the efficient generation of an anti-tumor immune response. As evidenced from studies with L-selectin^{-/-} mice or blocking antibodies, L-selectin is critical for the homing of circulating naïve lymphocytes to PLN. In addition, L-selectin plays an important role in the migration of myeloid cells, such as neutrophils and monocytes, to sites of inflammation. These effects of leukocyte-expressed L-selectin are mediated via interactions with its ligands on the vascular endothelium, which are constitutively expressed on HEV in PLN and upregulated in post-capillary venules near inflammatory sites.

Tumor growth is associated with the release of soluble factors that drive the generation and accumulation of immunosuppressive MDSC, which enhance tumor progression via multiple mechanisms. Importantly, MDSC inhibit CTL activation in the TDLN and CTL function in the tumor. Thus the ability of MDSC to enter TDLN and the tumor may be critical for suppression of the anti-tumor response. This warrants further investigation of the mechanisms of MDSC migration to tumors and TDLN. The role of L-selectin in leukocyte migration to PLN and sites of inflammation has been characterized for lymphocytes and conventional myeloid cells, but its contribution to MDSC migration is unknown.

L-selectin^{-/-} mice have been generated to study L-selectin function (92). Hallmark characteristics of these mice include inhibition of lymphocyte homing to PLN resulting in dramatically decreased PLN cellularity, as well as inhibition of neutrophil recruitment to sites of inflammation resulting in the alleviation of inflammation-induced tissue damage. In light of these observations, in the context of tumor progression, decreased MDSC abundance tumors and TDLN of L-selectin^{-/-} mice relative to wild type may be a sign of impaired MDSC migration to these tissues due to lack of L-selectin expression. However, contribution of other factors such as differential MDSC survival or egress from these tissues cannot be excluded. More direct evidence of the contribution of L-selectin in MDSC migration can be gained from adoptive transfer of cell tracker-labeled wild type or L-selectin^{-/-} MDSC into the circulation of tumor-bearing mice, followed by enumeration of the labeled MDSC in the tumor and TDLN shortly thereafter. This time-restricted approach minimizes the cumulative possible contribution of differential MDSC survival or egress on the abundance of tumor- or TDLN-resident MDSC. Thus any differences in the number of tracker-labeled wild type *vs.* L-selectin^{-/-} MDSC in the tumor or TDLN would be primarily the result of altered MDSC migration to these sites.

With this experimental design in mind, we sought to compare tumor progression and MDSC accumulation in wild type and L-selectin^{-/-} mice and to validate a model system, in which tumor-bearing wild type and L-selectin^{-/-} mice would be equivalent MDSC sources for adoptive transfer experiments, except for the lack of L-selectin on MDSC from L-selectin^{-/-} mice. We used the 4T1 transplantable murine breast cancer model, which is widely used as a model for stage IV human metastatic breast cancer. We observed similar tumor growth rates and kinetics of tumor-induced PMN-MDSC and M-

MDSC accumulation in wild type *vs.* L-selectin^{-/-} mice (Fig. 3). We also confirmed the expression of L-selectin on PMN-MDSC and M-MDSC (Fig. 4). We further quantified the accumulation of these subsets in various tissues in wild type and L-selectin^{-/-} mice (Fig. 5) and examined their localization within the spleen (Fig. 8), TDLN (Fig. 9, 10), and tumor (Fig. 11). Interestingly, we were able to detect low levels of PMN-MDSC in the thymus, which correlated with a decreased thymic cellularity and a tendency for a decrease in CD4⁺CD8⁺ double positive thymocytes (Fig. 12). On a different note, we showed expression of FR β on both MDSC subsets (Fig. 13), which may provide a potential strategy for the targeted elimination of MDSC.

Small, but statistically significant acceleration of tumor growth was observed in L-selectin^{-/-} mice relative to wild type (Fig. 3A). It can be speculated that a lack of L-selectin expression, via inhibiting T cell migration to TDLN, would decrease the anti-tumor T cell activation, ultimately resulting in faster tumor growth. However, this putative pro-tumor effect of decreased T cell access to TDLN may have little significance in the context of an inherently aggressive cancer such as the 4T1. In addition, this effect may be further negated by decreased migration of L-selectin^{-/-} immunosuppressive cells, such as regulatory T cells or MDSC to the TDLN or to the tumor, thus alleviating immunosuppression at these sites in L-selectin^{-/-} mice. Therefore, the finding that L-selectin expression has some contribution in the control of tumor growth is not surprising, but likely has little functional significance, at least in this model system.

MDSC generation is driven by tumor-derived soluble factors and MDSC accumulation correlates with tumor burden. This well established fact was extended to L-selectin^{-/-} mice with 4T1 tumors. As expected, both wild type and L-selectin^{-/-} mice

exhibited a dramatic increase in circulating MDSC numbers, which correlated with tumor burden. In addition, the small increase in tumor growth rate in L-selectin^{-/-} mice was not sufficient to cause a statistically significant increase in the rate of MDSC accumulation in the blood of L-selectin^{-/-} mice relative to wild type (Fig. 3C).

MDSC do not only accumulate in the blood. Many studies have shown a dramatic accumulation of MDSC in the spleen during tumor progression and other inflammatory pathologies. In the spleen of 4T1 tumor-bearing wild type mice, there were 88-fold more PMN-MDSC and 35-fold more M-MDSC compared to conventional polymorphonuclear and monocytic myeloid cells in healthy mice, respectively (Fig. 5). In the L-selectin^{-/-} tumor-bearing mice, the increase was 76-fold and 37-fold, respectively, not statistically different from that observed in wild type mice. For comparison, the increase in blood averaged to 156-fold and 24-fold for PMN-MDSC and M-MDSC, respectively (Fig. 3C). The spleen is important for removal of aged or damaged red blood cells from the circulation and also plays a role in the immune surveillance against blood-borne pathogens. For these functions, the spleen must filter the blood very efficiently and is equipped with sinusoids with large fenestrations that allow easier entry of cells into the tissue. It is possible that the splenic accumulation of MDSC, paralleling the increase in blood-borne MDSC numbers, is merely the result of blood filtration through the spleen. Thus, it was not surprising that splenic MDSC localized largely in the red pulp that is rich in sinusoids (Fig. 8). In addition, the liver, another organ rich in sinusoids is also a site of preferential MDSC homing and accumulation in cancer, irrespective of liver metastasis (229). In agreement, we observed an increased frequency of PMN-MDSC and M-MDSC in the liver. Interestingly, during cancer progression there are increased numbers of

clonogenic myeloid progenitors in the spleen and liver, suggestive of a role of these organs in supporting extramedullary hematopoiesis and thus contributing to MDSC accumulation (229, 230).

Regardless of the mechanism of MDSC accumulation in the spleen, the organ is a convenient and commonly used experimental source of large numbers of cancer-induced MDSC in mice. Its cellularity is dramatically increased in late stages of cancer, it is easily dissociated to single cells without the need for enzymatic digestion, and immunolabeling gives clean and unambiguous identification of leukocyte subsets with flow cytometry. All these factors made it the source of choice for large numbers of MDSC for further sorting or adoptive transfer into recipient mice. In addition, our data showed that splenic PMN-MDSC and M-MDSC expressed similar levels of L-selectin as the corresponding blood-borne MDSC, further validating this organ as a source of MDSC for the study of L-selectin function.

Interestingly, for efficient L-selectin detection in blood samples from mice with advanced 4T1 tumors, the blood had to be washed with an excess volume of PBS to remove soluble plasma proteins. Various inflammatory conditions are characterized by elevated soluble L-selectin (sL-selectin) in the bloodstream, generated by endoproteolytic cleavage of membrane-bound L-selectin upon leukocyte activation. High levels of sL-selectin in the test samples would block antibody labeling of membrane-bound L-selectin due to competitive binding to the anti-L-selectin antibody. Thus, the requirement for removal of soluble plasma proteins for efficient immunolabeling of L-selectin on leukocytes suggests high levels of sL-selectin in the blood of wild type mice with advanced 4T1 tumors. A functional significance of sL-selectin during inflammation

comes from its ability to compete against membrane-bound L-selectin for endothelial binding partners, thus interfering with L-selectin-dependent leukocyte adhesion and migration (82, 231). Thus, sL-selectin may serve as a regulatory mechanism to tune down over-activated immune responses (66). The protease that cleaves membrane-bound L-selectin is the cell surface-expressed ADAM17, which functions in a *cis* manner, cleaving L-selectin expressed by the same cell (232, 233). Importantly, ADAM17 is expressed on MDSC and it has been suggested that MDSC-expressed ADAM17 cleaves T cell-expressed L-selectin, thus inhibiting T cell homing to the TDLN and providing yet another mechanism of MDSC-mediated suppression of the anti-tumor T cell response (234). While such a *trans* mechanism of action may be controversial, it is likely that MDSC-expressed ADAM17 cleaves MDSC-expressed L-selectin in a *cis* manner and contributes to the high circulating sL-selectin levels. Given this, the relatively high and uniform expression of L-selectin observed on the surface of both MDSC subsets is unexpected (Fig. 4). Thus, MDSC-expressed ADAM17 may indirectly inhibit T cell homing to the TDLN and contribute to the suppression of the anti-tumor T cell response.

Interestingly, a role of L-selectin in MDSC migration to TDLN was suggested by decreased numbers of MDSC in the TDLN of L-selectin^{-/-} mice relative to wild type (Fig. 5B). On the other hand, the opposite effect was observed in the tumor: at least in part due to an increased tumor burden, there were increased MDSC numbers in the tumor of L-selectin^{-/-} mice, suggesting that L-selectin may not be required for MDSC migration to the tumor. Furthermore, L-selectin influenced the ratio between the numbers of M-MDSC and PMN-MDSC in the lymph nodes (Fig. 6). Specifically, L-selectin expression favored a M-MDSC/PMN-MDSC ratio in NDLN that was 17-fold higher than in blood,

while loss of L-selectin expression completely eliminated this effect. For TDLN, L-selectin expression was associated with a 26-fold higher M-MDSC/PMN-MDSC ratio relative to the bloodstream, while L-selectin deficiency reduced this effect by greater than 60%. These results hint at a more efficient migration of M-MDSC from the blood to PLN compared to PMN-MDSC, but factors such as enhanced M-MDSC survival or greater PMN-MDSC egress from PLN cannot be excluded as contributors to the high M-MDSC/PMN-MDSC ratio in PLN. In addition, L-selectin may have a greater impact on M-MDSC migration to PLN relative to PMN-MDSC. This could be due to higher L-selectin expression levels on M-MDSC than PMN-MDSC, as indicated by the higher fluorescence intensities observed by flow cytometry (Fig. 4). Furthermore, other adhesion molecules, preferentially expressed on M-MDSC that synergize with L-selectin could also contribute. On the other hand, L-selectin deficiency alters the cellular composition of the PLN, thus possibly affecting chemokine production and recruitment of other leukocytes. Therefore, to conclusively address the involvement of L-selectin in MDSC migration to PLN, a more direct approach is necessary. Here, we validated a model system, in which tumor-bearing wild type and L-selectin^{-/-} mice can be used as MDSC sources for adoptive transfer experiments for the study of L-selectin involvement in MDSC migration.

FIGURE LEGENDS

Figure 3. The kinetics of systemic MDSC accumulation correlate with tumor growth rate.

Wild type and L-selectin^{-/-} mice were injected s.c. in the mammary fat pad with 10⁴ 4T1 cells. Total numbers of each MDSC subset were calculated from the leukocyte count. A) At weeks 1, 2, 3, 4, and 5 after 4T1 cell injection, the tumor volumes were determined with caliper measurements using the formula $V = (L \times W^2) / 2$, where W (width) is the short tumor axis and L (length) is the long tumor axis. *p<0.05 vs. wild type at each indicated time point. Results are from 22-165 independent experiments per genotype per time point. B), C) At weeks 1, 2, 3, 4, and 5 after tumor induction, blood was collected from the retro-orbital sinus and the leukocyte concentration was determined. The blood was labeled with anti-CD11b, anti-Ly-6G, and anti-Ly-6C antibodies and the frequencies of CD11b⁺Ly6G⁻Ly6C^{high} M-MDSC and CD11b⁺Ly6G⁺Ly6C^{low} PMN-MDSC were determined with flow cytometry (B), and PMN-MDSC and M-MDSC numbers were calculated (C). Results are from 4-11 independent experiments per genotype per time point.

Figure 4. PMN-MDSC and M-MDSC from spleen and blood of 4T1 tumor-bearing mice express L-selectin.

A) Spleen cells from advanced stage 4T1 tumor-bearing BALB/c mice were labeled with FITC-conjugated anti-CD11b, PE-conjugated anti-Ly-6G, PE/Cy7-conjugated anti-Ly-6C and biotinylated anti-L-selectin (detected with avidin-APC) antibodies. The expression level of L-selectin by CD11b⁺Ly6G⁺Ly6C^{low} PMN-MDSC and CD11b⁺Ly6G⁻Ly6C^{high} M-MDSC was determined with flow cytometry using

constant voltage settings between experiments. FACS histogram plots (left) are representative of 4 experiments with solid lines showing L-selectin expression levels on PMN-MDSC or M-MDSC and dashed lines showing isotype control labeling. The bar graph (right) represents the mean relative fluorescence intensity of L-selectin-labeled PMN-MDSC and M-MDSC. * $p < 0.05$ vs. PMN-MDSC.

B) Blood was collected from the retro-orbital sinus from advanced stage 4T1 tumor-bearing mice using a heparinized Pasteur pipette. After a wash in excess PBS or without washing, the blood was labeled as above and L-selectin expression was determined with flow cytometry. Solid lines represent L-selectin labeling on PMN-MDSC or M-MDSC in washed blood (bold solid line) or non-washed blood (thin solid line); dashed line represents the negative control. Histogram plots (left) are representative of a minimum of 3 independent experiments. The bar graph (right) represents the mean relative fluorescence intensity of L-selectin-labeled PMN-MDSC and M-MDSC from washed blood samples.

Figure 5. MDSC accumulation in tissues of wild type and L-selectin^{-/-} mice with advanced stage 4T1 tumors.

Wild type (WT) or L-selectin^{-/-} mice were injected s.c. in the mammary fat pad with 10^4 4T1 cells in supplement-free RPMI. Supplement-free RPMI alone was injected in the contra-lateral fat pad and served as an internal vehicle control. After 4-5 weeks, mice were sacrificed and the indicated tissues collected. TDLN were the inguinal PLN next to the site of 4T1 injection, while NDLN were the contralateral inguinal PLN next to the vehicle injection site. Single-cell suspensions were immunolabeled against CD11b, Ly-6G, and Ly-6C to quantify PMN-MDSC and M-MDSC. Conventional

polymorphonuclear and monocytic myeloid cells from control WT mice without tumors were quantified for comparison. Frequencies (A) and total numbers (B) of CD11b⁺Ly6G⁺Ly-6C^{low} polymorphonuclear and CD11b⁺Ly-6G⁻Ly-6C^{high} monocytic cells were determined with flow cytometry. Tissue cellularities (C) were determined using a hemocytometer. *p<0.05 vs. PMN-MDSC (A and B) or p<0.05 vs. control (C); †p<0.05 vs. WT. Results are from 3-10 independent experiments per genotype per tissue.

Figure 6. High M-MDSC/PMN-MDSC ratio in PLN of mice with advanced stage 4T1 tumors is dependent on L-selectin expression.

The M-MDSC/PMN-MDSC ratio in the blood and various tissues from tumor-bearing mice was calculated from the data shown in figure 5. Dashed line represents equal abundance of M-MDSC and PMN-MDSC; BM, bone marrow; *p<0.05 vs. wild type. Results are from 5-14 independent experiments per genotype per tissue.

Figure 7. MDSC from spleen of 4T1 tumor-bearing mice suppress T cell proliferation in a dose-dependent manner.

MDSC were sorted from the spleens of advanced stage 4T1 tumor-bearing BALB/c mice and their ability to suppress T cell proliferation was tested in a mixed lymphocyte reaction in a 96-well plate format. The responder cells (10⁵ per well) were spleen cells from a non-tumor-bearing BALB/c mouse, labeled with CFSE to detect proliferation. Stimulator cells (10⁵ per well) were spleen cells from a C57BL/6 mouse, pretreated with mitomycin C to prevent proliferation. The frequency of T cells within the responder spleen cell population was determined with flow cytometry and sorted MDSC were added to the wells at various ratios relative to the responder T cells. Negative control was responders incubated alone and positive control was stimulators co-incubated

with responders without added MDSC. Triplicate wells for each combination were cultured for 4 days, pooled, and labeled with anti-CD4 and anti-CD8 antibodies. Flow cytometric analysis was done by collecting data for the whole sample. A) Events with high forward light scatter (FSC) were analyzed to enumerate proliferated CFSE^{low} CD4⁺ and CFSE^{low} CD8⁺ T cells in each well. Negative control – responder spleen cells cultured without stimulator cells or MDSC; positive control – responder cells cultured with stimulator cells, but without MDSC; 1:1 through 1:64 – MDSC/T cell responder ratios, responder cells were cultured with stimulator cells and decreasing numbers of MDSC; CFSE^{low} gate indicates CFSE^{low} CD4⁺ T cell population; numbers next to the gate indicate total counts of CFSE^{low} CD4⁺ T cells. B) The total counts of CFSE^{low} CD4⁺ and CFSE^{low} CD8⁺ T cells were plotted. Data represent the results from one of two independent experiments.

Figure 8. Localization of MDSC in the spleen of advanced stage 4T1 tumor-bearing mice.

Spleens were harvested from advanced stage (4-5 weeks) 4T1 tumor-bearing wild type mice. Cryosections were immunolabeled against the pan T cell marker Thy1.2, the pan B cell marker IgD, and the MDSC markers CD11b, Ly-6G, and Ly-6C. The sections were analyzed with fluorescence microscopy. Digital monochromatic images were acquired at a constant exposure, and pseudocolored and overlaid using MetaVue™ software. Overlays include Ly-6G (green), Ly-6C (red), Thy1.2 (magenta) and IgD (blue). CD11b was expressed by Ly-6G⁺Ly-6C^{low/-} and Ly-6G⁻Ly-6C^{high} cells, but was not included in overlays for the sake of clarity. Thus, representative images are of CD11b⁺Ly-6G⁺Ly-6C^{low/-} PMN-MDSC (yellow arrowheads in inset) and CD11b⁺Ly-6G⁻

Ly-6C^{high} M-MDSC (white arrows in inset), relative to T cell zones (magenta) and B cell follicles (blue). Scale bar (50 μ m) is for all images. Images are representative of 3 independent experiments.

Figure 9. Localization of PMN-MDSC in the TDLN of advanced stage 4T1 tumor-bearing mice.

Spleens were harvested from advanced stage (4-5 weeks) 4T1 tumor-bearing wild type mice. Cryosections were immunolabeled against the T cell marker Thy1.2, the B cell marker IgD, and the MDSC markers CD11b, Ly-6G, and Ly-6C. The sections were analyzed with fluorescence microscopy. Digital monochromatic images were acquired at a constant exposure, and pseudocolored and overlaid using MetaVue™ software. Representative images are of cells co-expressing Ly-6G (green) and CD11b, but no to low levels of Ly-6C, relative to T cell zones (Thy1.2, red) and B cell follicles (IgD, blue). CD11b and Ly-6C are not included in overlays for the sake of clarity. Arrows point to some of the CD11b⁺Ly-6G⁺ Ly-6C^{low/-} cells. Scale bar (50 μ m) is for all images. Images are representative of 3 independent experiments.

Figure 10. Localization of M-MDSC in the TDLN of advanced stage 4T1 tumor-bearing mice.

TDLN were harvested from advanced stage (4-5 weeks) 4T1 tumor-bearing wild type mice. Cryosections were immunolabeled against the T cell marker Thy1.2, the B cell marker IgD, and the MDSC markers CD11b, Ly-6G, and Ly-6C. The sections were analysed with fluorescence microscopy. Digital monochromatic images were acquired at a constant exposure, and pseudocolored and overlaid using MetaVue™ software. Representative images are of cells expressing CD11b and high levels of Ly-6C (green),

but no Ly-6G, relative to T cell zones (Thy1.2, red) and B cell follicles (IgD, blue). CD11b and Ly-6G are not included in overlays for the sake of clarity. Arrows point to some of the CD11b⁺Ly-6G⁺ Ly-6C^{low/-} cells. Scale bar (50 μm) is for all images. Images are representative of 3 independent experiments.

Figure 11. Localization of MDSC in advanced stage 4T1 tumors

To visualize hypoxic regions within the tumor microenvironment, mice with advanced stage (4-5 weeks) 4T1 tumors were injected with pimonidazole·HCl 1 h prior to euthanasia. Cryosections of tumors were labeled with antibodies against pimonidazole and the MDSC markers CD11b, Ly-6G and Ly-6C. The sections were analyzed with fluorescence microscopy. Digital monochromatic images were acquired at a constant exposure, and pseudocolored and overlaid using MetaVue™ software. Overlays include Ly-6G (green), Ly-6C (red), and pimonidazole (blue). CD11b was expressed by Ly-6G⁺Ly-6C^{low/-} and Ly-6G⁻Ly-6C^{high} cells, but was not included in overlays for the sake of clarity. Thus, representative images are of CD11b⁺Ly-6G⁺Ly-6C^{low/-} PMN-MDSC (yellow arrowheads in inset) and CD11b⁺Ly-6G⁻Ly-6C^{high} M-MDSC (white arrows in inset), relative to hypoxic regions (blue). Scale bar (50 μm) is for all images. Images are representative of 3 independent experiments.

Figure 12. PMN-MDSC are present in the thymus of advanced stage 4T1 tumor-bearing mice.

Thymus was collected from healthy or tumor-bearing wild type mice with advanced stage 4T1 tumors. A) Single-cell suspensions from thymi were immunolabeled against CD11b, Ly-6G, and Ly-6C to quantify polymorphonuclear (PMN) and monocytic (M) myeloid cells, or against CD4 and CD8 to quantify CD4⁻CD8⁻ double-negative

thymocytes (DN), CD4⁺CD8⁺ double-positive thymocytes (DP) and CD4⁺ and CD8⁺ single-positive thymocytes with flow cytometry. Thymus cellularity was determined using a hemocytometer. *p<0.05 vs. healthy control, †p<0.05 vs. PMN-MDSC. Results are from 3-12 independent experiments. B) Cryosections from thymi of wild type mice with advanced stage 4T1 tumors were labeled with antibodies against CD11b, Ly-6G, Ly-6C, CD4 and CD8. The sections were analyzed with fluorescence microscopy. Digital monochromatic images were acquired at a constant exposure, and pseudocolored and overlaid using MetaVue™ software. Overlays include Ly-6G (green), CD8 (red) and CD4 (blue). Ly-6G⁺ cells expressed CD11b, but no Ly-6C. CD11b and Ly-6C are not included in overlays for the sake of clarity. Thus, representative images are of CD11b⁺Ly-6G⁺Ly-6C^{low/-} PMN-MDSC (white arrows) relative to CD8⁺ thymocytes (red), CD4⁺ thymocytes (blue), and CD4⁺CD8⁺ double-positive thymocytes (magenta resulting from the overlay of CD4 and CD8). Scale bar (50 μm) is for all images. Images are representative of 3 independent experiments.

Figure 13. MDSC from 4T1 tumor-bearing mice express folate receptor β (FRβ).

Blood and spleen were collected from mice with advanced stage (4-5 weeks) 4T1 tumors. Spleen single-cell suspensions and blood were labeled with antibodies against CD11b, Ly-6G and Ly-6C and a rabbit anti-FRβ antibody, detected with AlexaFluor® 647-conjugated goat anti-rabbit IgG antibody. The primary rabbit anti-FRβ antibody was omitted from the negative control. Solid lines represent FRβ labeling on PMN-MDSC or M-MDSC; dashed line is negative control. Histogram plots are representative of a minimum of 3 independent experiments.

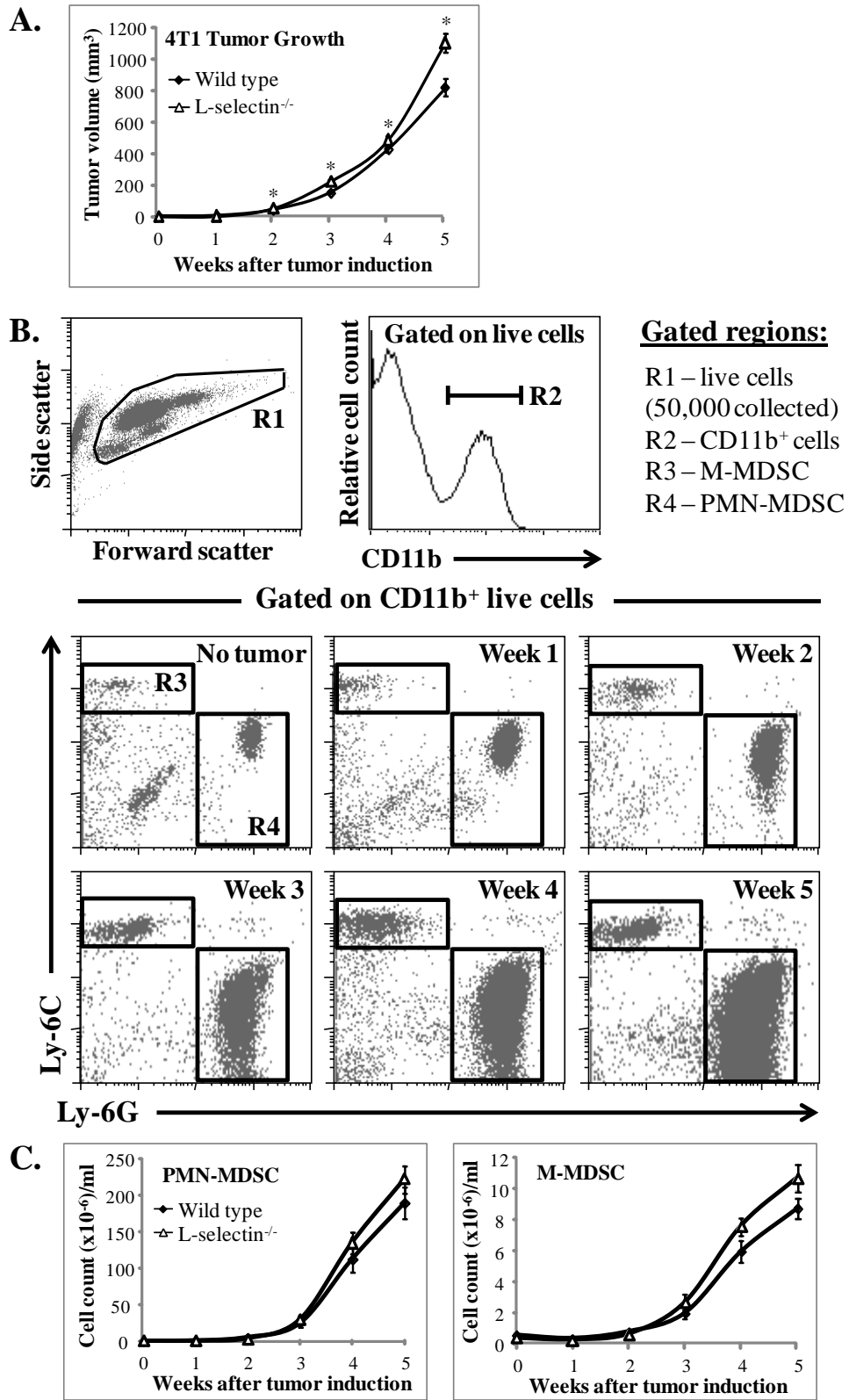
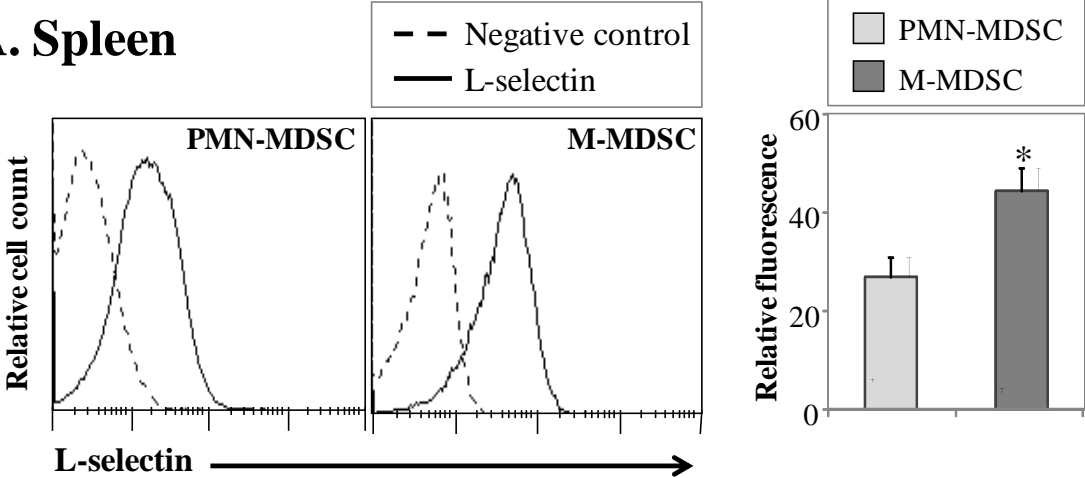


Figure 3

A. Spleen



B. Blood

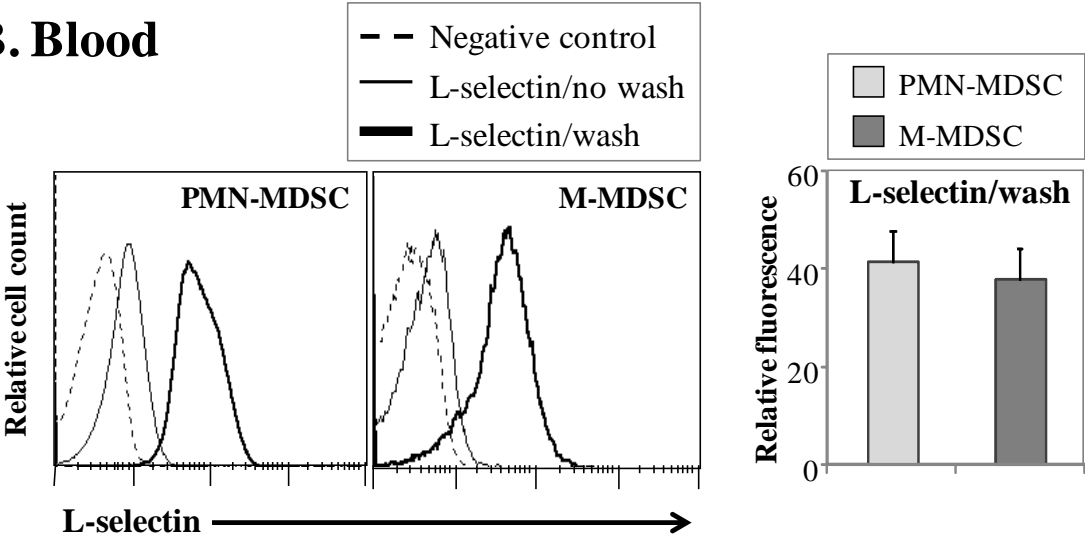
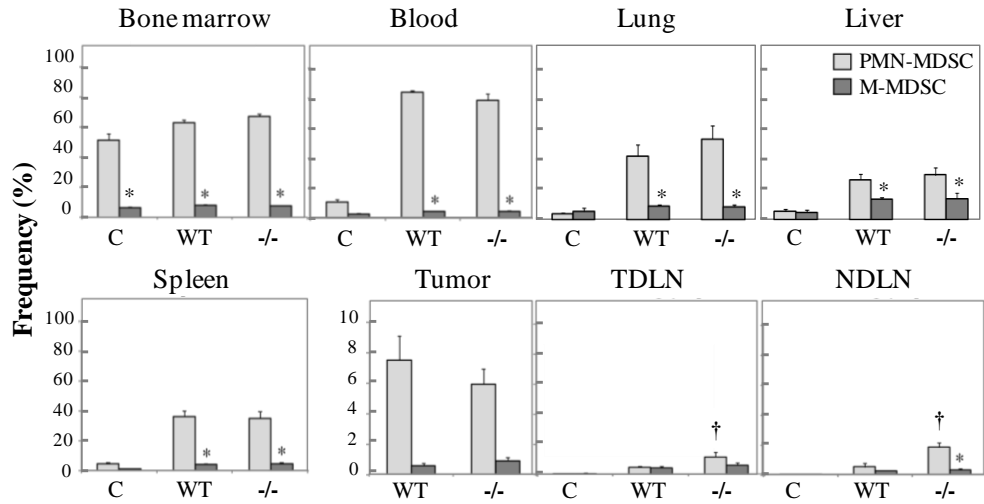
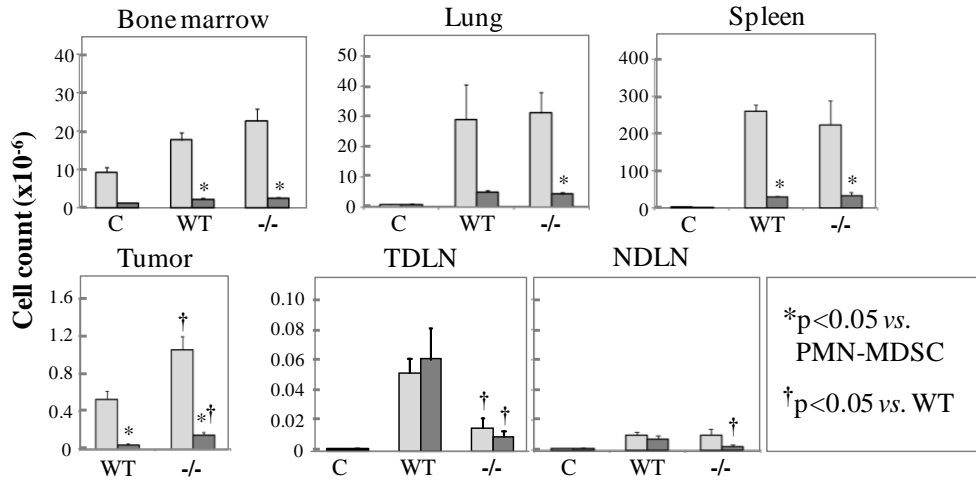


Figure 4

A. MDSC frequency



B. MDSC count



C. Tissue cellularity

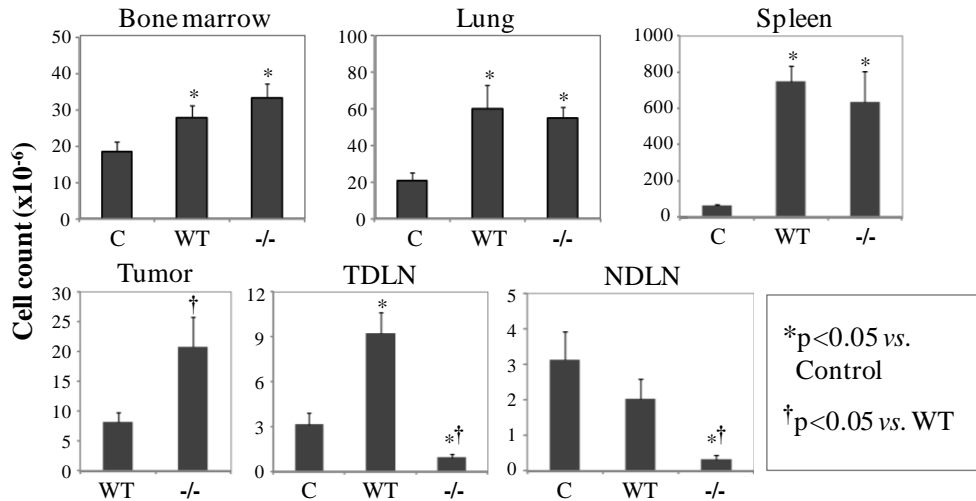


Figure 5

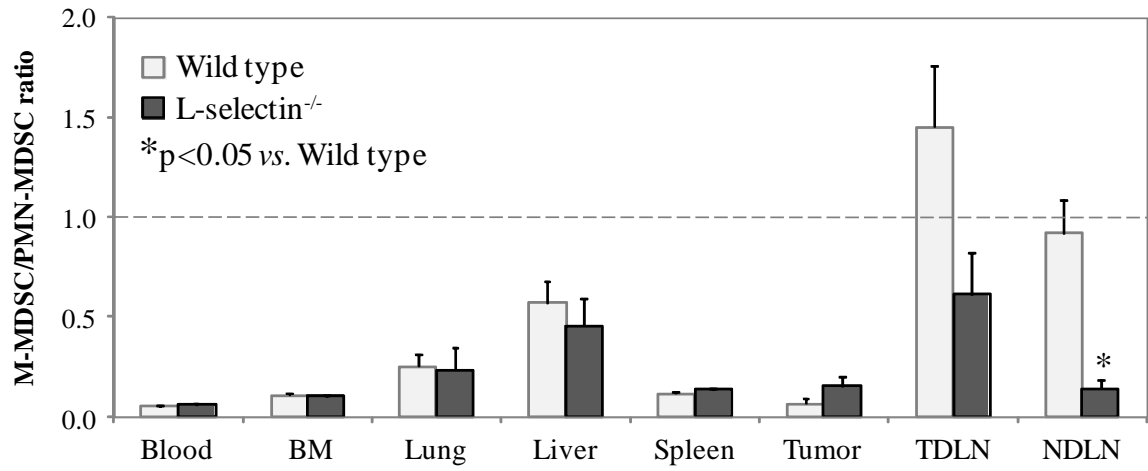
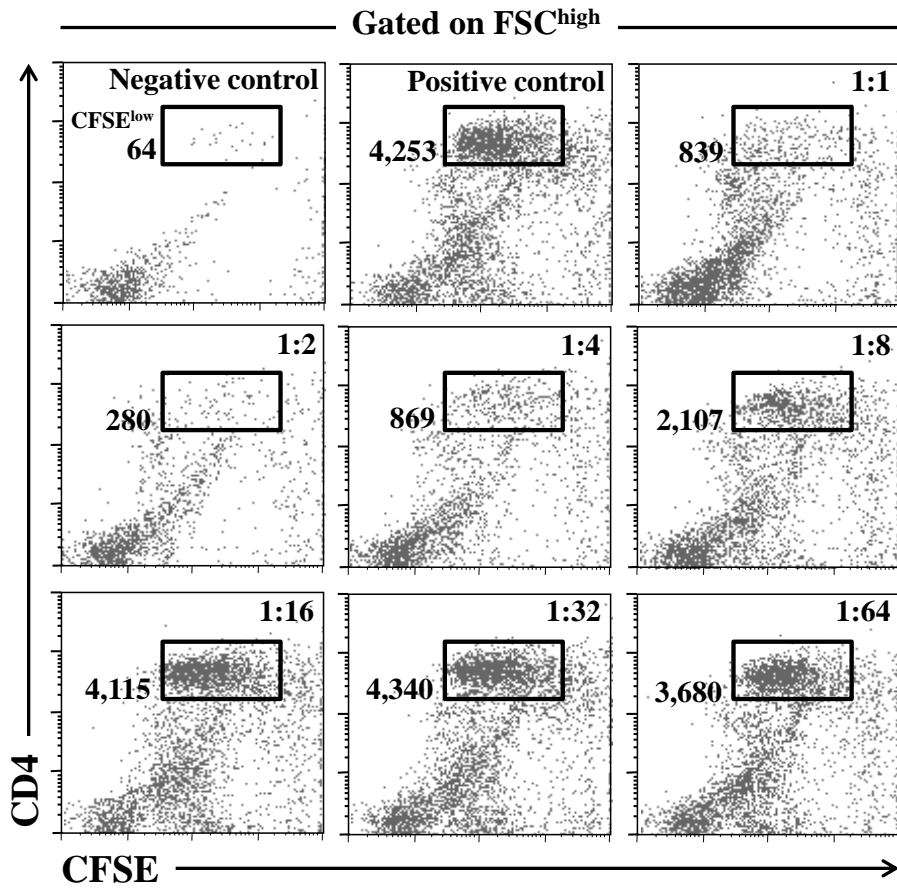


Figure 6

A. FACS analysis of T cell proliferation (4 days MLR)



B. T cell proliferation (4 days MLR)

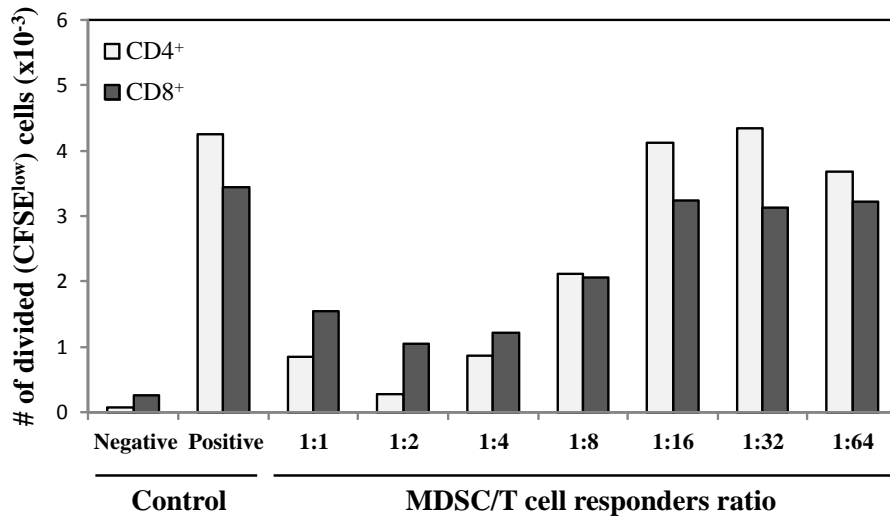


Figure 7

Spleen

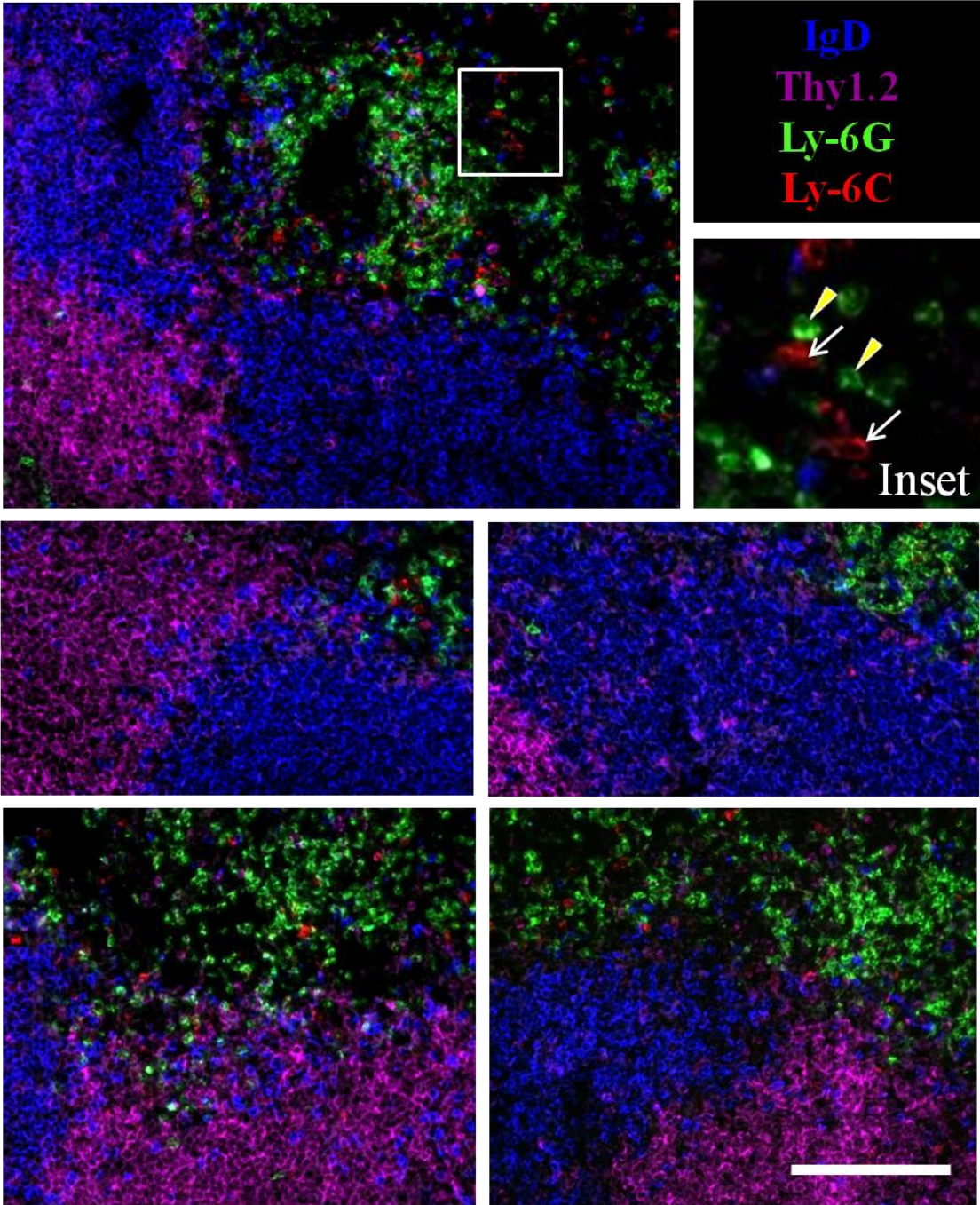


Figure 8

TDLN

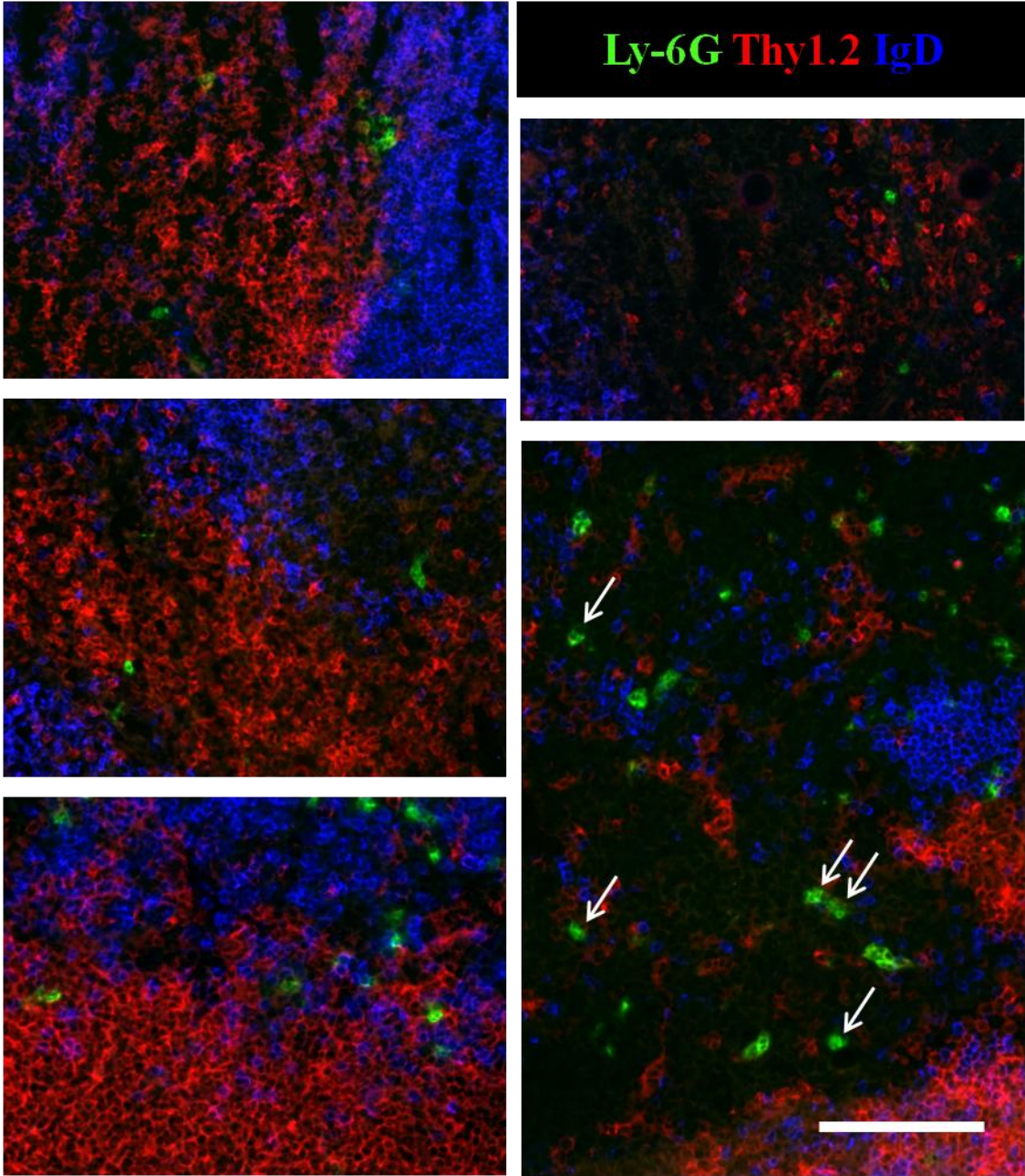


Figure 9

TDLN

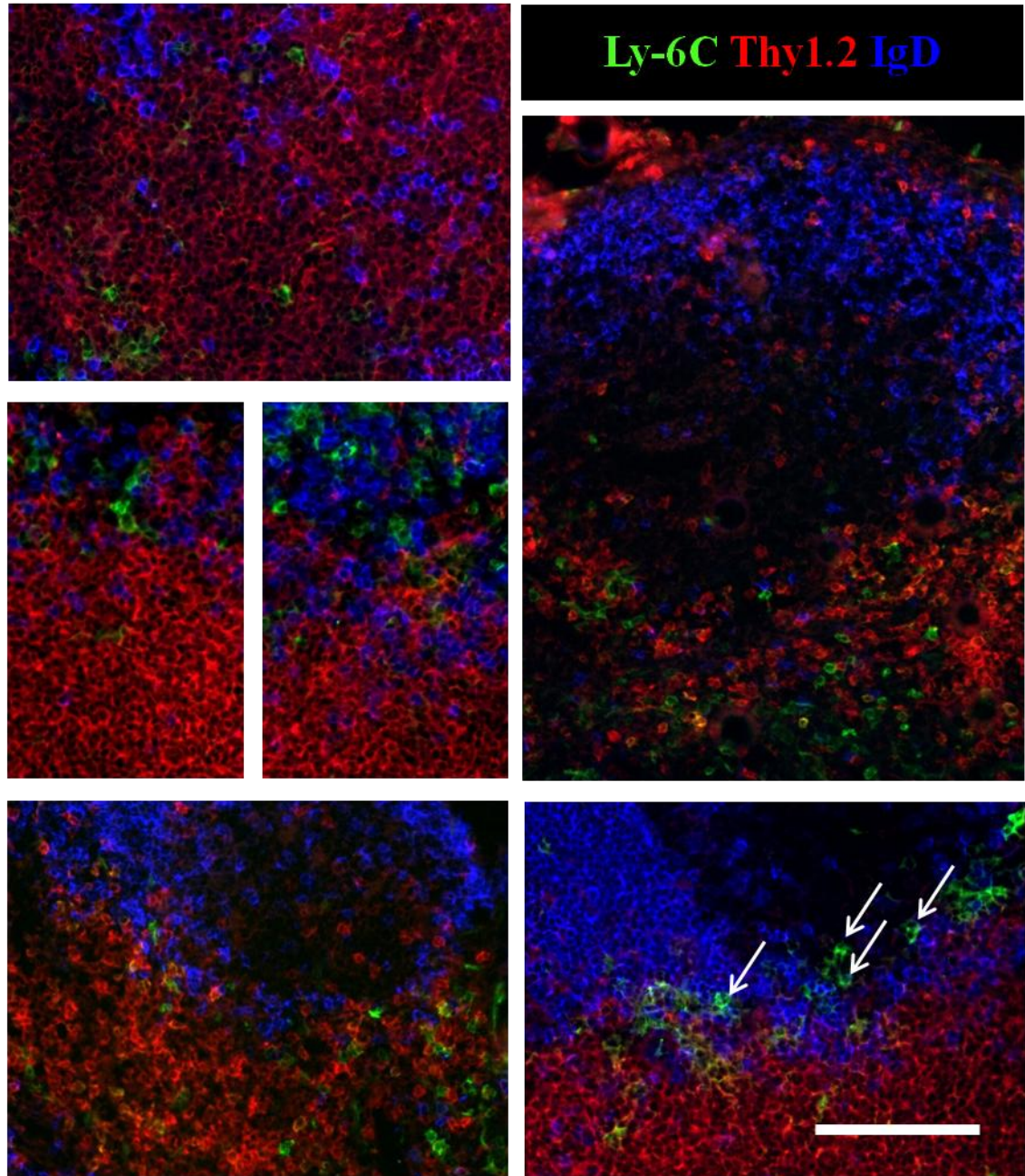


Figure 10

Tumor

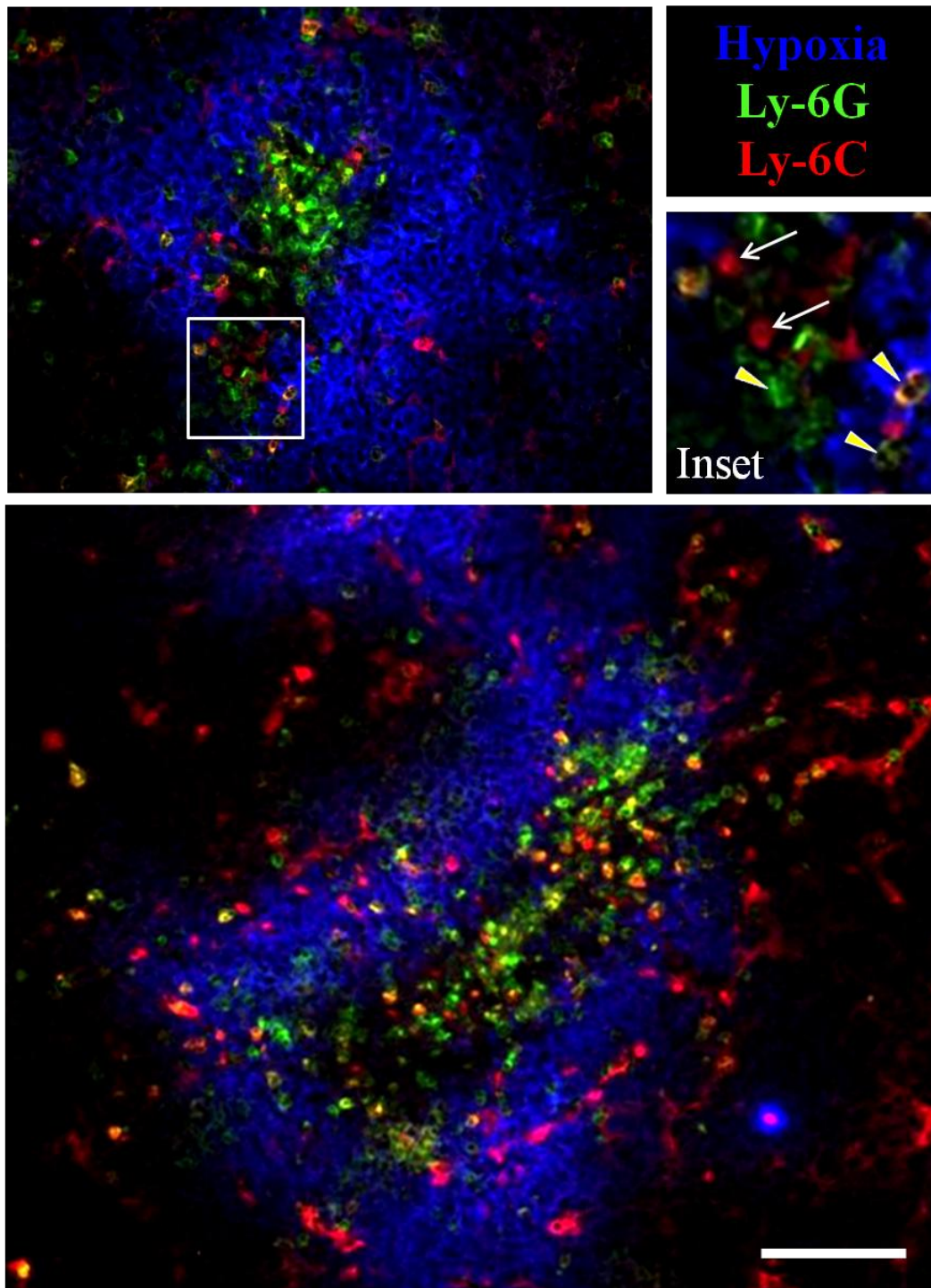
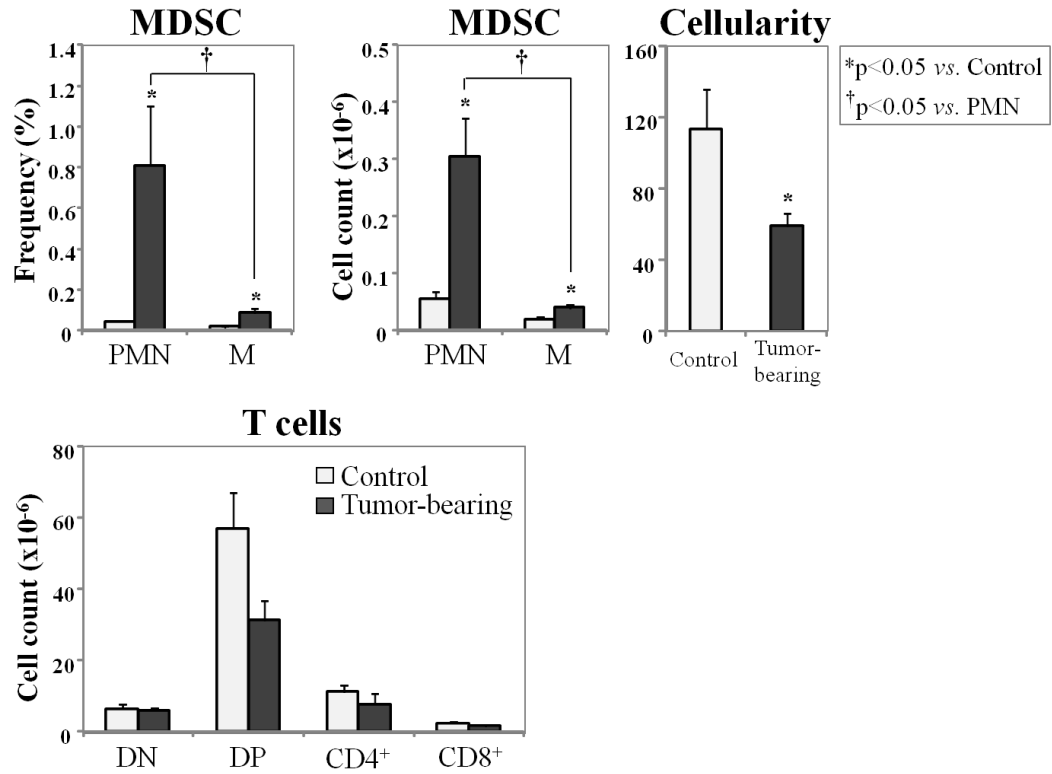


Figure 11

A. Thymus from control and tumor-bearing mice



B. Thymus from tumor-bearing mice

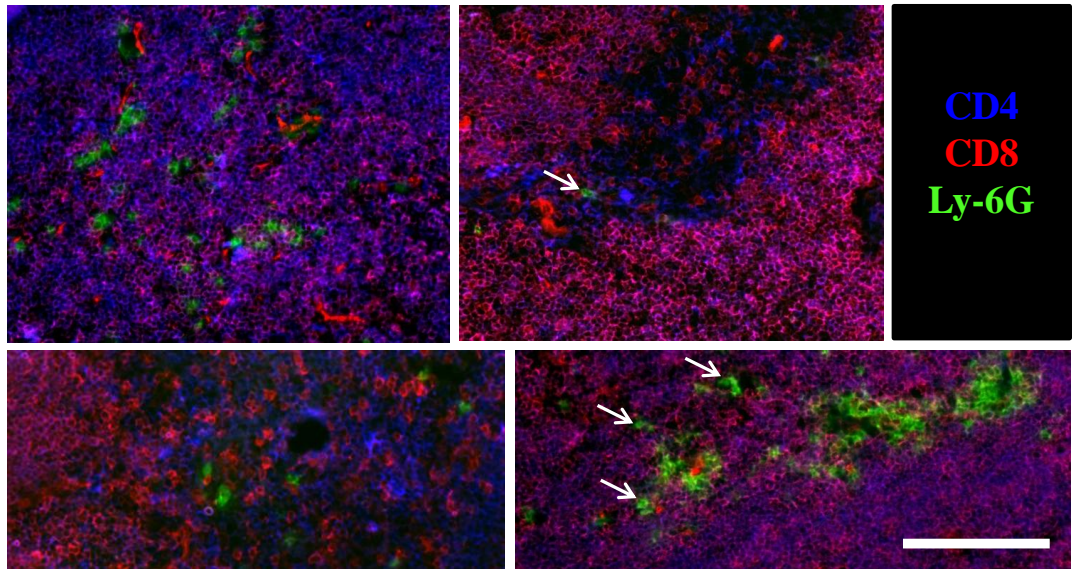


Figure 12

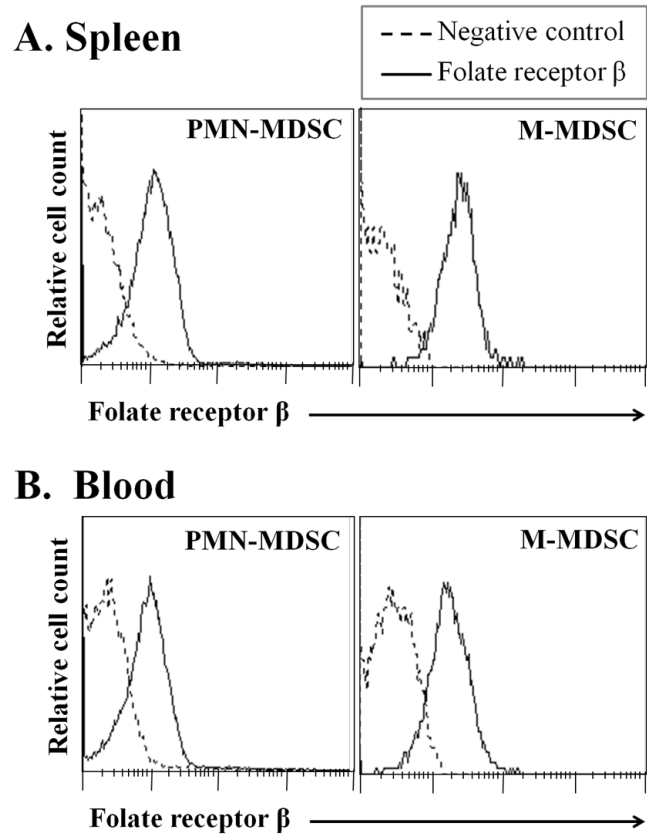


Figure 13

Table I. Tumor growth rate and kinetics of MDSC accumulation in 4T1 tumor-bearing wild type and L-selectin^{-/-} mice^a.

Tumor volume (mm³)			
Genotype	Control (no tumor)	1 wk^b tumor	2 wk tumor
Wild type	N/A	2.78 ± 0.36	41.25 ± 1.86
L-selectin ^{-/-}	N/A	1.48 ± 0.35	53.21 ± 3.25*
Genotype	3 wk tumor	4 wk tumor	5 wk tumor
Wild type	154.68 ± 7.35	434.15 ± 19.37	830.48 ± 53.43
L-selectin ^{-/-}	227.24 ± 10.76*	493.91 ± 22.21*	1,120.08 ± 58.63*
Number of PMN-MDSC (x10⁻⁶)/ml of blood			
Genotype	Control (no tumor)	1 wk tumor	2 wk tumor
Wild type	1.4 ± 0.2	1.7 ± 0.3	6.3 ± 0.9
L-selectin ^{-/-}	1.2 ± 0.2	1.6 ± 0.1	4.7 ± 0.6
Genotype	3 wk tumor	4 wk tumor	5 wk tumor
Wild type	25.0 ± 3.9	111.3 ± 16.6	186.7 ± 21.3
L-selectin ^{-/-}	30.0 ± 5.4	133.6 ± 14.5	219.0 ± 18.4
Number of M-MDSC (x10⁻⁶)/ml of blood			
Genotype	Control (no tumor)	1 wk tumor	2 wk tumor
Wild type	0.53 ± 0.13	0.31 ± 0.04	0.75 ± 0.08
L-selectin ^{-/-}	0.34 ± 0.08	0.24 ± 0.02	0.61 ± 0.05
Genotype	3 wk tumor	4 wk tumor	5 wk tumor
Wild type	1.95 ± 0.32	5.99 ± 0.71	8.84 ± 0.67
L-selectin ^{-/-}	2.65 ± 0.53	7.65 ± 0.59	10.81 ± 0.87

^aTumors were induced by a s.c. injection of 10⁴ 4T1 cells in 50 µl supplement-free RPMI. Tumors were measured with calipers and the tumor volume was calculated according to the formula: (LxW²)/2, where L (length) is the long diameter and W (width) is the short

diameter of the tumor. At the indicated time points after tumor injection, blood was collected from the retro-orbital sinus. Leukocyte count was determined using a hemocytometer and the blood was labeled with antibodies against CD11b, Ly-6G, and Ly-6C. The frequencies of PMN-MDSC and M-MDSC were determined with flow cytometry and the counts of PMN-MDSC and M-MDSC per 1 ml of blood were calculated. * $p < 0.05$ vs. wild type. Results are from 22-165 mice per genotype per time point for tumor growth rate and from 4-11 mice per genotype per time point for MDSC accumulation kinetics in the blood.

^bAbbreviations used: wk, week(s); PMN-MDSC, polymorphonuclear myeloid-derived suppressor cell(s); M-MDSC, monocytic myeloid-derived suppressor cell(s).

Table II. Frequencies of MDSC subsets in tissues of wild type and L-selectin^{-/-} mice with advanced stage 4T1 tumors^a.

MDSC^b frequency				
Genotype	BONE MARROW		BLOOD	
	% PMN-MDSC	% M-MDSC	% PMN-MDSC	% M-MDSC
Control	51.54 ± 4.04	6.28 ± 0.60*	10.86 ± 1.91	3.10 ± 0.36
Wild type	63.06 ± 1.82	7.78 ± 0.60*	84.12 ± 1.24	4.68 ± 0.22*
L-selectin ^{-/-}	61.15 ± 1.96	7.40 ± 0.29*	78.99 ± 4.22	4.64 ± 0.49*
Genotype	LUNG		LIVER	
	% PMN-MDSC	% M-MDSC	% PMN-MDSC	% M-MDSC
Control	3.92 ± 0.41	5.31 ± 2.58	5.41 ± 1.61	4.70 ± 1.88
Wild type	41.91 ± 7.49	8.88 ± 0.91*	26.84 ± 4.10*	13.68 ± 1.18*
L-selectin ^{-/-}	53.09 ± 9.06	8.37 ± 1.53*	30.13 ± 4.98*	14.11 ± 3.99*
Genotype	SPLEEN		TUMOR	
	% PMN-MDSC	% M-MDSC	% PMN-MDSC	% M-MDSC
Control	4.63 ± 1.21	1.37 ± 0.06	N/A	N/A
Wild type	36.12 ± 4.30	4.30 ± 0.63*	7.46 ± 1.62	0.54 ± 0.20
L-selectin ^{-/-}	35.00 ± 4.73	4.79 ± 0.67*	5.90 ± 0.99	0.90 ± 0.21
Genotype	TDLN		NDLN	
	% PMN-MDSC	% M-MDSC	% PMN-MDSC	% M-MDSC
Control	0.06 ± 0.02	0.06 ± 0.03	0.06 ± 0.02	0.06 ± 0.03
Wild type	0.59 ± 0.11	0.56 ± 0.12	0.70 ± 0.32	0.35 ± 0.07
L-selectin ^{-/-}	1.51 ± 0.45 [†]	0.81 ± 0.20	2.45 ± 0.41 [†]	0.42 ± 0.13*

^aWild type or L-selectin^{-/-} BALB/c mice were injected s.c. in the mammary fat pad with 10⁴ 4T1 cells in supplement-free RPMI. Supplement-free RPMI alone was injected in the contra-lateral fat pad and served as an internal vehicle control. After 4-5 weeks, mice were sacrificed and the indicated tissues collected. TDLN was represented by the inguinal PLN next to the site of 4T1 injection, while NDLN was represented by the contralateral inguinal PLN next to the vehicle injection site. Single-cell suspensions were

immunolabeled against CD11b, Ly-6G, and Ly-6C to quantify PMN-MDSC and M-MDSC. Conventional polymorphonuclear and monocytic myeloid cells from control wild type mice without tumors were also labeled for comparison. Cells suspensions were counted using a hemacytometer. Frequencies of CD11b⁺Ly6G⁺Ly-6C^{low/-} polymorphonuclear and CD11b⁺Ly-6G⁻Ly-6C^{high} monocytic cells were determined with flow cytometry. *p<0.05 vs. PMN-MDSC, †p<0.05 vs. tumor-bearing wild type. Results are from 3-10 mice per genotype per tissue.

^bAbbreviations used: MDSC, myeloid-derived suppressor cell(s); PMN-MDSC, polymorphonuclear myeloid-derived suppressor cell(s); M-MDSC, monocytic myeloid-derived suppressor cell(s); TDLN, tumor-draining lymph node(s); NDLN, non-draining lymph node(s).

Table III. Numbers of MDSC subsets in tissues of wild type and L-selectin^{-/-} mice with advanced stage 4T1 tumors^a.

MDSC ^b count (x10 ⁻⁶)				
Genotype	BONE MARROW		LUNG	
	# PMN-MDSC	# M-MDSC	# PMN-MDSC	# M-MDSC
Control	9.2 ± 1.4	1.2 ± 0.2	0.8 ± 0.2	0.8 ± 0.4
Wild type	17.6 ± 2.0	2.2 ± 0.3*	28.9 ± 11.7	5.0 ± 0.7
L-selectin ^{-/-}	22.7 ± 3.1	2.5 ± 0.3*	31.3 ± 6.7	4.3 ± 0.5*
Genotype	SPLEEN		TUMOR	
	# PMN-MDSC	# M-MDSC	# PMN-MDSC	# M-MDSC
Control	3.0 ± 0.8	0.9 ± 0.1	N/A	N/A
Wild type	259.9 ± 18.3	30.7 ± 2.2*	0.53 ± 0.93	0.04 ± 0.02*
L-selectin ^{-/-}	224.4 ± 64.5	32.7 ± 10.1*	1.06 ± 0.14 [†]	0.15 ± 0.03* [†]
Genotype	TDLN		NDLN	
	# PMN-MDSC	# M-MDSC	# PMN-MDSC	# M-MDSC
Control	0.001 ± 0.0003	0.001 ± 0.0006	0.001 ± 0.0003	0.001 ± 0.0006
Wild type	0.052 ± 0.0095	0.061 ± 0.0206	0.010 ± 0.0025	0.008 ± 0.0024
L-selectin ^{-/-}	0.015 ± 0.0062 [†]	0.009 ± 0.0039 [†]	0.008 ± 0.0029	0.002 ± 0.0010 [†]

^aTumors were induced in wild type or L-selectin^{-/-} mice and antibody labeling was performed as described for Table II. The number of CD11b⁺Ly6G⁺Ly-6C^{low/-} polymorphonuclear and CD11b⁺Ly-6G⁻Ly-6C^{high} monocytic cells were determined with flow cytometry. *p<0.05 vs. PMN-MDSC, [†]p<0.05 vs. tumor-bearing wild type. Results are from 3-10 mice per genotype per tissue.

^bAbbreviations used: MDSC, myeloid-derived suppressor cell(s); PMN-MDSC, polymorphonuclear myeloid-derived suppressor cell(s); M-MDSC, monocytic myeloid-derived suppressor cell(s); TDLN, tumor-draining lymph node(s); NDLN, non-draining lymph node(s).

Table IV. Tissue cellularity of wild type and L-selectin^{-/-} mice with advanced stage 4T1 tumors^a.

Tissue cell count (x10⁻⁶)		
Genotype	BONE MARROW	LUNG
Control	18.7 ± 2.8	21.0 ± 4.2
Wild type	27.9 ± 3.4*	60.2 ± 12.8*
L-selectin ^{-/-}	33.4 ± 4.0*	55.2 ± 5.9*
Genotype	SPLEEN	TUMOR
Control	63.9 ± 4.8	N/A
Wild type	750.2 ± 81.1*	8.2 ± 1.6
L-selectin ^{-/-}	636.0 ± 169.7*	20.8 ± 5.1 [†]
Genotype	TDLN^b	NDLN
Control	3.1 ± 0.8	3.1 ± 0.8
Wild type	9.2 ± 1.4*	2.0 ± 0.6
L-selectin ^{-/-}	0.9 ± 0.2* [†]	0.3 ± 0.1* [†]

^aTumors were induced in wild type or L-selectin^{-/-} mice as described for Table II. Single-cell suspensions from the indicated tissues were counted using a hemacytometer *p<0.05 vs. no tumor control, [†]p<0.05 vs. tumor-bearing wild type. Results are from 3-10 mice per genotype per tissue.

^bAbbreviations used: TDLN, tumor-draining lymph node(s); NDLN, non-draining lymph node(s).

CHAPTER 3

INVOLVEMENT OF L-SELECTIN IN MDSC MIGRATION TO TUMOR AND TUMOR-DRAINING LYMPH NODES

ABSTRACT

Myeloid-derived suppressor cells (MDSC) consist of two major subsets, monocytic MDSC (M-MDSC) and polymorphonuclear MDSC (PMN-MDSC), both of which expand in cancer and suppress the activation of naïve T cells in the tumor-draining lymph node (TDLN) and the function of effector cells in the tumor microenvironment. Thus, the ability of MDSC to enter TDLN and the tumor is likely to be critical for suppression of the anti-tumor immune response and elucidating the mechanisms of MDSC migration to these sites may create a basis for novel immunotherapeutic approaches for the treatment of cancer. L-selectin mediates the homing of circulating naïve lymphocytes to lymph nodes and the migration of conventional myeloid cells, such as neutrophils and monocytes, to sites of inflammation, but its contribution to MDSC migration is unknown. In this part of the study, we evaluated the expression on MDSC of various integrins supporting leukocyte migration to lymph nodes, mucosal lymphoid tissues in the gut, and inflammatory sites, such as the tumor. Specifically, both MDSC subsets expressed comparable levels of the integrins LFA-1 and Mac-1 known to be involved in migration to lymph nodes and inflammatory sites. By contrast, VLA-4, which also supports migration to lymph nodes and inflammatory sites, was differentially expressed at higher levels on M-MDSC relative to PMN-MDSC. The $\alpha_4\beta_7$ integrin, involved in migration to mucosa-associated lymphoid tissues, was virtually absent from the surface of most MDSC and was only expressed by a subset of M-MDSC. Together with previously demonstrated expression of L-selectin, these observations indicate that MDSC are equipped with a set of adhesion molecules necessary for migration to the TDLN and tumor. We then evaluated the efficiency of MDSC migration to these sites, as

well as the involvement of L-selectin in this process. Specifically, we demonstrated involvement of L-selectin in the migration of PMN-MDSC, but not M-MDSC, to tumors and TDLN. However, the efficiency of MDSC migration to the TDLN was low. This observation is in agreement with previously observed low MDSC numbers in the TDLN and questions the functional significance of TDLN-infiltrating MDSC in the suppression of the anti-tumor T cell response in this tumor model.

INTRODUCTION

Leukocytes carried with the blood can enter peripheral tissues via a complex, but well-regulated process, called the adhesion cascade (see Fig. 1 in Chapter 1). The adhesion cascade involves adhesive and signaling interactions between the leukocyte and the endothelium. These interactions are sequentially organized in 4 main stages: 1) leukocyte capture and rolling over the endothelium, 2) activation, 3) firm adhesion or arrest, and 4) transendothelial migration or diapedesis (64). Each of these stages is characterized by interactions between distinct groups of molecules. Specifically, the capture and rolling events are dependent on interactions between selectins and their ligands (65, 66). Via these interactions, the leukocyte slows down and during the activation stage senses chemokines displayed on the endothelial surface. Chemokines secreted in the inflamed tissue in response to inflammatory mediators are transcytosed by endothelial cells and presented on the luminal endothelial surface in association with proteoglycans (235). The chemokine signals improve the adhesiveness of leukocyte-expressed integrins, which, via interactions with endothelial immunoglobulin-like superfamily of adhesion molecules, are involved in decreasing the rolling velocity and transitioning to the next stage, firm adhesion (64, 68-72, 236). Integrins are also involved in all subsequent locomotion events in the adhesion cascade leading to diapedesis, as well as leukocyte migration in the extracellular matrix to reach sites of tissue injury or inflammation (73).

Leukocyte migration is essential for the proper function of the immune system in both physiologic and pathologic conditions. During physiologic conditions, as part of the immunosurveillance process, naïve lymphocytes constantly re-circulate between the

blood and the PLN, where they scan for cognate antigens, displayed on antigen-presenting cells. On the other hand, during pathologic conditions, as part of the immune response, activated lymphocytes and myeloid cells such as macrophages and neutrophils migrate to damaged or inflamed tissues. In addition, during pathologic conditions, there is increased migration of lymphocytes to the PLN draining the inflammatory site, where the lymphocytes become activated and enabled to execute an efficient adaptive immune response. During both physiologic and pathologic conditions, the migration of lymphocytes to the PLN occurs in specialized post-capillary venules, named high endothelial venules (HEV) to acknowledge the plump cuboidal shape of their endothelial cells. Importantly, in the physiologic steady state, HEV express a diverse group of adhesion molecules, collectively termed peripheral node addressins (PNAd), which bind to L-selectin (CD62L) expressed on lymphocytes to initiate the adhesion cascade. Among the PNAd are glycosylation-dependent cell adhesion molecule-1 (GlyCAM-1), CD34, endomucin, podocalyxin, nepmucin, and Spg200 (237, 238). Thus, the tissue-specific expression of L-selectin ligands in PLN directs lymphocyte homing to PLN in the steady state. Consequently, L-selectin-deficient (L-selectin^{-/-}) lymphocytes are largely impaired in their ability to migrate to PLN *in vivo* (66), an effect similar to that of antibody-mediated blockade of L-selectin binding (91), and L-selectin^{-/-} mice show a 70% decrease in PLN cellularity (92). Importantly, during pathologic conditions, inflammatory cytokines (*e.g.* TNF- α , IL-1 β), ROS, complement components, immune complexes and other factors cause an upregulation of adhesion molecules, including L-selectin ligands, on the endothelium in inflamed tissues, thus leading to increased leukocyte migration to the inflammatory site (66). Contribution of L-selectin in leukocyte migration to sites of

inflammation has been documented in various conditions (66). For instance, L-selectin is involved in the recruitment of neutrophils (239, 240) and T cells (95) to the inflammatory site in ischemia-reperfusion injury, and concanavalin A-induced liver injury, respectively. Furthermore, L-selectin plays a role in the recruitment of T cells (96) as well as neutrophils, macrophages, lymphocytes and eosinophils (241, 242) to the site of pulmonary inflammation in murine and sheep models of asthma, respectively. As another example of pulmonary inflammation, mice with pulmonary fibrosis showed an L-selectin-dependent infiltration of neutrophils and lymphocytes in the lung (99). Taken together these data implicate L-selectin in lymphocyte migration to PLN in steady state and disease, as well as in myeloid cell migration to sites of inflammation.

In addition to selectins, integrins also play a role in determining the destination of leukocyte migration. For instance, migration to PLN is dependent on the leukocyte expressed $\alpha_L\beta_2$ integrin (CD11a/CD18), also known as lymphocyte function-associated antigen-1 (LFA-1). Migration to sites of inflammation depends on the $\alpha_M\beta_2$ integrin (CD11b/CD18), also known as macrophage-1 antigen (Mac-1), the $\alpha_4\beta_1$ integrin (CD49d/CD29), also known as very late activation-4 (VLA-4) antigen, and/or LFA-1. The $\alpha_4\beta_7$ integrin is primarily responsible for migration to mucosa-associated lymphoid tissue in the gut. The major binding partner of LFA-1 and Mac-1 are the intercellular adhesion molecules ICAM-1 and ICAM-2. Both of these molecules are constitutively expressed on endothelial cells; however, ICAM-1 is additionally upregulated upon endothelial activation by inflammatory mediators (243, 244). VLA-4 primarily binds to vascular cell adhesion molecule-1 (VCAM-1) expressed on inflamed endothelium (124). An alternative binding partner of α_4 is the β_7 integrin and the $\alpha_4\beta_7$ integrin dimer, via

binding to mucosal vascular addressin cell adhesion molecule-1 (MAdCAM-1), is responsible for leukocyte migration to mucosa-associated lymphoid tissues. Thus, the combination of adhesion molecules and chemokine receptors expressed by leukocyte subsets determines their migratory preferences in the steady state and inflammation.

Migration of myeloid leukocytes such as neutrophils and monocytes/macrophages to sites of inflammation is an important part of the innate immune response and an initial line of defense against invading pathogens. Due to the production of reactive oxygen and nitrogen species, a process called the respiratory burst, these cells directly kill pathogens in the inflammatory site. In addition, they release pro-inflammatory mediators and chemokines and thus play a further role in the activation and execution of the adaptive immune response. Finally, after the contraction of the immune response, they participate in the repair of the tissue damaged during the inflammatory processes. In the context of unresolved chronic inflammation; however, there is an abnormal accumulation of immature myeloid leukocytes with immunosuppressive functions, called myeloid-derived suppressor cells (MDSC). For instance, MDSC accumulate during cancer progression and are one of the major mechanisms of tumor-induced immunosuppression.

Most of the suppressive mechanisms of MDSC are related to the upregulation of arginase-1 and inducible nitric oxide synthase (iNOS), which control L-arginine metabolism. L-arginine depletion from the tumor microenvironment by these enzymes causes T cell unresponsiveness by interfering with signaling from the TCR complex and the IL-2 receptor on T cells. In addition, L-arginine deficiency also causes proliferative arrest of activated T cells. Furthermore, hydrogen peroxide and peroxynitrites, products of the cooperative function of arginase-1 and iNOS, cause apoptosis in antigen-activated

T cells (55, 56). Additional pro-tumor effects of MDSC include induction of regulatory T cells, as well as participation in the processes of angiogenesis within the tumor microenvironments and the establishment of distant site metastases.

Two major MDSC subsets have been identified morphologically: polymorphonuclear (PMN-MDSC) and monocytic (M-MDSC), which differ in frequency, immunosuppressive potency and mechanisms of immunosuppression (207, 245, 246). For instance, in mice, PMN-MDSC are usually more abundant than M-MDSC with some dependence of the M-MDSC/PMN-MDSC ratio on the type of tumor. However, M-MDSC are more suppressive on a per-cell basis *in vitro* (207, 245, 246). PMN-MDSC-mediated immunosuppression depends primarily on the upregulation of arginase-1 and ROS production, while M-MDSC-mediated immunosuppression depends on upregulation of both arginase-1 and iNOS and production of reactive nitrogen species (206). In light of these differences, it is important to discriminate between the two subsets when studying MDSC biology. In addition to their morphological differences, murine PMN-MDSC and M-MDSC can be identified by flow cytometry based on their expression of the markers CD11b (also known as α_M integrin and complement receptor type 3) and Gr-1. Specifically, PMN-MDSC and M-MDSC can be distinguished from non-myeloid cells by the expression of the myeloid-specific marker CD11b, while distinction between PMN-MDSC and M-MDSC is based on the expression levels of Gr-1: thus PMN-MDSC are identified as CD11b⁺Gr-1^{high}, while M-MDSC are identified as CD11b⁺Gr-1^{low}. However, this labeling combination usually results in a continuum of events with various levels of Gr-1 labeling, and a clear distinction between Gr-1^{low} and Gr-1^{high} populations remains ambiguous. The anti-Gr-1 antibody (Clone RB6-8C5) binds

epitopes present in two different proteins belonging to the Ly-6 superfamily: Ly-6C and Ly-6G. The substitution of the RB6-8C5 antibody in MDSC staining protocols with antibodies individually specific to Ly-6C and Ly-6G allows unambiguous distinction between PMN-MDSC and M-MDSC subsets (206). Thus, the CD11b⁺Gr-1^{high} PMN-MDSC are identified as CD11b⁺Ly-6G⁺Ly-6C^{low/-}, while the CD11b⁺Gr-1^{low} M-MDSC are identified as CD11b⁺Ly-6G⁻Ly-6C^{high}.

MDSC are generated in the bone marrow and accumulate in the blood, spleen, and tumor. Although MDSC are found in great numbers in the spleen, studies suggest that splenic MDSC have limited effect on the immune response to solid tumors compared to tumor-resident MDSC. Specifically, tumor-resident MDSC have higher expression of arginase-1 and iNOS and higher suppressive activity in assays of T cell function (4, 181). In addition, an immunosuppressive role of MDSC in the TDLN has also been demonstrated (1, 2, 5). These observations, together with the fact that the suppressive function of MDSC against T cells is dependent on cell proximity, highlight the importance of TDLN and tumor-resident MDSC in the suppression of anti-tumor T cell activation in the TDLN and anti-tumor T cell function within the tumor microenvironment. Thus, MDSC migration to TDLN and tumor may be a limiting factor in MDSC-mediated suppression of the anti-tumor T cell response.

Over the last two decades, parallel to a surge in cancer immunotherapy research, the study of tumor-induced MDSC has received increasing interest because these cells hinder the success of various immunotherapeutic methodologies. As a result, a significant number of studies have been published focused on elucidating the mechanisms of MDSC-mediated immunosuppression, as well as on developing strategies for MDSC

depletion and inhibition of their function. By contrast, there are far fewer studies of MDSC migration, most of which focus on the involvement of chemokines in MDSC recruitment. Importantly, the involvement of adhesion molecules in regulation of MDSC migration remains largely unknown. We previously demonstrated that MDSC from the blood and spleen of mice with 4T1 mammary carcinoma expressed L-selectin (see Fig. 4 in Chapter 2). In this part of the study, we demonstrated that MDSC expressed the integrins LFA-1 and Mac-1 involved in migration to PLN and inflammatory sites. In addition VLA-4 was differentially expressed at higher levels on M-MDSC relative to PMN-MDSC. By contrast, only a subset of M-MDSC expressed the $\alpha_4\beta_7$ integrin, involved in migration to mucosa-associated lymphoid tissues. We then evaluated the efficiency of MDSC migration, as well as the involvement of L-selectin in MDSC migration to secondary lymphoid tissues, such as the lymph nodes, and to inflammatory sites, such as the primary tumor. Specifically, using adoptive transfer experiments of L-selectin-deficient MDSC, we demonstrated involvement of L-selectin in the migration of PMN-MDSC, but not M-MDSC, to tumors and TDLN. However, the efficiency of MDSC migration to the TDLN was low. This observation is in agreement with the low MDSC numbers found in the TDLN (see Fig. 5 in Chapter 2) and questions the functional significance of TDLN-resident MDSC in the suppression of the anti-tumor T cell response in this tumor model.

MATERIALS AND METHODS

Cell lines and reagents

The 4T1 murine mammary carcinoma cell line (ATCC CRL 2539) was purchased from ATCC (Manassas, VA) and maintained as described in Chapter 2, “Materials and Methods.”

Antibodies used in the flow cytometry and fluorescence microscopy experiments included: FITC- or APC-conjugated, or biotinylated anti-CD11b (Clone M1/70, BD Biosciences, San Jose, CA); FITC- or PE-conjugated anti-Ly-6G (Clone 1A8, BD Biosciences); PerCP-Cy5.5- or PE/Cy7-conjugated anti-Ly-6C (Clone HK1.4, BioLegend, San Diego, CA; Clone AL-21, BD Biosciences), FITC-conjugated anti-Gr-1 (Clone RB6-8C5) and anti-CD11a (Clone M17/4); PE-conjugated anti-CD18 (Clone C71/16), anti- β_7 integrin (Clone M293), and anti- $\alpha_4\beta_7$ integrin (Clone DATK32); PE/Cy7-conjugated anti-CD29 (Clone HM β 1-1); AlexaFluor[®] 647-conjugated CD49d (Clone R1-2); biotinylated anti-CD34 (Clone RAM43, eBioscience, San Diego, CA). Biotinylated antibodies were detected with AlexaFluor[®] 350- or AlexaFluor[®] 488-conjugated avidin (Life Technologies, Grand Island, NY), or TRITC- or APC-conjugated neutralite avidin (SouthernBiotech).

EZ link-sulfo-NHS-biotin (Pierce, Rockford, IL) was used to label the surface of cells and subsequently track them in adoptive transfer assays. Normal goat serum (Sigma, St. Louis, MO) and HyClone[®] and normal horse serum (ThermoFisher Scientific, Waltham, MA) were used in buffers to reduce non-specific antibody labeling. Deoxyribonuclease I (DNase I) from bovine pancreas and collagenase type VIII from *Clostridium histolyticum* were used for tissue digestion (both from Sigma). Bovine serum

albumin fraction V, also used in the tissue digestion buffer, was purchased from ThermoFisher Scientific.

Animals and tumor induction

BALB/c (wild type) mice were originally purchased from the Jackson Laboratories (Bar Harbor, ME) and further housed and bred in a specific pathogen-free barrier facility at the University of Wisconsin-Milwaukee and screened regularly for pathogens. L-selectin^{-/-} mice were generated as described (247) and back-crossed against the BALB/c genetic background for twelve generations. All procedures were approved by the Animal Care and Use Committee of the University of Wisconsin-Milwaukee. Tumors were induced as described in Chapter 2, “Materials and Methods.”

Integrin labeling on MDSC

Spleens from advanced stage (4-5 weeks) 4T1 tumor-bearing BALB/c mice were harvested and single-cell suspensions were prepared as described in Chapter 2 “Materials and Methods.” To label for α_L integrin (CD11a) expression on MDSC, cells were incubated with a combination of APC-conjugated anti-CD11b, FITC-conjugated anti-Ly-6G, PE/Cy7-conjugated anti-Ly-6C, and PE-conjugated anti-CD11a antibodies. To label for β_2 integrin (CD18) expression, cells were incubated with a combination of APC-conjugated anti-CD11b, FITC-conjugated anti-Ly-6G, PE/Cy7-conjugated anti-Ly-6C, and PE-conjugated anti-CD18 antibodies. To label for α_4 integrin (CD49d) expression, cells were incubated with a combination of FITC-conjugated anti-CD11b, PE-conjugated anti-Ly-6G, PE/Cy7-conjugated anti-Ly-6C, and AlexaFluor[®] 647-conjugated anti-CD49d antibodies. To label for β_1 integrin (CD29) expression, cells were incubated with a combination of biotinylated anti-CD11b, FITC-conjugated anti-Gr-1, and PE/Cy7-

conjugated anti-CD29 antibodies. To label for β_7 or $\alpha_4\beta_7$ integrin expression on MDSC, cells were labeled with AlexaFluor[®] 647-conjugated anti-CD11b, FITC-conjugated anti-Ly-6G, PE/Cy7-conjugated anti-Ly-6C, and PE-conjugated anti- β_7 or anti- $\alpha_4\beta_7$ integrin antibodies. In the negative control samples, the anti-CD11a, anti-CD18, anti-CD49d, anti-CD29, anti- β_7 integrin, and anti- $\alpha_4\beta_7$ integrin antibodies were replaced with fluorochrome-conjugated isotype control antibodies. All samples were incubated for 30 min on ice. The biotinylated anti-CD11b antibody was detected by APC-conjugated avidin added for 30 min on ice. Following antibody labeling all cells were washed in PBS. All samples were then fixed in 1.5% formaldehyde in PBS and analyzed with a FACSCalibur flow cytometer (BD Biosciences) using BD CellQuest[™] Pro software. One to four experiments were analyzed per labeling combination.

Adoptive transfer assay

Spleen single-cell suspensions from advanced stage 4T1 tumor-bearing wild type or L-selectin^{-/-} mice were prepared as described in Chapter 2, “Materials and Methods.” At a concentration of 12.5×10^6 cells/ml, the spleen cells were labeled with 80 $\mu\text{g/ml}$ EZ link-sulfo-NHS-biotin in PBS for 15 min at room temperature with gentle mixing. The cells were washed 3 times with PBS, counted on a hemacytometer, and adjusted to 100×10^6 cells/ml. Forty million cells were injected i.v. into the lateral tail vein of wild type mice bearing mid stage (2-2.5 weeks) 4T1 tumors. In addition, aliquots of the spleen cell suspensions were immunolabeled against the MDSC markers CD11b, Ly-6G, and Ly-6C, the frequencies of CD11b⁺Ly-6G⁺Ly-6C^{low/-} PMN-MDSC and CD11b⁺Ly-6G⁻Ly-6C^{high} M-MDSC present in the injected population were determined with flow cytometry, and the total number of injected PMN-MDSC and M-MDSC was calculated. Sixteen

hours after injection, the recipient mice were euthanized. In some experiments, tumors from recipient mice were harvested and cryosectioned for immunofluorescence microscopy. Alternatively, blood, bone marrow, spleen, tumor, TDLN, and NDLN were collected and used to prepare single-cell suspensions as described in Chapter 2 “Materials and Methods.” The single-cell suspensions were labeled with APC-conjugated anti-CD11b, PE-conjugated anti-Ly-6G, PerCP/Cy5.5-conjugated anti-Ly-6C antibodies and AlexaFluor[®] 488-conjugated avidin for 30 min on ice, washed in PBS, fixed with 1.5% formaldehyde in PBS, and analyzed with flow cytometry. The number of migrated PMN-MDSC and M-MDSC in each tissue was determined by multiplying the frequency of biotinylated PMN-MDSC or M-MDSC present in each tissue by the total tissue cell count. The number of migrated PMN-MDSC or M-MDSC in each tissue was expressed as percentage of the total injected PMN-MDSC or M-MDSC, respectively.

Labeling of tumor cryosections for fluorescence microscopy

The tumor sections were fixed in -20°C acetone for 5 min and stored at -20°C until labeling. The sections were thawed for 5 min and rehydrated in PBS for 10 min. The sections were then incubated in 5% normal goat serum in PBS to block non-specific antibody binding. Antibody dilutions were prepared in 2% normal horse serum in PBS. To visualize the localization of biotinylated (*i.e.* transferred) MDSC, the tumor sections were incubated with fluorochrome-conjugated avidin and antibodies against the MDSC markers CD11b, Ly-6G, and Ly-6C for 30 min at room temperature. To visualize the localization of MDSC relative to blood vessels, the tumor sections were labeled with antibodies against the MDSC markers CD11b, Ly-6G, and Ly-6C, in combination with the blood vessel marker CD34. The slides were then washed for 5 min in PBS and

mounted in ProLong Gold[®] antifade mounting medium. The mounting medium was allowed to cure overnight and the tumor sections were imaged with a Nikon Eclipse TE2000-U epifluorescence microscope (Nikon Instruments Inc., Melville, NY) equipped with a Cool Snap ES digital monochromatic camera (Photometrics, Tuscon, AZ). The MetaVUE[™] software (Universal Imaging Corporation, Downingtown, PA) was used for imaging and analysis. Images are representative of a minimum of 3 independent experiments.

Statistical analysis

Data are presented as mean \pm SEM. Significant differences between sample means were determined using a Student's *t* test with $p < 0.05$ considered to be significant.

RESULTS

PMN-MDSC and M-MDSC from 4T1 tumor-bearing mice exhibit uniform expression of LFA-1 and Mac-1, but differential expression of VLA-4 and $\alpha_4\beta_7$ integrin

Leukocyte migration to PLN and sites of inflammation requires the orchestrated function of various signaling and adhesion molecules. L-selectin and integrins are among the leukocyte-expressed adhesion molecules. Using the 4T1 mouse breast cancer model, we previously demonstrated with flow cytometry that L-selectin is expressed by both PMN-MDSC and M-MDSC, albeit at lower levels on PMN-MDSC compared to M-MDSC (see Fig. 4 in Chapter 2). In this part of the study, we further examined the expression of various integrins on PMN-MDSC and M-MDSC. In these experiments, PMN-MDSC were identified as either CD11b⁺Gr-1^{high}, or CD11b⁺Ly-6G⁺Ly-6C^{low/-} and M-MDSC were identified as either CD11b⁺Gr-1^{low}, or CD11b⁺Ly-6G⁻Ly-6C^{high} (Fig. 14). CD11b is also known as α_M integrin, which combines with β_2 integrin (CD18) to form the $\alpha_M\beta_2$ heterodimer, known as Mac-1. The β_2 integrin also combines with α_L integrin (CD11a) to form the $\alpha_L\beta_2$ heterodimer known as LFA-1. Both LFA-1 and Mac-1 bind ICAM-1 expressed on HEV or inflamed endothelium and support migration to PLN and inflammatory sites. All myeloid leukocytes, including MDSC, express α_M integrin (CD11b). Specifically, in the 4T1 tumor model, PMN-MDSC and M-MDSC expressed similar levels of the α_M integrin (Fig. 14B). In addition, all 4T1 tumor-induced splenic MDSC also expressed α_L and β_2 integrins and no significant differences in the expression levels of these adhesion molecules were detected between PMN-MDSC and M-MDSC populations with flow cytometry (Fig. 15). Therefore, PMN-MDSC and M-MDSC

express similar levels of LFA-1 and Mac-1, both of which have the potential to support MDSC migration to tumors and TDLN via interactions with endothelium-expressed ICAM-1.

We also tested MDSC for expression of the α_4 integrin pairs $\alpha_4\beta_1$ (VLA-4) and $\alpha_4\beta_7$. Both VLA-4 and $\alpha_4\beta_7$ integrin bind VCAM-1, which is upregulated on inflamed endothelium, and to MAdCAM-1, constitutively expressed on HEV of mucosa-associated lymphoid tissues. However, VLA-4 binds with higher affinity to VCAM-1 and $\alpha_4\beta_7$ integrin binds with higher affinity to MAdCAM-1. Thus VLA-4 primarily supports migration to sites of inflammation, while $\alpha_4\beta_7$ integrin primarily supports migration to mucosa-associated lymphoid tissues. In the present study, α_4 integrin (CD49d) was expressed by all PMN-MDSC and M-MDSC from spleens of 4T1 tumor-bearing mice, albeit at 2.6-fold higher levels on M-MDSC compared to PMN-MDSC (Fig. 16A). The β_1 integrin (CD29) was also expressed by both subsets, albeit at 3-fold higher levels on M-MDSC (Fig. 16B). In contrast, expression of β_7 integrin was limited to a subset of M-MDSC (Fig. 16C). Similar results were obtained when MDSC were labeled with an antibody specific to the $\alpha_4\beta_7$ integrin pair, rather than the monomeric forms of either α_4 or β_7 integrins. Specifically, only a small subset of M-MDSC and none of the PMN-MDSC expressed the $\alpha_4\beta_7$ dimer (Fig. 16D). Taken together, these results demonstrate differential expression of VLA-4 and $\alpha_4\beta_7$ integrin, which may result in differential efficiency of migration to inflammatory sites and mucosa-associated lymphoid tissues.

MDSC migration to the tumor and TDLN is partially dependent on L-selectin

To determine whether L-selectin is involved in MDSC migration to tumors and TDLN, we compared *in vivo* migration of 4T1 tumor-induced MDSC from wild type and

L-selectin^{-/-} mice. Specifically, we biotinylated spleen cell suspensions from wild type or L-selectin^{-/-} mice with advanced stage 4T1 tumors and transferred the biotinylated cells into the circulation of wild type mice bearing medium stage 4T1 tumors. Advanced stage 4T1 tumor-bearing mice were used as donors because of the higher yield of MDSC, while recipients with smaller tumors were used to minimize the amount of endogenous circulating MDSC that may compete with the adoptively transferred MDSC for interactions with the endothelium within target tissues. In addition, single-cell suspensions of smaller tumors show less ambiguity and allow for a clearer subset distinction between PMN-MDSC and M-MDSC with flow cytometric analysis compared to larger, more advanced, tumors. Leukocytes can migrate to TDLN directly from the blood via HEV, as occurs normally during recirculation. Alternatively, leukocytes could first enter the tumor or peritumoral tissue, and then carried with the lymph, may enter the TDLN via the afferent lymphatics. To allow ample time for maximal leukocyte migration to TDLN directly from the bloodstream, but insufficient time for indirect entry via the lymphatic route, the transferred cells were allowed to circulate and migrate for 16 h before analysis. Following migration, the number of biotinylated PMN-MDSC and M-MDSC in the tested tissues was determined and expressed as a percentage of all initially injected PMN-MDSC and M-MDSC, respectively. The numbers of initially injected PMN-MDSC and M-MDSC were $13.1 (\pm 0.8) \times 10^6$ and $0.61 (\pm 0.09) \times 10^6$, respectively.

Sixteen hours after MDSC transfer, the largest number of recovered PMN-MDSC and M-MDSC were from the spleen of the recipient mice (approximately 9.6% of injected for either subset), independent of L-selectin expression (Fig.17, Table V). Per 1 ml of blood, there remained approximately 3.1% of the initially injected PMN-MDSC or

M-MDSC regardless of L-selectin expression. Mice have approximately 2 ml of blood and thus the extrapolated total number of circulating transferred PMN-MDSC or M-MDSC (around 6.2% of initially injected) would still be lower than that in the spleen. The numbers of biotinylated M-MDSC recovered from the bone marrow from both femurs of recipient mice was also independent of L-selectin expression, and comprised approximately 1% of the initially injected M-MSDC. By contrast, 2.4% and 1.3% of the initially injected wild type and L-selectin^{-/-} PMN-MDSC, respectively, were recovered from the bone marrow; however, this difference did not reach statistical significance ($p = 0.09$).

Smaller numbers of biotinylated MDSC were detected in the tumors. Specifically, 0.28% and 0.08% of the initially injected wild type and L-selectin^{-/-} PMN-MDSC, respectively, were recovered from the tumor, which represented a statistically significant 3.5-fold decrease in migration resulting from the loss of L-selectin expression (see lower graphs in Fig. 17, representing the same results as the upper graph, but on a smaller scale). By contrast, M-MDSC migration to tumors tended to decrease with the loss of L-selectin expression, but the decrease did not reach statistical significance ($p = 0.16$).

The inguinal PLN in the vicinity of the tumor in recipient mice was used as TDLN. The contralateral inguinal PLN from the same recipient mice was used as NDLN to show the baseline levels of MDSC migration to PLN in the absence of a nearby tumor. The NDLN is located in the vicinity of the mammary fat pad, which instead of 4T1 cell injection, received a vehicle control injection and did not develop a tumor. Of note, the TDLN was bigger than the NDLN (Table VI), which may in part be due to tumor-induced immune activation in the TDLN, resulting in increased recruitment and

proliferation of lymphocytes. In addition, establishment and growth of tumor metastases within the TDLN may also contribute to its increased size. Small numbers of biotinylated MDSC were recovered from TDLN and NDLN (Table V), suggesting inefficient migration of MDSC from the bloodstream to these secondary lymphoid organs. Loss of L-selectin expression on PMN-MDSC resulted in a 3.1-fold and 4.7-fold decrease in migration to TDLN and NDLN, respectively (Fig. 17, Table V). By contrast, M-MDSC migration to TDLN and NDLN was independent of L-selectin expression. These results were surprising in light of previously observed higher expression of L-selectin on splenic M-MDSC compared to PMN-MDSC (see Fig. 4A in Chapter 2).

Interestingly, M-MDSC migrated more efficiently to TDLN, NDLN and tumors compared to PMN-MDSC. Specifically, the percentages of injected wild type M-MDSC recovered from TDLN, NDLN and tumor were higher than PMN-MDSC by 38-fold, 9.4-fold and 2.5-fold, respectively (Fig. 17, Table V). This difference reached statistical significance only in the NDLN, while the p values for tumor and TDLN remained at 0.18 and 0.09, respectively. In the case of L-selectin^{-/-} MDSC, there was a statistically significant increase in efficiency of M-MDSC migration to TDLN, NDLN and tumor (129-, 62- and 3.5-fold higher, respectively) compared to PMN-MDSC.

Taken together, in the 4T1 breast cancer model, these results demonstrate that L-selectin supported PMN-MDSC migration to tumor, TDLN and NDLN. By contrast, M-MDSC migration to TDLN and NDLN was independent of L-selectin, while a role of L-selectin in M-MDSC migration to the tumor was not conclusively determined due to sample variability. However, the low efficiency of MDSC migration from the

bloodstream to lymph nodes suggests that this may not be the primary route of MDSC entry into the TDLN.

Sixteen hours after adoptive transfer of biotinylated spleen cells, tumor-infiltrating MDSC are localized outside or in the periphery of endogenous MDSC aggregates

To complement the flow cytometry results from the 16-h *in vivo* migration assays described above, we visualized the adoptively transferred biotinylated MDSC within the tumor using fluorescence microscopy. We had previously observed that in the 4T1 breast cancer model, tumor-infiltrating MDSC were not randomly distributed throughout the tumor, but were clustered together in aggregates. Results from the adoptive transfer experiments showed that while some of the transferred tumor-infiltrating MDSC were found located at the edges of endogenous MDSC aggregates, a similar number were found away from the aggregates, and virtually none were found inside the aggregates (Fig. 18A). These results suggest that MDSC likely enter tumors from blood vessels located outside of the aggregates and then migrate through the parenchyma to associate with existing aggregates. To visualize localization of blood vessels relative to the endogenous MDSC aggregates, tumor sections were labeled with antibodies against the endothelial cell marker CD34 and the MDSC markers CD11b, Ly-6C, and Ly-6G. Blood vessels were rarely observed within MDSC clusters, but often there were blood vessel networks in the vicinity of larger MDSC clusters (Fig. 18B). Single MDSC were often found in the immediate vicinity of the blood vessels and in some cases directly associated with the blood vessels, suggesting that these blood vessel networks may be a point of entry of MDSC into the tumor.

DISCUSSION

In leukocyte migration, L-selectin is one of the major adhesion molecules that mediates the initial interactions between the leukocyte and the endothelium. Specifically, leukocyte-expressed L-selectin interacts with endothelium-expressed ligands via rapid catch and release events, which allow the leukocyte to roll along the endothelial layer. During the rolling phase, the leukocyte via chemokine receptors senses chemokine signals displayed on the endothelium and activates the subsequent phases of migration, largely dependent on interactions between leukocyte-expressed integrins and endothelium-expressed immunoglobulin-like superfamily molecules. Leukocyte migration to PLN is an important part of immunosurveillance against infections and activation of adaptive immunity, while migration to inflammatory sites is vital for proper execution of the immune response followed by repair of damaged tissue. On the other hand, migration of immunosuppressive leukocytes, such as MDSC, to PLN and inflammatory sites is potentially critical for the suppression of immune response activation and execution, respectively.

The destination of a leukocyte during steady state and disease depends on the adhesion and signaling molecule profile of the leukocyte. In this part of the study we examined the expression of several integrins on PMN-MDSC and M-MDSC as well as the involvement of L-selectin in MDSC migration to TDLN and tumor in the mouse 4T1 breast cancer model. We demonstrated that all PMN-MDSC and M-MDSC from the spleen of tumor-bearing mice expressed the integrins LFA-1 and Mac-1 (Fig. 14 and 15), which can support migration to PLN and sites of inflammation. In addition, we demonstrated differential expression of the α_4 integrin (CD49d) between M-MDSC and

PMN-MDSC (Fig. 16). Specifically, all MDSC expressed CD49d, however the M-MDSC showed a 2.6-fold higher expression with flow cytometry. These results are in partial agreement with a previous report, which demonstrated that M-MDSC but not PMN-MDSC expressed CD49d in several mouse tumor models (248). The authors further proposed the use of CD49d as a marker, alternative to Gr-1 or Ly-6C and Ly-6G, for the identification and distinction between the M-MDSC and PMN-MDSC subsets. Based on our data, such use is also feasible with the 4T1 tumor model; however, the distinction between the two subsets would be based on high *vs.* low levels of CD49d. It is possible that the expression of CD49d on MDSC subsets is dependent on the type of tumor, and that unique combinations of tumor-derived factors determine the phenotype of MDSC subsets in different types of cancer.

CD49d (α_4 integrin) combines with the β_1 integrin to form VLA-4 or with less preference, with the β_7 integrin. VLA-4 and $\alpha_4\beta_7$ integrin have somewhat overlapping functions, but VLA-4 is primarily involved in migration to inflammatory sites, while $\alpha_4\beta_7$ integrin is involved in migration to mucosal lymphoid tissues in the gut. An alternative partner for the β_7 integrin is the α_E integrin and the $\alpha_E\beta_7$ heterodimer, via interaction with its primary ligand E-cadherin, is also involved in leukocyte migration and retention in mucosal lymphoid tissues in the gut (249). Similar to CD49d (α_4 integrin), the β_1 integrin was also expressed by both subsets, albeit at higher levels on M-MDSC (Fig. 16). By contrast, the β_7 integrin and the $\alpha_4\beta_7$ heterodimer were expressed on a small subset of M-MDSC and absent from PMN-MDSC. Although we did not test for expression of the α_E integrin, given the limited expression of the β_7 integrin, it is likely that efficient migration

to mucosal lymphoid tissues in the gut would be possible only for a small subset of M-MDSC.

In adoptive transfer experiments, L-selectin was involved in PMN-MDSC migration to the TDLN, NDLN, and the tumor; however, the efficiency of PMN-MDSC migration, especially to the lymph nodes, was low. On the contrary, M-MDSC migration to the TDLN and NDLN was independent of L-selectin expression suggesting a compensatory role of other adhesion molecules mediating the capture and fast rolling of M-MDSC. For instance, α_4 integrins, such as VLA-4, via interactions with VCAM-1 have been reported to mediate capture and rolling of lymphocytes, myeloid cell lines, and hematopoietic progenitor cells both *in vitro* and *in vivo* (71, 72, 250-252). Interestingly, reports suggest that α_4 integrins are constitutively active and have higher binding affinities in hematopoietic progenitor cells (253, 254). M-MDSC expressed high levels of VLA-4 (Fig. 16) and their close relation to hematopoietic progenitors suggests a possibility for constitutive activation and a high binding affinity of this integrin. In addition, P-selectin expressed on endothelium in response to inflammatory mediators, such as TNF- α , IL-1 β , ROS, *etc.*, may also mediate M-MDSC capture and rolling independently of L-selectin. That would require expression of P-selectin ligands such as PSGL-1 (255, 256) and heat stable antigen (CD24) (257) on M-MDSC. In addition, P-selectin expressed on activated platelets may support leukocyte migration to PLN or sites of inflammation in an L-selectin-independent manner via a process similar to secondary tethering. Specifically, activated P-selectin expressing platelets bound to circulating leukocytes via interactions with PSGL-1 may serve as a bridge to potentiate tethering and rolling interactions over vascular endothelium or HEV that express P-selectin ligands,

including PNAd. For instance, this mechanism of L-selectin-independent lymphocyte homing to PLN has been implicated in the restoration of lymphocyte homing to PLN by injection of activated platelets into the circulation of L-selectin^{-/-} mice (104, 105). Furthermore, a similar mechanism has been implicated in the migration of myeloid leukocytes to inflamed tissues in models of inflammatory diseases (106, 109, 258). In addition to their role in mediating leukocyte capture and rolling, activated platelets are also involved in the upregulation of leukocyte and endothelial adhesion molecules, as well as in the deposition of inflammatory mediators for leukocyte recruitment to sites of inflammation (109, 259, 260). Thus, activated platelets, rather than L-selectin, may play a critical role in MDSC migration to tumors or TDLN. Such an assumption is in agreement with a well-established relationship between platelet activation and tumor progression. Specifically, various types of cancer are associated with increased platelet count (thrombocytosis) (261-267) and activation (268-272), resulting from tumor-derived factors that drive the generation and differentiation of megakaryocytes, the precursors of platelets, in the bone marrow, as well as platelet activation in the bloodstream and in the tumor microenvironment (273-278). In turn, activated platelets aid in tumor progression via a variety of mechanisms, including the promotion of tumor metastasis, angiogenesis, and inflammation, and increased platelet counts correlate with poor prognosis (279, 280). In light of these findings, the involvement of activated platelets in MDSC migration to tumors and TDLN, as well as other effects of putative MDSC-platelet interactions on cancer progression, warrants further investigation.

Interestingly, Ly-6C expressed at high levels on M-MDSC has been shown to enhance the homing of a subset of memory lymphocytes to lymph nodes via interaction

with an unknown ligand expressed on HEV (212). Specifically, antibody crosslinking of Ly-6C resulted in clustering of LFA-1 on the lymphocyte surface and increased adhesion to ICAM-1. Individual blockade of Ly-6C or L-selectin binding resulted in similar degrees of inhibition of lymphocyte recruitment to lymph nodes and combined blockade of both Ly-6C and L-selectin did not result in further inhibition (212). Therefore, it was concluded that Ly-6C may function downstream of L-selectin in a shared PLN homing pathway in the tested memory lymphocyte subset, which involves LFA-1. However the requirement of Ly-6C for PLN homing is not universal, because naïve lymphocytes, which home successfully to PLN, do not express Ly-6C. In addition, whether Ly-6C is involved in M-MDSC migration to lymph nodes and tumor is unknown. In the absence of L-selectin, Ly-6C expressed on M-MDSC may play a compensatory role in the recruitment to lymph nodes and tumor. If that is the case, the differential expression of Ly-6C on M-MDSC and PMN-MDSC may in part explain why Ly-6C^{low/-} PMN-MDSC migration to PLN and tumor was dependent on L-selectin, while the migration of Ly-6C^{high} M-MDSC did not depend on L-selectin expression. Furthermore, it is of interest to define the role of Ly-6C in M-MDSC migration, because Ly-6C may emerge as a candidate for targeted blockade of Ly-6C^{high} M-MDSC migration to PLN and tumor, while sparing the homing ability of Ly-6C⁻ lymphocytes to PLN.

Another interesting finding from the adoptive transfer experiments of MDSC into tumor-bearing animals is that M-MDSC migrated more efficiently to tumors and lymph nodes compared to PMN-MDSC. A higher efficiency of M-MDSC migration to TDLN and NDLN is in agreement with the increased M-MDSC/PMN-MDSC ratio in these tissues relative to that in the blood (see Fig. 6 in Chapter 2). However, the M-

MDSC/PMN-MDSC ratio in the tumor is as low as in the blood, suggesting that the more efficient M-MDSC migration to this site is countered by events promoting PMN-MDSC accumulation in the tumor. For instance, such events may include M-MDSC egress from the tumor or favored survival of PMN-MDSC in the tumor microenvironment compared to M-MDSC. In addition, *in situ* proliferation of PMN-MDSC within the tumor microenvironment, or conversion of M-MDSC to PMN-MDSC may in theory lower the M-MDSC/PMN-MDSC ratio. Mature myeloid cells do not normally proliferate in peripheral tissues and mature monocytic cells do not differentiate into PMN cells. However, given the immature nature of MDSC, further differentiation or proliferation events outside of the bone marrow may not be fully excluded. For instance, it has been suggested that the spleen is a site of extramedullary proliferation of both M-MDSC and PMN-MDSC subsets (281) and that M-MDSC can differentiate to PMN-MDSC (282) in the tumor-bearing host. Interestingly, the M-MDSC-to-PMN-MDSC transition was the result of epigenetic histone deacetylase 2 (HDAC-2)-mediated transcriptional silencing of the retinoblastoma 1 gene (282). Inhibition of HDAC-2 activity favored the differentiation of M-MDSC to conventional macrophages and dendritic cells in culture. These findings provide a fresh perspective on the use of HDAC inhibitors as anti-cancer drugs, as restoration of normal myeloid cell differentiation may remove MDSC-mediated immunosuppression from the tumor-bearing host and improve immunotherapy.

It remains unclear why M-MDSC seemed to migrate more efficiently than did PMN-MDSC to lymph nodes and tumor. One possibility is a preferential expression of appropriate chemokine receptors on M-MDSC. Interestingly, several chemokines and chemokine receptors are expressed at higher levels by M-MDSC than by PMN-MDSC in

hepatocellular carcinoma (283). For instance, a study using both real-time PCR and flow cytometry, demonstrated dramatically higher levels of CC chemokine receptor 2 (CCR2) on M-MDSC relative to PMN-MDSC (283). In cancer and other inflammatory conditions, CCR2 is involved in the egress of monocytic cells from the bone marrow and their migration to the tumor or inflammatory site (284-287). A role of CCR2 in directing myeloid cell recruitment to reactive lymph nodes after virus infection has been demonstrated (288); however, the significance CCR2 signaling in M-MDSC recruitment to the TDLN in cancer remains to be determined. The chemokine receptor CXCR2 was also differentially expressed on MDSC subsets in hepatocellular carcinoma, with higher levels present on PMN-MDSC than on M-MDSC (283). CXCR2 mediates the release of polymorphonuclear cells from the bone marrow to the bloodstream via interactions with its ligand CXCL2 expressed by bone marrow endothelial cells in response to inflammatory cytokines such as granulocyte colony stimulating factor (G-CSF) (289). In addition, production of G-CSF and CXCL2 within the tumor microenvironment is implicated in PMN-MDSC accumulation in the tumor (285), suggesting a role of CXCR2 in PMN-MDSC recruitment to the tumor. Collectively, these studies suggest that M-MDSC and PMN-MDSC migration to tumors may be differentially regulated by the various chemokines present in the tumor microenvironment.

FIGURE LEGENDS

Figure 14. Flow cytometric identification of PMN-MDSC and M-MDSC subpopulations.

Spleen single-cell suspensions from wild type mice bearing advanced stage 4T1 tumors were labeled with antibodies against CD11b, Ly-6C, and Ly-6G (A) or CD11b and Gr-1 (B) and analyzed with flow cytometry. FACS plots are representative of 5 independent experiments. Gated regions (C) included live cell gating based on forward and side light scatter (R1), followed by gating of M-MDSC (R3) and PMN-MDSC (R4) based on expression of CD11b (R2), Ly-6C, and Ly-6G, or CD11b and Gr-1.

Figure 15. Expression of α_L and β_2 integrins on PMN-MDSC and M-MDSC.

Spleen single-cell suspensions from wild type mice bearing advanced stage 4T1 tumors were labeled with APC-conjugated anti-CD11b, PE/Cy7-conjugated anti-Ly-6C, and PE-conjugated anti-Ly-6G in combination with FITC-conjugated anti-CD11a or isotype control antibody (A) or APC-conjugated anti-CD11b, PE/Cy7-conjugated anti-Ly-6C, and FITC-conjugated anti-Ly-6G in combination with PE-conjugated anti-CD18 or isotype control antibody (B). The expression levels of CD11a and CD18 on the MDSC subsets were determined with flow cytometry using constant voltage settings between experiments. FACS histograms are representative of 4 experiments with solid lines showing CD11a or CD18 expression levels on PMN-MDSC or M-MDSC and dashed lines showing isotype control labeling. Bar graphs represent the mean relative fluorescence intensity of CD11a-labeled (A) or CD18-labeled (B) PMN-MDSC and M-MDSC.

Figure 16. Expression of α_4 , β_1 , and β_7 integrins on PMN-MDSC and M-MDSC.

Spleen single-cell suspensions from wild type mice bearing advanced stage 4T1 tumors were labeled with FITC-conjugated anti-CD11b, PE/Cy7-conjugated anti-Ly-6C, and PE-conjugated anti-Ly-6G antibodies in combination with AlexaFluor[®] 647-conjugated anti-CD49d or isotype control antibody (A) or biotinylated anti-CD11b and FITC-conjugated anti-Gr-1 antibodies in combination with PE/Cy7-conjugated anti-CD29 or isotype control antibody (B) or biotinylated anti-CD11b and FITC-conjugated anti-Gr-1 antibodies in combination with PE-conjugated anti- β_7 integrin or isotype control antibody (C), or biotinylated anti-CD11b and FITC-conjugated anti-Gr-1 antibodies in combination with PE-conjugated anti- $\alpha_4\beta_7$ integrin or isotype control antibody (D). The expression levels of CD49d, CD29, β_7 integrin, and $\alpha_4\beta_7$ integrin were determined with flow cytometry using constant voltage settings between experiments. FACS histograms are representative of 1-4 experiments with solid lines showing CD49d, CD29, β_7 integrin, or $\alpha_4\beta_7$ integrin labeling levels on PMN-MDSC or M-MDSC and dashed lines showing isotype control labeling. Bar graphs represent the mean relative fluorescence intensity of CD49d-labeled (A) or CD29-labeled (B) PMN-MDSC and M-MDSC from 4 experiments. * $p < 0.05$ vs. PMN-MDSC.

Figure 17. *In vivo* migration of adoptively transferred 4T1 tumor-induced MDSC.

Wild type and L-selectin^{-/-} mice were injected s.c. with 10^4 4T1 cells into the mammary fat pad. Four to 5 weeks after tumor induction, the mice were euthanized and splenocytes were labeled with biotin. Forty million biotinylated spleen cells were injected i.v. into the lateral tail vein of wild type mice bearing mid stage 4T1 tumors, induced as above. The frequencies within the donor spleen suspensions of CD11b⁺Ly-6G⁺Ly-6C^{low/-}

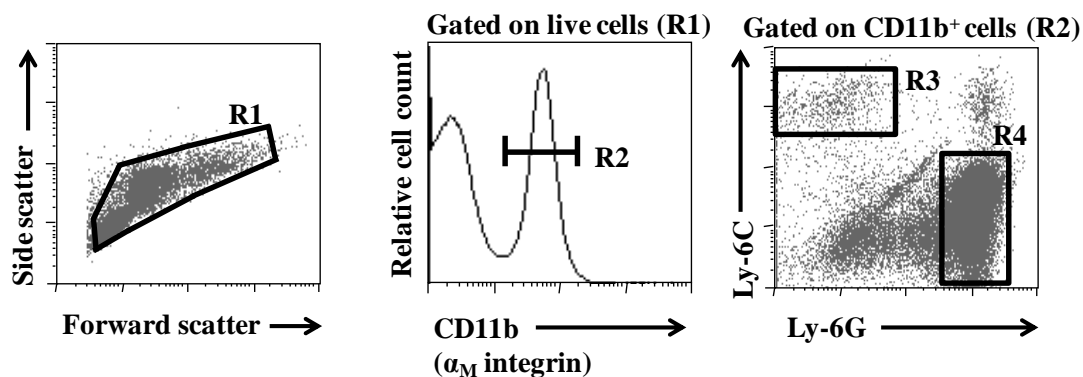
PMN-MDSC and CD11b⁺Ly-6G⁻Ly-6C^{high} M-MDSC were determined with flow cytometry and the total number of injected PMN-MDSC and M-MDSC was calculated. Sixteen hours after injection, the mice were euthanized and blood, and single-cell suspensions of bone marrow, spleen, tumor, TDLN and NDLN were labeled with fluorochrome-conjugated avidin and anti-CD11b, anti-Ly-6G, and anti-Ly-6C antibodies. The frequencies of biotinylated PMN-MDSC and M-MDSC in each tissue were determined with flow cytometry and the number of migrated PMN-MDSC and M-MDSC in each tissue was calculated. The number of migrated PMN-MDSC or M-MDSC in each tissue was expressed as percentage of the total number of initially injected PMN-MDSC or M-MDSC, respectively. The lower graphs represent the same results for tumor, TDLN and NDLN as the upper graph, but with decreased scales to better show the differences. Results are from 7-11 independent experiments. *p<0.05 vs. wild type.

Figure 18. Localization of migrated MDSC relative to blood vessels and endogenous MDSC clusters in the tumor microenvironment.

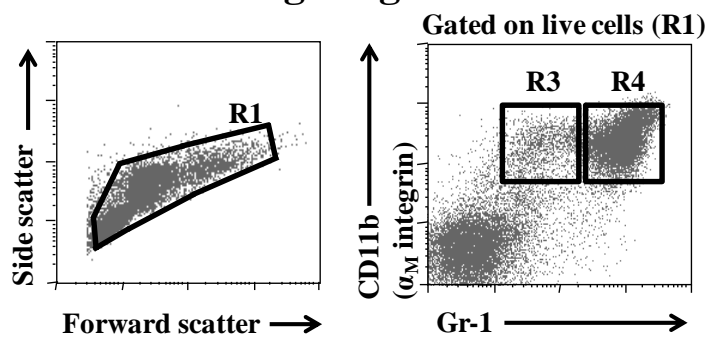
Biotinylated spleen cells from mice with advanced stage 4T1 tumors were injected i.v. into recipient mice bearing mid stage 4T1 tumors and recipients were euthanized 16h after the injection. A) Cryosections of tumors were labeled with TRITC-conjugated avidin and APC-conjugated anti-CD11b, FITC-conjugated anti-Ly-6G and PerCP/Cy5.5-conjugated anti-Ly-6C antibodies. The sections were analyzed by fluorescence microscopy with digital monochromatic images acquired at a constant exposure, and pseudocolored and overlaid using MetaVue™ software. Overlays include Ly-6G (green), avidin (red), and Ly-6C (blue). CD11b was not included in overlays for the sake of clarity. Tumor cryosections from mice that were not injected with biotinylated

donor spleen cells were labeled the same way and used as negative control for avidin labeling. Thus, representative images are of biotinylated CD11b⁺Ly-6G⁺Ly-6C^{low/-} PMN-MDSC associated with MDSC clusters (white arrows) and biotinylated CD11b⁺Ly-6G⁺Ly-6C^{low/-} PMN-MDSC localized outside of the MDSC clusters (yellow arrows). B) Tumor cryosections from mice with mid stage 4T1 cancer were labeled with biotinylated anti-CD34 (blood vessel marker, detected with TRITC-conjugated avidin), APC-conjugated anti-CD11b, FITC-conjugated Ly-6G, and PerCP/Cy5.5-conjugated anti-Ly-6C antibodies, and analyzed by fluorescence microscopy as above. Overlays include Ly-6G (green), Ly-6C (red), and CD34 (blue) labeling. CD11b was not included in overlays for the sake of clarity. White arrows indicate CD11b⁺Ly-6G⁺Ly-6C^{low/-} cells associated with blood vessels. Images in A and B are representative of 3 independent experiments. Scale bar (100 μ m) is for all images.

A. CD11b/Ly-6C/Ly-6G gating



B. CD11b/Gr-1 gating

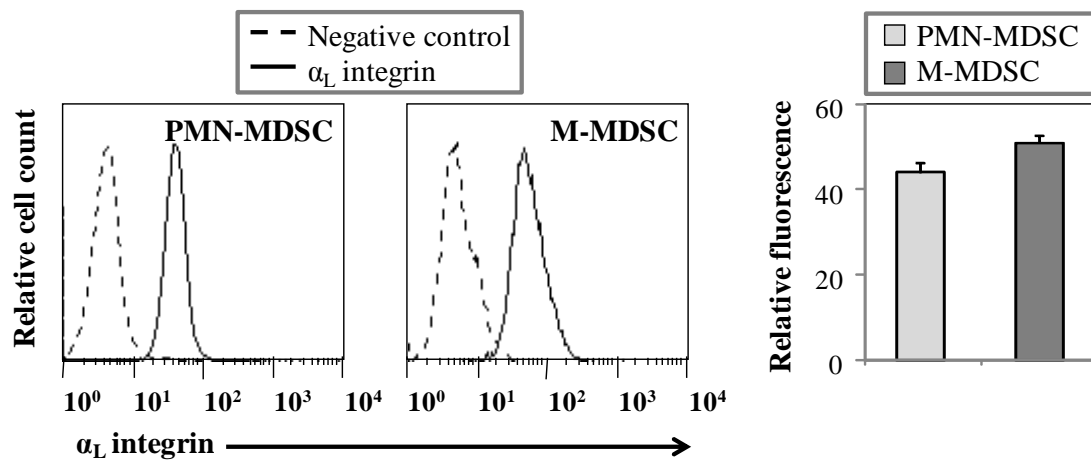


C. Gated regions

R1 – live cells
 R2 – CD11b⁺ cells
 R3 – M-MDSC:
 CD11b⁺Gr-1^{low} or
 CD11b⁺Ly6G⁺Ly-6C^{high}
 R4 – PMN-MDSC:
 CD11b⁺Gr-1^{high} or
 CD11b⁺Ly6G⁺Ly-6C^{low/-}

Figure 14

A. α_L integrin (CD11a)



B. β_2 integrin (CD18)

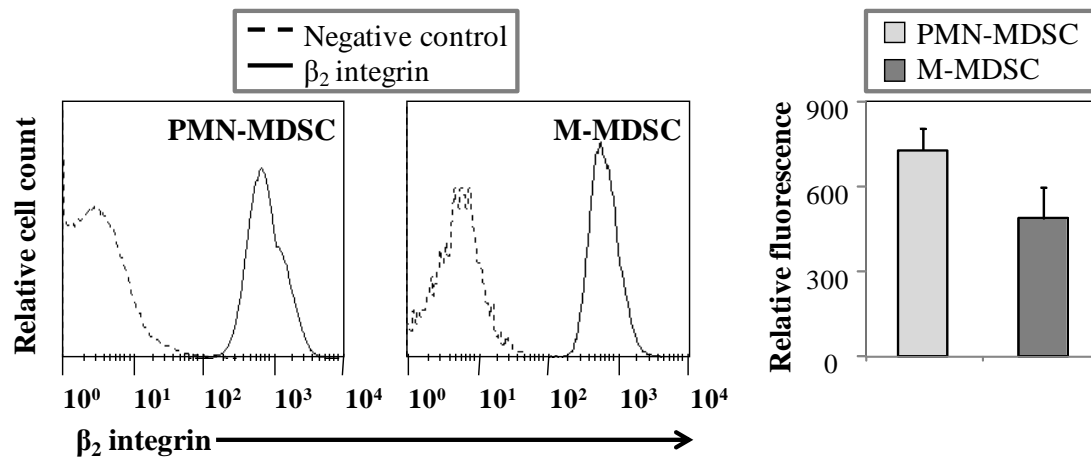
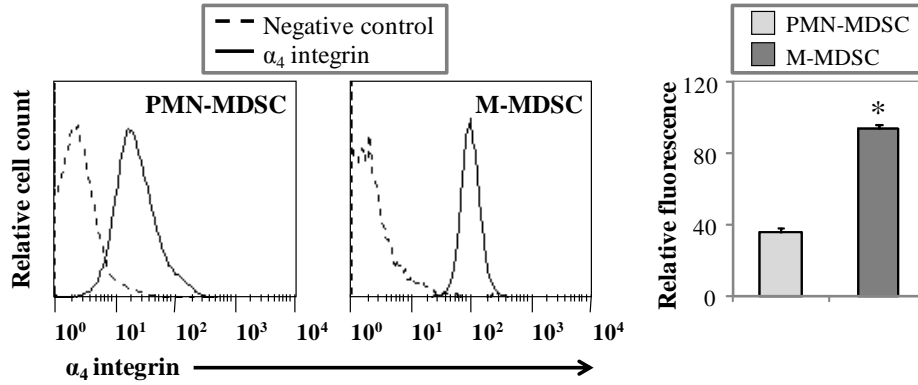
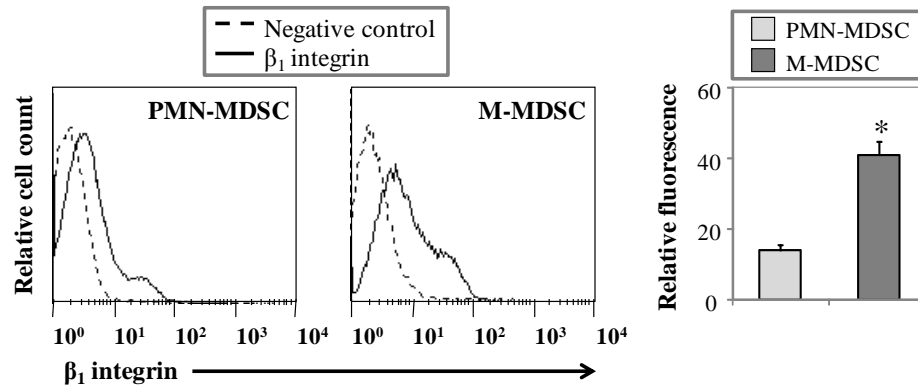


Figure 15

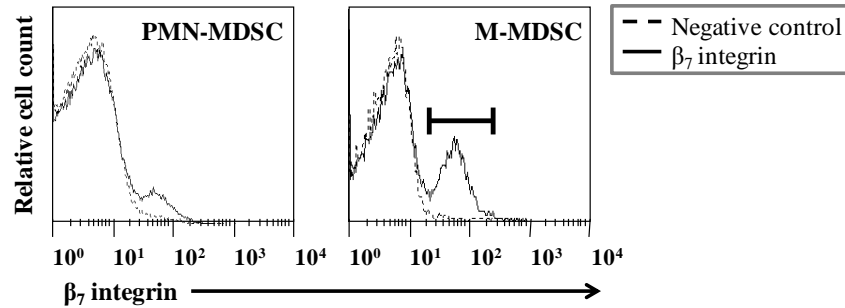
A. α_4 integrin (CD49d)



B. β_1 integrin (CD29)



C. β_7 integrin



D. $\alpha_4\beta_7$ integrin

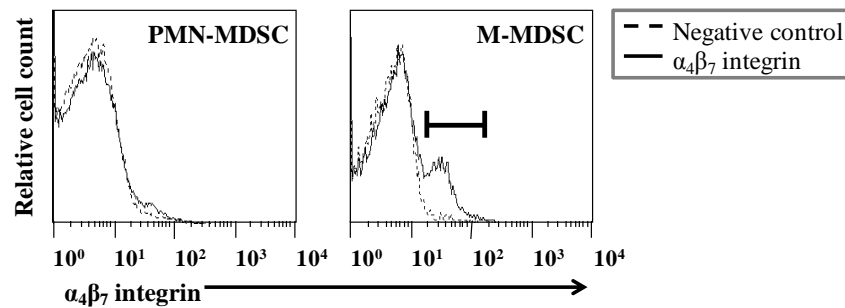


Figure 16

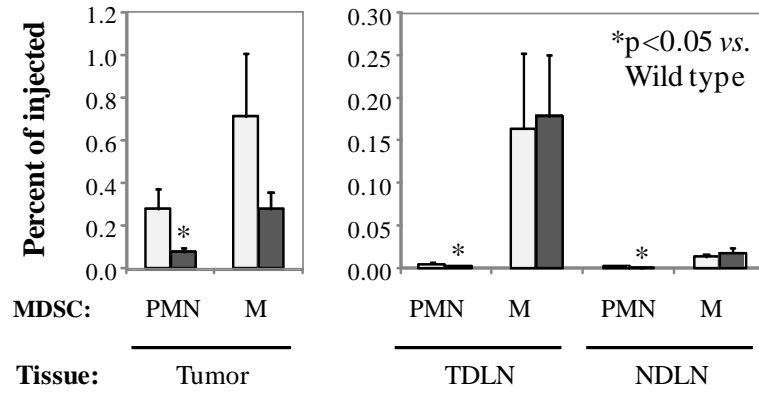
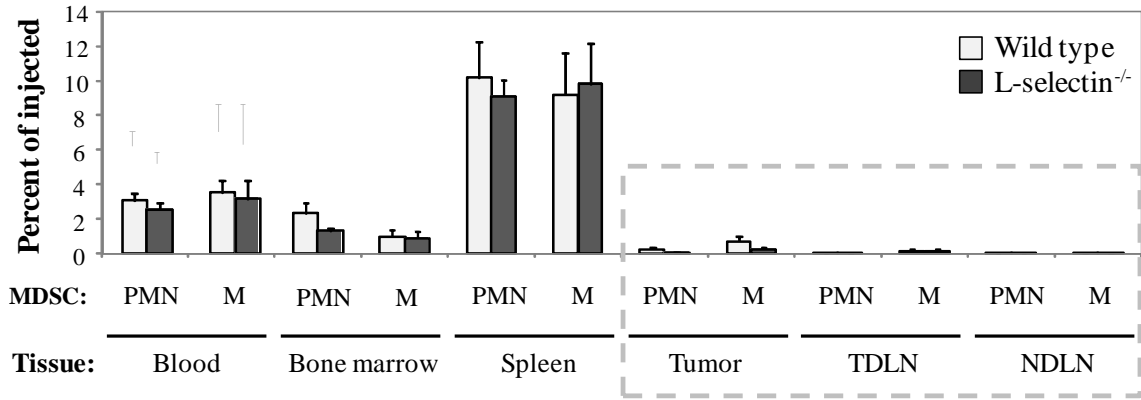
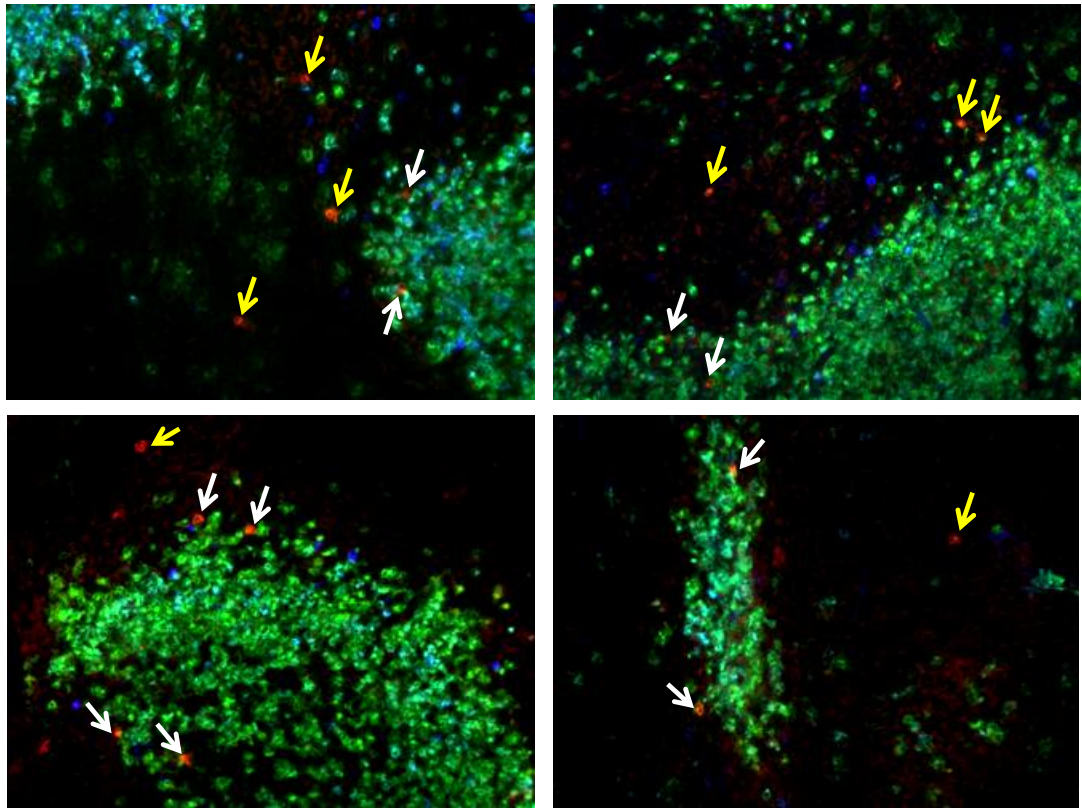


Figure 17

A. Ly-6G Ly-6C Biotin (migrated cells)



B. Ly-6G Ly-6C CD34 (blood vessels)

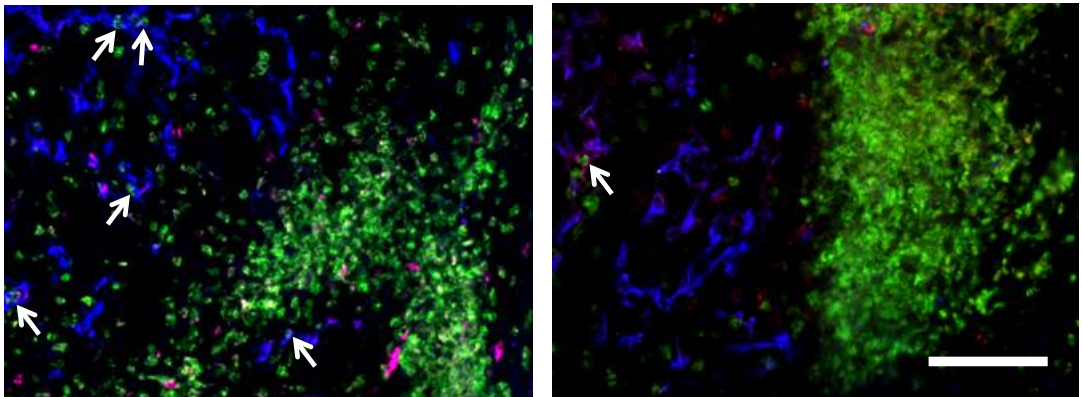


Figure 18

Table V. Efficiency of MDSC migration quantified as numbers and percent of injected PMN-MDSC and M-MDSC recovered 16 h after adoptive transfer^a

Numbers of recovered MDSC (x10⁻³)				
Donor genotype	Blood (1 ml)		Bone marrow	
	PMN-MDSC^b	M-MDSC	PMN-MDSC	M-MDSC
Wild type	385 ± 35	20 ± 5	328 ± 93	4 ± 1
L-selectin ^{-/-}	377 ± 81	12 ± 4	177 ± 27	4 ± 1

Donor genotype	Spleen		Tumor	
	PMN-MDSC	M-MDSC	PMN-MDSC	M-MDSC
Wild type	1,262 ± 213	49 ± 8	39.9 ± 14.1	2.4 ± 0.7
L-selectin ^{-/-}	1,223 ± 169	38 ± 4	12.3 ± 3.4	1.3 ± 0.4

Donor genotype	TDLN		NDLN	
	PMN-MDSC	M-MDSC	PMN-MDSC	M-MDSC
Wild type	0.50 ± 0.14	0.82 ± 0.25	0.16 ± 0.04	0.10 ± 0.03
L-selectin ^{-/-}	0.18 ± 0.06	0.57 ± 0.24	0.04 ± 0.01*	0.06 ± 0.01

Recovered MDSC (% of injected)				
Donor genotype	Blood (1ml)		Bone marrow	
	PMN-MDSC	M-MDSC	PMN-MDSC	M-MDSC
Wild type	3.1 ± 0.4	3.5 ± 0.8	2.4 ± 0.6	1.0 ± 0.4
L-selectin ^{-/-}	2.6 ± 0.3	3.2 ± 1.1	1.3 ± 0.1	0.9 ± 0.3

Donor genotype	Spleen		Tumor	
	PMN-MDSC	M-MDSC	PMN-MDSC	M-MDSC
Wild type	10.2 ± 2.1	9.2 ± 2.4	0.28 ± 0.09	0.71 ± 0.29
L-selectin ^{-/-}	9.1 ± 0.9	9.8 ± 2.4	0.08 ± 0.02*	0.28 ± 0.08

Donor genotype	TDLN		NDLN	
	PMN-MDSC	M-MDSC	PMN-MDSC	M-MDSC
Wild type	0.0043 ± 0.0013	0.1632 ± 0.0890	0.0014 ± 0.0004	0.0131 ± 0.0029
L-selectin ^{-/-}	0.0014 ± 0.0004*	0.1789 ± 0.0723	0.0003 ± 0.0001*	0.0184 ± 0.0057

^aWild type and L-selectin^{-/-} mice with advanced stage 4T1 tumors were euthanized and spleen single-cell suspensions were labeled with EZ link-sulfo-NHS-biotin. Forty million biotinylated spleen cells were injected i.v. into the lateral tail vein of wild type mice bearing mid stage 4T1 tumors. The frequencies within the donor spleen suspensions of CD11b⁺Ly-6G⁺Ly-6C^{low/-} PMN-MDSC and CD11b⁺Ly-6G⁺Ly-6C^{high} M-MDSC were determined by flow cytometry and the total number of injected PMN-MDSC and M-MDSC was calculated. Sixteen hours after injection, the mice were euthanized and blood, and single-cell suspensions of bone marrow, spleen, tumor, TDLN and NDLN were labeled with fluorochrome-conjugated avidin and anti-CD11b, anti-Ly-6G, and anti-Ly-6C antibodies. The numbers of migrated PMN-MDSC and M-MDSC were calculated from the frequencies of biotinylated PMN-MDSC and M-MDSC present in each tissue, determined by flow cytometry. Then, the number of migrated PMN-MDSC or M-MDSC in each tissue was expressed as percentage of the total number of initially injected PMN-MDSC or M-MDSC, respectively. *p<0.05 vs. wild type. Results are from 7-11 mice per genotype.

^bAbbreviations: PMN-MDSC, polymorphonuclear myeloid-derived suppressor cells; M-MDSC, monocytic myeloid-derived suppressor cells; TDLN, tumor-draining lymph node(s); NDLN, non-draining lymph node(s).

Table VI. Tissue cellularity of recipient mice bearing mid stage 4T1 tumors^a.

Recipient tissue cellularity (x10⁻⁶)	
Blood (1ml)	Bone marrow
17 ± 1	19 ± 2
Spleen	Tumor
125 ± 9	4 ± 0.4
TDLN^b	NDLN
17 ± 2	4 ± 0.4

^aMigration assays were performed as described in Table V. Following migration, blood and cells from the indicated tissues were counted on a hemocytometer. Results are from 15-19 mice per tissue.

^bAbbreviations used: TDLN, tumor-draining lymph node(s); NDLN, non-draining lymph node(s).

Table VII. Numbers of endogenous PMN-MDSC and M-MDSC in wild type recipient mice bearing mid stage 4T1 tumors^a.

MDSC count (x10⁻⁶)			
Blood (1 ml)		Bone marrow	
PMN-MDSC^b	M-MDSC	PMN-MDSC	M-MDSC
8.2 ± 0.8	0.4 ± 0.04	12.1 ± 1.3	0.5 ± 0.1
Spleen		Tumor	
PMN-MDSC	M-MDSC	PMN-MDSC	M-MDSC
22.3 ± 1.7	0.7 ± 0.08	0.37 ± 0.06	0.04 ± 0.01
TDLN		NDLN	
PMN-MDSC	M-MDSC	PMN-MDSC	M-MDSC
0.005 ± 0.001	0.020 ± 0.008	0.002 ± 0.0003	0.002 ± 0.0009

^aMigration assays were performed as described in Table V. Following migration, blood and cells from the indicated tissues were counted using a hemocytometer and labeled with fluorochrome-conjugated avidin and anti-CD11b, anti-Ly-6G, and anti-Ly-6C antibodies. The frequencies of resident PMN-MDSC and M-MDSC in each tissue were determined by flow cytometry and the total numbers calculated. Results are from 15-19 mice per tissue.

^bAbbreviations used: PMN-MDSC, polymorphonuclear myeloid-derived suppressor cells; M-MDSC, monocytic myeloid-derived suppressor cells; TDLN, tumor-draining lymph node(s); NDLN, non-draining lymph node(s).

CHAPTER 4

TUMOR-INFILTRATING MYELOID-DERIVED SUPPRESSOR CELLS
AGGREGATE NEAR REGIONS OF HYPOXIA WITHIN THE PRIMARY TUMOR

ABSTRACT

Areas of decreased tissue oxygenation (hypoxia) are a hallmark of the tumor microenvironment. Hypoxia-inducible factor (HIF) is an intracellular sensor of hypoxia, which functions to activate the expression of genes necessary for adaptation to hypoxia. There are several HIF isoforms with both overlapping and opposing roles in various processes, but overall hypoxia promotes tumor progression. In addition, it has been suggested that HIF activation in the tumor microenvironment increases the immunosuppressive activity of myeloid-derived suppressor cells (MDSC). MDSC expand in cancer and inhibit the function of anti-tumor effector T cells in the tumor microenvironment, thus severely suppressing the immune response. We previously observed that in the 4T1 mouse breast cancer model, tumor-infiltrating MDSC preferentially aggregated in the immediate vicinity of hypoxic regions. In this part of the study we quantified the extent of this co-localization, as well as addressed aspects of the dynamics of MDSC aggregate formation. Our results show that an average of 81% of MDSC aggregates localized next to areas of hypoxia. In addition, there was substantial contact between MDSC aggregates and hypoxic regions, averaging ~60% of total MDSC cluster circumference. We further demonstrated that MDSC enter the tumor in areas located outside of hypoxic regions and outside of MDSC aggregates, followed by migration through the tumor parenchyma to associate with MDSC aggregates. Interestingly, BrdU incorporation experiments showed that an average of 19% of tumor-infiltrating MDSC were undergoing *in situ* proliferation in the tumor microenvironment. Thus, in addition to MDSC recruitment to tumors, intratumoral proliferation of MDSC may also contribute to MDSC accumulation. It is of interest to determine the role hypoxia

plays in MDSC proliferation. As a preliminary experiment to test whether HIF induces proliferation of MDSC in the tumor microenvironment we treated mice with a HIF-activating drug. Although the treatment did not increase MDSC proliferation, the specific roles of the different HIF isoforms in MDSC recruitment, proliferation, and function in the tumor microenvironment require further study.

INTRODUCTION

The improperly upregulated proliferation of cancer cells causes tumors to outgrow the existing vasculature, reducing blood supply and consequently oxygen tension, a condition called hypoxia. Hypoxia is not a condition unique to cancer, but also occurs transiently in inflamed tissues due to increased metabolic activity of resident cells or recruited inflammatory cells (290, 291). Given the dependence of eukaryotic cells on oxygen, the existence of a mechanism for sensing and adapting to hypoxia is not surprising. The central pathway for adaptation to hypoxia is regulated by the transcription factor hypoxia-inducible factor-1 (HIF-1), a heterodimer of HIF-1 α and HIF-1 β subunits regulated by cellular oxygen tension (129). Specifically, both subunits are constitutively expressed (133), but in well-oxygenated (normoxic) environments, dioxygenase enzymes (PHD) hydroxylate an oxygen-dependent degradation domain (ODDD) of HIF-1 α thus marking the subunit for ubiquitination and proteasomal degradation (132, 133). Conversely, hydroxylation of ODDD does not occur in hypoxic conditions, resulting in stabilization of HIF-1 α (129, 131, 138) and its translocation to the nucleus, where it dimerizes with HIF-1 β and binds to hypoxia response elements (HREs) of target genes (139, 140). Thus HIF-1 α is also a sensor of intracellular oxygen levels. HIF-2 α is an isoform HIF-1 α , originally described in lung and endothelium (147, 148), but later it was demonstrated that HIF-2 α is detectable in hypoxic conditions in a wide range of tissues and cell types (155). HIF-2 α can bind HIF-1 β and HREs, but induces the expression of genes distinct from the HIF-1 target genes (147-151). Similar to HIF-1 α , in normoxic conditions, HIF-2 α protein levels are regulated by proline hydroxylation within the ODDD, and CBP/p300 coactivator binding to HIF-2 α is inhibited by asparagine

hydroxylation in the C-terminal transactivation domain (134). Inhibitors of PHD, such as dimethyl-oxalyl-glycine (DMOG), prevent the oxygen-induced degradation of HIF-1 α and HIF-2 α , thus activating HIF-1 and HIF-2 target genes in normoxic conditions.

Among the targets of HIF are genes that stimulate formation of new blood vessels (angiogenesis), growth of existing blood vessels (vasculogenesis), metabolic switch to anaerobic glycolysis, cell survival and proliferation, which ultimately help the tissue to adapt to and counteract oxygen deficiency. Thus, it is not surprising that in various types of cancer, intratumoral hypoxia and HIF-1 α stabilization aid in tumor growth and correlate with a poor prognosis (292). In addition, intratumoral hypoxia in a HIF-dependent manner promotes tumor metastasis by upregulating genes involved in various steps of the metastatic process, including formation of the pre-metastatic niche (216, 293-295). Furthermore, hypoxia, via HIF-1 and HIF-2, differentially regulates cell cycle progression. While HIF-1 stabilization favors cycle arrest (310-312), HIF-2 has been shown to induce proliferation (313-315). Importantly, intratumoral hypoxia may indirectly enhance tumor progression by increasing the immunosuppressive activity of MDSC. Specifically, it has been shown that tumor-infiltrating MDSC are more potent inhibitors of T cell function than splenic MDSC, likely due to HIF-1 α -mediated upregulation of arginase-1 and iNOS (4, 181).

Interestingly, in the 4T1 mouse breast cancer model, tumor-infiltrating MDSC aggregated next to hypoxic regions in the tumor microenvironment (see Fig. 11 in Chapter 2). In this part of the study we quantified the extent of this co-localization, as well as addressed aspects of the dynamics of MDSC aggregate formation. Our results demonstrate that the location of MDSC entry into the tumors is outside of hypoxic

regions and outside of the regions of MDSC aggregation. In addition, our results indicate that after their entry into tumors, the tumor-infiltrating MDSC migrate through the parenchyma to associate with MDSC aggregates. BrdU incorporation experiments further showed that in addition to MDSC recruitment to tumors, intratumoral proliferation of MDSC may also contribute to MDSC accumulation. A possible role of intratumoral hypoxia and HIF in the regulation of MDSC proliferation within the tumor requires further study.

MATERIALS AND METHODS

Cell lines and reagents

The 4T1 murine mammary carcinoma cell line (ATCC CRL 2539) was purchased from ATCC (Manassas, VA) and maintained as described in Chapter 2, “Materials and Methods.”

Antibodies used in the flow cytometry and fluorescence microscopy experiments include APC-conjugated, or biotinylated anti-CD11b (Clone M1/70, BD Biosciences, San Jose, CA), PE- or FITC-conjugated anti-Ly-6G (Clone 1A8, BD Biosciences), PerCP/Cy5.5- or PE/Cy7-conjugated anti-Ly-6C (Clone HK1.4, BioLegend, San Diego, CA; Clone AL-21, BD Biosciences), and biotinylated anti-CD34 (Clone RAM43, eBioscience, San Diego, CA). Biotinylated antibodies were detected with APC- or TRITC-conjugated Neutralite avidin (SouthernBiotech, Birmingham, AL). Hypoxiprobe™ RedAPC Kit, containing pimonidazole·HCl and APC-conjugated anti-pimonidazole antibody (Clone 4.3.11.3) or Hypoxiprobe™ 1 Omni Kit, containing pimonidazole·HCl and affinity-purified AlexaFluor® 647-conjugated anti-pimonidazole rabbit antisera (PAb2627AP) were purchased from Hypoxiprobe (Burlington, MA) and used to detect hypoxic regions in the tumor microenvironment with fluorescence microscopy.

EZ link-sulfo-NHS-biotin (Pierce, Rockford, IL) was used to track cells in adoptive transfer assays. Normal goat serum (Sigma, St. Louis, MO) and HyClone® normal horse serum (ThermoFisher Scientific, Waltham, MA) were used in buffers to reduce non-specific binding of antibodies. 5-Bromo-2-deoxyuridine (BrdU), a thymidine analog used to measure cell proliferation was purchased from Sigma. Deoxyribonuclease

I (DNase I) from bovine pancreas and collagenase type VIII from *Clostridium histolyticum* were used for tissue digestion (both from Sigma). Bovine serum albumin fraction V, also used in the tissue digestion buffer, was purchased from ThermoFisher Scientific. DMOG, a PHD inhibitor used to stabilize HIF- α *in vivo*, was purchased from Cayman Chemical (Ann Arbor, MI).

Animals and tumor induction

BALB/c (wild type) mice were originally purchased from the Jackson Laboratories (Bar Harbor, ME) and further housed and bred in a specific pathogen-free barrier facility at the University of Wisconsin-Milwaukee and screened regularly for pathogens. All procedures were approved by the Animal Care and Use Committee of the University of Wisconsin-Milwaukee. Tumors were induced as described in Chapter 2, “Materials and Methods.”

Labeling of tumor cryosections for fluorescence microscopy

4T1 tumor-bearing mice were injected i.p. with 60 mg/kg body weight of pimonidazole-HCl dissolved in PBS at a concentration of 5 mg/ml. One hour after the injection, the mice were euthanized and tumors were harvested. A middle slice of each tumor was snap frozen in tissue freezing medium (Triangle Biomedical Sciences, Inc, Durham, NC). Five- μ m thick tissue sections were cut on a cryostat, adhered to poly-L-lysine-coated microscope slides, fixed in -20°C acetone for 5 min and stored at -20°C until labeling. The sections were thawed for 5 min and rehydrated in PBS for 10 min. The sections were then incubated in 5% normal goat serum in PBS to block non-specific antibody binding. Antibody dilutions were prepared in 2% normal horse serum in PBS. To visualize the localization of MDSC relative to hypoxic regions within the primary

tumor, the sections were incubated with anti-pimonidazole antibody for 1 h at 37°C in a humidified chamber, followed by a 30-min incubation at room temperature with antibodies against the MDSC markers CD11b, Ly-6G, and Ly-6C. Alternatively, to visualize the localization of blood vessels relative to hypoxic regions within the primary tumor, the sections were incubated as above with anti-pimonidazole antibody and then followed by a 30-min incubation at room temperature with a biotinylated anti-CD34 antibody. The sections were then washed in PBS and the biotinylated anti-CD34 antibody was detected with TRITC-conjugated avidin. All sections were washed in PBS and mounted in ProLong Gold[®] antifade reagent for fluorescence. The samples were imaged using a Nikon Eclipse TE2000-U epifluorescence microscope (Nikon Instruments Inc., Melville, NY) equipped with a Cool Snap ES digital monochromatic camera (Photometrics, Tuscon, AZ). A minimum of 3 sections per tumor were labeled, out of which one representative section per tumor was used for further analysis. Successive images of tumor sections were taken in a scanning manner to visualize the whole tissue. Each image was assigned a number, by which the location of the image within the tissue could be determined. The MetaVUE[™] software (Universal Imaging Corporation, Downingtown, PA) was used for imaging and analysis. One tumor section per mouse from 3 mice per labeling combination was analyzed.

Analysis of MDSC localization relative to hypoxia

Images of Ly-6G (representing MDSC aggregates) and hypoxia staining were overlaid. For best accuracy, the hypoxic regions were outlined with the Ly-6G overlay turned off and the MDSC clusters were outlined with the hypoxic overlay turned off. The areas of the MDSC clusters, the hypoxic regions and the remaining part of the tissue were

recorded. The circumference of MDSC clusters and hypoxic areas, as well as the length of the contact border between the MDSC clusters and the hypoxic areas, were recorded. The number of MDSC clusters in contact with hypoxia and the number of MDSC clusters located separate from hypoxia were recorded. It was taken into account that some MDSC clusters spanned 2 or more images and these clusters were scored only once.

Analysis of blood vessel localization relative to hypoxia

Images of CD34 and hypoxia labeling were overlaid. Three region categories were assigned and outlined: hypoxic (HP), corresponding to hypoxia labeling; near-hypoxic (near-HP), located within 100 μm from the border of the HP regions; and non-hypoxic (non-HP), located beyond 100 μm from the border of the HP regions. The areas of the HP, near-HP and non-HP regions were recorded. The number and lengths of CD34⁺ blood vessels in each region were recorded.

Adoptive transfer assay

Splenic single-cell suspensions from 4T1 tumor-bearing donor mice were prepared, biotinylated and injected into tumor-bearing recipient mice as described in Chapter 2, "Materials and Methods." One or 47 h after injection, the recipients were injected with pimonidazole-HCl as described above and euthanized 1 h later. Tumors were harvested, cryosectioned, fixed and stored as described above. The sections were then labeled to visualize the localization of biotinylated MDSC relative to hypoxic regions and endogenous non-biotinylated MDSC clusters in the tumor environment. Specifically, sections were thawed, rehydrated and blocked as described above. Then, the sections were incubated with anti-pimonidazole antibody for 1 h at 37°C in a humidified chamber, followed by a 30-min incubation at room temperature with TRITC-conjugated

avidin, FITC-conjugated Ly-6G, and PerCP/Cy5.5-conjugated anti-Ly-6C antibodies. The sections were then washed, mounted and visualized as described above. The localization of each detected biotinylated Ly-6G⁺Ly-6C^{low/-} or Ly-6G⁻Ly-6C^{high} cell relative to endogenous non-biotinylated MDSC clusters was defined as cluster-associated (within cluster) or not associated (outside of cluster) and recorded.

BrdU labeling

BrdU was used to quantify *in situ* MDSC proliferation in the bone marrow, spleen and tumor. BrdU is a thymidine analog that incorporates into replicating DNA during the S-phase of cell division. In its bound form, it can be detected by anti-BrdU antibody and dividing cells can be quantified with flow cytometry. Tumor-bearing mice were injected i.p. with a single dose of 100 µg/mg body weight of freshly prepared 10 mg/ml BrdU in PBS. The chemical was allowed to circulate for 1 h before mouse euthanasia. Single-cell suspensions of bone marrow, spleen and tumor were prepared as described in Chapter 2 “Materials and Methods.” Five million cells from bone marrow, spleen and tumor were labeled in a final volume of 200 µl with biotinylated anti-CD11b, PE/Cy7-conjugated anti-Ly-6C, and PE-conjugated anti-Ly-6G antibodies for 30 min on ice. The cells were then washed, resuspended in 500 µl of ice-cold 0.15 M NaCl, fixed by the drop-wise addition of 1.2 ml of 95% ethanol, and incubated for 30 min on ice. The cells were then washed in PBS and incubated in 1% paraformaldehyde and 0.1% Tween-20 in PBS for 30 min at room temperature to permeabilize cell and nuclear membranes and further fix cellular components. The cells were washed in PBS and incubated in 50 U/ml DNase I in DNase buffer (4.2 mM MgCl₂, 0.15M NaCl, pH 5) for 15 min at 37°C. After another wash in PBS, 5 µl of FITC-conjugated anti-BrdU or FITC-conjugated isotype-matched

irrelevant antibody (negative control), together with 1 μ l of APC-conjugated Neutralite avidin, was added to the cells and incubated for 30 min on ice. The cells were then washed, fixed in 1.5% formaldehyde in PBS, and analyzed with flow cytometry. First, live cells were gated based on their forward and side light scatter properties. Of the live cells, the CD11b⁺Ly-6G⁺Ly-6C^{low/-} PMN-MDSC and the CD11b⁺Ly-6G⁺Ly-6C^{high} M-MDSC were gated. Finally, the frequencies of BrdU⁺ cells in the PMN-MDSC or M-MDSC subsets were determined. Three to four mice were used per tissue.

DMOG treatment

The PHD inhibitor DMOG was used to enhance HIF-1 α and HIF-2 α stabilization in tumor-bearing mice. *In vivo*, maximal HIF- α stabilization is reached at 4 to 6 h after i.p. injection of DMOG (296). We tested 2 DMOG treatment regimens, which we termed “1-dose” or “2-dose” DMOG treatment. In the “1-dose” regimen, the tumor-bearing mice received an i.p. injection of 8 mg of DMOG in 0.5 ml of PBS. After seven hours, the mice were injected with BrdU as described above and 1 h after BrdU injection, the mice were sacrificed and the tumors were analyzed for BrdU incorporation in PMN-MDSC and M-MDSC subsets as described above. In the “2-dose” regimen, tumor-bearing mice were first injected i.p. with 8 mg DMOG, followed by a second i.p. injection of 8 mg DMOG 8 h after the first one. Thirteen hours after the second DMOG dose, the mice were injected with BrdU as described above, and 1 h after BrdU injection the mice were sacrificed and the tumors were analyzed for BrdU incorporation as described above. In control mice, the DMOG injections were substituted by PBS. Three to six mice were used per treatment.

Statistical analysis

Results are presented as mean \pm SEM. Significant differences between sample means were determined using a Student's *t* test with $p < 0.05$ considered to be significant.

RESULTS

Tumor-infiltrating MDSC are localized in aggregates of various sizes, most of which are found next to areas of hypoxia.

Tissue oxygenation, or lack thereof, is emerging as a major regulator of tumor progression, as it generates intracellular signals that modulate tumor cell metabolism, increase the metastatic potential of tumor cells, trigger tumor vascularization, and even increase the suppressive function of MDSC, thus leading to a more aggressive cancer phenotype. We used the 4T1 mouse breast cancer model to determine the localization of tumor-infiltrating MDSC relative to hypoxic regions in the primary tumor. Low oxygen tension within tumors was indirectly detected by binding of the intraperitoneally injected cell-permeable chemical pimonidazole·HCl to exposed thiol groups in the structures of proteins and peptides. Due to the reduction of protein disulfide bonds in hypoxic conditions, regions of low oxygen tension contain more thiol groups and retain the bound pimonidazole, which is then detected by antibody labeling. MDSC were not uniformly distributed within the tumor, but rather were localized together forming aggregates with only a few individual cells observed around the aggregates. Interestingly these MDSC clusters were often localized immediately next to areas of hypoxia (Fig. 19).

To quantify MDSC co-localization with hypoxic regions, images of tumor sections from 3 mice were collected in a scanning manner using epifluorescence microscopy (Fig. 20A). Hypoxic regions and MDSC aggregates were outlined (Fig. 20B), and the number of MDSC clusters co-localized next to hypoxic regions, as well as those localized separately from hypoxic regions, were counted. Although the total number of MDSC aggregates varied, most of the MDSC aggregates (81±8%) were co-localized next to hypoxic regions (Fig. 20C). This level of co-localization was unlikely to be random,

because the total area of MDSC clusters was only $8\pm 3\%$ of the entire tissue and the total hypoxic area was only $13\pm 1\%$ of the whole tissue (Fig. 20D). In addition to the percentage of area taken by MDSC clusters and hypoxic regions, the shape of these elements should also be considered when quantifying their co-localization, as more complex “branching” shapes may increase the chance of random co-localization. In the examined tumor sections, the shape of the MDSC aggregates was not complex and more often approximated an oval. The shape of the hypoxic regions displayed a minimal degree of “branching” in the 2D images without dominating the whole tissue. In most of the images, there was substantial contact between the hypoxic regions and MDSC clusters, and the MDSC clusters were often partially or entirely surrounded by hypoxia (Fig. 19). To quantify this aspect of co-localization, we measured the length of the outlines of the MDSC aggregates and hypoxic regions, as well as the length of the contact border between the MDSC aggregates and the hypoxic regions (Fig. 21A). Although there was some variability in the outline lengths, in all mice, most of the MDSC cluster outline ($63\pm 6\%$) was in contact with hypoxia (Fig. 21B). Collectively, these results demonstrate that tumor-infiltrating MDSC are predominantly located next to hypoxic regions in 4T1 tumors.

Blood vessels are evenly distributed between hypoxic and non-hypoxic regions within the 4T1 tumor microenvironment.

It was unclear whether the preferential MDSC localization next to hypoxic regions in the 4T1 tumors was due to the recruitment of MDSC from other locations within the tumor microenvironment or whether the MDSC clusters represented the preferential location of MDSC entry into the tumor, possibly due to blood vessel

enrichment in areas near hypoxia. To begin addressing this question, we quantified the number and length of blood vessels per unit of area in hypoxic regions, in regions near hypoxia (within 100 μm , near-hypoxic regions), and in regions farther than 100 μm away from hypoxia (non-hypoxic regions; Fig. 22A). There were no significant differences in the blood vessel density or the length of blood vessels per unit area between the regions defined as hypoxic, near-hypoxic and non-hypoxic (Fig. 22B). These results do not exclude the possibility that MDSC primarily enter tumors within near-hypoxic regions. However, a possible preferential use of any of the regions defined above as an entry point of MDSC into 4T1 tumors would not be due to blood vessel enrichment within the preferred region.

MDSC enter tumors within near- and non-hypoxic regions and migrate toward pre-existing MDSC aggregates.

We previously observed that 16 h after adoptive transfer of biotinylated MDSC into the circulation of tumor-bearing recipients, approximately 50% of the tumor-infiltrating biotinylated MDSC were found outside of endogenous MDSC aggregates and the remaining 50% were found in the periphery of the MDSC aggregates (see Fig. 18A in Chapter 3). In addition, in the vicinity of MDSC clusters, regions that stained rich in blood vessels were also often enriched in individually dispersed MDSC, some of which were associated with the blood vessels (see Fig. 18B in Chapter 3). This led us to hypothesize that MDSC enter tumors in areas in the vicinity of MDSC clusters, after which they migrate through the tumoral extracellular matrix to join clusters. To determine the location of initial MDSC entry into the tumor relative to hypoxic regions and MDSC clusters, we harvested recipient tumors 2 h after injection of biotinylated

MDSC and labeled tumor sections with avidin and antibodies against MDSC and hypoxia markers. Two hours after adoptive transfer, $92\pm 6\%$ of tumor-infiltrating biotinylated MDSC were localized in near-hypoxic and non-hypoxic regions outside of MDSC clusters, while the remaining 8% were found in the periphery of the MDSC aggregates and none was found within hypoxic regions (Fig. 23). To determine where the biotinylated MDSC accumulated over time, we harvested recipient tumors 48 h after injection of biotinylated MDSC and labeled tumor sections as above. Forty-eight hours after adoptive transfer, $91\pm 2\%$ of tumor-infiltrating biotinylated MDSC were now localized within MDSC clusters, including in the middle of the clusters, while the remaining $\sim 9\%$ were found outside of the MDSC aggregates and none was within hypoxic regions (Fig. 23). These results demonstrate that after adoptive transfer, MDSC are first located outside of MDSC clusters and over time accumulate inside the clusters, suggesting that upon their entry into tumors, the tumor-infiltrating MDSC were recruited to endogenous MDSC clusters.

MDSC proliferate within the 4T1 tumors.

The accumulation and aggregation of MDSC within 4T1 tumors are due to the extravasation of circulating MDSC followed by their migration through the tumoral extracellular matrix to the sites of aggregation. Previous studies have demonstrated that extramedullary MDSC proliferation occurs in the spleen of tumor-bearing mice (229, 230). If MDSC proliferation occurs similarly within the tumor, it may also contribute to the intratumoral accumulation of MDSC and aggregate formation. We used BrdU incorporation to determine whether MDSC proliferated within the tumor microenvironment. BrdU is a thymidine analog, which is incorporated within the DNA

double helix in the process of DNA replication during the S phase of the cell cycle. BrdU was injected i.p. into tumor-bearing mice and the mice were euthanized 1 h later. Thus, BrdU marked any cells that were in S phase within the 1-h period. One hour is not sufficient time for the completion of MDSC division and exit from the bone marrow or spleen and their subsequent extravasation into the tumor tissue. Therefore, the use of this time-frame allows the detection of *in situ* proliferation of MDSC within the tumor-microenvironment. From flow cytometric analysis of the CD11b⁺Ly-6G⁺Ly-6C^{low/-} PMN-MDSC and CD11b⁺Ly-6G⁻Ly-6C^{high} M-MDSC populations (Fig. 24A), we determined the frequency of BrdU⁺ proliferating cells within each of these subsets in the bone marrow, spleen and tumor (Fig. 24B). A higher frequency of M-MDSC, 31±4%, stained BrdU⁺ in the bone marrow compared to 7±0.6% of PMN-MDSC, while a difference in proliferative rate between the two subsets was not observed in the spleen or tumor. Importantly, both subsets of MDSC showed high levels of intratumoral proliferation, with an average of 19% being BrdU⁺. Relative to bone marrow, there was a 3-fold higher frequency of BrdU⁺ PMN-MDSC in the tumor, suggesting a higher proliferation rate of PMN-MDSC in the tumor, or a premature egress of proliferating PMN-MDSC from the bone marrow. By contrast, the frequency of tumor-infiltrating BrdU⁺ M-MDSC was 2-fold lower compared to that in the bone marrow, suggesting a lower proliferation rate of M-MDSC in the tumor. Importantly, the finding that the tumor is a site of high levels of extramedullary MDSC proliferation suggests that factors characteristic of the tumor microenvironment may drive this proliferation.

DMOG, an inhibitor of HIF- α degradation, did not increase the frequency of BrdU⁺ MDSC in the 4T1 tumor microenvironment.

Both HIF-1 α and HIF-2 α upregulate genes involved in cell proliferation. Generally, HIF-1 α and HIF-2 α have opposing effects on cell proliferation: HIF-1 α targets induce cell cycle arrest, while HIF-2 α targets induce proliferation. However, crosstalk between HIF-1 α signaling and inflammatory signaling via STAT3 or NF- κ B may upregulate genes that induce proliferation. It was of interest to determine whether hypoxia was one of the factors that caused the observed proliferation of MDSC in the tumor microenvironment. As a preliminary experiment in that direction of research, we asked whether additional HIF activation could produce a further increase in MDSC proliferation in the tumor microenvironment. We treated tumor-bearing mice with DMOG, an inhibitor of the PHD enzymes that mark HIF-1 α and HIF-2 α for degradation. DMOG causes HIF- α stabilization regardless of the cellular oxygenation levels, thus in effect mimicking hypoxic conditions and leading to hypoxia-independent upregulation of HIF-1 and/or HIF-2 target genes. *In vivo*, maximal HIF- α stabilization is reached at 4 to 6 h after i.p. injection of DMOG (296). We tested 2 DMOG treatment regimens, which we termed “1-dose” and “2-dose” DMOG treatment (Fig. 25A). In the “1-dose” regimen, tumor-bearing mice received 8 mg of DMOG, 7 h after which the mice were injected with BrdU and 1 h after BrdU injection, the mice were sacrificed and the tumors were analyzed for BrdU incorporation in PMN-MDSC and M-MDSC subsets. In the “2-dose” regimen, tumor-bearing mice were injected with 8 mg DMOG, followed by a second DMOG injection (also 8 mg) 8 h after the first. Thirteen hours after the second DMOG dose, the mice were injected with BrdU; 1 h after BrdU injection the mice were sacrificed

and the tumors were analyzed for BrdU incorporation into PMN-MDSC and M-MDSC subsets. There was no change in the frequency of BrdU⁺ PMN-MDSC or M-MDSC in tumors of mice that received the “1-dose” DMOG treatment relative to mice receiving vehicle control (Fig. 25B). In the mice that received the “2-dose” DMOG treatment the frequency of BrdU⁺ cells within the PMN-MDSC population decreased by 33% relative to control. The frequency of BrdU⁺ cells within the M-MDSC also appeared smaller (by 23%); however, this decrease did not reach statistical significance. Thus, the experiments using DMOG treatment *in vivo* did not demonstrate involvement of HIF in driving MDSC proliferation in the tumor microenvironment.

DISCUSSION

We previously observed that tumor-infiltrating MDSC aggregated next to hypoxic regions in the tumor microenvironment. In this part of the study we quantified the extent of this co-localization as well as addressed aspects of the dynamics of MDSC aggregate formation. In advanced 4T1 tumors, approximately 81% of MDSC aggregates counted within fluorescence microscopy images were localized next to areas of hypoxia (Fig. 20). The 2-D nature of the images leaves a possibility that some or all of the remaining 19% of MDSC aggregates that did not localize next to hypoxia in the observed sections may be in contact with hypoxic regions in farther, parallel Z-planes in the 3-D structure of the tumor. To quantify the extent of contact between MDSC aggregates and hypoxic regions, we determined the percentage of the 2-D MDSC cluster circumference that was in contact with hypoxia. There was substantial contact (63% of total MDSC cluster circumference) between MDSC aggregates and hypoxic regions (Fig. 21).

Despite the large extent of contact between MDSC clusters and hypoxic regions, the overlapping area between these elements of the tumor microenvironment appeared negligible. Interestingly, areas of MDSC clusters were largely non-hypoxic, while hypoxic regions contained only sparse numbers of MDSC. This suggests a possibility that hypoxic areas in the tumor may actually serve as a barrier to MDSC migration throughout the tissue, thus confining and concentrating MDSC within certain locations. Although myeloid cells rely primarily on anaerobic glycolysis for ATP production, thus being largely equipped to survive low oxygen conditions (297), hypoxic areas are unfavorable environments and unless there is a chemotactic gradient originating beyond the hypoxic area, it is not surprising that MDSC may not be “inclined” to enter hypoxic regions. Myeloid cells consume large amounts of oxygen, necessary for production of ROS. Thus,

there is a possibility that the MDSC clusters contribute to the generation of hypoxia, resulting in the observed preferential co-localization between MDSC clusters and hypoxic regions. However, that would imply that the highest levels of hypoxia should be observed within the MDSC aggregates, which, as indicated above, is not the case. Thus, a possibility remains that the MDSC aggregate formation, at least in its initial stages, may result from MDSC recruitment toward hypoxic tissues. Then, MDSC-derived chemotactic factors may drive further recruitment of MDSC. Indeed, adoptively transferred biotinylated MDSC initially localized outside of hypoxic regions or MDSC clusters and over time accumulated within MDSC clusters. This suggests the presence of a chemotactic gradient originating within the MDSC clusters.

As a major sensor of hypoxia and transcriptional activator of hypoxia-driven genes, HIF-1 α may play a role in the recruitment of MDSC toward hypoxic regions by inducing the secretion of chemotactic factors. For instance, among the products upregulated by HIF-1 are vascular endothelial growth factor (VEGF) and stromal cell-derived factor-1 (SDF-1, also known as CXCL12), a ligand for CXCR4 (298, 299). These factors synergistically recruit monocytic cells, pericytes and endothelial progenitor cells, which support angiogenesis within the tumor tissue (300-303). Whether these or other chemokines induced by HIF participate in the recruitment of MDSC to tumors remains to be determined. Interestingly, HIF-1 can also upregulate expression of CXCR4 on tumor cells, which has been implicated in tumor metastasis to tissues expressing CXCR4 ligands (304). A putative induction of CXCR4 expression on tumor-infiltrating MDSC, together with the increased SDF-1 levels, may constitute a HIF-1 α -dependent mechanism for MDSC retention within tumors.

In addition to suspected recruitment and retention of MDSC within tumors, hypoxia, via HIF-1 α , may generate pro-survival signals for MDSC, thus further contributing to the observed preferential localization of MDSC clusters near hypoxic regions. For instance, HIF-1 has been shown to cooperate with the transcription factors NF- κ B and STAT3, thus linking hypoxic and inflammatory signaling (305-309). STAT3 and NF- κ B are the major factors involved in MDSC expansion and acquisition of suppressive phenotype, respectively (18-22, 24). In addition, synergism between these transcription factors and HIF-1 in cancer may result not only in induction of genes involved in MDSC expansion and function, but also in the expression of genes favoring cell survival (*e.g.*, *BCL-XL*, *BCL-2*, *CXCR1*, *CXCR2*, *survivin*) and proliferation (*e.g.*, *c-Myc*, *cyclin D1*) (24, 305-309). Interestingly, using the BrdU incorporation method, we determined that an average of 19% of tumor-infiltrating MDSC were undergoing proliferation during the 1-h time-frame of BrdU exposure (Fig. 24). This short window of BrdU exposure eliminated a possible contribution of BrdU⁺ MDSC recruited from the bloodstream to the BrdU⁺ events detected in the tumor, thus ensuring that the presence of BrdU⁺ MDSC within the tumor was due to *in situ* proliferation. Interestingly, the frequency of intratumoral BrdU⁺ PMN-MDSC was 3-fold higher than in the bone marrow, suggesting that there may be signals within the tumor microenvironment that are stronger stimulators of PMN-MDSC proliferation compared to those in the bone marrow. The PMN-MDSC and M-MDSC populations found in extramedullary tissues are heterogeneous and likely include progenitor cells with some proliferative potential as demonstrated for the spleen and liver (229, 230). Thus, the high levels of intratumoral MDSC proliferation may also result from preferential recruitment of myeloid progenitor

cells with proliferative potential over myeloid cells at more advanced stages of differentiation that are unable to proliferate.

Hypoxia has been shown to play opposing roles in the regulation of cell proliferation. On one end, HIF-1 α stabilization in hypoxia may induce cell cycle inhibitors such as p21 and p27 resulting in cell cycle arrest (310-312). On the other hand, hypoxic stabilization of HIF-2 α , a HIF- α isoform homologous to HIF-1 α , promotes cell proliferation via several mechanisms (313-315). In addition, cross-talk between HIF-1 α signaling and other signaling pathways, such as STAT3 and NF- κ B, may also induce genes that activate cell cycle progression, as mentioned above. It remains to be determined whether intratumoral hypoxia serves as an inducer of the observed MDSC proliferation within the tumor microenvironment. As a preliminary experiment in that direction of research, we treated tumor-bearing mice with the PHD inhibitor, DMOG, which leads to HIF- α stabilization regardless of the cellular oxygenation levels, thus in effect mimicking hypoxic conditions. As is evident from the MDSC/hypoxia co-localization experiments, only 13 \pm 1% of the area of tumor sections labeled positive for the hypoxic probe pimonidazole-HCl (Fig. 20D). Therefore, the majority (87%) of the tumor microenvironment was not hypoxic. With the DMOG injection we sought to maximally stabilize HIF- α throughout the entire tumor and determine whether that results in an increase in MDSC proliferation. An 8-h treatment of tumor-bearing mice with a single dose of DMOG (“1-dose” regimen) did not affect the frequency of BrdU⁺ PMN-MDSC or M-MDSC compared to vehicle control (Fig. 25). A 22-h total treatment of tumor-bearing mice with 2 doses of DMOG, the second dose given 8 h after the first dose (“2-dose” regimen), resulted in a small decrease in the frequency of cycling PMN-MDSC

within the tumor. Notably, neither of the treatment regimens resulted in an increase in MDSC proliferation. However, this result does not conclusively exclude a role of HIF in driving MDSC proliferation within the tumor microenvironment. Specifically, it is possible that HIF- α is maximally activated in tumor-infiltrating MDSC and in this case, the DMOG treatment would not show an effect. Although MDSC do not stain as hypoxic, they can use hypoxia-independent mechanisms for HIF- α stabilization, allowing for the possibility of a more profound HIF activation than the relatively small hypoxic content in the tumor. For instance, MDSC produce nitric oxide, which stabilizes HIF- α subunits by nitrosylation of cysteine residues within the ODDD (316). Considering the opposing effects of HIF-1 α and HIF-2 α on cell proliferation, it would be of further interest to determine the expression levels of these subunits in tumor-infiltrating MDSC, as well as to dissect the mechanism via which hypoxia may affect recruitment, function, and proliferation of tumor-infiltrating MDSC.

FIGURE LEGENDS

Figure 19. Co-localization of MDSC clusters next to hypoxic regions in 4T1 tumors.

To visualize hypoxic regions within the tumor microenvironment, 4T1 tumor-bearing mice were injected with pimonidazole·HCl 1 h prior to euthanasia. Cryosections of tumors were labeled with antibodies against pimonidazole and the MDSC markers CD11b, Ly-6G and Ly-6C. The sections were analyzed with fluorescence microscopy. Digital monochromatic images were acquired at a constant exposure, and pseudocolored and overlaid using MetaVue™ software. Overlays include Ly-6G (green), Ly-6C (red), and pimonidazole (hypoxia probe, blue). CD11b was expressed by Ly-6G⁺Ly-6C^{low/-} and Ly-6G⁻Ly-6C^{high} cells, but was not included in overlays for the sake of clarity. Scale bars are 100 μm. Images are from 3 independent experiments and represent examples of MDSC clusters localized next to hypoxic regions.

Figure 20. Quantitation of co-localized MDSC clusters next to hypoxic regions in 4T1 tumors.

Three 4T1 tumor-bearing mice were injected with pimonidazole·HCl 1 h prior to euthanasia. A) The middle slice of each tumor was frozen. Cryosections of tumors were labeled with antibodies against pimonidazole and the MDSC markers CD11b, Ly-6G and Ly-6C. One cryosection was analyzed from each tumor with fluorescence microscopy. Digital monochromatic images were acquired in a scanning manner covering the entire section. B) Images of hypoxia (pimonidazole, blue) and Ly-6G (MDSC clusters, green) were pseudocolored and overlaid using MetaVue™ software. CD11b labeling corresponded to the Ly-6G-labeled clusters and most of the Ly-6C-labeled cells were included within the Ly-6G-labeled clusters. CD11b and Ly-6C labeling was not included

in overlays for the sake of clarity. The hypoxic regions and MDSC clusters were outlined (dashed line) and the areas of the hypoxic regions and MDSC clusters, as well as the area of the remaining tissue, were recorded. The number of co-localized MDSC clusters in contact with hypoxia and the number of the separate MDSC clusters not in contact with hypoxia were recorded. The scale bar is 100 μm . C) The number of co-localized MDSC clusters and the number of the separate MDSC clusters for each of the three analyzed tumor sections (1 per mouse; 3 mice used: Mo 1, Mo 2, and Mo 3) were plotted. The percentage of co-localized MDSC clusters out of the total number of MDSC clusters in each sample was calculated (white numbers in bar graph). D) The total areas of hypoxic regions, MDSC clusters and the remaining tissue areas were calculated and plotted for each of the 3 mice (Mo 1, Mo 2, and Mo 3). The percentage of hypoxic area out of the total tissue area for each mouse was calculated (grey numbers). The percentage of MDSC cluster area out of the total tissue area for each mouse was calculated (black bold numbers).

Figure 21. Quantitation of contact between MDSC clusters and hypoxic regions in 4T1 tumors.

Tumors were labeled and imaged as described for Fig. 20. A) Images of hypoxia (pimonidazole, blue) and Ly-6G (MDSC clusters, green) were pseudocolored and overlaid using MetaVue™ software. CD11b labeling corresponded to the Ly-6G-labeled clusters and most of the Ly-6C-labeled cells were included within the Ly-6G-labeled clusters. CD11b and Ly-6C labeling was not included in overlays for the sake of clarity. The hypoxic regions and MDSC clusters were outlined: the dashed line is the portion of the outline of hypoxic regions, which is not in contact with MDSC clusters (Hypoxia

only); the solid thin line is the portion of the outline of MDSC clusters, which is not in contact with hypoxic regions (MDSC only); the solid bold line represents the contact borderline between MDSC clusters and hypoxic regions (MDSC/Hypoxia border). The length of each line was recorded. Scale bar is 100 μm . B) The total lengths of the “Hypoxia only”, “MDSC only” and the “MDSC/Hypoxia border” lines were calculated for each of the 3 mice (Mo 1, Mo 2, and Mo 3) and plotted as numbers (left) and percentages (right).

Figure 22. Quantitation of blood vessels in areas of hypoxia, areas near hypoxia, and areas far from hypoxia in 4T1 tumors.

Tumors from pimonidazole-injected mice were sectioned as described for Fig. 20 and immunolabeled against pimonidazole and the blood vessel marker CD34. A) Images of hypoxia (pimonidazole, green) and blood vessels (CD34, red) were pseudocolored and overlaid using MetaVue™ software. Three region categories were assigned and outlined: hypoxic (HP) corresponding to hypoxia labeling, near-hypoxic (near-HP) located within 100 μm from the border of the HP regions, and non-hypoxic (non-HP) located beyond 100 μm from the border of the HP regions. The areas of the HP, near-HP and non-HP regions were recorded. The number and lengths of CD34⁺ blood vessels in each region were recorded. White arrows indicate examples of blood vessels in HP, near-HP and non-HP regions. Scale bar is 100 μm . B) The average numbers (left) and lengths (right) per unit of area from the three tumors were calculated and plotted for each region (HP, near-HP, and non-HP).

Figure 23. MDSC enter tumors in areas located outside of MDSC clusters and accumulate within MDSC clusters over time.

Spleen single-cell suspensions from 4T1 tumor-bearing donor mice were prepared, biotinylated and injected into tumor-bearing recipient mice. One or 47 h after injection, the recipients were injected with pimonidazole·HCl and euthanized 1 h later. Three tumors (from 3 mice) per time point were harvested, cryosectioned, fixed and labeled with avidin and antibodies against pimonidazole, Ly-6G and Ly-6C. Three sections per tumor were analyzed. A) Images of hypoxia (pimonidazole, blue), PMN-MDSC (Ly-6G, green) or M-MDSC (Ly-6C, not shown) and avidin (biotinylated migrated cells, red) were pseudocolored and overlaid using MetaVue™ software. The localization of each biotinylated MDSC (arrows) relative to endogenous non-biotinylated MDSC aggregates was defined as within or outside of the aggregates and the numbers of biotinylated MDSC in each of these two categories were recorded for each section. B) The total numbers of cluster-associated or not associated biotinylated MDSC from the three sections analyzed per tumor were summed and the sums of the three tumors analyzed per time point were averaged and plotted.

Figure 24. Quantitation of MDSC proliferation within bone marrow, spleen and tumor from mice with 4T1 breast cancer.

Tumor-bearing mice were injected i.p. with a single dose of 100 µg/mg body weight of freshly prepared 10 mg/ml BrdU in PBS. The BrdU was allowed to circulate for 1 h before mouse euthanasia. Single-cell suspensions of bone marrow, spleen and tumor were prepared and labeled with antibodies against CD11b, Ly-6C, Ly-6G and BrdU. In negative control samples, the anti-BrdU antibody was substituted with an

isotype-matched irrelevant antibody. MDSC proliferation was analyzed with flow cytometry. A) Live cells were gated based on their forward and side light scatter and the CD11b⁺ population was further analyzed (upper left). The CD11b⁺Ly-6G⁺Ly-6C^{low/-} PMN-MDSC and the CD11b⁺Ly-6G⁻Ly-6C^{high} M-MDSC were gated (upper right) and further analysed for BrdU expression (lower; the dashed line represents negative control labeling; the solid line represents BrdU labeling). Plots are representative of tumor samples. B) The frequencies of BrdU⁺ cells out of the PMN-MDSC (left) or M-MDSC (right) subsets were plotted for each tissue. Three to 4 mice were used per tissue. *p<0.05 vs. bone marrow (BM).

Figure 25. Effect of *in vivo* DMOG treatment on the proliferation of tumor-infiltrating MDSC.

Tumor-bearing mice were subjected to 1 of 2 alternative DMOG treatment regimens (“1-dose” or “2-dose”) or vehicle control. A) In the “1-dose” regimen, the tumor-bearing mice received an i.p. injection 8 mg of DMOG dissolved in 0.5 ml of PBS. Seven hours after DMOG administration, the mice were injected i.p. with 100 µg/mg body weight of freshly prepared 10 mg/ml BrdU in PBS. In the “2-dose” regimen, tumor-bearing mice were injected with 8 mg DMOG or vehicle control. Eight hours thereafter, the mice were injected with a second dose of DMOG or vehicle control. Thirteen hours after the second injection, the mice were injected with BrdU. One hour after BrdU injection, all mice were sacrificed and the tumors were analyzed for BrdU incorporation in PMN-MDSC and M-MDSC subsets with flow cytometry. B) The frequencies of BrdU⁺ cells out of the tumor-infiltrating PMN-MDSC (left) or M-MDSC (right) subsets

were plotted for each treatment regimen. Three to 6 mice were used per regimen; * $p < 0.05$
vs. vehicle control.

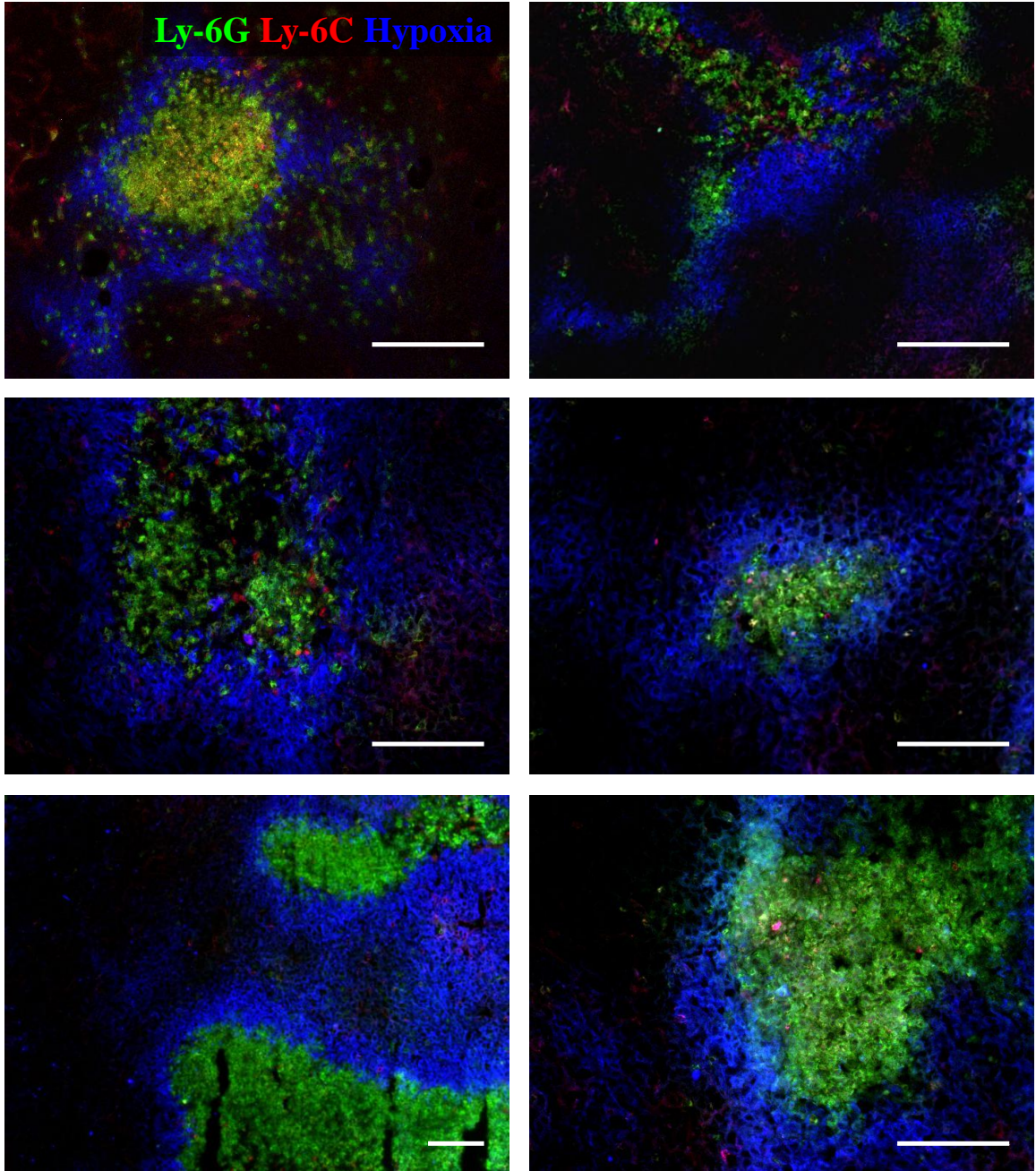


Figure 19

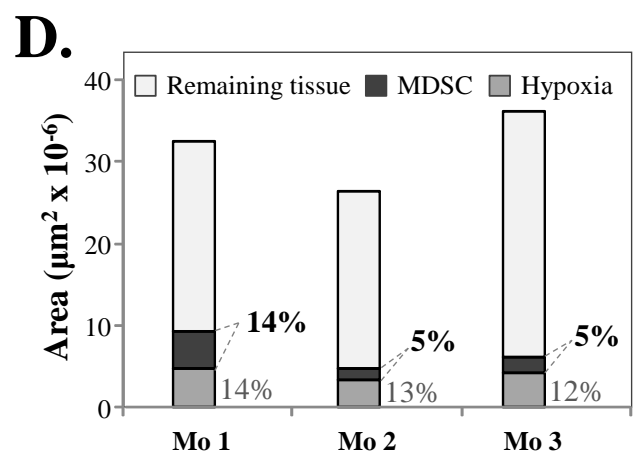
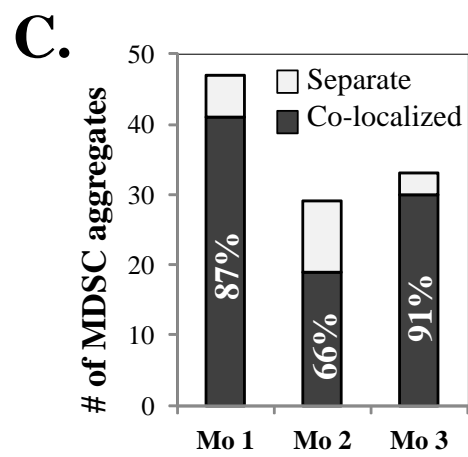
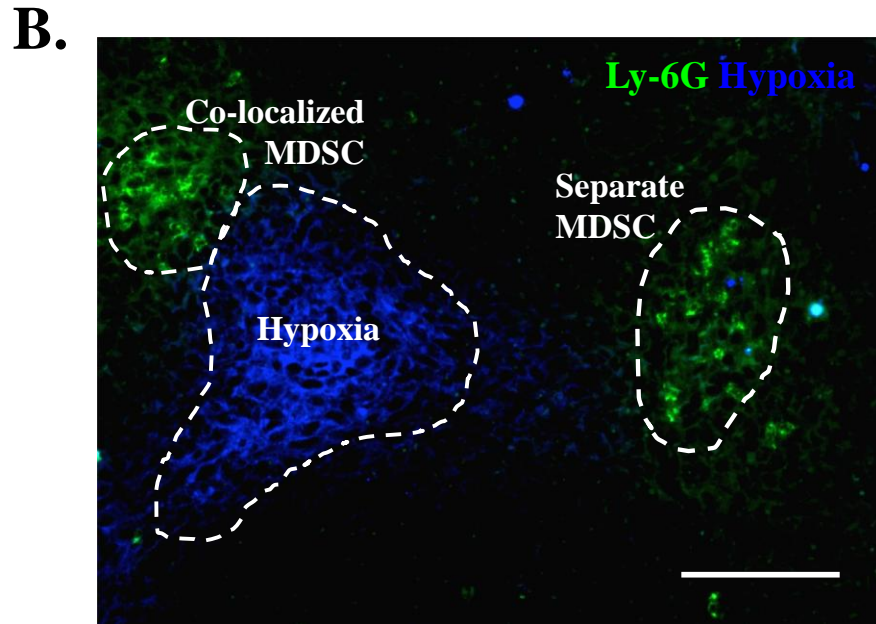
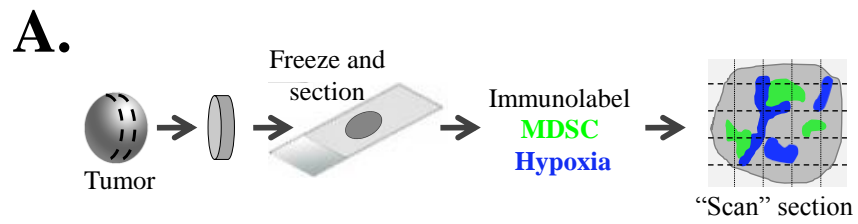
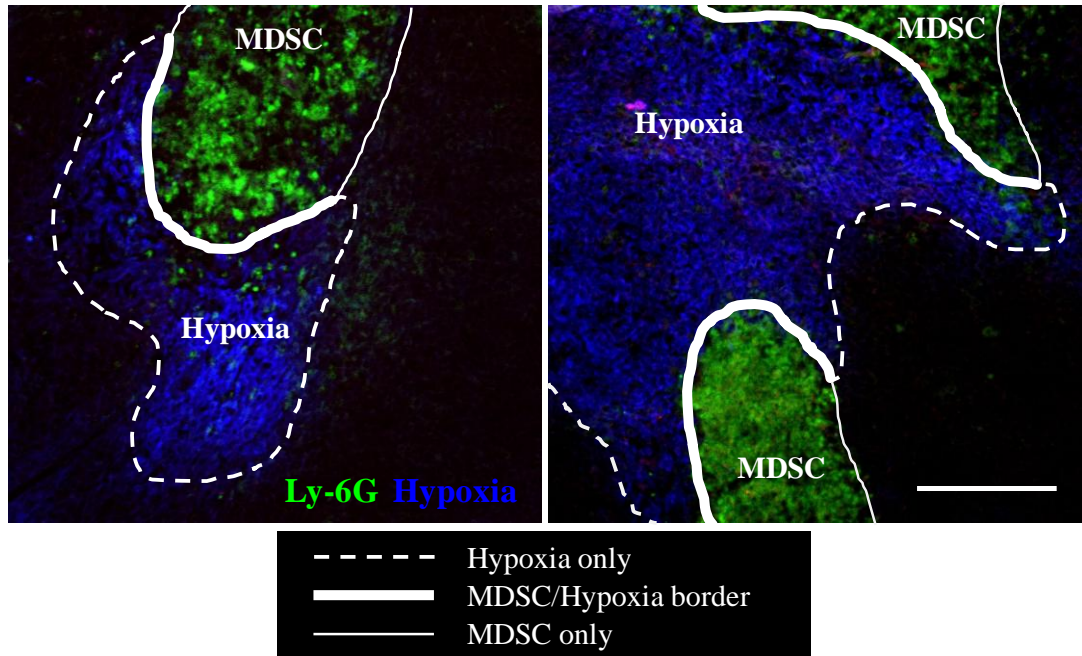


Figure 20

A.



B.

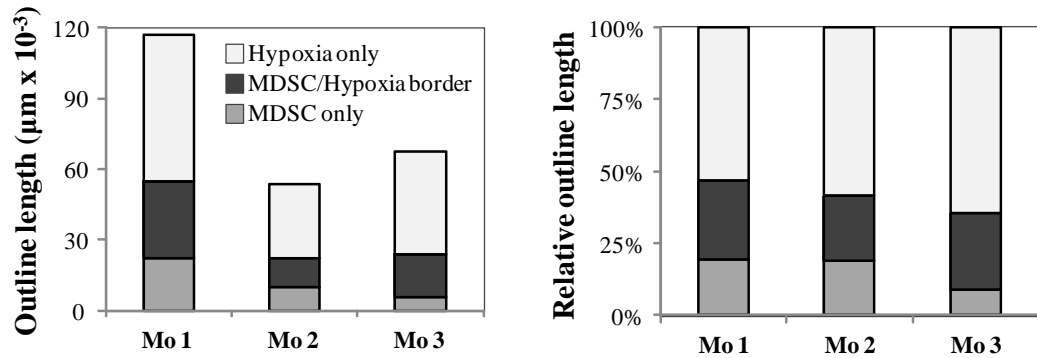
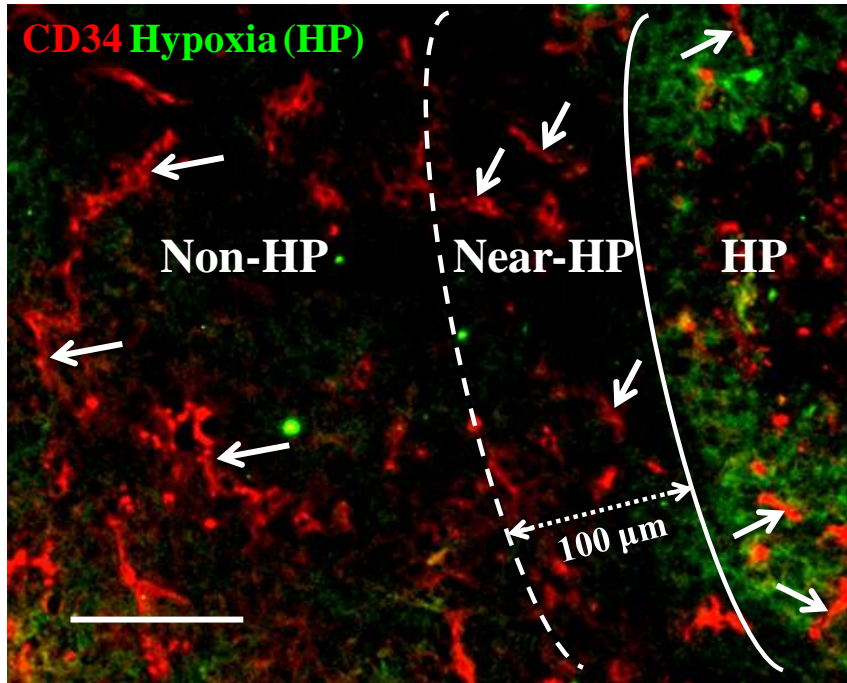


Figure 21

A.



B.

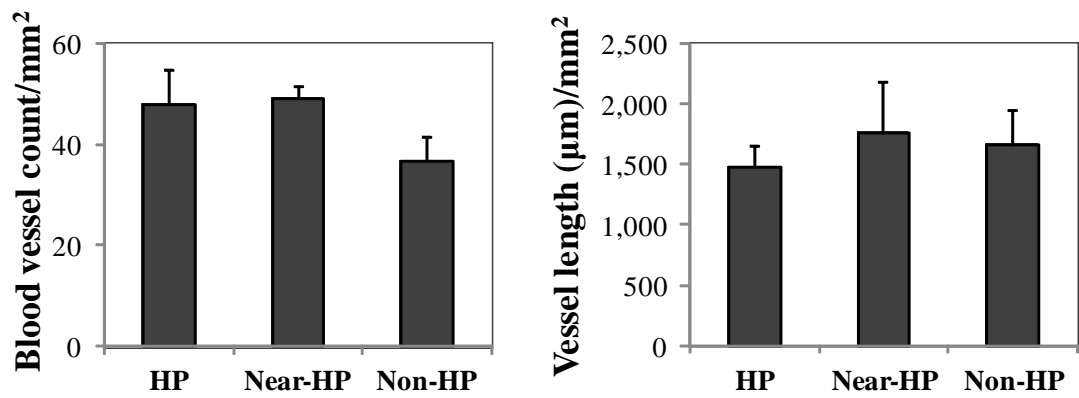
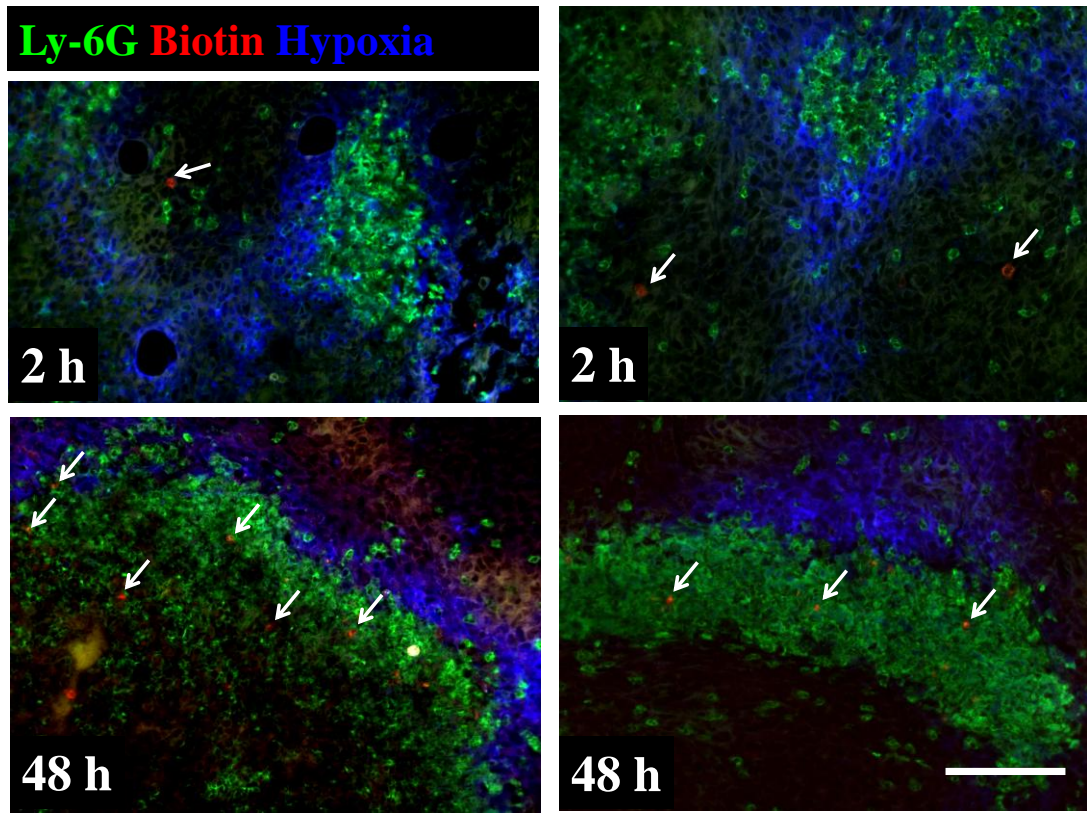


Figure 22

A.



B.

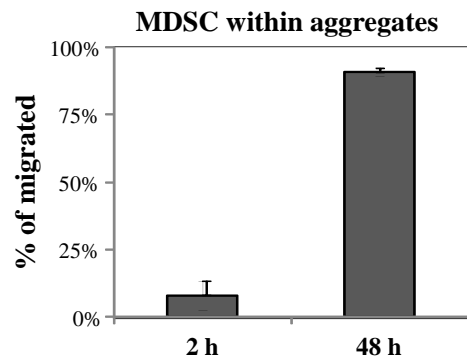
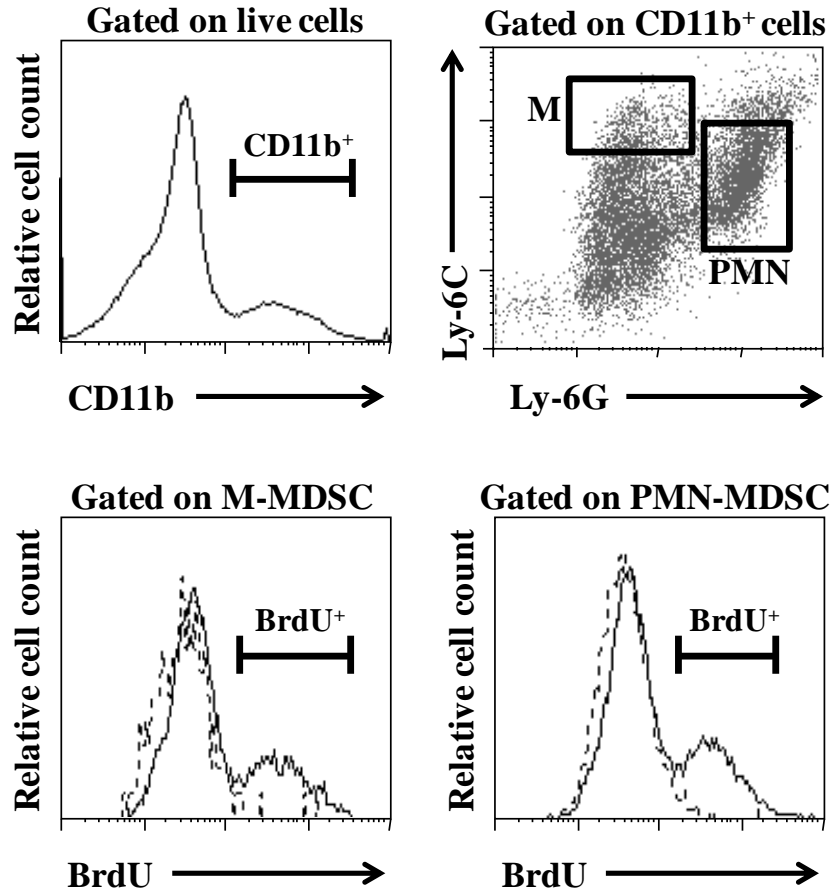


Figure 23

A.



B.

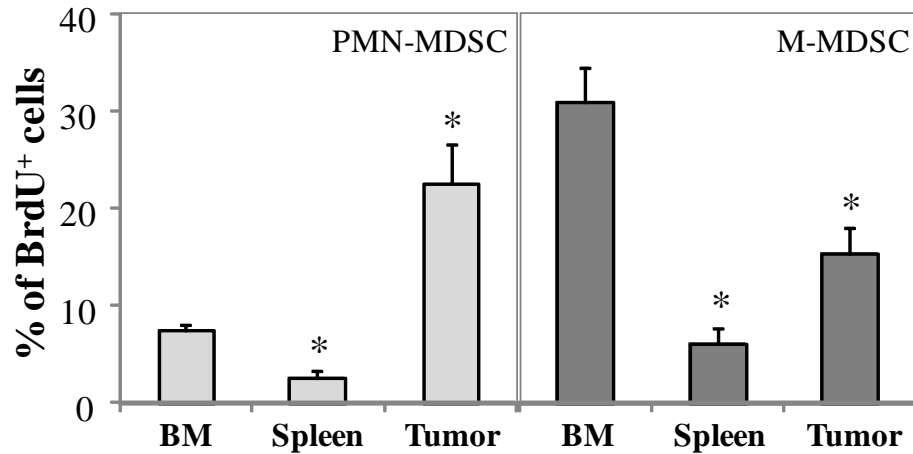
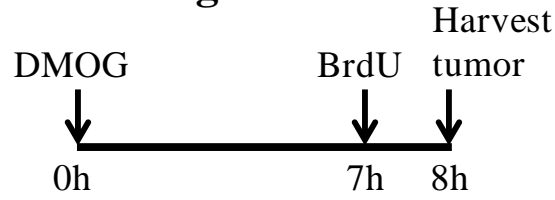


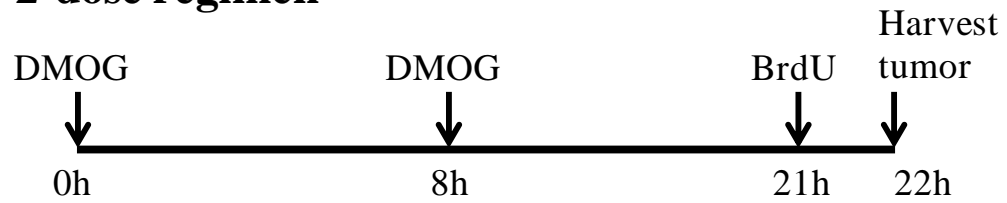
Figure 24

A.

1-dose regimen



2-dose regimen



B.

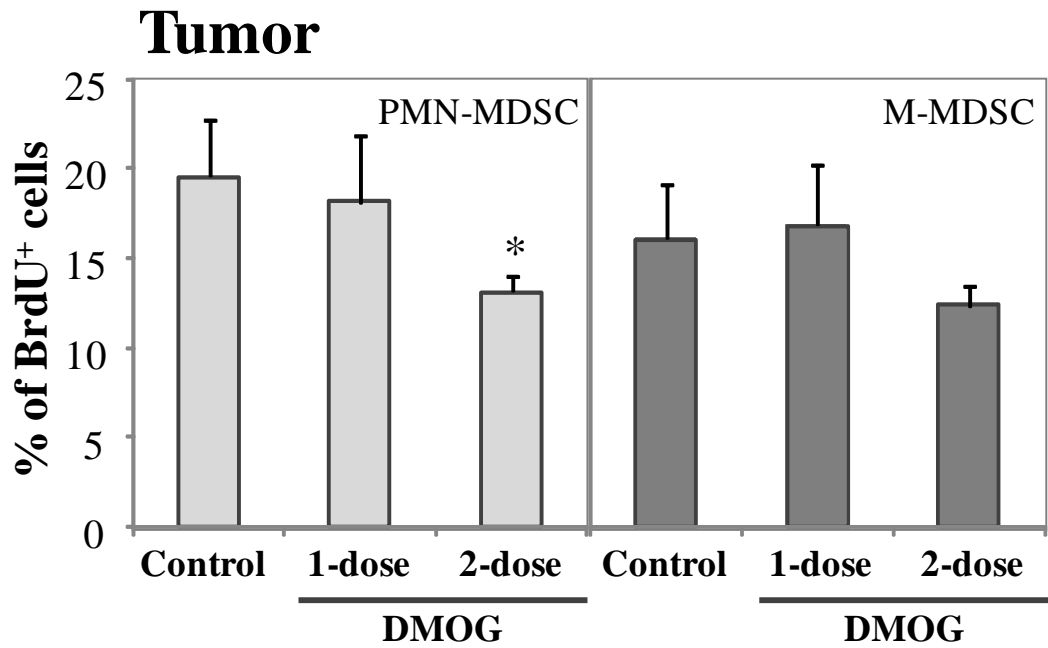


Figure 25

CHAPTER 5

CONCLUSIONS

CONCLUSIONS

CTL can kill tumor cells upon contact and are the most potent effectors in the anti-tumor immune response. Thus, higher numbers of tumor-infiltrating CTL correlate with a positive prognosis in cancer patients and various immunotherapeutic strategies utilize activated anti-tumor CTL. However, major factors limiting the success of immunotherapy are tumor-driven mechanisms of immunosuppression, such as the generation of MDSC, which inhibit CTL activation in the TDLN and CTL function in the tumor. The mechanisms of MDSC-mediated immunosuppression are dependent on direct cell contact or close proximity to target cells. Thus, the ability of MDSC to enter TDLN and the tumor is likely to be critical for suppression of the anti-tumor response and elucidating the mechanisms of MDSC migration to these sites may create a basis for novel immunotherapeutic approaches for the treatment of cancer. For instance, targeted MDSC-specific blockade of migration to the tumor would decrease the numbers of tumor-infiltrating MDSC, thus relieving some of the suppressive pressure that the tumor microenvironment exerts on adoptively transferred engineered or *ex vivo* activated anti-tumor CTL. Of note, a decrease in tumor-infiltrating MDSC and enhanced anti-tumor immune reactivity can also be achieved by antibody-mediated MDSC depletion (317). However, this strategy of MDSC depletion reportedly results in increased production of MDSC in the bone marrow, possibly via a mechanism similar to lymphopenia-induced homeostatic lymphocyte proliferation (318). Thus the beneficial effect of MDSC depletion may not only be short-lived, but may also result in an undesirable increase in MDSC accumulation in the long run. On the contrary, immunotherapeutic interference with MDSC migration to the tumor and TDLN should eliminate the immunosuppressive

activities of MDSC at those sites without increasing the production of MDSC in the bone marrow. While the mechanisms of MDSC-mediated immunosuppression are a popular area of research, far fewer studies are focused on the mechanisms of MDSC migration to the tumor and TDLN.

The initial capture and rolling stage of the adhesion cascade is largely mediated by leukocyte-expressed L-selectin, an adhesion molecule critical for the homing of circulating lymphocytes to PLN and the migration of myeloid cells to sites of inflammation. These effects of L-selectin are mediated via interactions with its endothelial ligands constitutively expressed on HEV in PLN and upregulated in post-capillary venules in response to inflammatory cytokines. The role of L-selectin in leukocyte migration to PLN and sites of inflammation has been characterized for lymphocytes and conventional myeloid cells, but its contribution specifically to MDSC migration to tumor and TDLN is unknown. Here, we used L-selectin^{-/-} mice to determine the involvement of L-selectin in the migration of MDSC subsets to tumor and TDLN in the 4T1 murine breast cancer model. Although both the PMN-MDSC and M-MDSC subsets expressed L-selectin (see Fig. 4 in Chapter 2), this adhesion molecule was critical only for PMN-MDSC migration to tumor and TDLN, while migration of M-MDSC was independent of L-selectin expression (see Fig. 17 and Table V in Chapter 3 and Fig. 26). This could be due to a possible involvement of VLA-4, expressed at higher levels on M-MDSC relative to PMN-MDSC (see Fig 16 in Chapter 3), in mediating L-selectin-independent capture and rolling of M-MDSC on VCAM-1-expressing endothelium. Integrin-mediated leukocyte tethering and rolling are not novel concepts, as VLA-4 has been reported to mediate capture and rolling of lymphocytes, myeloid cell lines, and

hematopoietic progenitor cells both *in vitro* and *in vivo* (71, 72, 250-252). It is also noteworthy that Ly-6C, expressed at higher levels on M-MDSC relative to PMN-MDSC, may play a role in the adhesion cascade by increasing LFA-1-mediated adhesion to ICAM-1. Specifically, Ly-6C has been shown to enhance the homing of a subset of memory lymphocytes to lymph nodes via its interaction with an unknown ligand expressed on HEV (212). Whether Ly-6C or VLA-4 mediate MDSC migration to TDLN and tumor is unknown but warrants further investigation, as these molecules may emerge as candidates for targeted blockade of M-MDSC migration to TDLN and tumor.

Another interesting finding described herein is that tumor-infiltrating MDSC preferentially localize in aggregates near hypoxic regions and adoptively transferred MDSC appeared to actively migrate to endogenous MDSC aggregates after entry into the tumor (see Chapter 4). This is likely due to chemotactic gradients generated by the MDSC aggregates (Fig. 26). However, it is unclear what signals initiate the *de-novo* formation of intratumoral MDSC aggregates and whether hypoxia is the trigger or the result of this event. If homotypic interactions between tumor-infiltrating MDSC during aggregation result in the secretion of chemokines for further MDSC recruitment, it would be of interest to identify the mechanisms driving the initial events of MDSC aggregation, as it may provide a basis for targeted inhibition of MDSC recruitment to tumors.

As a major sensor of hypoxia and a transcriptional activator of hypoxia-driven genes, HIF may play a role in the recruitment of MDSC toward hypoxic regions by inducing the secretion of chemotactic factors (Fig. 26). In addition, by upregulating the expression of chemokine receptors on MDSC, HIF may play a role in MDSC retention within the aggregates. Furthermore, HIF has been shown to synergize with other

transcription factors, such as STAT3 and NF- κ B, resulting in upregulation of genes favoring cell survival and proliferation (24, 305-309). Whether such events occur in tumor-infiltrating MDSC is unknown. Interestingly, flow cytometric analysis of BrdU incorporation showed proliferation of intratumoral MDSC in the 4T1 model (see Fig 24 in Chapter 4); however, the mechanisms driving MDSC proliferation in the tumor microenvironment require further investigation. Preliminary experiments with a PHD inhibitor which results in HIF stabilization did not show evidence of HIF involvement in the induction of MDSC proliferation in the tumor. However, HIF may exert pro- or anti-proliferative effects depending on which isoform of its α subunit is stabilized. For instance HIF-1 α stabilization leads to suppression of proliferation (310-312), but in synergism with STAT3 or NF- κ B, it may also induce genes that activate cell cycle progression. In contrast, HIF-2 α stabilization has pro-proliferative effects (313-315). Interestingly, HIF-2 α is stabilized by higher oxygen tension compared to HIF-1 α , which is relevant to the localization of MDSC clusters in the immediate vicinity of hypoxic regions, where the oxygen concentration gradient may favor HIF-2 α stabilization. In addition, both HIF isoforms can also be activated via oxygen-independent mechanisms, such as ROS- and RNS-mediated events (167-175), and a hallmark of MDSC function is the production of these reactive species. Since the PHD inhibitor used in the preliminary experiments described here has the potential to stabilize both HIF-1 α and HIF-2 α , resulting in opposing signals regarding cell proliferation, further studies are required to determine whether HIF-1 α or HIF-2 α is involved in MDSC proliferation in the tumor microenvironment.

FIGURE LEGENDS

Figure 26. Roles of L-selectin and hypoxia in MDSC migration to TDLN and tumor in the 4T1 breast cancer model.

During cancer progression, tumor-derived factors modulate myelopoiesis in the bone marrow (BM) resulting in abnormal expansion and accumulation of PMN-MDSC and M-MDSC (grey arrows). From the bloodstream, MDSC migrate to the TDLN (thin red arrows), where they suppress the activation of the anti-tumor T cell response. PMN-MDSC migration to the TDLN is L-selectin-dependent, while M-MDSC migration to the TDLN does not require L-selectin. In addition, larger numbers of MDSC migrate to the tumor (bold red arrows), where they suppress the function of the anti-tumor T cell response. Similar to TDLN, PMN-MDSC migration to the tumor is L-selectin-dependent, while the involvement of L-selectin in M-MDSC migration to the tumor is unclear. As tumors outgrow existing vasculature, hypoxic areas arise characterized by low oxygen tension due to insufficient blood supply (blue area). In hypoxic conditions, the transcription factor HIF becomes stabilized and activates the expression of genes involved in adaptation to hypoxia, cell survival, and proliferation. Importantly, tumor-infiltrating MDSC preferentially aggregate next to areas of hypoxia. It remains unclear whether HIF activates the expression of chemokines, which recruit MDSC to the hypoxic site or whether increased oxygen consumption within MDSC aggregates results in the generation of hypoxic areas around the aggregates. MDSC enter tumors in areas outside of the hypoxic sites and the pre-existing MDSC clusters, after which they migrate through the tumor parenchyma and associate with the pre-existing MDSC clusters. It remains unclear whether the MDSC within the aggregates secrete chemokines for the

recruitment of newly migrated MDSC resulting in expansion of the pre-existing aggregates over time. Approximately 20% of tumor-infiltrating MDSC undergo proliferation. It remains unclear whether HIF is stabilized in tumor-infiltrating MDSC and whether it induces proliferation of these cells. If in place, such a mechanism could have a significant contribution to the formation and expansion of MDSC aggregates within the tumor.

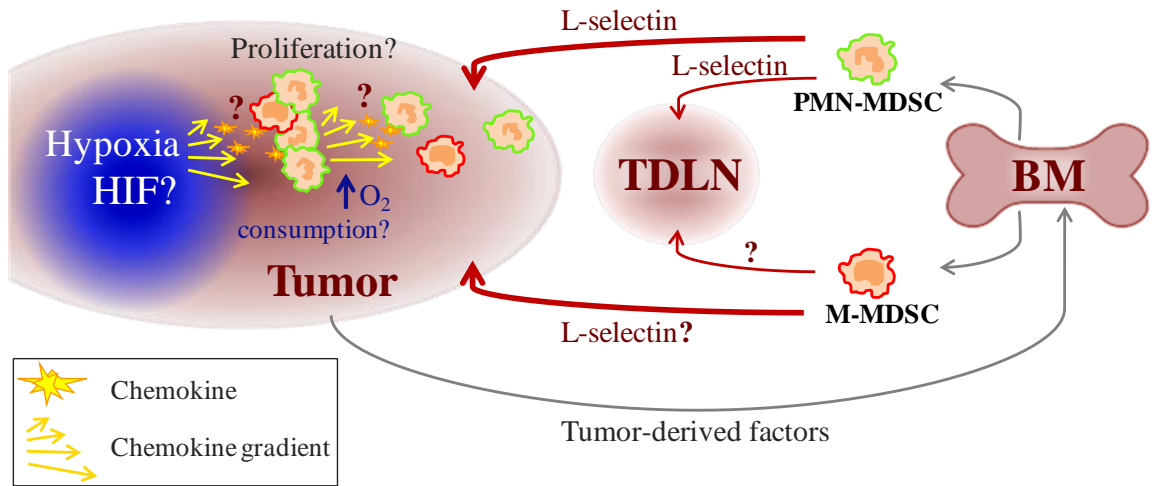


Figure 26

REFERENCES

1. Nagaraj S, Gupta K, Pisarev V, Kinarsky L, Sherman S, Kang L, Herber DL, Schneck J, Gabrilovich DI. 2007. Altered recognition of antigen is a mechanism of CD8+ T cell tolerance in cancer. *Nat Med* 13: 828-35
2. Marigo I, Dolcetti L, Serafini P, Zanovello P, Bronte V. 2008. Tumor-induced tolerance and immune suppression by myeloid derived suppressor cells. *Immunol Rev* 222: 162-79
3. Radoja S, Rao TD, Hillman D, Frey AB. 2000. Mice bearing late-stage tumors have normal functional systemic T cell responses in vitro and in vivo. *J Immunol* 164: 2619-28
4. Haverkamp JM, Crist SA, Elzey BD, Cimen C, Ratliff TL. 2011. In vivo suppressive function of myeloid-derived suppressor cells is limited to the inflammatory site. *Eur J Immunol* 41: 749-59
5. Watanabe S, Deguchi K, Zheng R, Tamai H, Wang LX, Cohen PA, Shu S. 2008. Tumor-induced CD11b+Gr-1+ myeloid cells suppress T cell sensitization in tumor-draining lymph nodes. *J Immunol* 181: 3291-300
6. Escamilla-Tilch M, Filio-Rodriguez G, Garcia-Rocha R, Mancilla-Herrera I, Mitchison NA, Ruiz-Pacheco JA, Sanchez-Garcia FJ, Sandoval-Borrego D, Vazquez-Sanchez EA. 2013. The interplay between pathogen-associated and danger-associated molecular patterns: an inflammatory code in cancer? *Immunol Cell Biol* 91: 601-10
7. Mittal D, Gubin MM, Schreiber RD, Smyth MJ. 2014. New insights into cancer immunoediting and its three component phases--elimination, equilibrium and escape. *Curr Opin Immunol* 27: 16-25
8. Dunn GP, Old LJ, Schreiber RD. 2004. The three Es of cancer immunoediting. *Annu Rev Immunol* 22: 329-60
9. Kusmartsev S, Eruslanov E, Kubler H, Tseng T, Sakai Y, Su Z, Kaliberov S, Heiser A, Rosser C, Dahm P, Siemann D, Vieweg J. 2008. Oxidative stress regulates expression of VEGFR1 in myeloid cells: link to tumor-induced immune suppression in renal cell carcinoma. *J Immunol* 181: 346-53
10. Serafini P, Carbley R, Noonan KA, Tan G, Bronte V, Borrello I. 2004. High-dose granulocyte-macrophage colony-stimulating factor-producing vaccines impair the immune response through the recruitment of myeloid suppressor cells. *Cancer Res* 64: 6337-43
11. Bronte V, Chappell DB, Apolloni E, Cabrelle A, Wang M, Hwu P, Restifo NP. 1999. Unopposed production of granulocyte-macrophage colony-stimulating factor by tumors inhibits CD8+ T cell responses by dysregulating antigen-presenting cell maturation. *J Immunol* 162: 5728-37
12. Song X, Krelin Y, Dvorkin T, Bjorkdahl O, Segal S, Dinarello CA, Voronov E, Apte RN. 2005. CD11b+/Gr-1+ immature myeloid cells mediate suppression of T cells in mice bearing tumors of IL-1beta-secreting cells. *J Immunol* 175: 8200-8
13. Bunt SK, Yang L, Sinha P, Clements VK, Leips J, Ostrand-Rosenberg S. 2007. Reduced inflammation in the tumor microenvironment delays the accumulation of myeloid-derived suppressor cells and limits tumor progression. *Cancer Res* 67: 10019-26
14. Pan PY, Wang GX, Yin B, Ozao J, Ku T, Divino CM, Chen SH. 2008. Reversion of immune tolerance in advanced malignancy: modulation of myeloid-derived suppressor cell development by blockade of stem-cell factor function. *Blood* 111: 219-28
15. Cheng P, Corzo CA, Luetsteke N, Yu B, Nagaraj S, Bui MM, Ortiz M, Nacken W, Sorg C, Vogl T, Roth J, Gabrilovich DI. 2008. Inhibition of dendritic cell differentiation and accumulation of myeloid-derived suppressor cells in cancer is regulated by S100A9 protein. *J Exp Med* 205: 2235-49

16. Menetrier-Caux C, Montmain G, Dieu MC, Bain C, Favrot MC, Caux C, Blay JY. 1998. Inhibition of the differentiation of dendritic cells from CD34(+) progenitors by tumor cells: role of interleukin-6 and macrophage colony-stimulating factor. *Blood* 92: 4778-91
17. Obermajer N, Wong JL, Edwards RP, Odunsi K, Moysich K, Kalinski P. 2012. PGE(2)-driven induction and maintenance of cancer-associated myeloid-derived suppressor cells. *Immunol Invest* 41: 635-57
18. Yu H, Kortylewski M, Pardoll D. 2007. Crosstalk between cancer and immune cells: role of STAT3 in the tumour microenvironment. *Nat Rev Immunol* 7: 41-51
19. Gabrilovich D. 2004. Mechanisms and functional significance of tumour-induced dendritic-cell defects. *Nat Rev Immunol* 4: 941-52
20. Sinha P, Okoro C, Foell D, Freeze HH, Ostrand-Rosenberg S, Srikrishna G. 2008. Proinflammatory S100 proteins regulate the accumulation of myeloid-derived suppressor cells. *J Immunol* 181: 4666-75
21. Nefedova Y, Nagaraj S, Rosenbauer A, Muro-Cacho C, Sebt SM, Gabrilovich DI. 2005. Regulation of dendritic cell differentiation and antitumor immune response in cancer by pharmacologic-selective inhibition of the janus-activated kinase 2/signal transducers and activators of transcription 3 pathway. *Cancer Res* 65: 9525-35
22. Nefedova Y, Huang M, Kusmartsev S, Bhattacharya R, Cheng P, Salup R, Jove R, Gabrilovich D. 2004. Hyperactivation of STAT3 is involved in abnormal differentiation of dendritic cells in cancer. *J Immunol* 172: 464-74
23. Kortylewski M, Kujawski M, Wang T, Wei S, Zhang S, Pilon-Thomas S, Niu G, Kay H, Mule J, Kerr WG, Jove R, Pardoll D, Yu H. 2005. Inhibiting Stat3 signaling in the hematopoietic system elicits multicomponent antitumor immunity. *Nat Med* 11: 1314-21
24. Gabrilovich DI, Nagaraj S. 2009. Myeloid-derived suppressor cells as regulators of the immune system. *Nat Rev Immunol* 9: 162-74
25. Strober S. 1984. Natural suppressor (NS) cells, neonatal tolerance, and total lymphoid irradiation: exploring obscure relationships. *Annu Rev Immunol* 2: 219-37
26. Argyris BF. 1978. Suppressor activity in the spleen of neonatal mice. *Cell Immunol* 36: 354-62
27. Okada S, Strober S. 1982. Spleen cells from adult mice given total lymphoid irradiation (TLI) or from newborn mice have similar regulatory effects in the mixed leukocyte reaction (MLR). II. Generation of antigen-specific suppressor cells in the MLR after the addition of spleen cells from newborn mice. *J Immunol* 129: 1892-7
28. Maier T, Holda JH, Claman HN. 1989. Natural suppressor cells. *Prog Clin Biol Res* 288: 235-44
29. Forghani P, Khorramizadeh MR, Waller EK. 2012. Natural suppressor cells; past, present and future. *Front Biosci (Elite Ed)* 4: 1237-45
30. Billingham RE, Brent L, Medawar PB. 1953. Actively acquired tolerance of foreign cells. *Nature* 172: 603-6
31. Munder M, Eichmann K, Moran JM, Centeno F, Soler G, Modolell M. 1999. Th1/Th2-regulated expression of arginase isoforms in murine macrophages and dendritic cells. *J Immunol* 163: 3771-7
32. Munder M, Eichmann K, Modolell M. 1998. Alternative metabolic states in murine macrophages reflected by the nitric oxide synthase/arginase balance: competitive regulation by CD4+ T cells correlates with Th1/Th2 phenotype. *J Immunol* 160: 5347-54
33. Boutard V, Havouis R, Fouqueray B, Philippe C, Moulinoux JP, Baud L. 1995. Transforming growth factor-beta stimulates arginase activity in macrophages. Implications for the regulation of macrophage cytotoxicity. *J Immunol* 155: 2077-84
34. Jost MM, Ninci E, Meder B, Kempf C, Van Royen N, Hua J, Berger B, Hoefler I, Modolell M, Buschmann I. 2003. Divergent effects of GM-CSF and TGFbeta1 on bone

- marrow-derived macrophage arginase-1 activity, MCP-1 expression, and matrix metalloproteinase-12: a potential role during arteriogenesis. *Faseb j* 17: 2281-3
35. Rutschman R, Lang R, Hesse M, Ihle JN, Wynn TA, Murray PJ. 2001. Cutting edge: Stat6-dependent substrate depletion regulates nitric oxide production. *J Immunol* 166: 2173-7
 36. Ganster RW, Taylor BS, Shao L, Geller DA. 2001. Complex regulation of human inducible nitric oxide synthase gene transcription by Stat 1 and NF-kappa B. *Proc Natl Acad Sci U S A* 98: 8638-43
 37. Chicoine LG, Paffett ML, Young TL, Nelin LD. 2004. Arginase inhibition increases nitric oxide production in bovine pulmonary arterial endothelial cells. *Am J Physiol Lung Cell Mol Physiol* 287: L60-8
 38. Zhang C, Hein TW, Wang W, Miller MW, Fossum TW, McDonald MM, Humphrey JD, Kuo L. 2004. Upregulation of vascular arginase in hypertension decreases nitric oxide-mediated dilation of coronary arterioles. *Hypertension* 44: 935-43
 39. Lee J, Ryu H, Ferrante RJ, Morris SM, Jr., Ratan RR. 2003. Translational control of inducible nitric oxide synthase expression by arginine can explain the arginine paradox. *Proc Natl Acad Sci U S A* 100: 4843-8
 40. Santhanam L, Lim HK, Lim HK, Miriel V, Brown T, Patel M, Balanson S, Ryoo S, Anderson M, Irani K, Khanday F, Di Costanzo L, Nyhan D, Hare JM, Christianson DW, Rivers R, Shoukas A, Berkowitz DE. 2007. Inducible NO synthase dependent S-nitrosylation and activation of arginase1 contribute to age-related endothelial dysfunction. *Circ Res* 101: 692-702
 41. Rodriguez PC, Quiceno DG, Zabaleta J, Ortiz B, Zea AH, Piazuelo MB, Delgado A, Correa P, Brayer J, Sotomayor EM, Antonia S, Ochoa JB, Ochoa AC. 2004. Arginase I production in the tumor microenvironment by mature myeloid cells inhibits T-cell receptor expression and antigen-specific T-cell responses. *Cancer Res* 64: 5839-49
 42. Rodriguez PC, Zea AH, DeSalvo J, Culotta KS, Zabaleta J, Quiceno DG, Ochoa JB, Ochoa AC. 2003. L-arginine consumption by macrophages modulates the expression of CD3 zeta chain in T lymphocytes. *J Immunol* 171: 1232-9
 43. Zea AH, Rodriguez PC, Atkins MB, Hernandez C, Signoretti S, Zabaleta J, McDermott D, Quiceno D, Youmans A, O'Neill A, Mier J, Ochoa AC. 2005. Arginase-producing myeloid suppressor cells in renal cell carcinoma patients: a mechanism of tumor evasion. *Cancer Res* 65: 3044-8
 44. Bingisser RM, Tilbrook PA, Holt PG, Kees UR. 1998. Macrophage-derived nitric oxide regulates T cell activation via reversible disruption of the Jak3/STAT5 signaling pathway. *J Immunol* 160: 5729-34
 45. Mazzoni A, Bronte V, Visintin A, Spitzer JH, Apolloni E, Serafini P, Zanovello P, Segal DM. 2002. Myeloid suppressor lines inhibit T cell responses by an NO-dependent mechanism. *J Immunol* 168: 689-95
 46. Macphail SE, Gibney CA, Brooks BM, Booth CG, Flanagan BF, Coleman JW. 2003. Nitric oxide regulation of human peripheral blood mononuclear cells: critical time dependence and selectivity for cytokine versus chemokine expression. *J Immunol* 171: 4809-15
 47. Fischer TA, Palmetshofer A, Gambaryan S, Butt E, Jassoy C, Walter U, Sopper S, Lohmann SM. 2001. Activation of cGMP-dependent protein kinase Ibeta inhibits interleukin 2 release and proliferation of T cell receptor-stimulated human peripheral T cells. *J Biol Chem* 276: 5967-74
 48. Rishi L, Dhiman R, Raje M, Majumdar S. 2007. Nitric oxide induces apoptosis in cutaneous T cell lymphoma (HuT-78) by downregulating constitutive NF-kappaB. *Biochim Biophys Acta* 1770: 1230-9

49. Rodriguez PC, Quiceno DG, Ochoa AC. 2007. L-arginine availability regulates T-lymphocyte cell-cycle progression. *Blood* 109: 1568-73
50. Rodriguez PC, Hernandez CP, Morrow K, Sierra R, Zabaleta J, Wyczechowska DD, Ochoa AC. 2010. L-arginine deprivation regulates cyclin D3 mRNA stability in human T cells by controlling HuR expression. *J Immunol* 185: 5198-204
51. Bronte V, Zanovello P. 2005. Regulation of immune responses by L-arginine metabolism. *Nat Rev Immunol* 5: 641-54
52. Otsuji M, Kimura Y, Aoe T, Okamoto Y, Saito T. 1996. Oxidative stress by tumor-derived macrophages suppresses the expression of CD3 zeta chain of T-cell receptor complex and antigen-specific T-cell responses. *Proc Natl Acad Sci U S A* 93: 13119-24
53. Schmielau J, Finn OJ. 2001. Activated granulocytes and granulocyte-derived hydrogen peroxide are the underlying mechanism of suppression of T-cell function in advanced cancer patients. *Cancer Res* 61: 4756-60
54. Bronte V, Kasic T, Gri G, Gallana K, Borsellino G, Marigo I, Battistini L, Iafrate M, Prayer-Galetti T, Pagano F, Viola A. 2005. Boosting antitumor responses of T lymphocytes infiltrating human prostate cancers. *J Exp Med* 201: 1257-68
55. Hildeman DA, Mitchell T, Aronow B, Wojciechowski S, Kappler J, Marrack P. 2003. Control of Bcl-2 expression by reactive oxygen species. *Proc Natl Acad Sci U S A* 100: 15035-40
56. Brito C, Naviliat M, Tiscornia AC, Vuillier F, Gualco G, Dighiero G, Radi R, Cayota AM. 1999. Peroxynitrite inhibits T lymphocyte activation and proliferation by promoting impairment of tyrosine phosphorylation and peroxynitrite-driven apoptotic death. *J Immunol* 162: 3356-66
57. Li H, Han Y, Guo Q, Zhang M, Cao X. 2009. Cancer-expanded myeloid-derived suppressor cells induce anergy of NK cells through membrane-bound TGF-beta 1. *J Immunol* 182: 240-9
58. Suzuki E, Kapoor V, Jassar AS, Kaiser LR, Albelda SM. 2005. Gemcitabine selectively eliminates splenic Gr-1⁺/CD11b⁺ myeloid suppressor cells in tumor-bearing animals and enhances antitumor immune activity. *Clin Cancer Res* 11: 6713-21
59. Sinha P, Clements VK, Bunt SK, Albelda SM, Ostrand-Rosenberg S. 2007. Cross-talk between myeloid-derived suppressor cells and macrophages subverts tumor immunity toward a type 2 response. *J Immunol* 179: 977-83
60. Pan PY, Ma G, Weber KJ, Ozao-Choy J, Wang G, Yin B, Divino CM, Chen SH. 2010. Immune stimulatory receptor CD40 is required for T-cell suppression and T regulatory cell activation mediated by myeloid-derived suppressor cells in cancer. *Cancer Res* 70: 99-108
61. Huang B, Pan PY, Li Q, Sato AI, Levy DE, Bromberg J, Divino CM, Chen SH. 2006. Gr-1⁺CD115⁺ immature myeloid suppressor cells mediate the development of tumor-induced T regulatory cells and T-cell anergy in tumor-bearing host. *Cancer Res* 66: 1123-31
62. Serafini P, Mgebrouff S, Noonan K, Borrello I. 2008. Myeloid-derived suppressor cells promote cross-tolerance in B-cell lymphoma by expanding regulatory T cells. *Cancer Res* 68: 5439-49
63. Yang L, DeBusk LM, Fukuda K, Fingleton B, Green-Jarvis B, Shyr Y, Matrisian LM, Carbone DP, Lin PC. 2004. Expansion of myeloid immune suppressor Gr⁺CD11b⁺ cells in tumor-bearing host directly promotes tumor angiogenesis. *Cancer Cell* 6: 409-21
64. Steeber DA, Venturi GM, Tedder TF. 2005. A new twist to the leukocyte adhesion cascade: intimate cooperation is key. *Trends Immunol* 26: 9-12
65. Bullard DC. 2007. P- and E-selectin. In *Adhesion Molecules: Function and Inhibition*, ed. K Ley, pp. 71-95: Birkhäuser Basel

66. Steeber DA, Subramanian H, Grailer JJ, Conway RM. 2007. L-selectin-mediated leukocyte adhesion and migration. In *Adhesion Molecules: Function and Inhibition*, ed. K Ley, pp. 27-70: Birkhäuser Basel
67. Dunne JL, Ballantyne CM, Beaudet AL, Ley K. 2002. Control of leukocyte rolling velocity in TNF-alpha-induced inflammation by LFA-1 and Mac-1. *Blood* 99: 336-41
68. Dunne JL, Collins RG, Beaudet AL, Ballantyne CM, Ley K. 2003. Mac-1, but not LFA-1, uses intercellular adhesion molecule-1 to mediate slow leukocyte rolling in TNF-alpha-induced inflammation. *J Immunol* 171: 6105-11
69. Henderson RB, Lim LH, Tessier PA, Gavins FN, Mathies M, Perretti M, Hogg N. 2001. The use of lymphocyte function-associated antigen (LFA)-1-deficient mice to determine the role of LFA-1, Mac-1, and alpha4 integrin in the inflammatory response of neutrophils. *J Exp Med* 194: 219-26
70. Chesnutt BC, Smith DF, Raffler NA, Smith ML, White EJ, Ley K. 2006. Induction of LFA-1-dependent neutrophil rolling on ICAM-1 by engagement of E-selectin. *Microcirculation* 13: 99-109
71. Berlin C, Bargatze RF, Campbell JJ, von Andrian UH, Szabo MC, Hasslen SR, Nelson RD, Berg EL, Erlandsen SL, Butcher EC. 1995. alpha 4 integrins mediate lymphocyte attachment and rolling under physiologic flow. *Cell* 80: 413-22
72. Alon R, Kassner PD, Carr MW, Finger EB, Hemler ME, Springer TA. 1995. The integrin VLA-4 supports tethering and rolling in flow on VCAM-1. *J Cell Biol* 128: 1243-53
73. Schenkel AR, Kim M. 2007. Lymphocyte function-associated antigen-1 (LFA-1) and macrophage antigen-1 (Mac-1): Cooperative partners in leukocyte emigration and function. In *Adhesion Molecules: Function and Inhibition*, ed. K Ley, pp. 175-97: Birkhäuser Basel
74. Hsu-Lin S, Berman CL, Furie BC, August D, Furie B. 1984. A platelet membrane protein expressed during platelet activation and secretion. Studies using a monoclonal antibody specific for thrombin-activated platelets. *J Biol Chem* 259: 9121-6
75. McEver RP, Martin MN. 1984. A monoclonal antibody to a membrane glycoprotein binds only to activated platelets. *J Biol Chem* 259: 9799-804
76. McEver RP, Beckstead JH, Moore KL, Marshall-Carlson L, Bainton DF. 1989. GMP-140, a platelet alpha-granule membrane protein, is also synthesized by vascular endothelial cells and is localized in Weibel-Palade bodies. *J Clin Invest* 84: 92-9
77. Bonfanti R, Furie BC, Furie B, Wagner DD. 1989. PADGEM (GMP140) is a component of Weibel-Palade bodies of human endothelial cells. *Blood* 73: 1109-12
78. Finger EB, Puri KD, Alon R, Lawrence MB, von Andrian UH, Springer TA. 1996. Adhesion through L-selectin requires a threshold hydrodynamic shear. *Nature* 379: 266-9
79. Tu L, Chen A, Delahunty MD, Moore KL, Watson S, McEver RP, Tedder TF. 1996. L-selectin binds to P-selectin glycoprotein ligand-1 on leukocytes. Interactions between the lectin, EGF and consensus repeat domains of the selectins determine ligand binding specificity. *J Immunol* 156: 3995-4004
80. Revelle BM, Scott D, Beck PJ. 1996. Single amino acid residues in the E- and P-selectin epidermal growth factor domains can determine carbohydrate binding specificity. *J Biol Chem* 271: 16160-70
81. Gibson RM, Kansas GS, Tedder TF, Furie B, Furie BC. 1995. Lectin and epidermal growth factor domains of P-selectin at physiologic density are the recognition unit for leukocyte binding. *Blood* 85: 151-8
82. Schleiffenbaum B, Spertini O, Tedder TF. 1992. Soluble L-selectin is present in human plasma at high levels and retains functional activity. *J Cell Biol* 119: 229-38
83. Ferri LE, Swartz D, Christou NV. 2001. Soluble L-selectin at levels present in septic patients diminishes leukocyte-endothelial cell interactions in mice in vivo: a mechanism for decreased leukocyte delivery to remote sites in sepsis. *Crit Care Med* 29: 117-22

84. Kansas GS. 1996. Selectins and their ligands: current concepts and controversies. *Blood* 88: 3259-87
85. Rosen SD. 2004. Ligands for L-selectin: homing, inflammation, and beyond. *Annu Rev Immunol* 22: 129-56
86. Rosen SD. 1999. Endothelial ligands for L-selectin: from lymphocyte recirculation to allograft rejection. *Am J Pathol* 155: 1013-20
87. Renkonen J, Tynninen O, Hayry P, Paavonen P, Renkonen R. 2002. Glycosylation might provide endothelial zip codes for organ-specific leukocyte traffic into inflammatory sites. *Am J Pathol* 161: 543-50
88. McEver RP. 2007. P-selectin glycoprotein ligand-1 (PSGL-1). In *Adhesion Molecules: Function and Inhibition*, ed. K Ley, pp. 3-25: Birkhäuser Basel
89. Yang J, Hirata T, Croce K, Merrill-Skoloff G, Tchernychev B, Williams E, Flaumenhaft R, Furie BC, Furie B. 1999. Targeted gene disruption demonstrates that P-selectin glycoprotein ligand 1 (PSGL-1) is required for P-selectin-mediated but not E-selectin-mediated neutrophil rolling and migration. *J Exp Med* 190: 1769-82
90. Steeber DA, Green NE, Sato S, Tedder TF. 1996. Lymphocyte migration in L-selectin-deficient mice. Altered subset migration and aging of the immune system. *J Immunol* 157: 1096-106
91. Gallatin WM, Weissman IL, Butcher EC. 1983. A cell-surface molecule involved in organ-specific homing of lymphocytes. *Nature* 304: 30-4
92. Arbones ML, Ord DC, Ley K, Ratech H, Maynard-Curry C, Otten G, Capon DJ, Tedder TF. 1994. Lymphocyte homing and leukocyte rolling and migration are impaired in L-selectin-deficient mice. *Immunity* 1: 247-60
93. Yan ZQ, Bolognesi MP, Steeber DA, Tedder TF, Chen LE, Seaber AV, Urbaniak JR. 2000. Blockade of L-selectin attenuates reperfusion injury in a rat model. *J Reconstr Microsurg* 16: 227-33
94. Yadav SS, Howell DN, Gao W, Steeber DA, Harland RC, Clavien P-A. 1998. L-selectin and ICAM-1 mediate reperfusion injury and neutrophil adhesion in the warm ischemic mouse liver. *Am J Physiol* 275: G1341-G52
95. Kawasuji A, Hasegawa M, Horikawa M, Fujita T, Matsushita Y, Matsushita T, Fujimoto M, Steeber DA, Tedder TF, Takehara K, Sato S. 2006. L-selectin and intercellular adhesion molecule-1 regulate the development of Concanavalin A-induced liver injury. *J Leukoc Biol* 79: 696-705
96. Fiscus LC, Van Herpen J, Steeber DA, Tedder TF, Tang ML. 2001. L-Selectin is required for the development of airway hyperresponsiveness but not airway inflammation in a murine model of asthma. *J Allergy Clin Immunol* 107: 1019-24
97. Abraham WM, Ahmed A, Sabater JR, Lauredo IT, Botvinnikova Y, Bjercke RJ, Hu X, Revelle M, Kogan TP, Scott IL, Dixon RAF, Yeh ETH, Beck PJ. 1999. Selectin blockade prevents antigen-induced late bronchial responses and airway hyperresponsiveness in allergic sheep. *Am J Respir Crit Care Med* 159: 1205-14
98. Rosen SD, Tsay D, Hemmerich S, Abraham WM. 2005. Therapeutic targeting of endothelial ligands for L-selectin (PNAd) in a sheep model of asthma. *Am J Pathol* 166: 935-44
99. Hamaguchi Y, Nishizawa Y, Yasui M, Hasegawa M, Kaburagi Y, Komura K, Nagaoka T, Saito E, Shimada Y, Takehara K, Kadono T, Steeber DA, Tedder TF, Sato S. 2002. Intercellular adhesion molecule-1 and L-selectin regulate bleomycin-induced lung fibrosis. *Am J Pathol* 161: 1607-18
100. Falati S, Liu Q, Gross P, Merrill-Skoloff G, Chou J, Vandendries E, Celi A, Croce K, Furie BC, Furie B. 2003. Accumulation of tissue factor into developing thrombi in vivo is dependent upon microparticle P-selectin glycoprotein ligand 1 and platelet P-selectin. *J Exp Med* 197: 1585-98

101. Larsen E, Celi A, Gilbert GE, Furie BC, Erban JK, Bonfanti R, Wagner DD, Furie B. 1989. PADGEM protein: a receptor that mediates the interaction of activated platelets with neutrophils and monocytes. *Cell* 59: 305-12
102. Geng JG, Bevilacqua MP, Moore KL, McIntyre TM, Prescott SM, Kim JM, Bliss GA, Zimmerman GA, McEver RP. 1990. Rapid neutrophil adhesion to activated endothelium mediated by GMP-140. *Nature* 343: 757-60
103. Frenette PS, Johnson RC, Hynes RO, Wagner DD. 1995. Platelets roll on stimulated endothelium in vivo: an interaction mediated by endothelial P-selectin. *Proc Natl Acad Sci U S A* 92: 7450-4
104. Diacovo TG, Puri KD, Warnock RA, Springer TA, von Andrian UH. 1996. Platelet-mediated lymphocyte delivery to high endothelial venules. *Science* 273: 252-5
105. Diacovo TG, Catalina MD, Siegelman MH, von Andrian UH. 1998. Circulating activated platelets reconstitute lymphocyte homing and immunity in L-selectin-deficient mice. *J Exp Med* 187: 197-204
106. Singbartl K, Forlow SB, Ley K. 2001. Platelet, but not endothelial, P-selectin is critical for neutrophil-mediated acute postischemic renal failure. *Faseb j* 15: 2337-44
107. Kuligowski MP, Kitching AR, Hickey MJ. 2006. Leukocyte recruitment to the inflamed glomerulus: a critical role for platelet-derived P-selectin in the absence of rolling. *J Immunol* 176: 6991-9
108. Zarbock A, Singbartl K, Ley K. 2006. Complete reversal of acid-induced acute lung injury by blocking of platelet-neutrophil aggregation. *J Clin Invest* 116: 3211-9
109. Zarbock A, Polanowska-Grabowska RK, Ley K. 2007. Platelet-neutrophil-interactions: linking hemostasis and inflammation. *Blood Rev* 21: 99-111
110. Evangelista V, Manarini S, Sideri R, Rotondo S, Martelli N, Piccoli A, Totani L, Piccardoni P, Vestweber D, de Gaetano G, Cerletti C. 1999. Platelet/polymorphonuclear leukocyte interaction: P-selectin triggers protein-tyrosine phosphorylation-dependent CD11b/CD18 adhesion: role of PSGL-1 as a signaling molecule. *Blood* 93: 876-85
111. Piccardoni P, Sideri R, Manarini S, Piccoli A, Martelli N, de Gaetano G, Cerletti C, Evangelista V. 2001. Platelet/polymorphonuclear leukocyte adhesion: a new role for SRC kinases in Mac-1 adhesive function triggered by P-selectin. *Blood* 98: 108-16
112. Davignon D, Martz E, Reynolds T, Kurzinger K, Springer TA. 1981. Lymphocyte function-associated antigen 1 (LFA-1): a surface antigen distinct from Lyt-2,3 that participates in T lymphocyte-mediated killing. *Proc Natl Acad Sci U S A* 78: 4535-9
113. Springer T, Galfre G, Secher DS, Milstein C. 1979. Mac-1: a macrophage differentiation antigen identified by monoclonal antibody. *Eur J Immunol* 9: 301-6
114. Marlin SD, Springer TA. 1987. Purified intercellular adhesion molecule-1 (ICAM-1) is a ligand for lymphocyte function-associated antigen 1 (LFA-1). *Cell* 51: 813-9
115. Diamond MS, Staunton DE, de Fougères AR, Stacker SA, Garcia-Aguilar J, Hibbs ML, Springer TA. 1990. ICAM-1 (CD54): a counter-receptor for Mac-1 (CD11b/CD18). *J Cell Biol* 111: 3129-39
116. Springer TA. 1994. Traffic signals for lymphocyte recirculation and leukocyte emigration: the multistep paradigm. *Cell* 76: 301-14
117. Rothlein R, Dustin ML, Marlin SD, Springer TA. 1986. A human intercellular adhesion molecule (ICAM-1) distinct from LFA-1. *J Immunol* 137: 1270-4
118. Roebuck KA, Finnegan A. 1999. Regulation of intercellular adhesion molecule-1 (CD54) gene expression. *J Leukoc Biol* 66: 876-88
119. Grakoui A, Bromley SK, Sumen C, Davis MM, Shaw AS, Allen PM, Dustin ML. 1999. The immunological synapse: a molecular machine controlling T cell activation. *Science* 285: 221-7

120. van Gisbergen KP, Sanchez-Hernandez M, Geijtenbeek TB, van Kooyk Y. 2005. Neutrophils mediate immune modulation of dendritic cells through glycosylation-dependent interactions between Mac-1 and DC-SIGN. *J Exp Med* 201: 1281-92
121. Iwata M, Hirakiyama A, Eshima Y, Kagechika H, Kato C, Song SY. 2004. Retinoic acid imprints gut-homing specificity on T cells. *Immunity* 21: 527-38
122. Mora JR, Iwata M, Eksteen B, Song SY, Junt T, Senman B, Otipoby KL, Yokota A, Takeuchi H, Ricciardi-Castagnoli P, Rajewsky K, Adams DH, von Andrian UH. 2006. Generation of gut-homing IgA-secreting B cells by intestinal dendritic cells. *Science* 314: 1157-60
123. Johnston B, Kubes P. 1999. The alpha4-integrin: an alternative pathway for neutrophil recruitment? *Immunol Today* 20: 545-50
124. Elices MJ, Osborn L, Takada Y, Crouse C, Luhowskyj S, Hemler ME, Lobb RR. 1990. VCAM-1 on activated endothelium interacts with the leukocyte integrin VLA-4 at a site distinct from the VLA-4/fibronectin binding site. *Cell* 60: 577-84
125. Ruegg C, Postigo AA, Sikorski EE, Butcher EC, Pytela R, Erle DJ. 1992. Role of integrin alpha 4 beta 7/alpha 4 beta P in lymphocyte adherence to fibronectin and VCAM-1 and in homotypic cell clustering. *J Cell Biol* 117: 179-89
126. Guan JL, Hynes RO. 1990. Lymphoid cells recognize an alternatively spliced segment of fibronectin via the integrin receptor alpha 4 beta 1. *Cell* 60: 53-61
127. Berlin C, Berg EL, Briskin MJ, Andrew DP, Kilshaw PJ, Holzmann B, Weissman IL, Hamann A, Butcher EC. 1993. Alpha 4 beta 7 integrin mediates lymphocyte binding to the mucosal vascular addressin MAdCAM-1. *Cell* 74: 185-95
128. Gazitt Y, Akay C. 2004. Mobilization of myeloma cells involves SDF-1/CXCR4 signaling and downregulation of VLA-4. *Stem Cells* 22: 65-73
129. Wang GL, Jiang BH, Rue EA, Semenza GL. 1995. Hypoxia-inducible factor 1 is a basic-helix-loop-helix-PAS heterodimer regulated by cellular O₂ tension. *Proc Natl Acad Sci U S A* 92: 5510-4
130. Reyes H, Reisz-Porszasz S, Hankinson O. 1992. Identification of the Ah receptor nuclear translocator protein (Arnt) as a component of the DNA binding form of the Ah receptor. *Science* 256: 1193-5
131. Kallio PJ, Pongratz I, Gradin K, McGuire J, Poellinger L. 1997. Activation of hypoxia-inducible factor 1alpha: posttranscriptional regulation and conformational change by recruitment of the Arnt transcription factor. *Proc Natl Acad Sci U S A* 94: 5667-72
132. Pugh CW, O'Rourke JF, Nagao M, Gleadle JM, Ratcliffe PJ. 1997. Activation of hypoxia-inducible factor-1; definition of regulatory domains within the alpha subunit. *J Biol Chem* 272: 11205-14
133. Salceda S, Caro J. 1997. Hypoxia-inducible factor 1alpha (HIF-1alpha) protein is rapidly degraded by the ubiquitin-proteasome system under normoxic conditions. Its stabilization by hypoxia depends on redox-induced changes. *J Biol Chem* 272: 22642-7
134. Masson N, Willam C, Maxwell PH, Pugh CW, Ratcliffe PJ. 2001. Independent function of two destruction domains in hypoxia-inducible factor-alpha chains activated by prolyl hydroxylation. *Embo j* 20: 5197-206
135. Srinivas V, Zhang LP, Zhu XH, Caro J. 1999. Characterization of an oxygen/redox-dependent degradation domain of hypoxia-inducible factor alpha (HIF-alpha) proteins. *Biochem Biophys Res Commun* 260: 557-61
136. Jeong JW, Bae MK, Ahn MY, Kim SH, Sohn TK, Bae MH, Yoo MA, Song EJ, Lee KJ, Kim KW. 2002. Regulation and destabilization of HIF-1alpha by ARD1-mediated acetylation. *Cell* 111: 709-20
137. Masson N, Ratcliffe PJ. 2003. HIF prolyl and asparaginyl hydroxylases in the biological response to intracellular O(2) levels. *J Cell Sci* 116: 3041-9

138. Huang LE, Arany Z, Livingston DM, Bunn HF. 1996. Activation of hypoxia-inducible transcription factor depends primarily upon redox-sensitive stabilization of its alpha subunit. *J Biol Chem* 271: 32253-9
139. Crews ST. 1998. Control of cell lineage-specific development and transcription by bHLH-PAS proteins. *Genes Dev* 12: 607-20
140. Wenger RH, Stiehl DP, Camenisch G. 2005. Integration of oxygen signaling at the consensus HRE. *Sci STKE* 2005: re12
141. Carrero P, Okamoto K, Coumailleau P, O'Brien S, Tanaka H, Poellinger L. 2000. Redox-regulated recruitment of the transcriptional coactivators CREB-binding protein and SRC-1 to hypoxia-inducible factor 1alpha. *Mol Cell Biol* 20: 402-15
142. Arany Z, Huang LE, Eckner R, Bhattacharya S, Jiang C, Goldberg MA, Bunn HF, Livingston DM. 1996. An essential role for p300/CBP in the cellular response to hypoxia. *Proc Natl Acad Sci U S A* 93: 12969-73
143. Ruas JL, Poellinger L, Pereira T. 2002. Functional analysis of hypoxia-inducible factor-1 alpha-mediated transactivation. Identification of amino acid residues critical for transcriptional activation and/or interaction with CREB-binding protein. *J Biol Chem* 277: 38723-30
144. Lando D, Peet DJ, Whelan DA, Gorman JJ, Whitelaw ML. 2002. Asparagine hydroxylation of the HIF transactivation domain a hypoxic switch. *Science* 295: 858-61
145. Lando D, Peet DJ, Gorman JJ, Whelan DA, Whitelaw ML, Bruick RK. 2002. FIH-1 is an asparaginyl hydroxylase enzyme that regulates the transcriptional activity of hypoxia-inducible factor. *Genes Dev* 16: 1466-71
146. Maynard MA, Qi H, Chung J, Lee EH, Kondo Y, Hara S, Conaway RC, Conaway JW, Ohh M. 2003. Multiple splice variants of the human HIF-3 alpha locus are targets of the von Hippel-Lindau E3 ubiquitin ligase complex. *J Biol Chem* 278: 11032-40
147. Ema M, Taya S, Yokotani N, Sogawa K, Matsuda Y, Fujii-Kuriyama Y. 1997. A novel bHLH-PAS factor with close sequence similarity to hypoxia-inducible factor 1alpha regulates the VEGF expression and is potentially involved in lung and vascular development. *Proc Natl Acad Sci U S A* 94: 4273-8
148. Tian H, McKnight SL, Russell DW. 1997. Endothelial PAS domain protein 1 (EPAS1), a transcription factor selectively expressed in endothelial cells. *Genes Dev* 11: 72-82
149. Gu YZ, Moran SM, Hogenesch JB, Wartman L, Bradfield CA. 1998. Molecular characterization and chromosomal localization of a third alpha-class hypoxia inducible factor subunit, HIF3alpha. *Gene Expr* 7: 205-13
150. Zhang P, Yao Q, Lu L, Li Y, Chen PJ, Duan C. 2014. Hypoxia-inducible factor 3 is an oxygen-dependent transcription activator and regulates a distinct transcriptional response to hypoxia. *Cell Rep* 6: 1110-21
151. Hu CJ, Iyer S, Sataur A, Covello KL, Chodosh LA, Simon MC. 2006. Differential regulation of the transcriptional activities of hypoxia-inducible factor 1 alpha (HIF-1alpha) and HIF-2alpha in stem cells. *Mol Cell Biol* 26: 3514-26
152. Makino Y, Cao R, Svensson K, Bertilsson G, Asman M, Tanaka H, Cao Y, Berkenstam A, Poellinger L. 2001. Inhibitory PAS domain protein is a negative regulator of hypoxia-inducible gene expression. *Nature* 414: 550-4
153. Hara S, Hamada J, Kobayashi C, Kondo Y, Imura N. 2001. Expression and characterization of hypoxia-inducible factor (HIF)-3alpha in human kidney: suppression of HIF-mediated gene expression by HIF-3alpha. *Biochem Biophys Res Commun* 287: 808-13
154. Maynard MA, Evans AJ, Shi W, Kim WY, Liu FF, Ohh M. 2007. Dominant-negative HIF-3 alpha 4 suppresses VHL-null renal cell carcinoma progression. *Cell Cycle* 6: 2810-6

155. Wiesener MS, Jurgensen JS, Rosenberger C, Scholze CK, Horstrup JH, Warnecke C, Mandriota S, Bechmann I, Frei UA, Pugh CW, Ratcliffe PJ, Bachmann S, Maxwell PH, Eckardt KU. 2003. Widespread hypoxia-inducible expression of HIF-2alpha in distinct cell populations of different organs. *Faseb j* 17: 271-3
156. Makino Y, Kanopka A, Wilson WJ, Tanaka H, Poellinger L. 2002. Inhibitory PAS domain protein (IPAS) is a hypoxia-inducible splicing variant of the hypoxia-inducible factor-3alpha locus. *J Biol Chem* 277: 32405-8
157. Semenza GL. 2007. Hypoxia-inducible factor 1 (HIF-1) pathway. *Sci STKE* 2007: cm8
158. Berra E, Benizri E, Ginouves A, Volmat V, Roux D, Pouyssegur J. 2003. HIF prolyl-hydroxylase 2 is the key oxygen sensor setting low steady-state levels of HIF-1alpha in normoxia. *Embo j* 22: 4082-90
159. Jaakkola P, Mole DR, Tian YM, Wilson MI, Gielbert J, Gaskell SJ, von Kriegsheim A, Hebestreit HF, Mukherji M, Schofield CJ, Maxwell PH, Pugh CW, Ratcliffe PJ. 2001. Targeting of HIF-alpha to the von Hippel-Lindau ubiquitylation complex by O2-regulated prolyl hydroxylation. *Science* 292: 468-72
160. Yuan Y, Hilliard G, Ferguson T, Millhorn DE. 2003. Cobalt inhibits the interaction between hypoxia-inducible factor-alpha and von Hippel-Lindau protein by direct binding to hypoxia-inducible factor-alpha. *J Biol Chem* 278: 15911-6
161. Ke Q, Costa M. 2006. Hypoxia-inducible factor-1 (HIF-1). *Mol Pharmacol* 70: 1469-80
162. Kuiper C, Vissers MC. 2014. Ascorbate as a co-factor for fe- and 2-oxoglutarate dependent dioxygenases: physiological activity in tumor growth and progression. *Front Oncol* 4: 359
163. Hon WC, Wilson MI, Harlos K, Claridge TD, Schofield CJ, Pugh CW, Maxwell PH, Ratcliffe PJ, Stuart DI, Jones EY. 2002. Structural basis for the recognition of hydroxyproline in HIF-1 alpha by pVHL. *Nature* 417: 975-8
164. Ivan M, Kaelin WG, Jr. 2001. The von Hippel-Lindau tumor suppressor protein. *Curr Opin Genet Dev* 11: 27-34
165. Gossage L, Eisen T, Maher ER. 2015. VHL, the story of a tumour suppressor gene. *Nat Rev Cancer* 15: 55-64
166. Keith B, Johnson RS, Simon MC. 2012. HIF1alpha and HIF2alpha: sibling rivalry in hypoxic tumour growth and progression. *Nat Rev Cancer* 12: 9-22
167. Guzy RD, Hoyos B, Robin E, Chen H, Liu L, Mansfield KD, Simon MC, Hammerling U, Schumacker PT. 2005. Mitochondrial complex III is required for hypoxia-induced ROS production and cellular oxygen sensing. *Cell Metab* 1: 401-8
168. Bell EL, Klimova TA, Eisenbart J, Moraes CT, Murphy MP, Budinger GR, Chandel NS. 2007. The Qo site of the mitochondrial complex III is required for the transduction of hypoxic signaling via reactive oxygen species production. *J Cell Biol* 177: 1029-36
169. Chua YL, Dufour E, Dassa EP, Rustin P, Jacobs HT, Taylor CT, Hagen T. 2010. Stabilization of hypoxia-inducible factor-1alpha protein in hypoxia occurs independently of mitochondrial reactive oxygen species production. *J Biol Chem* 285: 31277-84
170. Kohl R, Zhou J, Brune B. 2006. Reactive oxygen species attenuate nitric-oxide-mediated hypoxia-inducible factor-1alpha stabilization. *Free Radic Biol Med* 40: 1430-42
171. Brune B, Zhou J. 2007. Hypoxia-inducible factor-1alpha under the control of nitric oxide. *Methods Enzymol* 435: 463-78
172. Mateo J, Garcia-Lecea M, Cadenas S, Hernandez C, Moncada S. 2003. Regulation of hypoxia-inducible factor-1alpha by nitric oxide through mitochondria-dependent and -independent pathways. *Biochem J* 376: 537-44
173. Sumbayev VV, Budde A, Zhou J, Brune B. 2003. HIF-1 alpha protein as a target for S-nitrosation. *FEBS Lett* 535: 106-12

174. Yasinska IM, Sumbayev VV. 2003. S-nitrosation of Cys-800 of HIF-1alpha protein activates its interaction with p300 and stimulates its transcriptional activity. *FEBS Lett* 549: 105-9
175. Metzzen E, Zhou J, Jelkmann W, Fandrey J, Brune B. 2003. Nitric oxide impairs normoxic degradation of HIF-1alpha by inhibition of prolyl hydroxylases. *Mol Biol Cell* 14: 3470-81
176. Brune B, Zhou J. 2007. Nitric oxide and superoxide: interference with hypoxic signaling. *Cardiovasc Res* 75: 275-82
177. Sasabe E, Yang Z, Ohno S, Yamamoto T. 2010. Reactive oxygen species produced by the knockdown of manganese-superoxide dismutase up-regulate hypoxia-inducible factor-1alpha expression in oral squamous cell carcinoma cells. *Free Radic Biol Med* 48: 1321-9
178. Kasuno K, Takabuchi S, Fukuda K, Kizaka-Kondoh S, Yodoi J, Adachi T, Semenza GL, Hirota K. 2004. Nitric oxide induces hypoxia-inducible factor 1 activation that is dependent on MAPK and phosphatidylinositol 3-kinase signaling. *J Biol Chem* 279: 2550-8
179. de Lemos ML, de la Torre AV, Petrov D, Brox S, Folch J, Pallas M, Lazarowski A, Beas-Zarate C, Auladell C, Camins A. 2013. Evaluation of hypoxia inducible factor expression in inflammatory and neurodegenerative brain models. *Int J Biochem Cell Biol* 45: 1377-88
180. Westra J, Brouwer E, Bos R, Posthumus MD, Doornbos-van der Meer B, Kallenberg CG, Limburg PC. 2007. Regulation of cytokine-induced HIF-1alpha expression in rheumatoid synovial fibroblasts. *Ann N Y Acad Sci* 1108: 340-8
181. Corzo CA, Condamine T, Lu L, Cotter MJ, Youn JI, Cheng P, Cho HI, Celis E, Quiceno DG, Padhya T, McCaffrey TV, McCaffrey JC, Gabrilovich DI. 2010. HIF-1alpha regulates function and differentiation of myeloid-derived suppressor cells in the tumor microenvironment. *J Exp Med* 207: 2439-53
182. Haverkamp JM, Crist SA, Elzey BD, Cimen C, Ratliff TL. 2011. In vivo suppressive function of myeloid-derived suppressor cells is limited to the inflammatory site. *Eur J Immunol* 41: 749-59
183. Prevost-Blondel A, Zimmermann C, Stemmer C, Kulmburg P, Rosenthal FM, Pircher H. 1998. Tumor-infiltrating lymphocytes exhibiting high ex vivo cytolytic activity fail to prevent murine melanoma tumor growth in vivo. *J Immunol* 161: 2187-94
184. Dexter DL, Kowalski HM, Blazar BA, Fligiel Z, Vogel R, Heppner GH. 1978. Heterogeneity of tumor cells from a single mouse mammary tumor. *Cancer Res* 38: 3174-81
185. Miller FR, Miller BE, Heppner GH. 1983. Characterization of metastatic heterogeneity among subpopulations of a single mouse mammary tumor: heterogeneity in phenotypic stability. *Invasion Metastasis* 3: 22-31
186. Cardiff RD, Altrock BW. 1978. Biology of mammary tumor viruses. In *Origins of Inbred Mice*, ed. HC Morse, pp. 321-42: Academic Press
187. Pulaski BA, Ostrand-Rosenberg S. 2001. Mouse 4T1 breast tumor model. *Curr Protoc Immunol* Chapter 20: Unit 20.2
188. Matsushita H, Vesely MD, Koboldt DC, Rickert CG, Uppaluri R, Magrini VJ, Arthur CD, White JM, Chen YS, Shea LK, Hundal J, Wendl MC, Demeter R, Wylie T, Allison JP, Smyth MJ, Old LJ, Mardis ER, Schreiber RD. 2012. Cancer exome analysis reveals a T-cell-dependent mechanism of cancer immunoediting. *Nature* 482: 400-4
189. Gajewski TF. 2012. Cancer immunotherapy. *Mol Oncol* 6: 242-50
190. Gajewski TF, Woo SR, Zha Y, Spaapen R, Zheng Y, Corrales L, Spranger S. 2013. Cancer immunotherapy strategies based on overcoming barriers within the tumor microenvironment. *Curr Opin Immunol* 25: 268-76

191. Avram G, Sanchez-Sendra B, Martin JM, Terradez L, Ramos D, Monteagudo C. 2013. The density and type of MECA-79-positive high endothelial venules correlate with lymphocytic infiltration and tumour regression in primary cutaneous melanoma. *Histopathology* 63: 852-61
192. Koch M, Beckhove P, Op den Winkel J, Autenrieth D, Wagner P, Nummer D, Specht S, Antolovic D, Galindo L, Schmitz-Winnenthal FH, Schirmacher V, Buchler MW, Weitz J. 2006. Tumor infiltrating T lymphocytes in colorectal cancer: Tumor-selective activation and cytotoxic activity in situ. *Ann Surg* 244: 986-92; discussion 92-3
193. Ryschich E, Notzel T, Hinz U, Autschbach F, Ferguson J, Simon I, Weitz J, Frohlich B, Klar E, Buchler MW, Schmidt J. 2005. Control of T-cell-mediated immune response by HLA class I in human pancreatic carcinoma. *Clin Cancer Res* 11: 498-504
194. Fukunaga A, Miyamoto M, Cho Y, Murakami S, Kawarada Y, Oshikiri T, Kato K, Kurokawa T, Suzuoki M, Nakakubo Y, Hiraoka K, Itoh T, Morikawa T, Okushiba S, Kondo S, Katoh H. 2004. CD8+ tumor-infiltrating lymphocytes together with CD4+ tumor-infiltrating lymphocytes and dendritic cells improve the prognosis of patients with pancreatic adenocarcinoma. *Pancreas* 28: e26-31
195. Tedder TF, Penta AC, Levine HB, Freedman AS. 1990. Expression of the human leukocyte adhesion molecule, LAM1. Identity with the TQ1 and Leu-8 differentiation antigens. *J Immunol* 144: 532-40
196. Ley K, Bullard DC, Arbones ML, Bosse R, Vestweber D, Tedder TF, Beaudet AL. 1995. Sequential contribution of L- and P-selectin to leukocyte rolling in vivo. *J Exp Med* 181: 669-75
197. Tedder TF, Steeber DA, Pizcueta P. 1995. L-selectin-deficient mice have impaired leukocyte recruitment into inflammatory sites. *J Exp Med* 181: 2259-64
198. Steeber DA, Tedder TF. 2000. Adhesion molecule cascades direct lymphocyte recirculation and leukocyte migration during inflammation. *Immunol Res* 22: 299-317
199. Lee WT, Vitetta ES. 1991. The differential expression of homing and adhesion molecules on virgin and memory T cells in the mouse. *Cell Immunol* 132: 215-22
200. Witz IP. 2008. The selectin-selectin ligand axis in tumor progression. *Cancer Metastasis Rev* 27: 19-30
201. Paschos KA, Canovas D, Bird NC. 2009. The role of cell adhesion molecules in the progression of colorectal cancer and the development of liver metastasis. *Cell Signal* 21: 665-74
202. Shu SY, Chou T, Rosenberg SA. 1987. Generation from tumor-bearing mice of lymphocytes with in vivo therapeutic efficacy. *J Immunol* 139: 295-304
203. Hargadon KM, Brinkman CC, Sheasley-O'neill S L, Nichols LA, Bullock TN, Engelhard VH. 2006. Incomplete differentiation of antigen-specific CD8 T cells in tumor-draining lymph nodes. *J Immunol* 177: 6081-90
204. Munn DH, Mellor AL. 2006. The tumor-draining lymph node as an immune-privileged site. *Immunol Rev* 213: 146-58
205. Talmadge JE, Gabilovich DI. 2013. History of myeloid-derived suppressor cells. *Nat Rev Cancer* 13: 739-52
206. Damuzzo V, Pinton L, Desantis G, Solito S, Marigo I, Bronte V, Mandruzzato S. 2015. Complexity and challenges in defining myeloid-derived suppressor cells. *Cytometry B Clin Cytom* 88: 77-91
207. Movahedi K, Guillems M, Van den Bossche J, Van den Bergh R, Gysemans C, Beschin A, De Baetselier P, Van Ginderachter JA. 2008. Identification of discrete tumor-induced myeloid-derived suppressor cell subpopulations with distinct T cell-suppressive activity. *Blood* 111: 4233-44
208. Ross SR. 2008. MMTV infectious cycle and the contribution of virus-encoded proteins to transformation of mammary tissue. *J Mammary Gland Biol Neoplasia* 13: 299-307

209. Miller FR. 1983. Tumor subpopulation interactions in metastasis. *Invasion Metastasis* 3: 234-42
210. Steeber DA, Engel P, Miller AS, Sheetz MP, Tedder TF. 1997. Ligation of L-selectin through conserved regions within the lectin domain activates signal transduction pathways and integrin function in human, mouse, and rat leukocytes. *J Immunol* 159: 952-63
211. Kruisbeek AM, Shevach E, Thornton AM. 2004. Proliferative assays for T cell function. *Curr Protoc Immunol* Chapter 3: Unit 3.12
212. Hanninen A, Maksimow M, Alam C, Morgan DJ, Jalkanen S. 2011. Ly6C supports preferential homing of central memory CD8+ T cells into lymph nodes. *Eur J Immunol* 41: 634-44
213. Jutila MA, Kroese FG, Jutila KL, Stall AM, Fiering S, Herzenberg LA, Berg EL, Butcher EC. 1988. Ly-6C is a monocyte/macrophage and endothelial cell differentiation antigen regulated by interferon-gamma. *Eur J Immunol* 18: 1819-26
214. Wrammert J, Kallberg E, Agace WW, Leanderson T. 2002. Ly6C expression differentiates plasma cells from other B cell subsets in mice. *Eur J Immunol* 32: 97-103
215. Sato N, Yahata T, Santa K, Ohta A, Ohmi Y, Habu S, Nishimura T. 1996. Functional characterization of NK1.1 + Ly-6C+ cells. *Immunol Lett* 54: 5-9
216. Semenza GL. 2015. The hypoxic tumor microenvironment: A driving force for breast cancer progression. *Biochim Biophys Acta*
217. Leamon CP, Jackman AL. 2008. Exploitation of the folate receptor in the management of cancer and inflammatory disease. *Vitam Horm* 79: 203-33
218. Parker N, Turk MJ, Westrick E, Lewis JD, Low PS, Leamon CP. 2005. Folate receptor expression in carcinomas and normal tissues determined by a quantitative radioligand binding assay. *Anal Biochem* 338: 284-93
219. van Dam GM, Themelis G, Crane LM, Harlaar NJ, Pleijhuis RG, Kelder W, Sarantopoulos A, de Jong JS, Arts HJ, van der Zee AG, Bart J, Low PS, Ntziachristos V. 2011. Intraoperative tumor-specific fluorescence imaging in ovarian cancer by folate receptor-alpha targeting: first in-human results. *Nat Med* 17: 1315-9
220. Yang X, Grailer JJ, Rowland IJ, Javadi A, Hurley SA, Matson VZ, Steeber DA, Gong S. 2010. Multifunctional stable and pH-responsive polymer vesicles formed by heterofunctional triblock copolymer for targeted anticancer drug delivery and ultrasensitive MR imaging. *ACS Nano* 4: 6805-17
221. Xiao Y, Hong H, Matson VZ, Javadi A, Xu W, Yang Y, Zhang Y, Engle JW, Nickles RJ, Cai W, Steeber DA, Gong S. 2012. Gold Nanorods Conjugated with Doxorubicin and cRGD for Combined Anticancer Drug Delivery and PET Imaging. *Theranostics* 2: 757-68
222. Prabakaran M, Grailer JJ, Pilla S, Steeber DA, Gong S. 2009. Folate-conjugated amphiphilic hyperbranched block copolymers based on Boltorn H40, poly(L-lactide) and poly(ethylene glycol) for tumor-targeted drug delivery. *Biomaterials* 30: 3009-19
223. Prabakaran M, Grailer JJ, Steeber DA, Gong S. 2009. Thermosensitive micelles based on folate-conjugated poly(N-vinylcaprolactam)-block-poly(ethylene glycol) for tumor-targeted drug delivery. *Macromol Biosci* 9: 744-53
224. Krystofiak ES, Matson VZ, Steeber DA, Oliver JA. 2012. Elimination of tumor cells using folate receptor targeting by antibody-conjugated, gold-coated magnetite nanoparticles in a murine breast cancer model. *J. Nanomat.* 2012: Article ID 431012
225. Pan XQ, Zheng X, Shi G, Wang H, Ratnam M, Lee RJ. 2002. Strategy for the treatment of acute myelogenous leukemia based on folate receptor beta-targeted liposomal doxorubicin combined with receptor induction using all-trans retinoic acid. *Blood* 100: 594-602

226. Ross JF, Wang H, Behm FG, Mathew P, Wu M, Booth R, Ratnam M. 1999. Folate receptor type beta is a neutrophilic lineage marker and is differentially expressed in myeloid leukemia. *Cancer* 85: 348-57
227. Nakashima-Matsushita N, Homma T, Yu S, Matsuda T, Sunahara N, Nakamura T, Tsukano M, Ratnam M, Matsuyama T. 1999. Selective expression of folate receptor beta and its possible role in methotrexate transport in synovial macrophages from patients with rheumatoid arthritis. *Arthritis Rheum* 42: 1609-16
228. Paulos CM, Turk MJ, Breur GJ, Low PS. 2004. Folate receptor-mediated targeting of therapeutic and imaging agents to activated macrophages in rheumatoid arthritis. *Adv Drug Deliv Rev* 56: 1205-17
229. Ilkovitch D, Lopez DM. 2009. The liver is a site for tumor-induced myeloid-derived suppressor cell accumulation and immunosuppression. *Cancer Res* 69: 5514-21
230. Melani C, Chiodoni C, Forni G, Colombo MP. 2003. Myeloid cell expansion elicited by the progression of spontaneous mammary carcinomas in c-erbB-2 transgenic BALB/c mice suppresses immune reactivity. *Blood* 102: 2138-45
231. Ferri LE, Swartz D, Christou NV. 2001. Soluble L-selectin at levels present in septic patients diminishes leukocyte-endothelial cell interactions in mice in vivo: a mechanism for decreased leukocyte delivery to remote sites in sepsis. *Crit Care Med* 29: 117-22
232. Lajoie L, Congy-Jolivet N, Bolzec A, Gouilleux-Gruart V, Sicard E, Sung HC, Peiretti F, Moreau T, Vie H, Clemenceau B, Thibault G. 2014. ADAM17-mediated shedding of FcγRIIIA on human NK cells: identification of the cleavage site and relationship with activation. *J Immunol* 192: 741-51
233. Chen A, Engel P, Tedder TF. 1995. Structural requirements regulate endoproteolytic release of the L-selectin (CD62L) adhesion receptor from the cell surface of leukocytes. *J Exp Med* 182: 519-30
234. Hanson EM, Clements VK, Sinha P, Ilkovitch D, Ostrand-Rosenberg S. 2009. Myeloid-derived suppressor cells down-regulate L-selectin expression on CD4+ and CD8+ T cells. *J Immunol* 183: 937-44
235. Colditz IG, Schneider MA, Pruenster M, Rot A. 2007. Chemokines at large: in-vivo mechanisms of their transport, presentation and clearance. *Thromb Haemost* 97: 688-93
236. Dunne JL, Ballantyne CM, Beaudet AL, Ley K. 2002. Control of leukocyte rolling velocity in TNF- α -induced inflammation by LFA-1 and Mac-1. *Blood* 99: 336-41
237. Rosen SD. 2004. Ligands for L-selectin: homing, inflammation, and beyond. *Annu Rev Immunol* 22: 129-56
238. Umemoto E, Tanaka T, Kanda H, Jin S, Tohya K, Otani K, Matsutani T, Matsumoto M, Ebisuno Y, Jang MH, Fukuda M, Hirata T, Miyasaka M. 2006. Nepmucin, a novel HEV sialomucin, mediates L-selectin-dependent lymphocyte rolling and promotes lymphocyte adhesion under flow. *J Exp Med* 203: 1603-14
239. Yan ZQ, Bolognesi MP, Steeber DA, Tedder TF, Chen LE, Seaber AV, Urbaniak JR. 2000. Blockade of L-selectin attenuates reperfusion injury in a rat model. *J Reconstr Microsurg* 16: 227-33
240. Yadav SS, Howell DN, Gao W, Steeber DA, Harland RC, Clavien PA. 1998. L-selectin and ICAM-1 mediate reperfusion injury and neutrophil adhesion in the warm ischemic mouse liver. *Am J Physiol* 275: G1341-52
241. Abraham WM, Ahmed A, Sabater JR, Laredo IT, Botvinnikova Y, Bjercke RJ, Hu X, Revelle BM, Kogan TP, Scott IL, Dixon RA, Yeh ET, Beck PJ. 1999. Selectin blockade prevents antigen-induced late bronchial responses and airway hyperresponsiveness in allergic sheep. *Am J Respir Crit Care Med* 159: 1205-14
242. Rosen SD, Tsay D, Singer MS, Hemmerich S, Abraham WM. 2005. Therapeutic targeting of endothelial ligands for L-selectin (PNAd) in a sheep model of asthma. *Am J Pathol* 166: 935-44

243. Dustin ML, Rothlein R, Bhan AK, Dinarello CA, Springer TA. 1986. Induction by IL 1 and interferon-gamma: tissue distribution, biochemistry, and function of a natural adherence molecule (ICAM-1). *J Immunol* 137: 245-54
244. Lucas R, Lou J, Morel DR, Ricou B, Suter PM, Grau GE. 1997. TNF receptors in the microvascular pathology of acute respiratory distress syndrome and cerebral malaria. *J Leukoc Biol* 61: 551-8
245. Dolcetti L, Peranzoni E, Ugel S, Marigo I, Fernandez Gomez A, Mesa C, Geilich M, Winkels G, Traggiai E, Casati A, Grassi F, Bronte V. 2010. Hierarchy of immunosuppressive strength among myeloid-derived suppressor cell subsets is determined by GM-CSF. *Eur J Immunol* 40: 22-35
246. Youn JI, Nagaraj S, Collazo M, Gabrilovich DI. 2008. Subsets of myeloid-derived suppressor cells in tumor-bearing mice. *J Immunol* 181: 5791-802
247. Steeber DA, Green NE, Sato S, Tedder TF. 1996. Lymphocyte migration in L-selectin-deficient mice: altered subset migration and aging of the immune system. *J Immunol* 157: 1096-106
248. Haile LA, Gamrekelashvili J, Manns MP, Korangy F, Greten TF. 2010. CD49d is a new marker for distinct myeloid-derived suppressor cell subpopulations in mice. *J Immunol* 185: 203-10
249. Kilshaw PJ. 1999. Alpha E beta 7. *Mol Pathol* 52: 203-7
250. Jones DA, McIntire LV, Smith CW, Picker LJ. 1994. A two-step adhesion cascade for T cell/endothelial cell interactions under flow conditions. *J Clin Invest* 94: 2443-50
251. Mazo IB, Gutierrez-Ramos JC, Frenette PS, Hynes RO, Wagner DD, von Andrian UH. 1998. Hematopoietic progenitor cell rolling in bone marrow microvessels: parallel contributions by endothelial selectins and vascular cell adhesion molecule 1. *J Exp Med* 188: 465-74
252. Papayannopoulou T, Priestley GV, Nakamoto B, Zafiroopoulos V, Scott LM. 2001. Molecular pathways in bone marrow homing: dominant role of alpha(4)beta(1) over beta(2)-integrins and selectins. *Blood* 98: 2403-11
253. Oostendorp RA, Dormer P. 1997. VLA-4-mediated interactions between normal human hematopoietic progenitors and stromal cells. *Leuk Lymphoma* 24: 423-35
254. Wang MW, Consoli U, Lane CM, Durett A, Lauppe MJ, Champlin R, Andreeff M, Deisseroth AB. 1998. Rescue from apoptosis in early (CD34-selected) versus late (non-CD34-selected) human hematopoietic cells by very late antigen 4- and vascular cell adhesion molecule (VCAM) 1-dependent adhesion to bone marrow stromal cells. *Cell Growth Differ* 9: 105-12
255. Moore KL, Stults NL, Diaz S, Smith DF, Cummings RD, Varki A, McEver RP. 1992. Identification of a specific glycoprotein ligand for P-selectin (CD62) on myeloid cells. *J Cell Biol* 118: 445-56
256. Moore KL, Patel KD, Breuhl RE, Li F, Johnson DA, Lichenstein HS, Cummings RD, Bainton DF, McEver RP. 1995. P-selectin glycoprotein ligand-1 mediates rolling of human neutrophils on P-selectin. *J Cell Biol* 128: 661-71
257. Aigner S, Ruppert M, Hubbe M, Sammar M, Sthoeger Z, Butcher EC, Vestweber D, Altevogt P. 1995. Heat-stable antigen (mouse CD24) supports myeloid cell binding to endothelial and platelet P-selectin. *Int Immunol* 7: 1557-65
258. Pitchford SC, Momi S, Giannini S, Casali L, Spina D, Page CP, Gesele P. 2005. Platelet P-selectin is required for pulmonary eosinophil and lymphocyte recruitment in a murine model of allergic inflammation. *Blood* 105: 2074-81
259. Ghasemzadeh M, Hosseini E. 2013. Platelet-leukocyte crosstalk: Linking proinflammatory responses to procoagulant state. *Thromb Res* 131: 191-7
260. Semple JW, Freedman J. 2010. Platelets and innate immunity. *Cell Mol Life Sci* 67: 499-511

261. Ikeda M, Furukawa H, Imamura H, Shimizu J, Ishida H, Masutani S, Tatsuta M, Satomi T. 2002. Poor prognosis associated with thrombocytosis in patients with gastric cancer. *Ann Surg Oncol* 9: 287-91
262. Monreal M, Fernandez-Llamazares J, Pinol M, Julian JF, Broggi M, Escola D, Abad A. 1998. Platelet count and survival in patients with colorectal cancer--a preliminary study. *Thromb Haemost* 79: 916-8
263. Symbas NP, Townsend MF, El-Galley R, Keane TE, Graham SD, Petros JA. 2000. Poor prognosis associated with thrombocytosis in patients with renal cell carcinoma. *BJU Int* 86: 203-7
264. Gucer F, Moser F, Tamussino K, Reich O, Haas J, Arikian G, Petru E, Winter R. 1998. Thrombocytosis as a prognostic factor in endometrial carcinoma. *Gynecol Oncol* 70: 210-4
265. Menczer J, Schejter E, Geva D, Ginath S, Zakut H. 1998. Ovarian carcinoma associated thrombocytosis. Correlation with prognostic factors and with survival. *Eur J Gynaecol Oncol* 19: 82-4
266. Lopes A, Daras V, Cross PA, Robertson G, Beynon G, Monaghan JM. 1994. Thrombocytosis as a prognostic factor in women with cervical cancer. *Cancer* 74: 90-2
267. Zeimet AG, Marth C, Muller-Holzner E, Daxenbichler G, Dapunt O. 1994. Significance of thrombocytosis in patients with epithelial ovarian cancer. *Am J Obstet Gynecol* 170: 549-54
268. Yazaki T, Inage H, Iizumi T, Koyama A, Kanoh S, Koiso K, Narita M, Tojo S. 1987. Studies on platelet function in patients with prostatic cancer. Preliminary report. *Urology* 30: 60-3
269. Ferriere JP, Bernard D, Legros M, Chassagne J, Chollet P, Gaillard G, Plagne R. 1985. beta-Thromboglobulin in patients with breast cancer. *Am J Hematol* 19: 47-53
270. Milroy R, Douglas JT, Campbell J, Carter R, Lowe GD, Banham SW. 1988. Abnormal haemostasis in small cell lung cancer. *Thorax* 43: 978-81
271. Prisco D, Paniccia R, Coppo M, Filippini M, Francalanci I, Brunelli T, Comeglio P, Abbate R. 1995. Platelet activation and platelet lipid composition in pulmonary cancer. *Prostaglandins Leukot Essent Fatty Acids* 53: 65-8
272. Abbasciano V, Bianchi MP, Trevisani L, Sartori S, Gilli G, Zavagli G. 1995. Platelet activation and fibrinolysis in large bowel cancer. *Oncology* 52: 381-4
273. Gastl G, Plante M, Finstad CL, Wong GY, Federici MG, Bander NH, Rubin SC. 1993. High IL-6 levels in ascitic fluid correlate with reactive thrombocytosis in patients with epithelial ovarian cancer. *Br J Haematol* 83: 433-41
274. Kaser A, Brandacher G, Steurer W, Kaser S, Offner FA, Zoller H, Theurl I, Widder W, Molnar C, Ludwiczek O, Atkins MB, Mier JW, Tilg H. 2001. Interleukin-6 stimulates thrombopoiesis through thrombopoietin: role in inflammatory thrombocytosis. *Blood* 98: 2720-5
275. Estrov Z, Talpaz M, Mavligit G, Pazdur R, Harris D, Greenberg SM, Kurzrock R. 1995. Elevated plasma thrombopoietic activity in patients with metastatic cancer-related thrombocytosis. *Am J Med* 98: 551-8
276. Suzuki A, Takahashi T, Nakamura K, Tsuyuoka R, Okuno Y, Enomoto T, Fukumoto M, Imura H. 1992. Thrombocytosis in patients with tumors producing colony-stimulating factor. *Blood* 80: 2052-9
277. Jurasz P, Sawicki G, Duszyk M, Sawicka J, Miranda C, Mayers I, Radomski MW. 2001. Matrix metalloproteinase 2 in tumor cell-induced platelet aggregation: regulation by nitric oxide. *Cancer Res* 61: 376-82
278. van den Berg YW, Osanto S, Reitsma PH, Versteeg HH. 2012. The relationship between tissue factor and cancer progression: insights from bench and bedside. *Blood* 119: 924-32

279. van Es N, Sturk A, Middeldorp S, Nieuwland R. 2014. Effects of cancer on platelets. *Semin Oncol* 41: 311-8
280. Goubran HA, Burnouf T, Radosevic M, El-Ekiaby M. 2013. The platelet-cancer loop. *Eur J Intern Med* 24: 393-400
281. Younos IH, Dafferner AJ, Gulen D, Britton HC, Talmadge JE. 2012. Tumor regulation of myeloid-derived suppressor cell proliferation and trafficking. *Int Immunopharmacol* 13: 245-56
282. Youn JI, Kumar V, Collazo M, Nefedova Y, Condamine T, Cheng P, Villagra A, Antonia S, McCaffrey JC, Fishman M, Sarnaik A, Horna P, Sotomayor E, Gabrilovich DI. 2013. Epigenetic silencing of retinoblastoma gene regulates pathologic differentiation of myeloid cells in cancer. *Nat Immunol* 14: 211-20
283. Zhao W, Xu Y, Xu J, Wu D, Zhao B, Yin Z, Wang X. 2015. Subsets of myeloid-derived suppressor cells in hepatocellular carcinoma express chemokines and chemokine receptors differentially. *Int Immunopharmacol* 26: 314-21
284. Huang B, Lei Z, Zhao J, Gong W, Liu J, Chen Z, Liu Y, Li D, Yuan Y, Zhang GM, Feng ZH. 2007. CCL2/CCR2 pathway mediates recruitment of myeloid suppressor cells to cancers. *Cancer Lett* 252: 86-92
285. Sawanobori Y, Ueha S, Kurachi M, Shimaoka T, Talmadge JE, Abe J, Shono Y, Kitabatake M, Kakimi K, Mukaida N, Matsushima K. 2008. Chemokine-mediated rapid turnover of myeloid-derived suppressor cells in tumor-bearing mice. *Blood* 111: 5457-66
286. Tsou CL, Peters W, Si Y, Slaymaker S, Aslanian AM, Weisberg SP, Mack M, Charo IF. 2007. Critical roles for CCR2 and MCP-3 in monocyte mobilization from bone marrow and recruitment to inflammatory sites. *J Clin Invest* 117: 902-9
287. Serbina NV, Pamer EG. 2006. Monocyte emigration from bone marrow during bacterial infection requires signals mediated by chemokine receptor CCR2. *Nat Immunol* 7: 311-7
288. Nakano H, Lin KL, Yanagita M, Charbonneau C, Cook DN, Kakiuchi T, Gunn MD. 2009. Blood-derived inflammatory dendritic cells in lymph nodes stimulate acute T helper type 1 immune responses. *Nat Immunol* 10: 394-402
289. Eash KJ, Greenbaum AM, Gopalan PK, Link DC. 2010. CXCR2 and CXCR4 antagonistically regulate neutrophil trafficking from murine bone marrow. *J Clin Invest* 120: 2423-31
290. Manresa MC, Godson C, Taylor CT. 2014. Hypoxia-sensitive pathways in inflammation-driven fibrosis. *Am J Physiol Regul Integr Comp Physiol* 307: R1369-80
291. Schreml S, Szeimies RM, Prantl L, Karrer S, Landthaler M, Babilas P. 2010. Oxygen in acute and chronic wound healing. *Br J Dermatol* 163: 257-68
292. Semenza GL. 2003. Targeting HIF-1 for cancer therapy. *Nat Rev Cancer* 3: 721-32
293. Wong CC, Gilkes DM, Zhang H, Chen J, Wei H, Chaturvedi P, Fraley SI, Wong CM, Khoo US, Ng IO, Wirtz D, Semenza GL. 2011. Hypoxia-inducible factor 1 is a master regulator of breast cancer metastatic niche formation. *Proc Natl Acad Sci U S A* 108: 16369-74
294. Wong CC, Zhang H, Gilkes DM, Chen J, Wei H, Chaturvedi P, Hubbi ME, Semenza GL. 2012. Inhibitors of hypoxia-inducible factor 1 block breast cancer metastatic niche formation and lung metastasis. *J Mol Med (Berl)* 90: 803-15
295. Sceneay J, Chow MT, Chen A, Halse HM, Wong CS, Andrews DM, Sloan EK, Parker BS, Bowtell DD, Smyth MJ, Moller A. 2012. Primary tumor hypoxia recruits CD11b⁺/Ly6C^{med}/Ly6G⁺ immune suppressor cells and compromises NK cell cytotoxicity in the premetastatic niche. *Cancer Res* 72: 3906-11
296. Taniguchi CM, Miao YR, Diep AN, Wu C, Rankin EB, Atwood TF, Xing L, Giaccia AJ. 2014. PHD inhibition mitigates and protects against radiation-induced gastrointestinal toxicity via HIF2. *Sci Transl Med* 6: 236ra64

297. Cramer T, Yamanishi Y, Clausen BE, Forster I, Pawlinski R, Mackman N, Haase VH, Jaenisch R, Corr M, Nizet V, Firestein GS, Gerber HP, Ferrara N, Johnson RS. 2003. HIF-1alpha is essential for myeloid cell-mediated inflammation. *Cell* 112: 645-57
298. Ceradini DJ, Kulkarni AR, Callaghan MJ, Tepper OM, Bastidas N, Kleinman ME, Capla JM, Galiano RD, Levine JP, Gurtner GC. 2004. Progenitor cell trafficking is regulated by hypoxic gradients through HIF-1 induction of SDF-1. *Nat Med* 10: 858-64
299. Forsythe JA, Jiang BH, Iyer NV, Agani F, Leung SW, Koos RD, Semenza GL. 1996. Activation of vascular endothelial growth factor gene transcription by hypoxia-inducible factor 1. *Mol Cell Biol* 16: 4604-13
300. Petit I, Jin D, Rafii S. 2007. The SDF-1-CXCR4 signaling pathway: a molecular hub modulating neo-angiogenesis. *Trends Immunol* 28: 299-307
301. Yamaguchi J, Kusano KF, Masuo O, Kawamoto A, Silver M, Murasawa S, Bosch-Marce M, Masuda H, Losordo DW, Isner JM, Asahara T. 2003. Stromal cell-derived factor-1 effects on ex vivo expanded endothelial progenitor cell recruitment for ischemic neovascularization. *Circulation* 107: 1322-8
302. Askari AT, Unzek S, Popovic ZB, Goldman CK, Forudi F, Kiedrowski M, Rovner A, Ellis SG, Thomas JD, DiCorleto PE, Topol EJ, Penn MS. 2003. Effect of stromal-cell-derived factor 1 on stem-cell homing and tissue regeneration in ischaemic cardiomyopathy. *Lancet* 362: 697-703
303. Du R, Lu KV, Petritsch C, Liu P, Ganss R, Passegue E, Song H, Vandenberg S, Johnson RS, Werb Z, Bergers G. 2008. HIF1alpha induces the recruitment of bone marrow-derived vascular modulatory cells to regulate tumor angiogenesis and invasion. *Cancer Cell* 13: 206-20
304. Staller P, Sulitkova J, Lisztwan J, Moch H, Oakeley EJ, Krek W. 2003. Chemokine receptor CXCR4 downregulated by von Hippel-Lindau tumour suppressor pVHL. *Nature* 425: 307-11
305. Bruning U, Fitzpatrick SF, Frank T, Birtwistle M, Taylor CT, Cheong A. 2012. NFkappaB and HIF display synergistic behaviour during hypoxic inflammation. *Cell Mol Life Sci* 69: 1319-29
306. Maxwell PJ, Gallagher R, Seaton A, Wilson C, Scullin P, Pettigrew J, Stratford IJ, Williams KJ, Johnston PG, Waugh DJ. 2007. HIF-1 and NF-kappaB-mediated upregulation of CXCR1 and CXCR2 expression promotes cell survival in hypoxic prostate cancer cells. *Oncogene* 26: 7333-45
307. Jung JE, Lee HG, Cho IH, Chung DH, Yoon SH, Yang YM, Lee JW, Choi S, Park JW, Ye SK, Chung MH. 2005. STAT3 is a potential modulator of HIF-1-mediated VEGF expression in human renal carcinoma cells. *Faseb j* 19: 1296-8
308. Pawlus MR, Wang L, Hu CJ. 2014. STAT3 and HIF1alpha cooperatively activate HIF1 target genes in MDA-MB-231 and RCC4 cells. *Oncogene* 33: 1670-9
309. Balamurugan K. 2015. HIF-1 at the crossroads of hypoxia, inflammation, and cancer. *Int J Cancer*
310. Koshiji M, Kageyama Y, Pete EA, Horikawa I, Barrett JC, Huang LE. 2004. HIF-1alpha induces cell cycle arrest by functionally counteracting Myc. *Embo j* 23: 1949-56
311. Goda N, Ryan HE, Khadivi B, McNulty W, Rickert RC, Johnson RS. 2003. Hypoxia-inducible factor 1alpha is essential for cell cycle arrest during hypoxia. *Mol Cell Biol* 23: 359-69
312. Lim JH, Park JW, Kim MS, Park SK, Johnson RS, Chun YS. 2006. Bafilomycin induces the p21-mediated growth inhibition of cancer cells under hypoxic conditions by expressing hypoxia-inducible factor-1alpha. *Mol Pharmacol* 70: 1856-65
313. Gordan JD, Bertout JA, Hu CJ, Diehl JA, Simon MC. 2007. HIF-2alpha promotes hypoxic cell proliferation by enhancing c-myc transcriptional activity. *Cancer Cell* 11: 335-47

314. Covello KL, Kehler J, Yu H, Gordan JD, Arsham AM, Hu CJ, Labosky PA, Simon MC, Keith B. 2006. HIF-2alpha regulates Oct-4: effects of hypoxia on stem cell function, embryonic development, and tumor growth. *Genes Dev* 20: 557-70
315. Elorza A, Soro-Arnaiz I, Melendez-Rodriguez F, Rodriguez-Vaello V, Marsboom G, de Carcer G, Acosta-Iborra B, Albacete-Albacete L, Ordonez A, Serrano-Oviedo L, Gimenez-Bachs JM, Vara-Vega A, Salinas A, Sanchez-Prieto R, Martin del Rio R, Sanchez-Madrid F, Malumbres M, Landazuri MO, Aragonés J. 2012. HIF2alpha acts as an mTORC1 activator through the amino acid carrier SLC7A5. *Mol Cell* 48: 681-91
316. Li F, Sonveaux P, Rabbani ZN, Liu S, Yan B, Huang Q, Vujaskovic Z, Dewhirst MW, Li CY. 2007. Regulation of HIF-1alpha stability through S-nitrosylation. *Mol Cell* 26: 63-74
317. Ribechini E, Leenen PJ, Lutz MB. 2009. Gr-1 antibody induces STAT signaling, macrophage marker expression and abrogation of myeloid-derived suppressor cell activity in BM cells. *Eur J Immunol* 39: 3538-51
318. Condamine T, Kumar V, Ramachandran IR, Youn JI, Celis E, Finnberg N, El-Deiry WS, Winograd R, Vonderheide RH, English NR, Knight SC, Yagita H, McCaffrey JC, Antonia S, Hockstein N, Witt R, Masters G, Bauer T, Gabrilovich DI. 2014. ER stress regulates myeloid-derived suppressor cell fate through TRAIL-R-mediated apoptosis. *J Clin Invest* 124: 2626-39

VYARA Z. MATSON

University of Wisconsin-Milwaukee
3209 N Maryland Ave, Milwaukee, WI 53211
kamenova@uwm.edu; kamenovavz@gmail.com

EDUCATION

Ph.D. in Biological Sciences, Research Area in Immunology, 2015

University of Wisconsin-Milwaukee, Milwaukee, WI, United States

Dissertation: Migration of myeloid-derived suppressor cells to tumor and tumor-draining lymph node in a murine model of breast cancer

Advisor: Douglas Steeber, Ph.D.

B.S. in Biotechnology, 2008

Sofia University, Sofia, Bulgaria

RESEARCH

INTERESTS

From the earliest stages of its development, cancer interacts with the immune system, often triggering immunoregulatory processes that enhance tumor progression. Furthermore, cancer-induced immunosuppression counters various immunotherapeutic approaches for cancer treatment, decreasing their efficacy. I am interested in the mechanisms of cancer-induced immunosuppression and the development of innovative strategies for their blockade as ways of augmenting cancer immunotherapy.

GRADUATE RESEARCH

Myeloid-derived suppressor cells (MDSC) are a population of immature immunosuppressive cells generated in the bone marrow during cancer progression. MDSC migrate to the spleen, tumor, and tumor-draining lymph nodes, and suppress the anti-tumor T cell response. MDSC-mediated immunosuppression is considered one of the factors hindering the success of cancer immunotherapy. Thus, blockade of MDSC generation, migration and function, as well as targeted elimination of MDSC, are potential strategies for augmenting the immunotherapy of cancer. MDSC generation and function have been extensively studied, but the mechanisms governing MDSC migration

are largely unknown. Using a murine model of breast cancer, I studied the distribution and localization of MDSC within lymphoid tissues and tumors, as well as the involvement of adhesion molecules and other factors in MDSC migration to these sites.

COLLABORATIONS

2012-2014: Julie Oliver, Ph.D. - Department of Biological Sciences, University of Wisconsin-Milwaukee: *In vitro* evaluation of folate receptor-targeted magnetic nanoparticles for the targeted elimination of tumor cells.

2011-2012: Yi-Qiang Cheng, Ph.D. - Department of Pharmaceutical Sciences, University of North Texas Health Science Center: *In vitro* evaluation of novel histone deacetylase inhibitors as anti-cancer drugs; *In vivo* evaluation of genetically engineered tumor-targeted *Salmonella sp.* producing anti-cancer drugs for the treatment of solid tumors.

2009-2011: Shaoqin Gong, Ph.D. - Department of Biomedical Engineering, University of Wisconsin-Madison: *In vitro* evaluation of cytotoxicity and cell uptake of various formulations of doxorubicin-conjugated nanoparticles for targeted delivery of anti-cancer drugs.

PUBLICATIONS

IN PREPARATION

Matson VZ, Steeber DA. *Role of L-selectin in the migration of myeloid-derived suppressor cells to tumors and tumor-draining lymph nodes in breast cancer*

Ulicki J, Wang C, Biswas S, Li X, **Matson VZ**, Spindler B, Murphy D, Tang W, Steeber DA, Hossain MM, Cheng Y. *Design, synthesis and biological evaluation of small, potent histone deacetylase (HDAC) inhibitors, which reveal a selectivity profile for HDAC1 and HDAC2: based on the scaffolds of FK228 and thailandepsins A and B*

PUBLISHED

*Krystofiak ES, ***Matson VZ**, Steeber DA, Oliver JA. *Elimination of tumor cells using folate receptor targeting by antibody-conjugated, gold-coated magnetite nanoparticles in a murine breast cancer model*. 2012, Journal of Nanomaterials, volume 2012, article ID 431012

* indicates co-first author

Xiao Y, Hong H, **Matson VZ**, Javadi A, Xu W, Yang Y, Zhang Y, Engle JW, Nickles RJ, Cai W, Steeber DA, Gong S. *Gold nanorods conjugated with doxorubicin and cRGD for combined anti-cancer drug delivery and PET imaging*. 2012, *Theranostics*, 2 (8): 757-68

Yang X, Grailer JJ, Rowland JJ, Javadi A, Hurley SA, **Matson VZ**, Steeber DA, Gong S. *Multifunctional stable and pH-responsive polymer vesicles formed by heterofunctional triblock copolymer for targeted anticancer drug delivery and ultrasensitive MR imaging*. 2010, *ACS Nano*, 4 (11): 6805-17

CONFERENCES AND SYMPOSIA

ATTENDED

Blood Center of Wisconsin - Center for Human Immunology Symposium, Wauwatosa, WI, 2014: *Immune Cell: Genome, Transcriptome, and Signalosome*

American Association of Immunologists Annual Meeting, Honolulu, HI, 2013

Blood Center of Wisconsin - Center for Human Immunology Symposium, Wauwatosa, WI 2013: *Cellular Immunotherapy and Hematopoietic Stem Cells*

Autumn Immunology Conference, Chicago, IL 2012

POSTERS

American Association of Immunologists Annual Meeting, Honolulu, HI, 2013: *Differential migration of myeloid-derived suppressor cell subsets to tumor-draining lymph nodes in a murine model of breast cancer*; Vyara Z. Matson, Jessica J. Loppnow, and Douglas A. Steeber

Microscopy and Microanalysis Meeting, Phoenix, AZ, 2012: *Protein conjugation by non-ionic adsorption both functionalizes and stabilizes gold-coated magnetite nanoparticles*; Evan S. Krystofiak, Vyara Z. Matson, Douglas A. Steeber, Julie A. Oliver; presented by Evan Krystofiak

TALKS

Biological Sciences Colloquium, UW-Milwaukee, 2015: *Migration of myeloid-derived suppressor cells to tumor and tumor-draining lymph node in a mouse model of breast cancer*

Biological Sciences Research Symposium, UW-Milwaukee, 2014: *Myeloid-derived suppressor cells co-localize with hypoxic regions within the primary tumor in a murine model of breast cancer*

Biological Sciences Research Symposium, UW-Milwaukee, 2013: *Differential migration of myeloid-derived suppressor cell subsets to tumor-draining lymph nodes in a murine model of breast cancer*

Biological Sciences Research Symposium, UW-Milwaukee, 2010: *The 4T1 murine mammary carcinoma as a model for in vivo tumor targeting with nanoparticles containing anti-cancer drugs*

INVITED LECTURES

2015: *Flow Cytometry – Principles*; University of Wisconsin – Milwaukee, Experimental Microbiology Bio Sci 580, invited by Ching-Hong Yang, Ph.D.

2013: *Cancer and the immune system*; University of Wisconsin – Milwaukee, Immunology Bio Sci 401, invited by Douglas Steeber, Ph.D.

RESEARCH SUPERVISION AND TEACHING

2009-2015: Research Supervisor

- High school students
 - Nicolet High School, Glendale, WI: Nancy Gao
 - Divine Savior Holy Angels High School, Milwaukee, WI: Jenna Lieungh, Alyssa Myszewski
- Undergraduate/graduate/postdoctoral
 - University of Wisconsin – Milwaukee: Kate Rose, Daniel Schloegel, Samantha Willms, Ahmed Al-Muhairi, Rishi Sharma, Louis Palen, Sreya Biswas, Shah Gopitkumar, Ph.D., Amber Huffine, Margaret Linden, Jeffrey Denninger, Stephanie Bora

2009-2015: Teaching Assistant, University of Wisconsin-Milwaukee

- Immunological Techniques Laboratory
- Laboratory in Genetics and Cell Biology
- Anatomy and Physiology II Laboratory

SERVICE

2013-2014: Graduate Student Advisory Council: Governance Subcommittee, UW-Milwaukee

2013-2014: Graduate Faculty Committee - Graduate Student Representative, UW-Milwaukee

2011-2014: Graduate Organization of Biological Sciences, UW-Milwaukee

Positions served: President, Vice President, Symposium Chair

2012-2013: Project Judge, Badger State Science and Engineering Fair

AWARDS

2012 – 2014: UW-Milwaukee Joseph B. Baier Award

2011, 2013, 2014: UW-Milwaukee Ruth Walker Grant-in-Aid

2013: UW-Milwaukee Distinguished Dissertator Fellowship

2011: UW-Milwaukee James J. Magnino, M.D. Scholarship

2010 – 2014: UW-Milwaukee Chancellor's Award

2003 – 2008: Sofia University Scholarship for Academic Excellence